Study of long-term visual function and plasma biomarkers in patients with epilepsy receiving Vigabatrin

Kaleena Bulan Michael MBChB. FRCOphth

Submitted for the Degree of

Doctor of Philosophy

University of Glasgow

Glasgow Centre for Ophthalmic Research

Glasgow

September 2021

Abstract

Vigabatrin is a highly effective adjunctive treatment for adults with refractory epilepsy and for infantile spasms. After gaining its license in Europe in 1989, it was used widely with much success until 1997 when reports of permanent visual fields defects were observed in some patients. The use of Vigabatrin had fallen in Europe since, where significant number of patients were denied this treatment leading to inadequate seizure control, poorer quality of life and greater risk of death and injury. In the US, Vigabatrin was made available for their patients in 2009 involving costly and extensive monitoring programme of visual function. The result of long-term monitoring is varied, partly due to the mixed methods used for examination of visual function. Our centre previously completed one of the largest international studies investigating Vigabatrin associated retinal toxicity, differentiating the pathological from physiological effects of Vigabatrin on vision and to document pre-existing visual field defects in 25% of patients with epilepsy. More than 2 milliseconds timing delay on the peripheral retina on WF-mfERG was found to be a sensitive and specific indicator of Vigabatrin associated retinal toxicity.

28 subjects were examined in this study. The effect of Vigabatrin use (current versus previous) on their visual function and retinal structures with the Optical Coherence Tomography (OCT) was assessed. Subjects were also stratified based on the presence of >2ms peripheral timing delay to uncover specific patterns in their visual tests.

The results showed a strong relationship between >2ms peripheral timing delay with higher volume of the inner retinal microstructures based on the OCT ($p<0.05$). These changes are also predictive of their perimetry scores ($p<0.05$). OCT retinal nerve fibre layer however appear to have poor correlation with mfERG results making it an unsuitable biomarker. Several retinal microlayers appear be affected, suggesting VaRT to be more diffuse and widespread than previously believed. Sub-group analyses showed no difference in the concentration of serum Taurine and Ornithine in the current or previous user groups or those with and without the mfERG >2ms peripheral timing delay. We propose that OCT macula volume analysis to be a promising method to detect and monitor for presence of VaRT. Development of a customised analytical algorithm involving retinal auto-segmentation could help us progress in developing a practical and reliable tool for the detection and monitoring of VaRT.

ACKNOWLEDGEMENTS

Firstly, I am indebted to all the patients and their carers who have participated in this study, without whom all this work will not be possible. These patients have been recruited from the Glasgow Centre for Ophthalmic Research and the Epilepsy Unit, Western Infirmary/Glasgow Royal Infirmary, Glasgow, UK.

I am extremely grateful to Dr Linda Stephen and Professor John Paul Leach for all their enthusiastic input, criticisms and perspectives in shaping the journey of this research.

This endeavour would not have been possible for all my colleagues in the Glasgow Centre for Ophthalmic Research for welcoming me as part of their family:

Dr Stuart Parks for all his advice, direction and opportunities over the years, for this project and also for many others.

Dr David Keating for his supervisory input and guidance.

Dr Sinead Walker for her time with helping in interpretation of the ff-ERG and WF-mfERG results; and also for her friendship, perspective and advice.

Ann Mcquiston, Lindsey Steele, Kirsten Graham for helping me conduct and organise the study, particularly for their expertise and experience in testing the patients with ff-ERG, WF-ERG and OCT.

Aimi Phillips for helping with the administrative aspect of this work.

Dr Iain Livingstone for his initial invitation and encouragement to consider research alongside training.

Dr Pedro Gonzalez for the research materials of the previous work related to this study.

The Endowment Funds, NHS Greater Glasgow and Clyde for sponsoring this study.

LIST OF CONTENTS

Section B: Experimental Work

SECTION C FINAL DISCUSSION

List of Figures

LIST OF TABLES

LIST OF ABBREVIATIONS

5-HIAA	5-hydroxyindole acetic acid
ANOVA	Analysis of variance (Statistical method)
Asb	Apostilb
BM	Bruch's membrane
cd	Candela
cGMP	Cyclic guanosine monophosphate
C_{max}	Maximum concentration observed
CNS	Central nervous system
CPS	Complex partial seizure
CRT	Cathode ray tubes
CSF	Cerebrospinal fluid
CT	Computerised tomography
DA	Dark adaptation
dB	Decibels
DPP	Digital polysilicone projection
EEG	Electroencephalogram
ELM	External limiting membrane
EOG	Electrooculogram
ERG	Electroretinogram/electroretinograhy
ETDRS	Early treatment Diabetic Retinopathy Study (Standardised visual testing)

GABA	Gamma aminobutyric acid
GABA-T	GABA transaminase
GAD	Glutamic acid decarboxylase
GAT	GABA transporter
GCL	Ganglion Cell layer
HPLC	High performance liquid chromatography
HVA	Homovanillic acid
IC_{50}	Half maximal inhibitory concentration
ILM	Internal limiting membrane
INL	Inner nuclear layer
IPL	Inner Plexiform layer
ISCEV	International Society for Clinical Electrophysiology of Vision
LA	Light adaptation
LED	Light emitting diode
mfERG	Multifocal electroretinogram
MRI	Magnetic resonance imaging
NFL	Nerve fibre layer
OAT	Ornithine aminotransferase
OCT	Optical coherence tomography
ONL	Outer nuclear layer
OP	Oscillatory potentials
OPL	Outer Plexiform layer
PRL	Photoreceptors layer
PS	Perimetry score

RNFL	Retinal nerve fibre layer
RPE	Retinal pigment epithelium
SD-OCT	Spectral domain Optical Coherence tomography
SITA	Swedish Interactive Threshold Algorithm
SPSS	Statistical Package for Social Sciences (An application/product of IBM)
TD-OCT	Time Domain Optical Coherence tomography
TFT-LCD	Thin-film-transistor liquid crystal displays
T_{max}	Time of maximum concentration observed
VaRT	Vigabatrin associated retinal toxicity
VAVFL	Vigabatrin associated visual field defect
VF	Visual fields
WF-mfERG	Wide field multifocal electroretinogram

CHAPTER 1:

VIGABATRIN AND VISION

1.1 Pharmacology of GABA:

1.1.1 The GABA molecule

GABA is the well-known abbreviation for ɣ-aminobutyric acid, a primary inhibitory neurotransmitter within the mammalian central nervous system. GABA is the product of glutamic acid, through the action of glutamic acid decarboxylase (GAD). GABA undergoes metabolization by GABA transaminase (GABA-T) into succinic semialdehyde. Further breakdown occurs resulting in succinate and gamma-hydroxybutyrate. GAD is normally found in the synaptic regions of GABA-ergic cells. GABA-T is mitochondrial enzyme found in neurons and glial cells.

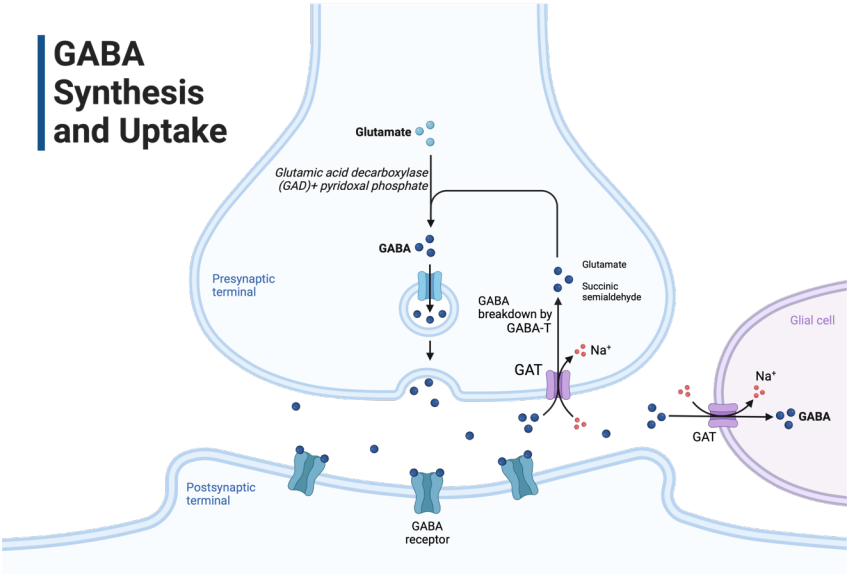

Figure 1.1: Diagram demonstrating the metabolism of GABA. (Image created with Biorender.com)

Several CNS disorders which include Huntington's chorea, Dystonia, Freidreich's ataxia, cerebellar ataxia and tardive dyskinesia have been implicated in the dysregulation of GABA within the CNS.

1.1.2 GABA receptors

The interaction between GABA and its receptors is inhibitory, as can be seen in its interaction with the following GABA receptors. Three forms of receptors are known to interact with the GABA molecule:

$GABA_A$

A bicuculline-sensitive macromolecular complex with five major binding sites for GABA, benzodiazepines, barbiturates, picrotoxin and anaesthetic steroids. They are ligand-gated ion channels that causes neuron hyperpolarisation through the influx of ions via the chloride channels. The Cl^- channel is key to the functioning of this receptor and is activated by the GABA-binding site. There is electrophysiological evidence of membrane hyperpolarisation, increasing the threshold for impulse firing. This reduces the chance to induce an action potential, therefore accomplishing its inhibitory effect.

The presence of $GABA_A$ is widespread in the retina, and are present in both the pre-synaptic and postsynaptic regions (Lukasiewicz and Shields, 1998).

$GABA_B$

They are more selective in their interaction, and do not interact with the same agents as $GABA_A$. $GABA_B$ receptors are metabotropic, obligatory heterodimers composed of the R1 and R2 subunits and belong to class C of the G-protein coupled receptor group. The main actions of activated $GABA_B$ receptor are to inhibit of adenylyl cyclase and inhibit voltage gated calcium channels that leads to propagated influx of ions through potassium channels. They are also present both in the presynaptic and postsynaptic regions. The presynaptic modulation of calcium channels coordinates the release of neurotransmitter in that region, while modulation of K^+ and adenylyl cyclase induces hyperpolarisation in the post-synaptic regions.

The large extracellular N-terminal domain of the receptor is the GABA binding site. Baclofen in particular, is found to have a potent effect and affinity for $GABA_B$ receptors. In the retina, $GABA_B$ receptors have been found in horizontal, amacrine, ganglion and muller glial cells in experimental animal models (Koulen *et al.*, 1998; Zhang, Bettler and Duvoisin, 1998; Nehring *et al.*, 2000; Rotolo and Dacheux, 2003).

$GABA_C$

This receptor was only later isolated due to observations where some GABA receptors appear to be insensitive to bicuculline and baclofen. However, they are more sensitive to GABA than $GABA_A$ itself, with the ability to sustain longer currents in the presence of agonists (Bormann and Feigenspan, 1995). Structurally, it is an integral membrane ionophore than responds to transmembrane Cl^- gradient change. The presence of ρ-subunits distinguishes them from the $GABA_A$ receptors.

$GABA_C$ receptors are composed of ρ (rho) subunits (rho1, rho2 and rho3), that form either homopentameric or heteropentameric complexes. They undergo selective activation by +CAMP, and inhibition by TPMPA. In rats, the heteropentameric structure has low sensitivity towards picrotoxin (Zhang and Slaughter, 1995). As $GABA_C$ is approximately 10 times more sensitive to GABA than $GABA_A$, it therefore requires a lower concentration of GABA for activation. They mediate a slower response with prolonged and sustained inhibitory currents in the presence of an agonist (Bormann and Feigenspan, 1995).

$GABA_C$ is found in the retina, although their population is less widespread than $GABA_A$. Their presence have been confirmed in cones, horizontal, amacrine, ganglion cells but are in especially higher density in the bipolar axon terminals (Popova, 2015).

1.1.3 GABA in Seizure disorders

During an epileptic seizure, it is believed that paroxysmal hypersynchronous transient electric charges occur in the brain where there is abnormal excitation or inhibition in the region of abnormality (Treiman, 2001). While several neurotransmitters were implicated, a deficiency in GABA as the principal neurotransmitter is believed to be key in the treatment of seizure disorders.

The key observations of GABA in seizures can be summarised by the following themes:

- GABA dysfunction is observed in both clinical and experimental animal models with seizures
- GABA agonist causes seizure suppression
- GABA antagonist promotes seizure
- Stimulation of GAD (Glutamic acid decarboxylase) increases pre-synaptic GABA levels
- Inhibition of GABA-T (GABA transaminase) increases synaptic GABA levels

The development of therapeutic agents has been directed towards increasing levels of GABA, especially in the pre-synaptic region. Several approaches were considered when attempting to modulate abnormal GABA levels.

The use of GABA agonists to interact with GABA receptors described above include drugs such as Muscimol ($GABA_c$), Baclofen ($GABA_B$) and Benzodiazepines ($GABA_A$).

The inhibition of GABA-T (Vigabatrin), with subsequent increase GABA levels within the synaptic region has been found to be effective. Simultaneous stimulation of GAD is also favoured to enhance GABA synthesis. GAT is known to be stimulated by Gabapentin and Sodium Valproate.

1.2 Vigabatrin

1.2.1 Origin and design

One of the earlier publications of 4-amino-hex-5-ynoic- acid (early version of Vigabatrin) detailed an in-vitro demonstration of the irreversible, covalent bonds with GABA-transaminase and the substrate was published in 1975 (Jung and Metcalf, 1975). This was subsequently followed by demonstration of its antiseizure activity in murine models. Peripheral administration of Vigabatrin (known by its molecular name as 4-amino-hex-5-enoic-acid *and* gamma-vinyl-GABA) was found to increase GABA concentration significantly, compared to controls (M J Jung *et al.*, 1977). Although an increase in total brain GABA does not always correlate with seizure control or suppression , GABA concentration increases from this novel substrate through selective inhibition of GABA-T appear to induce seizure control successfully (M. J. Jung *et al.*, 1977; Schechter *et al.*, 1977). Studies published at that time were also able to

demonstrate a predictable, dose-dependent relationship between GAD and the substrate, therefore increasing its therapeutic potential.

1.2.2 Chemical Structure

The substrate later became known as Gamma-Vinyl-GABA. Its molecular structure is illustrated in figure 1.2. It is a water-soluble chemical compound with the formula of $C_6H_{11}NO_2$, and a molecular weight of 129.16 (Hammond and Wilder, 1985).

In its drug form of Vigabatrin, it is a racemic mixture of the S(+)-enantiomers and the R(-)-enantiomers. The S(+)-enantiomer has a strong affinity towards GABA-T accounting for principal activity of Vigabatrin while the R(-)-enantiomers display very little activity. (Larsson *et al.*, 1986).

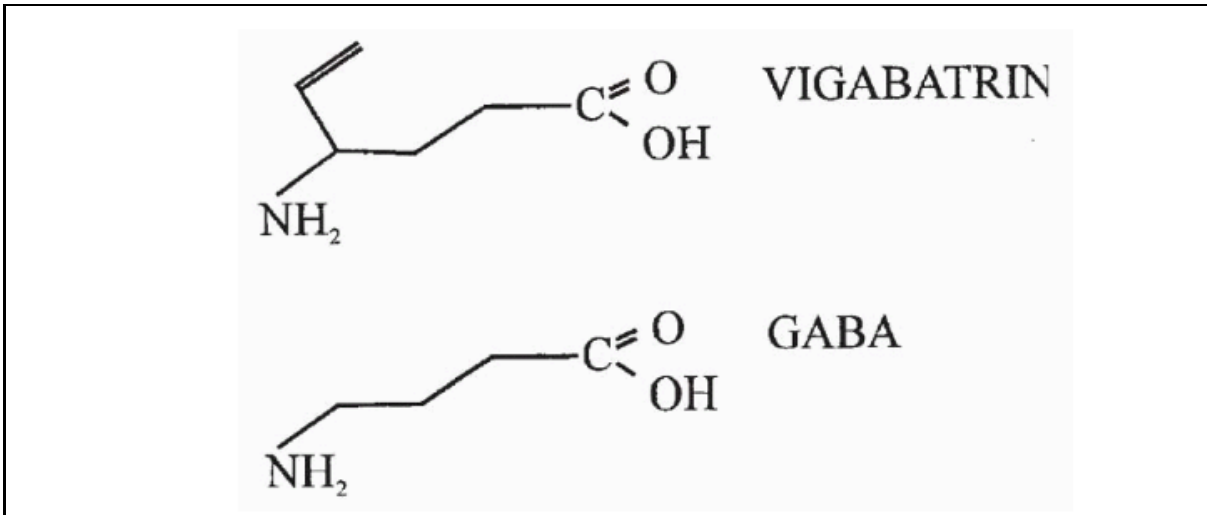

Figure 1.2: Chemical structure of Vigabatrin compared to GABA. (Image credit to https://neupsykey.com/vigabatrin-2/)

1.2.3 Mechanism of action

The primary action of Gamma-Vinyl-GABA is as an inhibitor to GABA-T, although some GAD activity was also observed. It is known to be a highly selective, catalytic irreversible inhibitor of GABA-T. Being a structural analogue of GABA, GABA-T accepts this substrate and converts it into a reactive compound that binds strongly to the enzyme. This interaction causes rapid increases in GABA, in a dose-dependent manner.

Because of the slow turnover rate of GABA-T, plasma concentration of Vigabatrin is not felt to be representative of its activity. Therefore CSF analyses were conducted by several groups to provide a better perspective of its efficacy.

Biochemical studies of the cerebrospinal fluid (CSF) in human subjects showed predictable increase in total and free GABA, and homocarnosine compared to baseline but does not appear to influence to seizure control (Pitkänen *et al.*, 1988). In another study, increases in 5-hydroxyindole acetic acid (5-HIAA) and homovanillic acid (HVA) was found in the CSF at the start of treatment, but then return to baseline levels after 4 weeks (Ben-Menachem *et al.*, 1989). Neurotransmitters dopamine and norepinephrine were also unaltered by Vigabatrin (Ben-Menachem *et al.*, 1991). A separate study examining human CSF confirmed the unaltered state of the cholinergic, dopaminergic, serotogenic and peptidergic systems (Riekkinen *et al.*, 1989). Homocarnosine, a dipeptide of GABA and histidine in the brain, known also as an inhibitory neuromodulator was also studied. Homocarnosine levels in CSF was found to be elevated in some, consistent with CSF Vigabatrin levels. Those with elevated

homocarnosine appear to have better seizure control and was thought to be predictive of good seizure control from Vigabatrin (Petroff *et al.*, 1998).

1.2.4 Experimental evidence of toxicity

In general, there is a low degree of toxicity from Vigabatrin found in experimental models. While the primary action of Vigabatrin is on GABA-T, work on murine models have also shown decreases in the activity of GAD, which subsequently reduces the GABA concentration and leads to seizures. The observation was likely to be due to the onset of negative feedback from the initial increase of GABA from GABA-T inhibition (M J Jung *et al.*, 1977) .

Vigabatrin was also observed to have dose related effects with decreased function in locomotor activities, sedation, thermoregulation, piloerection, lacrimation, ptosis and coma (Schechter and Tranier, 1977; Sabers and Gram, 1992).

1.2.5 Histopathological examination

Toxicity studies from chronic use of Vigabatrin in animal models showed varied results, which poses a challenge when interpreted for clinical use. In murine models, high daily doses are associated with reduced food consumption, weakness and death. After 3 months of exposure to 300mg/kg/day, increase in the frequency of tonic convulsions were observed with some ataxic movements; likely to due to changes within the brain rather than direct effect of Vigabatrin. Retinal degeneration has been observed in albino

rats, suggesting degenerative type changes due to interaction between light and Vigabatrin in this species (Butler, 1989).

In dogs, the observation was milder with no change in the general health or their serum biochemical profile. In monkeys, some loose stools were noted only at high doses. Mild change in serum alanine aminotransferase was noted, in both dogs and monkeys. The most prominent drug-related change in all species appear to be the finding of vacuolation in the white matter tracts of the brain. Vacuolation is defined as the separation between the outer layers of the myelin sheath, and macroscopically also termed as 'intramyelinic oedema'. The finding is most prominent in rats and mice within the following regions in the brain; fornix, thalamic areas, optic tract, inferior colliculus and hippocampus. This finding also appears to be reversible, as they are not seen in the recovering murine. In dogs, the vacuolation changes at 12 months do not appear to be more significant than the observation at 6 months suggesting that there is a 'maximal vacuolation effect'.

In all examined species, the CNS changes appear to be confined to the brain with sparing of the spinal cord, retina and the rest of the peripheral nervous system. (Gibson *et al.*, 1990; Sabers and Gram, 1992)

1.2.6 Pharmacodynamics in experimental models

GABA-T and Vigabatrin undergo rapid reaction, reaching half-life inactivation at 6 minutes following the first order enzyme kinetics. Withdrawal of Vigabatrin from this

culture shows complete reversibility, with GABA-T activity returning to baseline levels after 4-6 days (Lippert *et al.*, 1977). In another study, the incubation of rodent brain homogenate with Vigabatrin shows reduction of GABA-T activity by 50% (IC_{50})(Löscher, 1980).

The GABA-T inhibition by Vigabatrin appears to be preferentially higher in cultured mouse neurons, compared to cultured astrocytes (Grant and Heel, 1991). In mouse models, following systemic (intraperitoneal, intramuscular, intravenous, subcutaneous and oral) administration of Vigabatrin, whole brain GABA levels was observed to increase rapidly, reaching the maximum after 3 hours and sustained for the minimum of 20 hours (M. J. Jung *et al.*, 1977; Schechter *et al.*, 1977).

The increase in GABA levels is impressive, with 359% increase compared to control reported in in vitro studies (Gram *et al.*, 1988). Vigabatrin increases GABA levels in all parts of the nervous tissue, and appears to have greater effect in increasing the GABA in the synaptosomal region compared to the non-synaptosomal regions (Sarhan and Seiler, 1979) and is likely to suggest a preferential site of GABA-T action for Vigabatrin.

Additionally, Vigabatrin has also been shown to have a significant effect in blocking GABA uptake in cultured astrocytic cells, supporting GABA-T inhibition but also clarify the lack of clear relationship between time of maximal GABA-T inhibition and anti-convulsant effects in animals, or immediate loss of seizure control following Vigabatrin withdrawal (Bernasconi *et al.*, 1988; Leach *et al.*, 1996).

More recently, a high ratio of S(+)/R(-) enantiomers was found in retina of Vigabatrin treated mouse demonstrating high level of S(+) accumulation in the retina compared to the R(-). In the brain, the ratio between the enantiomers is more equal suggesting there is preferential accumulation of the S (+) enantiomers in the retina. They also reported dysregulation of taurine and ornithine, that seems to be confined to the eye bar the retina where no dysregulation was found (Walters *et al.*, 2019, 2021). A preferential accumulation of Vigabatrin in retinal tissue compared to the brain was also reported to be 5 – 20 fold greater (Chan *et al.*, 2020; Walters *et al.*, 2021). These findings may underlie the reason why a suitable plasma biomarker to detect Vigabatrin related toxicity is yet to be found, as dysregulation is not widespread but rather they appear to be limited to the retina.

1.2.7 Pharmacokinetics in humans

Vigabatrin exist as a racemic mixture of 2 enantiomers; S(+) and the R(-). The 2 enantiomers differ in their function and activity. The S(+) enantiomer is the pharmacokinetically active form. The R(-) is inactive and does not appear to interfere with the S(+) form. No chiral inversions have been reported (Rey, Pons and Olive, 1992).

There is rapid absorption of Vigabatrin following oral administration in human subjects, reaching mean plasma peak of 192 nmol/L at 1hr (Grove, Alken and Schechter, 1984). Food intake does not affect its absorption. In normal subjects, the half life of the S(+) enantiomer is 7.5 hours, and the R (-) enantiomer is 8.1 hours. The half-life in epileptic subjects however appear lower, between 4.1 – 5.6 hours.

Following gut absorption, Vigabatrin undergoes renal elimination where renal recovery is between 70 – 95%, in its unchanged form (Grove, Alken and Schechter, 1984; Rey, Pons and Olive, 1992). Renal clearance of Vigabatrin was also influenced by age, even in young healthy subjects(Haegele and Schechter, 1986). Elderly subjects experience delayed absorption accompanied by a major increase in peak values followed by prolonged half-life, due to slower renal clearance (Haegele *et al.*, 1988). Subjects with renal impairment undergo slower renal clearance of Vigabatrin, that can have clinical consequences and require dosing adjustments (Haegele *et al.*, 1988). Despite no strong evidence of protein binding for Vigabatrin, CSF level of Vigabatrin is only 10 – 15% of the serum levels.

1.2.8 Clinical Efficacy

The efficacy of Vigabatrin appear to be remarkable in treatment-resistant complex partial seizure (CPS) epilepsies, with approximately 50% patients achieving 50% reduction in seizure (Pedersen *et al.*, 1985; Tartara *et al.*, 1986; Michelucci and Tassinari, 1989). A meta-analysis of European trials of 390 patients showed 72% of patients achieved at least 25% reduction in seizures (Mumford and Dam, 1989). Some studies reported lower efficacy from Vigabatrin, likely due to the inclusion of a wide variety of seizure spectrum (Tassinari *et al.*, 1987).

The efficacy of Vigabatrin differs based on the type of seizures; drug resistant CPS have the best responses. In primary generalised epilepsies, Vigabatrin does not appear to have significant effect, and may exacerbate absences (Guberman, 1996). Subjects with one seizure type, have low seizure frequency and unifocal EEG abnormalities seem to have better response to Vigabatrin compared to those with partial seizures (other types, not CPS), high seizure frequency and multifocal EEG abnormalities with cognition defects; they tend to show poorer response. Exacerbation of seizures was reported to be 3% in a review study (Michelucci and Tassinari, 1989).

1.2.9 Clinical use

Vigabatrin has mainly been studied as an add-on therapy for seizure control, where more than 2/3 of patients experience improvement in seizure control and up to 40% were seizure free (Fisher *et al.*, 1996). A recently updated Cochrane review found add-on Vigabatrin to be associated with 2-3 times more likely to gain significant seizure control, compared to placebo (Bresnahan *et al.*, 2020).

As a monotherapy, an open label study involving newly diagnosed adults with partial epilepsy showed comparable efficacy with carbamazepine, although patients were 4 times more likely to drop out of the study compared to carbamazepine, from lack of efficacy (Kälviäinen *et al.*, 1995). In another study comparing Valproate to Vigabatrin in carbamazepine resistant subjects found 27% of patients were successfully switched to Vigabatrin monotherapy, with 7% of them being seizure free at the end of the study. In those with duotherapy, 10% were seizure free (Brodie and Mumford, 1999).

The current recommendation for adults aged 17 and above is to initiate at 1000mg/day, with increases of the daily dose in 500mg/day increments per week. The maximum recommended dose is 3000mg/day (usually in 2 divided doses of 1500mg).

1.2.10 Drug interactions

20% reduction in serum levels of Phenytoin have been reported in patients taking concurrent Vigabatrin, indicating an adjustment to phenytoin dosage is required (Tartara *et al.*, 1986; Tassinari *et al.*, 1987). This is likely to be due to the induction of 2C enzymes of the cytochrome P450.

An isolated study of healthy adult individuals showed Vigabatrin increases the C_{max} of clonazepam by 30%, and reduces the mean T_{max} by 45% ('Sabril Drug Information. HIghlights of perscribing information.', 2020).

In patients taking Vigabatrin, changes in plasma levels of phenobarbital was found to be reduced between 8 – 16%, and sodium Valproate by 8%. These reductions are concluded to be non-significant in the overall seizure management. Plasma levels of Vigabatrin appear unaffected by other anti-seizure medications.

1.2.11 Adverse effects

Prior to reports of visual effects, the adverse effects of Vigabatrin were generally well tolerated. Common side effects include drowsiness, confusion, constipation, nausea,

vertigo, headaches, dysarthria and ataxia (Pedersen *et al.*, 1985; Loiseau *et al.*, 1986; Tartara *et al.*, 1986). One study reported resolution of these symptoms at 3 months when they continued on treatment (Browne *et al.*, 1987).

1.3 Vigabatrin and Vision

The first most far-reaching case series reporting bilateral visual field constriction secondary to Vigabatrin use was published in early 1997. At that time the manufacturers have since received 28 reports of visual fields abnormality, with an incidence of 0.0002%. An earlier case report was found from 1993 in the Italian language (Faedda *et al.*, 1993), but with limited details (Eke, Talbot and Lawden, 1997).

Clinicians have subsequently began to publish similar findings, typically characterised by its bilaterality, concentric pattern, irreversibility, and later onset. This triggered concerns for the paediatric patients who were on Vigabatrin; as examining this cohort is more challenging and the impact of permanent visual loss is arguably more concerning. The current prevalence is much higher than initially thought, 25 -50% in adults, 15% in children and 15 – 31% in infants (Barrett *et al.*, 2014). In this thesis, discussion will primarily be focused on adult patients, with reference to paediatric data if necessary.

In the presence of bilateral visual field defect, it is essential to distinguish the cause from retinal, optic nerve or cortical. Case reports often provide results of their patients' visual fields, visual electrophysiology and intracranial imaging to support their discussions. Visual field defects have been reported in patients with epilepsy who have never been

exposed to Vigabatrin, adding to our diagnostic challenge (Wilson and Brodie, 1997; Gonzalez *et al.*, 2009). Multiple testing modalities are often employed to best ascertain the nature of field loss where Vigabatrin toxicity is suspected.

1.3.1 Visual problems from vigabatrin: What is the definition?

Several terms have been used to describe this phenomenon; this includes Vigabatrin associated visual field loss or VAVFL, Vigabatrin associated retinal toxicity or VaRT and retinal dysfunction secondary to Vigabatrin. For this thesis, the abbreviated term VaRT will be used.

Multiple testing methods which vary from psychometric to objective types, means that the results are not always comparable especially in a condition of undetermined aetiology such as this. The typical profile of visual disturbances suspected to be secondary to Vigabatrin is as follows:

- Bilateral
- Concentric
- Irreversible
- Maybe symptomatic
- Visual acuity and colour are unaffected.

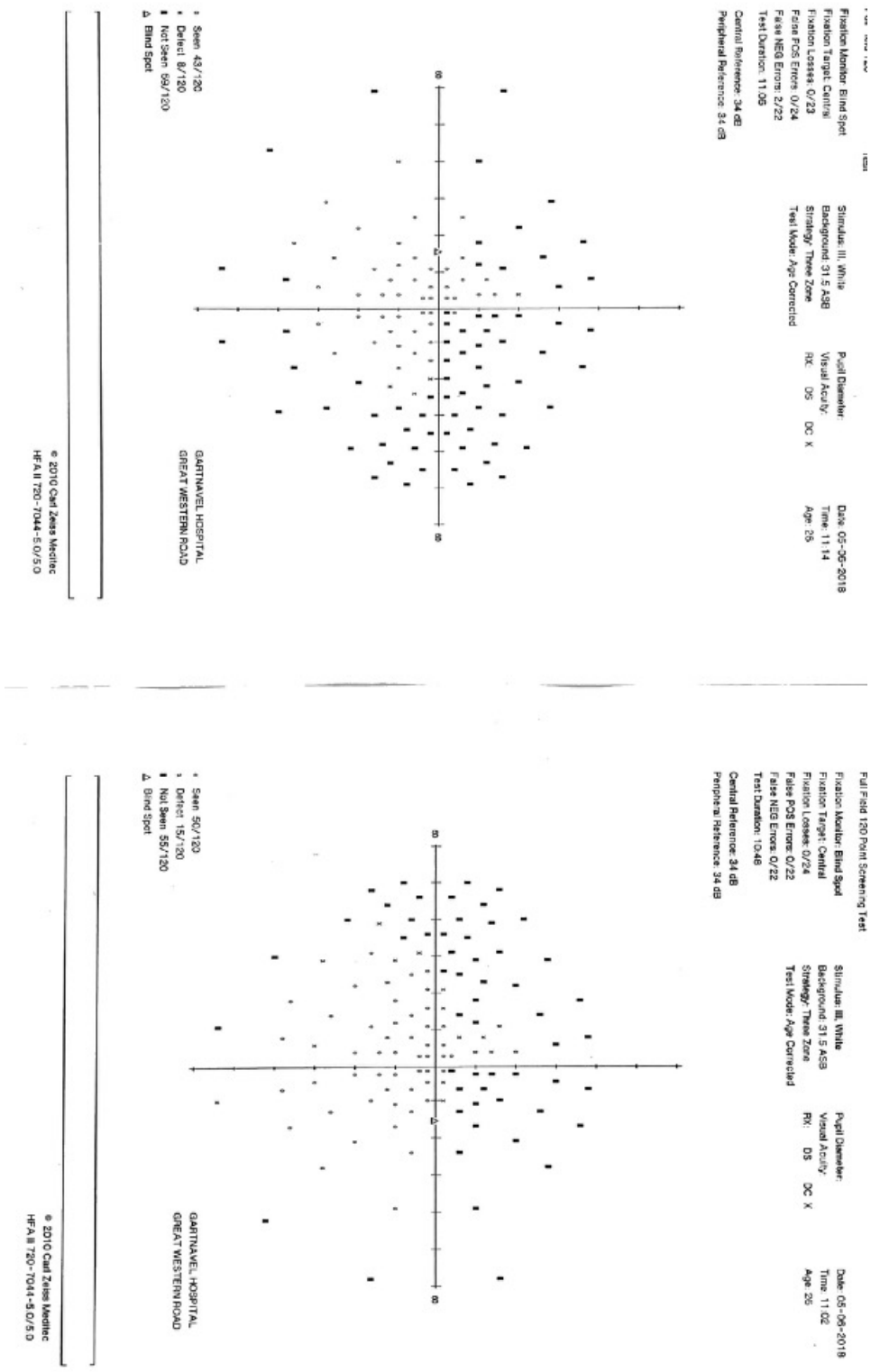

Figure 1.3 : Example of bilateral concentric visual loss record by the 120pt screening test (automated perimetry)

Various other findings and abnormalities have also been reported and will be discussed based on the type of examination. Discussion pertaining the following themes are discussed in other parts of this thesis, as part of the discussion section of the experimental works.

Visual fields (see Chapter 4)

Full field Electroretinogram (see Chapter 3.2)

Multifocal electroretinogram (see Chapter 2)

Serum amino acid analysis (see Chapter 6)

Optical coherence tomography (see Chapter 5)

1.3.2 The Sabril® Registry in the United States

Despite widespread use by epileptologists for complex partial seizures in Europe since 1989, the US FDA only approved Vigabatrin for use in complex partial seizures in 1997. This however was swiftly withdrawn in 1998 when they produced a 'non-approval' notice for use, following reports of severe visual field loss in the scientific literature.

Significant amendments were made for subsequent application to the FDA, incorporating an extensive program for visual monitoring. When the application was accepted and Vigabatrin was approved for use in 2009, it was accompanied by mandatory and extensive visual monitoring.

Participation in the US Sabril® Registry is mandatory, as such that patients can only obtain Vigabatrin through Support, Help and Resources for Epilepsy (SHARE) which runs a detailed registry. Prescribers are asked to complete:

Treatment Initiation form which collects information regarding treatment indication and current medication.

Ophthalmologic assessment form (OAF) which records visual assessments, required within 4 weeks from the start of treatment and every 3 months while on treatment. The form is also required within 3-6 months of stopping Vigabatrin. Notification of assessment exemption can also be provided here. Failure to complete this form within 90 days of the due date with see that Sabril prescription will not be renewed.

Treatment maintenance form at 3 months, for benefit-risk assessment of continuing Vigabatrin. (Krauss *et al.*, 2016)

Their publication in 2016 indicated that approximately 1200 patients were enrolled in their registry, where 35% were exempted from regular OAF completion due to other comorbidities affecting their ability to perform the test. This can include cognitive issues, blindness and others.

Obvious issues with the registry are related to the quality of data input, given the intensive information required from prescribers. The authors of the paper also reported previous relevant epileptic history such as surgery was not captured by the database.

The benefits of having the database are many; having all patients in a single database helps stratify the data when analysis and audit is due. The mandatory aspect forces prescribers and patient to be cooperative and involved in their monitoring, allowing for meticulous data capture.

1.3.4 Vigabatrin in Europe

After the start of clinical trials for Vigabatrin in 1979, it finally received marketing approval for the UK in 1989. However in 1995, a non-approval notice was received due to limited information regarding the safety and efficacy. Despite the report of visual loss in 1997, the European Medicines agency decision 1999 was that the benefit to risk profile was deemed favourable.

CHAPTER 2:

WIDE FIELD MULTIFOCAL ELECTRORETINOGRAPHY

In order to delve into Multifocal electroretinography, it is essential to grasp the basics of electroretinography. While the fundamentals are similar, multifocal ERG departs from the basic ERG as an enhanced testing arm of retinal function.

2.1 The Electroretinogram in brief

Curiosity about the electrical potentials in the eye dates as far back to 1865, where Holmgren discovered the change in electrical activity in the eye of an amphibian. Dewar and McKendrick in 1873 discovered 'electro-motive' force while operating in the eye of an anesthetised living cat and by placing a galvanometer near the eye of a living frog (Dewar and M Ckendrick, 1873). For several decades the study of light electrical responses of the eye continued on other species, allowing the study of retinal electrical waveforms. The first publication detailing clinical use of electroretinography was in 1945 by Gösta Karpe, by incorporating the electrodes onto a contact lens.

The electrical basis of ERG recordings is from studying the travel/path of electrical activity as it passes through living tissues, from the electrical resistance generated. The recordings are captured using externally placed electrodes, normally on both sides of the cornea.

Ohm's law in electricity could be applied when studying its course in biological tissues. The flow of electrical current through a resistor creates a gradient of electrical potential. This gradient matches the magnitude of current created by the resistance. Through this law, the ERG gathers global electrical responses from the retina.

2.1.1 Physiology

a-wave

In the scotopic state, higher concentrations of cyclic guanosine monophosphate (cGMP) lead to an opening of Na^+ and Ca^{2+} channels causing an influx of ions; the photoreceptors are depolarised with membrane potential of about -40mV. When light photons are absorped by the photoreceptor outer segments, rhodopsin photopigment is activated leading to activation of the G-protein, transducin. This leads to activation of the cGMP phosphodiesterase enzyme, reducing the levels of cGMP in the photoreceptors outersegments. This drastic change in intracellular cGMP causes the Na^+ channels to close resulting in hyperpolarisation with membrane potential of about -70mV (**the a-wave**).

b-wave

This state of hyperpolarisation reduces the release of neurotransmitter at their synaptic terminal causing subsequent depolarisation of the ON-bipolar cells. In the depolarised state, the increase in the extracellular K^+ within the outer plexiform layer causes depolarisation of the Müller cells. The positive waveform in the **b-wave** is the sum of the change in potentials of both the bipolar and Müller cells.

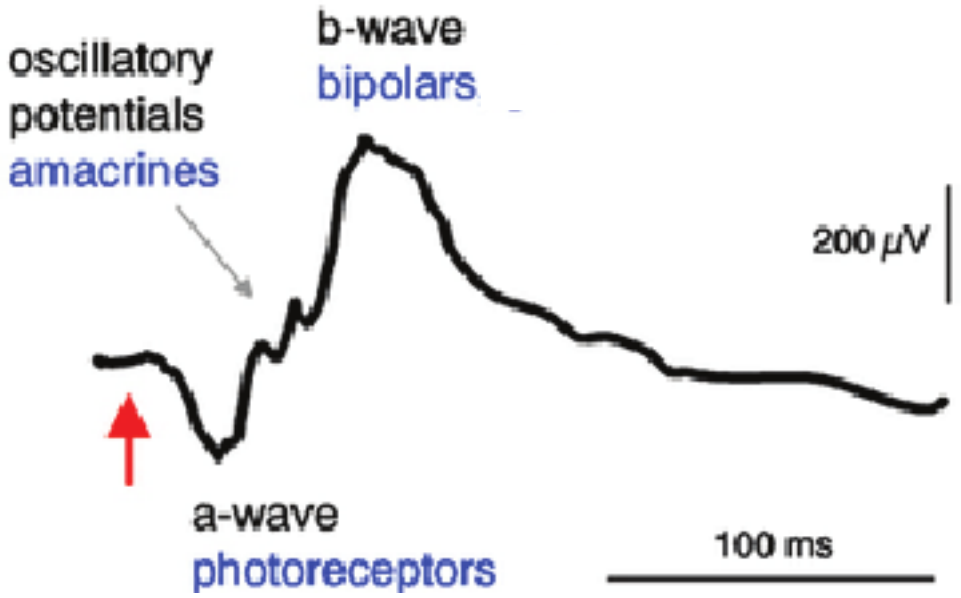

Figure 2.1 Light adapted ERG waveform in a normal patient. (modified from G.Niemeyer, "Das Elektroretinogramm: Nützlich und nicht kompliziert," Ophtha Schweizer, Faczeitschrift augenärztliche medizin, No. 5, 2004, pp. 7-13)

2.1.2 The test

The electrical responses are recorded by electrodes in contact with either the cornea or bulbar conjunctiva, or skin on the lower eyelids. The test must be performed in accordance with the ISCEV guidance (McCulloch *et al.*, 2015).

Testing conditions:

- Diffuse, uniform, white background with illumination of 17-34cd/m^2, normally achieved by an integrated dome or 'Ganzfeld'
- Dark-adapted conditions (*minimum 20 mins prior to start of test) to maximise rod-dominated retinal function
- Light adapted conditions (*minimum 10 mins if after dark adaptation stage) to minimise interference from rod responses.

(*The tests in this study were performed in accordance with the ISCEV guidelines published in 2015. This is now superseded by the latest version (2022 update) which is currently at draft for review stage)

2.1.2.1 Electrodes:

The main components of the electrodes are active, ground and reference. The active component may be in a contact form, or non-contact form. In the early days, contact electrodes are more common as they tended to provide higher quality readings.

1. Burrian Allen (BA) electrode: Provides stable and clear amplitude readings and virtually unaffected by eye movements. The downsides of this electrode is that it is normally re-usable (risk cross contamination), costly and carries the risk of eliciting corneal abrasions.
2. Jet electrode: Unipolar, disposable electrodes with gold plated plastic material as the active electrode. A separate reference electrode is also used on the patient's skin.

3. Dawson-Trick-Litzkow (DTL) electrodes: a unipolar disposable electrode that allows contact with the bulbar conjunctivae, lies deep in the inferior fornix. While reliable, the quality of the readings is often less than that of the BA electrodes. Additional electrode on the skin is required as the reference. The DTL electrodes were used for all subjects in this study as this is the standard practice for this research centre.
4. HK Loop and gold foil: thin and flexible silver wire, insulated with Teflon tucks on the lower eyelid. A reference electrode is required on the skin.

2.1.2.2 Interpretation of the ERG

The observed changes in the waveforms are the sum of elicited global responses of the retina. The clinical interpretation helps to distinguish between pathologies, especially in eyes that appear to have no apparent abnormalities on direct fundoscopy examination. The ERG can assist in distinguishing between rod or cone function, photoreceptor versus bipolar cell disorders, amacrine cell and ganglion cell function via the Oscillatory potentials.

Because of the nature of the recordings, the macula contributes very little to the overall readings. The results from the cones are predominantly from out with the central retina, where most of the cones are located, even though the highest density of cone population is within the fovea.

2.1.2.3 Dark adaptation stages

DA 0.01

During the dark adaptation stage, a dim flash (0.01cd/m^2) is used to elicit the 0.01 response, arising from the rod bipolar cells, which are also dependent on the function of the rod photoreceptors. The observed responses are believed to be virtually a pure rod-response, due to the low light intensities, below the level of cone sensitivity.

DA 3 and DA 10

The standard flash (3.0cd/m^2 and 10.0 cd/m^2) in the scotopic state gives a reading from both the cone and rod system, but the predominantly the rod system. The brighter 10.0 flash is normally more useful in subjects with issues such small sized pupil, media opacities, immature retina (McCulloch *et al.*, 2015).

DA 3 Oscillatory potentials

Within the recorded ERG waveforms, there is a high frequency and low amplitude response visible on the rising limb of the DA 3 and DA 10 waveforms. This is further recorded from the 3.0 cd/m2 by using a high pass filter, where frequencies below 75Hz are discarded. The OP reading is believed to be reflective of the amacrine and retinal ganglion cells.

2.1.2.4 Light adaptation stages

LA 3

Testing in the photopic state must allow at least 10 minutes of light adaptation. A 3.0 cd/m^2 standard flash is used. The waveforms are sharper and narrower, with smaller a-wave amplitude and shorter implicit times compared to results obtained during dark adaptation. In the responses, the observed a-wave is contributed by the cone photoreceptors, and the b-wave from the change in potentials in the outer plexiform layer (both ON and OFF bipolar cells).

LA 30

The system uses the 3.0 cd/m^2 standard flash, presented at 30Hz. As rods do not respond at this frequency, the observed waveform would be primarily driven by the cone ON and OFF bipolar cells.

2.1.3 Clinical applications of ERG

The clinical utility of the ERG is well established, particularly in individuals with apparently normal looking fundi. Because the ERG examines the function of cell groups, it can detect early disease activity prior to any apparent structural damage and change. Inherited conditions such as retinitis pigmentosa, Stargardt's disease and photoreceptor dystrophies can reveal abnormalities in the absence of any visible changes and can guide future management and diagnosis. It is also used in monitoring for drug toxicity from Quinine and Chloroquine (hydroxychloroquine).

2.1.3.1 ERG and Vigabatrin.

(This is discussed in Chapter 3.2, under Discussion)

2.2 The Multifocal Electroretinogram

The heterogeneity of the visual function across the retina cannot be adequately examined by the ERG, as it provides only global overall function of the retinal tissues without any spatial or localising capability. The cone system is especially varied and indeed more complex to examine from the ERG. The cones are highly concentrated in the macula region but is present throughout the retina. Despite the high concentration of cones on the macula region, proportionally the population of cones outwith the macula region is higher due to a larger area of spread. Because the ERG provides the sum of all electrical activity within cells under controlled conditions, response deficit because of isolated retinal lesions (rather than widespread) poses a challenge in the clinical interpretation of an ERG.

In 1991, Sutter and Tran described a novel modification of the ERG system that allows various areas of the retina to be stimulated simultaneously, and responses can be localised from the retinal field topography (Sutter and Tran, 1992). The original design employed a multi-input systems analysis and can study focal responses from up to 103 areas/element. Today several commercially available multi focal ERG software exist which includes VERIS™, RETIScan™, MetroVision™, Accumap™, Neuro-ERG™ and

Diopsys™. To our knowledge none of the above are able to test beyond 50°- 60° from fixation, making it limited in terms of assessing function of the retina in the far periphery.

Our centre developed a non-commercial system which uses similar principles to other mfERG devices in obtaining readings. The most obvious advantage is its ability examine peripheral retinal regions up to 120° (Keating, Parks and Evans, 2000; Keating *et al.*, 2001). In this thesis all study subjects are tested on this device, with up to 90° of eccentricity.

Multifocal ERG signals are delivered typically on a 61 or 103 hexagonal element array in photopic conditions to elicit cone-driven ERG signals. Each hexagon can display either an 'on' or 'off' state, or light and dark respectively. The change in its state is driven by the standard binary m-sequence, which is identical to all hexagons. The typical waveform on mfERG recordings is a biphasic wave, characterised by the initial negative N1, positive P1 followed by another negative N2. In terms of data collection, the waveforms in each hexagon do not directly measure the electrical responses from the corresponding retinal area, but rather are mathematical deductions from analysis of continuous ERG signals. The first ISCEV standards for mfERG was published in 2007, and subsequently updated in 2012 and 2021 (Hoffmann *et al.*, 2021).

2.2.1 Stimulus delivery

In the early days of mfERG, cathode ray tubes (CRT) were the popular choice for stimulus display. This has mainly been replaced by thin-film-transistor liquid crystal displays (TFT-LCD), organic light-emitting diode (LED) displays or in our centre the Digital Polysilicone Projection, which uses the liquid crystal technology (Keating *et al.*, 2001). Each type of stimulus delivery system has their advantages, initially in terms of screen resolution and ability to evoke responses at high screen refresh rate. The clear advantage of using the Digital Polysilicone projection technique is the wider field of examination, of up to 120° although examination at this extreme angle is mainly limited to research purposes.

The time lapse between the on or off change in a local hexagonal element is termed response time. Response times must be considered against the m-sequence frequency, and is usually a shorter duration. The rate of frame changes is usually 60 – 75Hz, and need to be bore in mind when interpreting the results. In the light or 'on' state, the luminance of the hexagonal element should at least reach 100cd/m^2. In the dark or 'off' state, the luminance should be low enough to achieve significant contrast of ≥ 90% on the Michelson scale.

2.2.2 Data recording

The same DTL electrodes as the ERG are used for mfERG in our study. (See chapter 2.1)

The conditions of the amplifiers and filters must be well controlled, to produce recognisable signals and to ensure reproducibility, and validity when compared to the software's normative values. The amplifiers used should have an alterable gain function that is able to yield discernible signals without saturation. A band-pass filter is an essential component, as it filters out additional unrelated electrical signals. 3-10 Hz is the acceptable range for a high pass cut-off, and 100 – 300Hz is the range for a low-pass cut-off.

2.2.3 Data Interpretation

First-order kernels are the standard response used for mfERG. Higher order kernels are possible but are out with the standard mfERG applications.

Spatial averaging describes the software's analysis that utilises a percentage from neighbouring hexagonal elements to create a smooth, discernible waveform within an element. The advantage of this step is the removal of artefactual interference, especially in a noisy signal. The disadvantage is its potential to obscure ambiguous signals which can be useful for clinical interpretation.

2.2.4 Artefacts

Systematic approach must be adopted when dealing with artefacts within the signals. The incorporated software algorithm for correction or rejection of artefacts must be used with care to not distort and alter the key aspects of the resulted waveform.

2.2.5 Patient factors

Refractive error

The available evidence to account for the effect of refractive blur on mfERG signal is mixed. Although there are documented differences in the effect of uncorrected refractive error on the mfERG response, the trend in the relationship is unclear. Plus (+) defocus appear to have different observation in those with minus (-) defocus, despite the same alleged magnitude (Chin *et al.*, 2015). No differences in readings was documented, but this was in systems that are different to ours (Palmowski *et al.*, 1999) . Despite these findings, it would be prudent to correct for refraction to ensure the clearest retinal signal is seen for best result.

Media opacities

The influence of media opacity on mfERG signal is recognised, due to lack of clear retinal image of the stimulus. The opacity in ocular media degrades the quality of the retinal image, by reducing the brightness and contrast. Concerns regarding the induced scatter

of light by these opacities (cataract, corneal scarring) was also acknowledged (Hood, 2000).

Pupil size

The consideration of pupil size during mfERG is essential. Smaller pupils have been associated with reduction in P1 latency and increase in P1 amplitudes (Gonzalez *et al.*, 2004). Fully dilated pupils are induced pharmacologically with 1% tropicamide, where pupil diameter of 7 – 8mm is preferred during testing.

Fixation monitoring

Problems with maintaining fixation can present artefacts in the mfERG readings. As the 3D topographic plot allows the location of signal deficit to be localised, issues with unstable fixation makes interpretation unreliable as the spatial relationship between the elements and the retina is poor. Adding a fixation target on the screen, as well direct observation of the fixation performance can aid test compliance.

2.2.6 mfERG interpretation

Reference values

Reference values for each system is recommended to be laboratory specific. Due to the complexity of the recording, interference from factors such as the electrodes and

lighting conditions can affect the resultant data (Mohidin, Yap and Jacobs, 1997). Lower responses from the 1st and 2nd central rings were documented in older individuals, believed to be associated with general decline in number of cones in an ageing eye (Nabeshima *et al.*, no date; Mohidin, Yap and Jacobs, 1999) or reduced temporal adaptation from ageing (Jackson *et al.*, 2002). Reduced amplitude with increased latency were also reported in myopes, thought to be due to loss of cone function and long axial length (Kawabata and Adachi-Usami, 1997; Chan and Mohidin, 2003).

Waveform profile

The examination of the trace array allows general inspection of the responses based on the corresponding retinal regions. It gives a general sense of the test, in terms of quality of tracing, stability of fixation (accuracy of blind spot location), and other artefacts.

Closer inspection of the waveform begins by determining the correct/discernible waveform from the presence of the trough N1, peak P1 and the N2. The amplitude is determined by measuring the difference between N1 to P1, and the timing would be the duration for reaching P1.

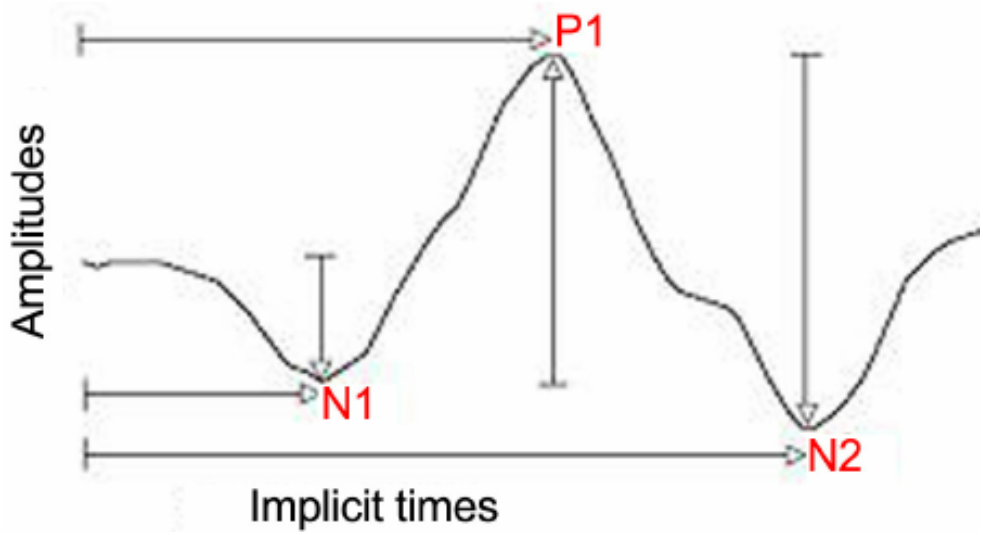

Figure 2.2: Typical mfERG waveform demonstrating N1, P1 and N2. (Image credit to Lee et al, 2010)

Regional averages

Ring or regional average values can be useful when diseases with retinal dysfunction in radial symmetry pattern is suspected. Responses can be grouped by successive rings of hexagons, quadrants or hemispheric. When regional average values are used, the response in a hexagon is the average value, contributed by the sum all the hexagons from the specified region. The normative values are laboratory-specific. As expected, when this step is taken, there is a chance of obscuring localised retinal dysfunction within that region.

3D topographic plots

Providing the topographic density plot as part of the result is recommended. This allows the interpreter and reader to visualise signal strength relative to the area, in colours

indicated through a heat map. It is visually engaging for the reader but must not be interpreted without the trace array display. Data regarding amplitudes and timing of the waveform is not visible and can be misleading especially when the colours of the heatmap is favourable.

2.3 Vigabatrin and Multifocal ERG

The first report detailing mfERG results in Vigabatrin treated patient found seemingly normal amplitudes and latency in the waveforms. Closer inspection however revealed abnormal waveform in some peripheral elements, consistent with the visual field defect (Ruether *et al.*, 1998). In contrast, a later publication detailed reduced peripheral amplitudes in two patients with evidence of macula sparing and felt to be consistent with the areas of defect on the visual fields. Due to small number of subjects, the main deduction here was that the observed change on mfERG is felt to be more relevant to vigabatrin compared to the reversible, but reduced, Arden ratio from the electro-oculogram (EOG) (Lawden *et al.*, 1999). Wide field (90°) mfERG findings in one case report showed normal central function up to 40°, but increase in implicit timings beyond this, with reduction in peripheral b-wave amplitudes (McDonagh *et al.*, 2001). Prospective study of 32 patients found the implicit time difference from the center to the periphery to be 100% sensitive and 86% specific to vigabatrin related toxicity, and has form the basis for the detection of vigabatrin associated retinal toxicity in this centre (McDonagh *et al.*, 2003a).

It is important to note that other abnormalities were also found in their cohort; differences in peripheral amplitude, peripheral implicit time but found the difference between the peripheral to central implicit timing to be the most significant.

Lack of reproducibility of the same findings by other centers is somewhat expected, given the distinct differences in the systems. The commercially available mfERG systems such VERIS™ can assess within 50° of fixation, versus the 90° from fixation in our custom build system. It is likely that angle deficit in other systems misses out on examination of the pathological retinal areas. In addition to this, the visual field defects seen in patients with epilepsy can be pre-existing in up to 24% of subjects with epilepsy who had no prior exposure to Vigabatrin (Gonzalez *et al.*, 2009). Therefore perpetual comparisons between the wide angle visual field test to the limited angle of mfERG is likely to bear poor concordance.

CHAPTER 3:

COHORT DESCRIPTION

3.1 The recruitment process

During the initial stages of the study, the intended study group were a proportion of patients who had previously participated in a large study examining pathological signals from multifocal electrophysiology (Gonzalez *et al.*, 2009). Their original cohort included patients on Vigabatrin as well as those only on other anti-epileptic drugs. As our study intends to examine the long-term effect of Vigabatrin on visual function, only Vigabatrin exposed subjects met inclusion criteria for this study. We also included patients who did not participated in the earlier study (who were referred by local epileptologist for visual tests following the start of Vigabatrin) in order to enhance potential number of participation.

126 Vigabatrin exposed subjects were identified; 10 are deceased and the remaining 116 subjects were contacted through mail. We provided the following in our correspondence:

- Patient information sheet

- Reply sheet for subject to indicate interest in participation
- Self-addressed stamped envelope

Participants	Number	Percentage %
Potential Identified	126	
Contacted	116	
Replied	**44**	**38**
Interested	30	68
Not interested	14	32
Tested so far	28	66
DNA	2	4

Table 3.1 Number illustrating response to the study invitation.

44 replies were received, where 30 indicated their interest in participation and 14 indicated that they were not interested. Out of the 30, 28 subjects attended the study visit and had given written consent to participate in the current study and future research. The study was approved by the West of Scotland Ethics committee, in accordance with the tenets of the Declaration of Helsinki.

3.2 Study Visit

At the study visit, subjects would have had at least 1 week to read the accompanying documents from our correspondence. Verbal and written consent was obtained at the start of the study visit. The typical flow of assessment during the study visit is as follows:

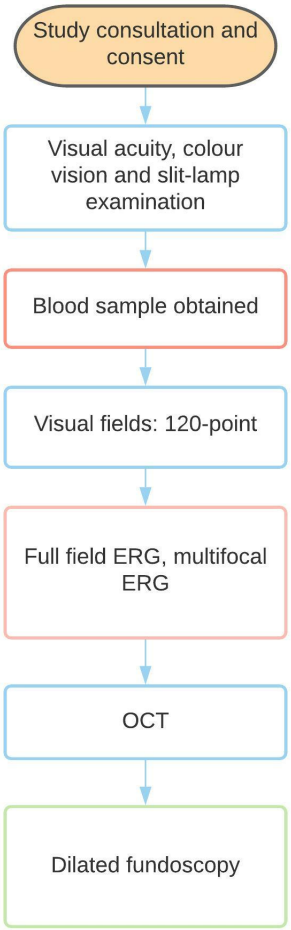

Figure 3.1 Flowchart demonstrating the flow of the study visit

(pupil dilation forms part of ERG testing)

3.3 Inclusion criteria:

Subjects' ability to give written consent, of male or female gender and of the age 18 and above can be included in the study. The diagnosis of epilepsy from an epilepsy specialist, alongside current or previous use of Vigabatrin for at least a year is essential.

3.4 Exclusion criteria:

A potential subject who was unable to provide written or verbal consent cannot be included, due to the level of cooperation required in most of the examinations. Previous or newly diagnosed glaucoma (open or narrow angled) and previous history of visual pathway pathology confirmed with CT or MRI imaging would also lead to exclusion due to potential interference with visual fields results. Visual acuity less than 6/9 on the Snellen chart or Logmar more than 0.2 would exclude subjects from the study.

3.5 Conditions for withdrawal of subjects:

Subjects are withdrawn from the study if they were diagnosed with a new condition that affected their level of vision or ability to follow instructions during the duration of this study. They were also withdrawn if they met any of the exclusion criteria during the duration of the study. All participants were given right and choice to withdraw from the study at any point for any reason.

Subjects who were unable to complete all the assessments were not automatically withdrawn from the study, unless specifically asked by the subject themselves.

No subjects were withdrawn from this study.

3.6 Comparison groups

Groups	Mean age (years)	Female	Male
Current user	44.3*	7	4
Previous user	50.7*	10	7
Delayed	47.5**	7	4
Non-delayed	53.4**	8	3

*(*p = 0.2, **p = 0.21 with the t-test)*

Table 3.2 Distribution of age-matched patient groups

In our experimental reports, two types of subject categories are used. The first is based on the current status of treatment; current exposure or previous exposure. The rationale for this is to assess long term visual effects as well as allow observation of serum concentration of ornithine and taurine, stratified by the vigabatrin exposure status.

The second type of grouping is based on the presence or absence of >2ms timing delay of the peripheral 45 – 90 °, compared to the central 0 – 45°. This change in the multifocal ERG signal is considered to be reflective of Vigabatrin associated retinal toxicity, based on previous studies in larger cohorts (McDonagh *et al.*, 2001, 2003a; Gonzalez *et al.*, 2009), associated with 100% sensitivity and 86% specificity.

This finding has not been replicated by other centres due to the different multifocal ERG software used by them, as well as the significantly more constricted field of assessment (usually up 50° of eccentricity).

The biological reasoning behind this is yet to be determined, hence the birth of this study which aims to examine all possible aspects of correlation in patients.

3.7 Strengths and weaknesses of this cohort

The profile of the cohorts altered slightly during each experimental analysis, depending on the availability of data for each subject. These are discussed in detail in the discussion section of each experimental report.

3.8 Issues around Statistical analyses

1-eye versus 2-eye

One of the common dilemmas in ophthalmology studies is the chosen analytic approach in analysis data from the 2 eyes individually of a subject or both eye treated as a single data point; the 1-eye vs 2-eye data interpretation. Many studies do not fully describe their approach and potentially overlook the need to correct by checking for type 1 or type 2 errors in their statistical assumptions.

In VaRT both eyes are assumed to affected to a very similar degree (high correlation) and it makes sense to view data from both eyes together as a single data point. This makes data interpretation much more straightforward, but at the expense of losing study power with less efficient use of data (Nowomiejska *et al.*, 2014).

In this study, both approaches are relevant and will be employed in data analysis depending on the experimental work. The 2-eye approach is used when we look at Visual fields versus Vigabatrin burden, and OCT RNFL and volume microstructure analysis. The 1-eye approach is used in the OCT RNFL and volume microstructure relationship with visual fields.

(**See page 114 for perimetry score where these approaches are used and explained.)**

Regression approach

In the Visual fields versus vigabatrin burden (chapter 4.2) report and the OCT RNFL and microstructure versus visual fields (chapter 5.3) report, the regression analyses are simple linear regression done individually for each correlation rather than the multiple linear regression approach. The latter approach was initially considered but due to significant issues with collinearity, where values from each independent variable (ie. Microlayers or quadrants) are highly interdependent, due to being biological tissues within the same vicinity. The high degree of correlation between the independent variables was uncovered using the Pearson correlation, and is a significant statistical issue it can undermine the statistical significance of an independent variable (Allen, 1997).

CHAPTER 3.2:

CASE SERIES: RETINAL ELECTROPHYSIOLOGY AND VISUAL FIELDS OF PATIENTS EXPOSED TO VIGABATRIN

Aim

To report the results of visual testing in patients treated with vigabatrin

Method

A prospective case series analysis of all our subjects that have participated in this study. Subjects are either currently on Vigabatrin or had previous exposure to Vigabatrin. All subjects underwent full ocular examination prior to inclusion into this study. Visual acuity, pupil examination and slit lamp examination which includes intraocular pressure measurements, anterior segment examination and dilated fundoscopy.

All subjects have undergone conventional full field electroretinogram (ERG), Wide Field multifocal electroretinogram (WF-mfERG), blood tests and optical coherence tomography. The ERG was performed in accordance with the standards of the International Society for Clinical Electrophysiology of Vision (ISCEV). The WF-mfERG responses were assessed with respect to the amplitude and latency (implicit time) of

individual response element. ERG and WF-mfERG results are interpreted by two clinical scientists with total combined duration of 35 years' experience in the subject.

The WF-mfERG protocol utilises back projection stimulus consisting of 61 element array with independent decimated binary m-sequence covering 90 degrees visual field, conducted by a custom-built software. Electrical responses from the central field (0-45 degrees) were compared to the peripheral field (45-90 degrees).

As part of the larger study, OCT examination was performed on all subjects using the spectral-domain OCT, Heidelberg SPECTRALIS, Heidelberg Engineering, Heidelberg, Germany. Results are discussed in Chapter 5.

Also as part of the larger study, blood test evaluating serum concentration of Taurine and ornithine was also performed. The results are discussed in Chapter 6.

Visual fields were assessed using the Humphrey 120-point suprathreshold, three zone static perimetry test. The visual fields are appraised in 2 ways; firstly based on Wild's modified classification to show consideration of visual fields grading in ordinal terms of normal, mild, moderate and severe(Wild *et al.*, 1999). As part of the larger study, the visual fields is assigned a perimetry but results relating to this method will be discussed in chapters 4.2 and 5.3.

Classification	Temporal	Nasal	Superior	Inferior
Normal	> 60°	> 50°	> 40°	> 55°
Mild	50° - 60°	36° - 50°	36° - 40°	45° - 55°
Moderate	30° - 50°	20° - 35°	20° - 35°	25° - 45°
Severe	< 30°	< 20°	< 20°	< 25°

Table 3.2.1 Modified Wild's classification for Vigabatrin associated visual field loss based on static perimetry.

Further background information on Wild's classification and perimetry score can be found on page 114.

Results:

28 subjects were recruited into the study once the set inclusion criteria were met. The subjects were first interviewed face to face for their seizure history, and underwent vision testing, slit lamp examination. Bloods samples were taken, and visual fields test is done prior to dilated fundoscopy. This is followed suit by full field ERG and WF-mfERG testing, and finally OCT testing.

Of the 28 subjects, 24 subjects completed all of examination. 11 out of the 28 were still on Vigabatrin during the study visit.

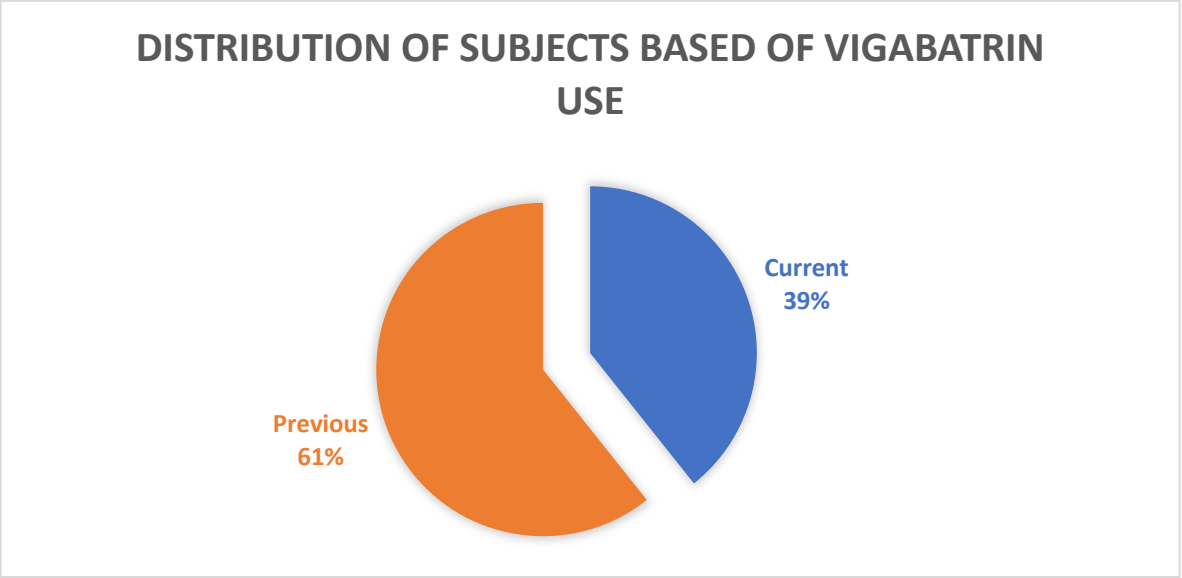

Figure 3.2.1: Pie chart illustrating the proportion of subjects based on Vigbatrin use.

61% (n=17) are previous users of Vigabatrin and 39% (n=11) are currently on Vigabatrin.

Visual Electrophysiology

3 subjects did not complete both the visual electrophysiology tests due to fatigue, and failure to attend subsequent visits to complete the tests. 1 additional subject did not have full field ERG performed due to technical issues. 11 of the 25 subjects who underwent WF-mfERG were found to have more than 2ms delay in the peripheral field from the central field.

Full Field ERG

The full field ERG results are illustrated in Diagram 3.2.2. 13 subjects had normal responses, 4 had unilateral reduced responses, 4 had bilateral reduced responses, 1 had negative b-wave, 1 had reduced and delayed photopic responses and 1 had bilateral photopic delay.

Full field ERG results	Number
Normal	13
Unilateral reduced responses	4
Abandoned	4
Negative b wave	1
Reduced responses all	4
Reduced and delayed photopic	1
Bilateral photopic delay	1

Table 3.2.2: Number of subjects with their full field ERG results

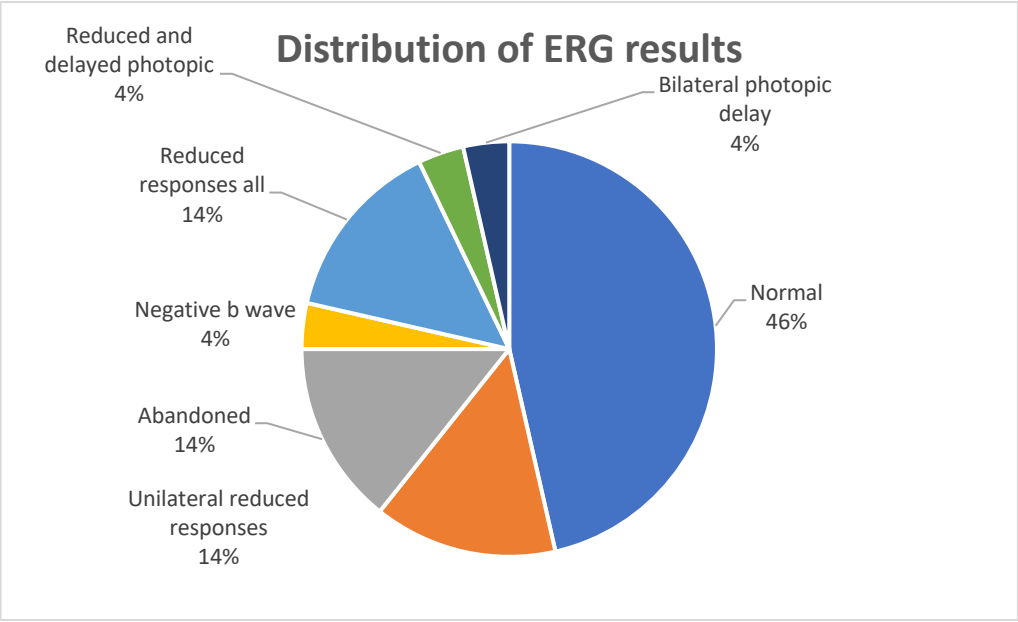

Figure 3.2.2: Pie chart illustrating the proportion of subjects with their full field ERG results.

WF-mfERG

The WF-mfERG results are illustrated in diagram 3.2.3. 11 had >2ms timing delay of the peripheral field compared to the central field, 3 had bilateral diffuse delay, 4 had mild diffuse amplitude reduction, 1 had unilateral diffuse delay, 2 had unilateral central delay and 4 had normal results.

WF-mfERG results	Number
>2ms delay	11
Diffuse delay (peripheral and central)	3
Mild diffuse amplitude reduction	4
Unilateral diffuse delay	1
Normal	4
Unilateral central delay	2
Abandoned	3

Table 3.2.3: Number of subjects with their WF-mfERG results

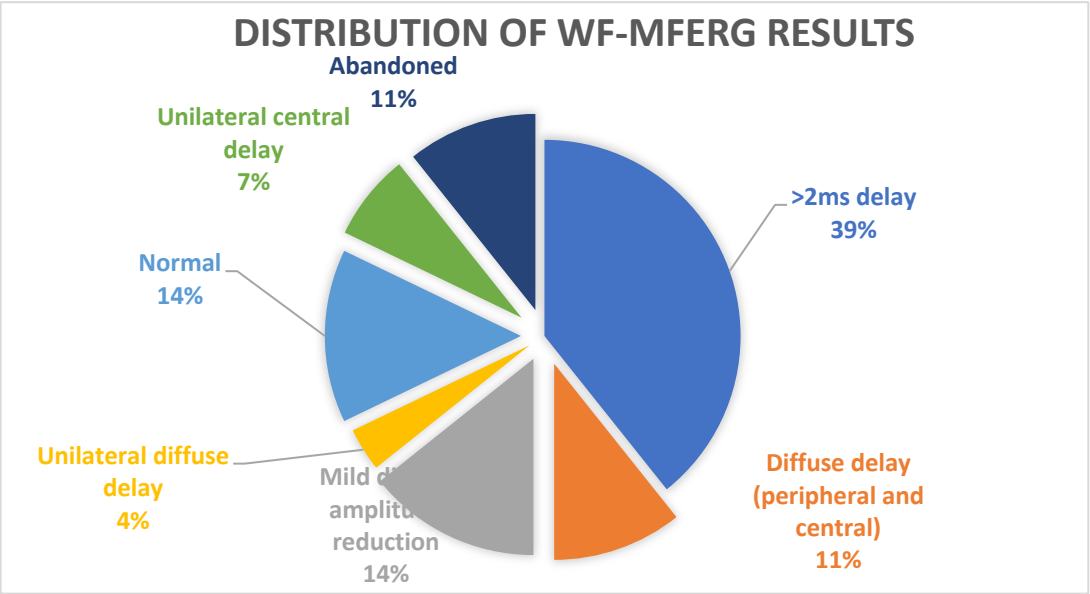

Figure 3.3.3: Pie-chart illustrating the proportion of subjects with final WF-mfERG results.

Visual Fields

Although all completed the visual fields tests, 9 results were bilaterally unreliable, and 2 had unilateral unreliable results; these individual tests were excluded. Of the included results, 1 was graded as normal, 3 were mild, 4 were moderate, and 8 were severe.

VF grading	Number
Normal	1
Mild	3
Moderate	4
Severe	8
Excluded	12

Table 3.2.4: Number of subjects with their VF grading (most recent tests only)

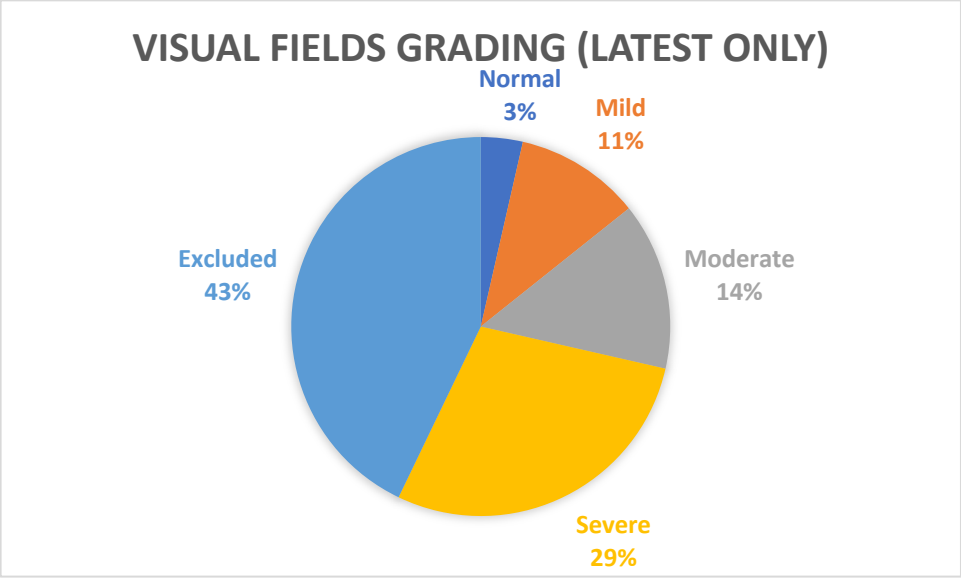

Figure 3.2.4: Pie-chart illustrating the proportion of visual fields grading (based on modified Wild's classification) in their most recent test.

Historical Visual fields

When analysing all visual fields including retrieved historical results, 21 were excluded; in the remaining visual fields, 19 were graded as severe, 8 graded as moderate, 6 graded as mild and 2 graded as normal.

VF grading	Number
Normal	2
Mild	6
Moderate	8
Severe	19
Excluded	21

Table 3.2.5: Number of retrieved visual fields and their respective gradings.

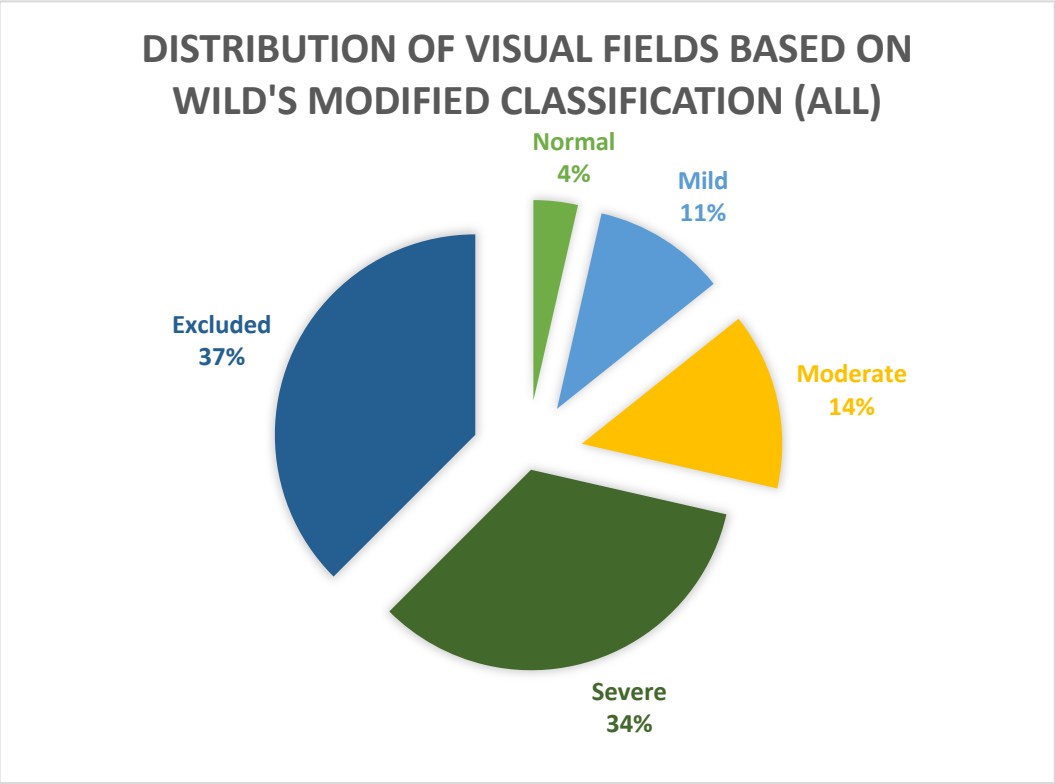

Figure 3.2.5: Pie-chart illustrating the proportion visual field grading (based on modified Wild's classification) in our cohort, including historical results.

Current Vigabatrin Users

In those who are still on Vigabatrin, 6 had >2ms delay in the peripheral field compared to the central field. 1 had diffuse timing delay in both the peripheral and central field. 1 had diffuse mild amplitude reduction, 1 had diffuse delay only in one eye. 2 subjects did not complete either of the visual electrophysiology tests. In this group, 4 had normal full field ERGs. 1 had the presence of a negative b wave, 1 had unilateral reduced responses, 1 had bilateral reduced responses, and 1 had bilateral reduced and delayed responses only in the photopic phase. 3 did not have full field ERG results. 2 sets of visual fields were excluded due to unreliability. In the remaining visual fields, 1 was normal, 1 was mild, 2 were moderate, 5 were severe.

Previous Vigabatrin users

Of the 17 who are no longer on Vigabatrin, 5 had >2ms delay in the peripheral field compared to the central field. 3 were normal, 2 had bilateral diffuse delay (central and peripheral), 3 had mild bilateral diffuse delay, and 2 had unilateral central delay. 1 did not complete either of the visual electrophysiology tests. In this group, 9 had normal full field ERGs, 3 had bilateral reduced responses, 1 had bilateral timing delay in the photopic phase, and 3 had unilateral reduced responses. 10 out of the 17 sets of visual fields were unreliable. Of the remaining 7 sets, 2 were mild, 2 were moderate, and 3 were severe.

Delayed

In those who displayed >2ms timing delay in the peripheral field compared to the central field, 4 had normal ERGs, 1 had negative B wave, 3 had bilateral reduced responses, 2

had unilateral reduced responses and 1 did not have a full field ERG done. 3 sets of visual fields were excluded and 1 had unilateral unreliable visual field.

Non-Delayed

In the remaining 14 who did not have the >2ms timing delay in the peripheral field compared to the central field, 9 had normal full field ERGs, 1 had bilateral reduced responses, 1 had bilateral delay in the photopic phase, 1 had bilateral delay and reduced amplitude responses and 2 had unilateral reduced responses. In this group 6 sets of visual fields had to be excluded due to unreliability, and 2 had unilateral unreliable visual fields; both of which were of severe grades. In the reliable visual fields 1 was mild, 1 was moderate and 4 were severe.

The results of all 28 patients are presented in Table 3.2.6.

ID	Vig status	Duration of treatment (months)	Treatment burden (Kg)	VF grading (Normal, mild, moderate, severe)	ERG findings	WF-mfERG findings
1	Current			Severe	Normal	>2ms delay
2	Current			Normal	Normal	>2ms delay
3	Current	154	12.6	Moderate	Unilateral reduced responses	>2ms delay
4	Current	183	30.6	Severe		>2ms delay
5	Current				Negative b wave	>2ms delay
6	Current	183	12.9	Mild	Normal	>2ms delay
7	Current	103	10.9	Severe	Reduced responses	Diffuse delay
8	Current	196	18.1	Severe	Reduced and delayed photopic response	Mild diffuse reduced amplitude
9	Current				Normal	Unilateral diffuse delay
10	Current			Moderate		
11	Current			Severe		
12	Ex		20.75	Severe	Reduced responses	>2ms delay

13	Ex		3.3	Moderate	Unilateral reduced responses	>2ms delay
14	Ex				Reduced responses	>2ms delay
15	Ex		1.64		Reduced responses	>2ms delay
16	Ex				Normal	>2ms delay
17	Ex		6.55		Bilateral photopic delay	Diffuse delay
18	Ex			Severe	Unilateral reduced responses	Diffuse delay
19	Ex				Normal	Normal
20	Ex			Mild	Normal	Mild diffuse reduced amplitude
21	Ex		11.6		Normal	Mild diffuse reduced amplitude
22	Ex				Normal	Mild diffuse reduced amplitude
23	Ex		12.38	Severe	Normal	Normal
24	Ex				Normal	Normal

25	Ex				Normal	Unilateral central delay
26	Ex		9.8	Moderate	Normal	Unilateral central delay
27	Ex		2.5		Unilateral reduced responses	Normal
28	Ex			Mild		

Table 3.2.6: List of study subjects with available data and results of Visual fields, Erg and WF-mf ERG.

ID	Vig status	Duration (months)	Burden (kg)	VF	Taurine and ornithine levels	OCT RNFL	OCT Macula	ERG	WF-mfERG
1	Current			✓	✓	✓		✓	✓
2	Current			✓	✓	✓	✓	✓	✓
3	Current	✓	✓	✓	✓	✓	✓	✓	✓
4	Current	✓	✓	✓	✓	✓	✓		✓
5	Current				✓	✓	✓	✓	✓
6	Current	✓	✓	✓	✓	✓	✓	✓	✓
7	Current	✓	✓	✓	✓	✓		✓	✓
8	Current	✓	✓	✓	✓	✓		✓	✓
9	Current				✓	✓	✓	✓	✓
10	Current			✓	✓		✓		
11	Current			✓	✓		✓		
12	Ex		✓	✓	✓	✓	✓	✓	✓
13	Ex		✓	✓	✓	✓	✓	✓	✓
14	Ex			½✓	✓	✓	✓	✓	✓
15	Ex		✓		✓	✓	✓	✓	✓
16	Ex				✓	✓	✓	✓	✓
17	Ex		✓		✓	✓		✓	✓
18	Ex			✓	✓	✓	✓	✓	✓
19	Ex				✓	✓	✓	✓	✓
20	Ex			✓	✓	✓	✓	✓	✓
21	Ex		✓		✓	✓	✓	✓	✓

22	Ex			½✓	✓	✓	✓	✓	✓
23	Ex		✓	✓	✓	✓	✓	✓	✓
24	Ex				✓	✓	✓	✓	✓
25	Ex				✓	✓	✓	✓	✓
26	Ex		✓	✓	✓	✓		✓	✓
27	Ex		✓	½✓	✓	✓	✓	✓	✓
28	Ex			✓	✓		✓		
% of available results				57% (62.5%)*	100%	89%	82%	85.7%	89%

*reliable unilateral results included

Table 3.2.7: The available results for analysis from each subject, and the percentage of included results by types of test.

ID	FOLLOW UP DURATION (MONTHS)	VIG STATUS	VIG BURDEN (KG)	VF GRADE
3	154	CURRENT	5.5	NORMAL
			6.6	MILD
			12.6	MODERATE
4	180	CURRENT	13.1	SEVERE
			16.4	SEVERE
			17.4	SEVERE
			18.6	SEVERE
			30.6	MODERATE
6	183	CURRENT	2.4	NORMAL
			4.37	MILD
			4.9	NORMAL
			6.36	NORMAL
			12.9	MILD
8	196	CURRENT	3.5	MODERATE
			6	MODERATE
			9	SEVERE
			12.1	SEVERE
12	148	EX	16.4	MODERATE
			19.6	MILD
			20.75	MODERATE
			20.75	MODERATE
13	152	EX	2.18	MODERATE
			3.2	MODERATE
			3.3	MODERATE
26	186	EX	6.55	MODERATE
			8.19	MODERATE
			9.8	MODERATE
			9.8	MODERATE
28	121	EX	2.2	SEVERE
			2.5	SEVERE
			2.5	SEVERE

Table 3.2.8: Visual field grading (based on modified Wild's) of the 8 subjects alongside the estimated Vigabatrin burden (kg). These were the only subjects within our cohort that had a series of visual fields (current and historical) with corresponding vigabatrin burden at the time of testing.

Discussion:

Visual fields

The chosen grading system used here was devised to aid visualisation and help comprehend the aetiology of the visual effects observed in Vigabatrin treated patients, particularly in the earlier years of when the issue with visual toxic effects was heavily discussed. Its translation into clinical and real-life practice nowadays is less certain, as treatment is often discontinued upon suspicion of visual effects and continued follow up is often poor (R. *et al.*, 2013; Sergott *et al.*, 2016a). Reliability of test results often vary, adding difficulties in assessing for progression. Historical visual fields were successfully retrieved in 18 of our subjects, but long-term analysis is only available in 8 due to unreliability of visual fields results. Despite the small numbers there is a subtle emerging pattern; where very gradual progression is seen in 3 out of 4 current vigabatrin users, and echoes previous report of the same (Clayton *et al.*, 2013). In the previous user group, all 3 out of 4 displayed static grading at each visit, also supportive of current assumption of non-progression and irreversibility following cessation of treatment (Wild, Smith and Knupp, 2019).

ERG findings

The advantage of ERG testing would be its ability to test tissue function objectively, which is especially advantageous in this group of patients. The barrier that lies ahead of adopting ERG for monitoring of Vigabatrin toxicity has been due to the lack of consistent pattern of abnormalities across all publications that has investigated the same. Results may be reproducible within their respective establishment where the research has taken place, but not reproducible on larger and wider scale forms part of the barrier of its full utilisation in the monitoring of Vigabatrin toxicity. ERG changes that had been linked to Vigabatrin toxicity includes increased photopic ERG b-wave latency (Harding, Mackenzie and Klistorner, 1998), reduced b-wave amplitude (Daneshvar *et al.*, 1999; Hardus *et al.*, 2001) diminished or altered oscillatory potentials (Gregory L. Krauss, Johnson and Miller, 1998; Arndt *et al.*, 1999; Harding *et al.*, 2000; Besch *et al.*, 2002; Comaish *et al.*, 2002; Jensen *et al.*, 2002), delayed b-wave in the 30Hz flicker (Harding *et al.*, 2000), reduced amplitude of the b-wave in the 30Hz flicker (Ponjavic and Andréasson, 2001). Normal ERGs were also reported in all (Lawden *et al.*, 1999). The wide variety of altered parameters posed a challenge in pinning down the exact site of altered tissue function; the suggested inner retinal damage (Gregory L. Krauss, Johnson and Miller, 1998; Coupland *et al.*, 2001; Besch *et al.*, 2002) would fit in with b-wave and oscillatory potential changes while outer retinal damage (van der Torren, Graniewski-Wijnands and Polak, 2002) is likely when combined with changes observed in the electro-oculogram (EOG). Despite the inconsistencies, ERG is likely to remain valuable especially an adjunct in the monitoring of Vigabatrin related retinal toxicity especially when it is not possible to obtain a reliable visual field. ERG changes is

likely to precede before any visual field or structural OCT changes manifest (Barrett *et al.*, 2014).

In our cohort, normal ERGs were seen in 2 subjects with severe field loss, 2 with mild field loss, 1 moderate field loss and 1 normal field. No conclusion can be drawn purely from this observation, which is partly due to the small number of subjects.

WF-mfERG findings

Our finding under this theme is discussed in chapter 2.3.

Main challenges of testing

The impact of fatigue on visual testing especially in perimetry is well documented. The impact on those with epilepsy is greater, with up to 46% prevalence in this population compared to the reported 18% in the normal population (Pawlikowska *et al.*, 1994; Ettinger *et al.*, 1998; Tellez-Zenteno, Matijevic and Wiebe, 2005; Lagogianni, Gatzonis and Patrikelis, 2021). While we did not specifically measure fatigue in our cohort, it is evident during testing that this was a major issue as subjects uncommonly fell asleep, or forget instructions mid-testing. The added effect of cognitive impairment affecting their attention, memory, learning and decline in executive functions lead to reduced ability to concentrate for prolonged periods of time (Chaudhuri and Behan, 2004). During the running of the study, it was essential that the schedule of the visit be kept as flexible as possible for the subjects to encourage cooperation and aid performance during the various assessments that had to be undertaken (Chaudhuri and Behan, 2004). This

meant that limited number of study visits can be arranged per day, while running the risk of not gaining any meaningful or reliable results from the session. While the presence of cognitive impairment is known to be a barrier to successful performance of visual fields test, fluctuating levels of focus and reduced attention duration can also impair the quality of testing. As it is, there is a high percentage of those with cognitive impairment in this population with up to 50% in some reports (Nowomiejska *et al.*, 2014). Additional characteristics such a learning disabilities and inability to follow instructions adds to the likelihood of gaining unreliable perimetry results. As our study includes a series of examinations, some which required minimum level of cooperation such as blood-taking to other more strenuous and focus-demanding tasks such as the visual fields testing – all subjects are included, provided they met the initial criteria for inclusion into the study (refer to Chapter 3.1 for details).

Study Visits

Each subject was given the option to either complete all assessment in one visit or in several visits; most chose the former option. Despite this, a balance must be struck between continuing the test on a fatiguing patient, or to keep the study visit shorter and continuing to offer the option of testing during subsequent visits. The latter option was riskier compared to the former, as there was a risk that the subject may not reattend. In our experience, this became an important barrier to the completion our data collection and may have resulted in several missing data points. If the visits are kept shorter, it is likely that fewer test results will be excluded as the subjects are less likely to be tested

under a fatigue state or on a 'bad day'. It would also give the opportunity to repeat other parts of the examination if necessary.

The potential cause behind poor attendance is discussed, mainly to identify issues in the strategy of the study and to allow the research team to take corrective measures in future research projects. Firstly, anxiety from visual field testing was previously reported (Chew *et al.*, 2016) and likely to form part of the reason behind low levels of re-attendance. The source of anxiety appears to be due to presumed or previous distressing and unpleasant experience of the test. Active participation of subject in general tests is often associated with apprehension linked to their performance anxiety (Frierson and Hoban, 1992). Treatment of anxiety depends heavily on the cause, ranging from medications to more holistic approaches including dietary and lifestyle changes. Chew et al alluded that patients with considerable experience tend to have less anxiety and therefore improve their performance. Ensuring a comfortable, quiet testing environment, continued presence of test administrator during the test, and clear test instructions (verbal or with the help of video and other instructive tools) can improve test reliability (Sherafat *et al.*, 2003).

Secondly, some subjects did not feel visual tests were essential as they are not aware of any adverse effects on their functional vision. It is known that many patients on Vigabatrin are asymptomatic from visual issues, and likely overlook any mild disturbances in vision that has not affected their daily functioning (Midelfart, Midelfart and Brodtkorb, 2000).

Thirdly, among the previous users of Vigabatrin they no longer felt that they are at continual risk of toxic effects from the medication. Certainly this also reflects our current state of knowledge of Vigabatrin, where the latency effect is only seen whilst on treatment but does not progress following cessation of Vigabatrin (Plant and Sergott, 2011) and has presented as a barrier to recruitment for this subgroup and the poor study retention is also not uncommon (Krauss *et al.*, 2016; Sergott *et al.*, 2016a).

Crabb et al reported that while patients find the visual fields examination unpleasant, their patients compliance improved following discussion to improve insight into their condition and appreciation of their doctors' care and empathy. (Glen, Baker and Crabb, 2014) In our case, the lack of established rapport between the subjects and the research team, and that the study visits were conducted at a separate site from their epilepsy outpatient gives the subjects the impression that the study is run separately from their epilepsy care have likely discouraged enthusiastic participation.

Unreliable and excluded results

Visual fields

Table 3.2.7 showed a high level of unreliable visual fields results compared to other examinations in our cohort and is higher compared to other reports (Conway *et al.*, 2014; Nowomiejska *et al.*, 2014). This was despite deliberately placing the visual fields test near the beginning of the study visit, and constant encouragement throughout the examination, to minimise the impact of mental fatigue. Breaks mid-testing was offered

to subjects who have difficulty during the exam, where some fell asleep mid-examination. The decreased level of alertness seen during the test have been reported in similar cohorts and could be attributed simply to decreased state of alertness in patients with epilepsy (Hawker and Astbury, 2008), or general lethargy from poor sleep (Swaminathan *et al.*, 2018).

OCT scans

Excluded test results were also seen for OCT scans, albeit to a much lower level. OCT scans are generally well received by patients and the device operator due to the rapid process of testing. Image capture is mere seconds, or less than a minute if multiple line scans are required or the targeted eye is not stationary. The advancement of spectral-domain (SD-OCT) with the 'eye-tracking' allowed successful data capture even in challenging population (paediatric and nystagmus), with improved reproducibility (Rajjoub *et al.*, 2015; Hwang *et al.*, 2016). Due to the requirement of the study, accurate cursor placement during a scan is essential for the ensuing image auto-segmentation. Despite the rapid testing, some of our subjects have difficulty maintaining their gaze on the internal fixation of the device, even after multiple attempts. Scan decentration and misalignment are common technical reasons for excluding an OCT scan result. One scan was excluded due to errors in auto-segmentation cause by significant epiretinal membrane. As the OCT scan is performed at the final section of their study visit; difficulty in maintaining fixation even for the brief duration may be due to either of the onset of mental fatigue, or progression of existing mental fatigue.

In our opinion, the quality of the scans can be improved if the scans were done in the earlier sections of the study visit. The challenge of maintaining fixation in this cohort was poorly anticipated and could have been better positioned among the order of examinations. Secondly, more accurate manual placement of the cursor during the scan can improve the scan quality. This was always attempted when fixation is poor during the scan, with variable results due to limited patient tolerance.

Electrophysiology

The issue with visual electrophysiology testing is usually in its lack of availability in general ophthalmology outpatient set ups, and usually restricted to large secondary care or tertiary level centres. Therefore the faculty of experts required to administer the test and interpret the results is limited, and can contribute to some variability in testing and result interpretation (Spence and Sankar, 2001). The reported ERG abnormalities in Vigabatrin patients vary in each publication, with little reproducibility and consistency in pattern. The full results are often lengthy, adding subjectivity to the overall test conclusion. Nevertheless it remains very valuable in retinal function testing, particularly as an adjunct to vision testing when visual fields results are equivocal (Arya *et al.*, 2015). The missing electrophysiology data in our cohort was due to failure to re-attend subsequent study visits for testing completion in all 4.

Visual testing is often fraught with artefacts of subjectivity and pinning down the actual visual function present as a real challenge. Visual acuity and perimetry testing nowadays form the norm of eye outpatient testing – most patients are able to perform them well.

In cohorts such as ours (epilepsy, vision at risk of toxic effect), these tests pose a challenge to both clinicians and patients alike, and not always truly representative of their visual function. Adjunctive assessment tools such as visual electrophysiology is hailed for its purported objectivity, often used as yardstick to clarify any dubiety in visual status. Despite this its adoption into the routine clinical use is limited by the complicated setup that it demands, making it a complex addition to a service.

Given the themes discussed above, there should be a constant impetus to develop an objective standardised test for vision in this population, bypassing the need to consider the impact of fatigue or cognitive decline. The following chapters discuss comparative analyses of each subgroup and test in more detail.

CHAPTER 4:

THE VISUAL FIELDS/ PERIMETRY TEST

4.1.1 Visual fields and history of its development

Visual fields assessment is a form of vision testing that maps the boundaries of vision, monocularly or binocularly. The test usually requires a minimum degree of cooperation form patient, which limits its objectivity when clinical correlation is required. The earliest record of a visual field defect was a hemianopia description by Hippocrates from the late 5th century B.C (Thompson and Wall, 2010; Johnson, 2013). The assessment of visual fields becomes a subject of interest since the plotting of the blind spot by Mariotte in 1668, and the mapping of the extent of visual fields by Purkinje and Young in the 1800s. Von Graefe, in 1856 became the first to successfully designed a clinical testing method for visual fields (Johnson, 2013).

The design for the ideal visual fields continued to progress from then on; Bjerrum visual field test which measured the central field was introduced in 1889. Aimark in 1930s introduced the Arc perimeter which was used to plot the peripheral field. The Goldmann perimeter was introduced in 1945, and remains in use until today (Rowe, 2006).

In 1966, the Friedmann perimeter was introduced as the first quantitative static perimetry for assessment of the central visual field. This led to the development of automated perimetry which takes allows some objective measure of the 'Hill of vision', a term used to describe the gradual change of visual sensitivity across the visual fields (Rowe, 2006)

4.1.2 The island of vision in a sea of darkness

The terms 'Hill of vision' and 'Island of vision' are 3 dimensional diagrams often used to describe the gradual change of retinal sensitivity on the visual map. It was first described in 1927 by Traquair as "an island of vision surrounded by a sea of darkness" (Grzybowski, 2009). Traquair's original representation of his concept assigned the horizontal and vertical meridian of the visual field on a base plane, with a third dimensional axis upwards for increasing DLS (differential light sensitivity).

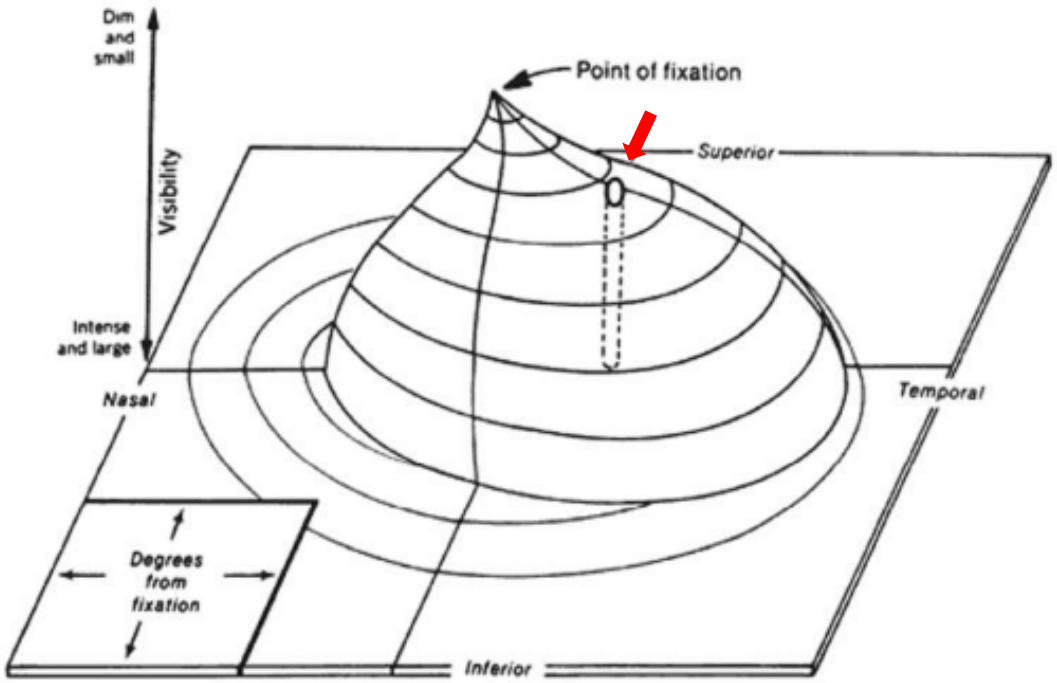

Figure 4.1: The normal island of vision with annotated key descriptions: Fovea at the 'Point of Fixation', the 'bottomless pit' or blindspot marked with a red arrow. (Image modified from Anderson DR: Perimetry with and without automation. 2nd edition. St Louis, MO: Mosby, 1987)

The Blind Spot

On the hill or the island a 'bottomless pit' exist, and corresponds with the location of the optic disc and called the 'blind spot'. The physiological blind spot is a limited area that appears approximately 15° temporal and 1.5° inferior to the are of fixation. In the normal population, it traverses 5.5° horizontally, and 7.5° vertically. It corresponds with the site of the optic disc, where there is complete absence of rods and cones.

4.1.3 Measurements of sensitivity on perimetry

The term ‘perimetry’ is often used interchangeably with ’visual fields’ to describe the same test. It is a form of examination that is widely used by ophthalmic, optometric and orthoptic colleagues in diagnosing and management of conditions where the visual map is affected.

Diseases affecting parts of the neural visual pathway produces specific patterns that can inform clinicians of the site of pathology.

Modern day perimetry testing allows the clinician to assess visual function through the visual fields, detect while quantifying changes in sensitivity within the visual field and monitor to change over time through repeated examinations.

The human visual field describes the perceived area or more accurately total space of vision, when the eye fixates, and the head and body is stationery. The approximate extents of visual field from point of fixation is 100° temporally, 60° nasally across the horizontal meridian, and 60° superiorly and 75°inferiorly across the vertical meridian.

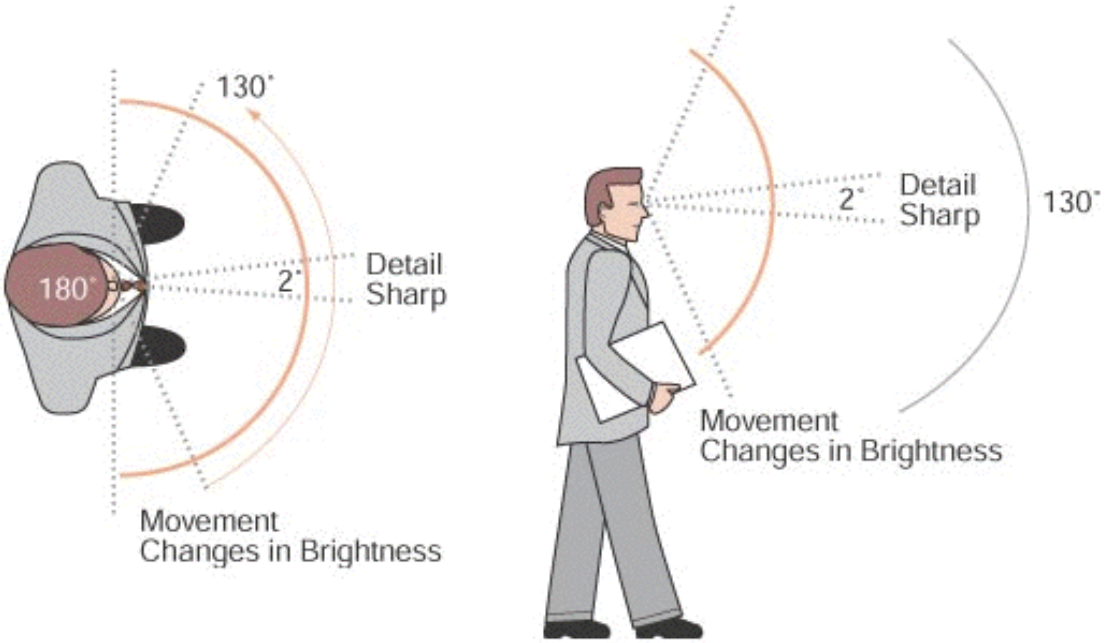

Figure 4.2: The full visual field in space, with respect to the location of the eye.

(Image credit to the Scottish Sensory Centre, The University of Edinburgh.)

Measurements of retinal sensitivity

The term 'sensitivity' is used to describe the ability of the eye to perceive brightness of target against the standard illuminated background. The standard illumination used is 31.5 asb

In order to describe the range retinal light sensitivity, the log scale unit with a base of 10 has been adopted. Decibels (dB) has been adopted into perimetric testing to allow larger numbers to be expressed in small numerical units;

- 10dB = 1 Lg = amplitude ratio of 3.162 = power ratio 10
- 20dB = 2 Lg = amplitude ratio of 3.162^2 = power ratio 100

The key standards of perimetric testing are:

- Background illumination
- Spot intensity – alterable via filter wheels
- Spot size – small to largest (I, II, III, IV, V)
- Spot duration – default is 200mS, can be increased for longer duration
- Spot speed – 4 degrees per second; only applies to Kinetic testing.

While the latter 4 key parameters can be altered, the background illumination tends to remain constant throughout at 31.5asb for the Goldmann and automated perimetry.

The value 31.5 asb is a historical standard that was originally employed during Goldmann perimetric testing, and later formally adopted as a standard background illumination for Perimetric testing by International Perimetric Society under the International Council of Ophthalmology in 1979. The value was chosen as it approximates the minimum level for photopic (daylight) conditions, which relies on retinal cone function. The standardisation of the background illumination is essential for test/retest repeatability.

4.1.4 The Visual Pathway

The responses recorded on the visual fields corresponds to the specific topographic arrangement of the photoreceptors within the retina.

The photoreceptors rods and cones form the most proximal part of the human visual pathway. They lie in the outer retinal layers and connect to the ganglion cell layers via several other retinal cell layers.

When photons of light are absorbed by the photoreceptors, the phototransduction cascade is triggered with a cis-trans isomerisation of the 11-cis chromophore, which leads to hyperpolarisation of the bipolar and horizontal cells and consequently the ganglion cells of the retinal nerve fibre layer. The axons of the retinal ganglion cell lie in the innermost surface of the retina, where they converge to exit the globe via the optic disc. The retinal nerve fibre layer lies in a distinct pattern where superior and inferior fibres radiates above and below the macula and the papillomacula bundle, with a horizontal raphe in between the two hemispheres before they converge at the optic disc. The optic disc is devoid of any photoreceptors, and corresponds to the presence of the blind spot on the visual fields.

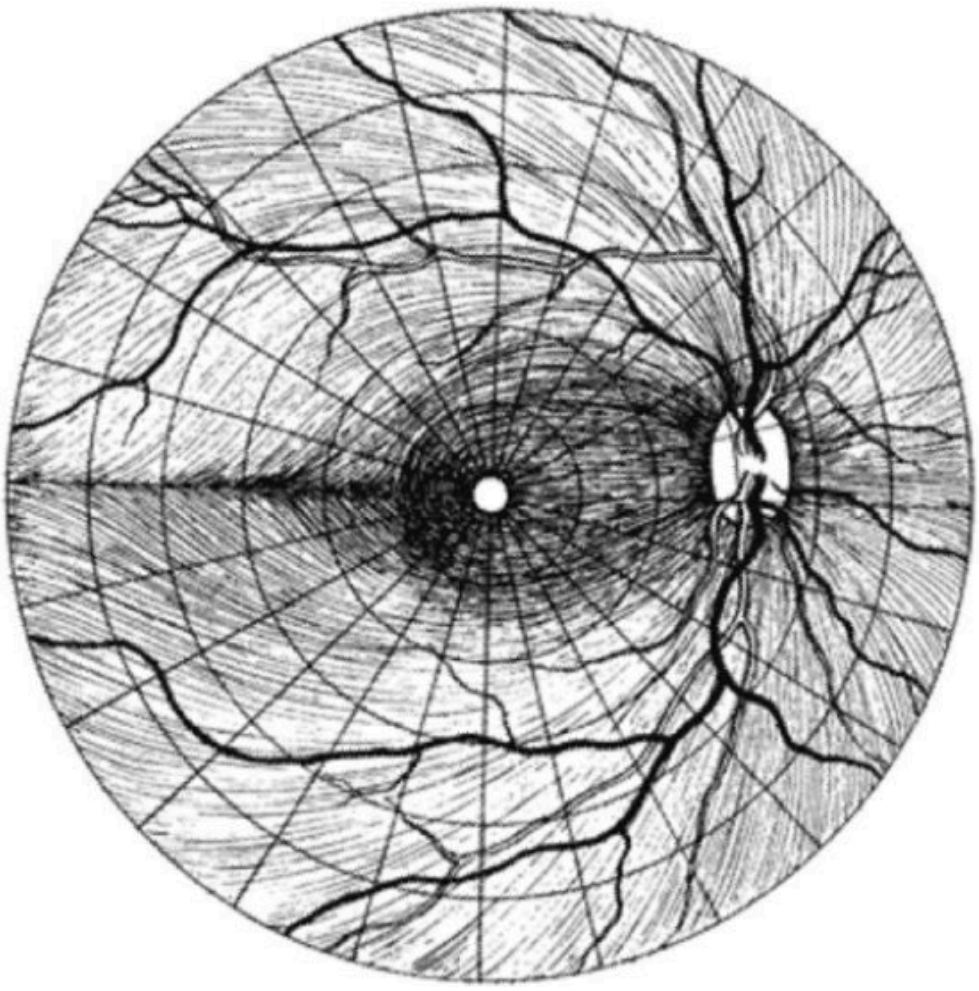

Figure 4.3: The arrangement of the retinal nerve fibre layer in the human fundus, modified from Harrington and Drake 1990.

This specific arrangement of the nerve fibre layer has a direct relationship to the pattern of visual defects detected on the visual fields. As an example, arcuate shaped scotomas in either the superior or inferior hemisphere of the visual fields indicate loss of retinal nerve fibre layers in the corresponding section (inferior or superior to the horizontal raphe, respectively).

From the optic disc, the converging nerves form the “Optic nerve”, and travels posteriorly through the optic canal via the optic foramen, and join the optic nerve from

the opposite eye at the optic chiasm. The nerves continue to travel posteriorly, forming the optic chiasm, the optic tract, the lateral geniculate nucleus, the optic radiation and finally the occipital cortex. At the optic chiasm, fibres from the nasal retina of either eye crosses over to the contralateral optic tract, while the fibres from the temporal retina remain uncrossed within the ipsilateral optic tract.

Throughout the journey of the neural visual pathway, the axons of the ganglion cells follow specific pattern of arrangement as such that patterns of visual field defect clinically can specifically indicate site of pathology.

Common types of visual defects and its causes:

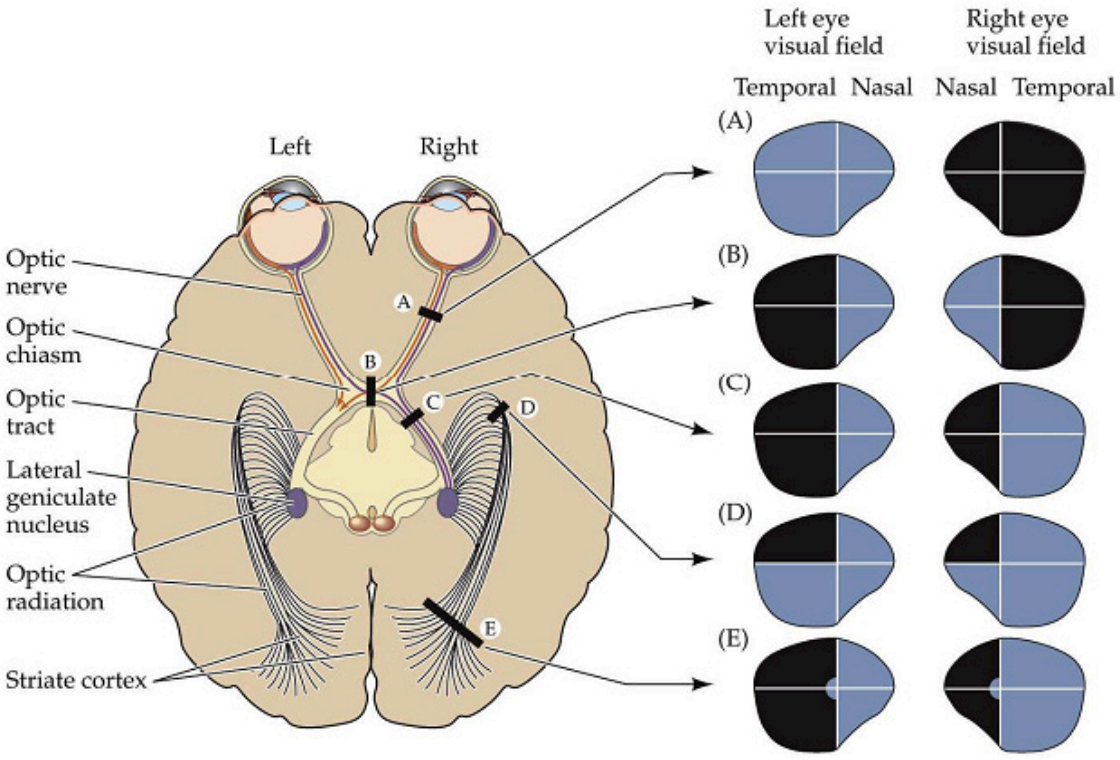

Figure 4.4: Common patterns of visual field defect and the corresponding site of pathology. (Image credit to Neuroscience, 5th Edition, Sinauer Assoc., Inc.)

4.1.5 Types of Perimetry

4.1.5.1 Kinetic

Most of the historical work appraising visual fields in vigabtrin associated visual field loss utilises kinetic perimetry which originates from the Goldmann perimetry. The target size and intensity remains constant, while moving from a non-seeing area to a seeing area along a set meridian to plot the extent of visual fields. The process is repeated in various meridians in order to map the visual isopters, usually at 15 degree spacing. A 2-dimensional 'Hill of Vision' can be plotted from the results. This form of testing is useful when steep gradients or dense scotoma is suspected.

4.1.5.2 Static

Our cohort was tested with static perimetry. It uses stationary targets that changes in brightness in order to measure retinal sensitivity at various points. The stimulus size is constant. Unlike kinetic perimetry, the border of the defect could not be clearly outlined. This form of perimetry is useful in detecting subtle or fluctuating scotomas, and gives useful illustration when dense scotoma is detected.

4.1.5.3 Automated perimetry

This assessment tool is a common finding in clinical setups, where visual fields/perimetric tests are assisted by computerised hardware carried out by a perimetric technician. The test strategy is commonly static perimetry, with the parameters of the stimulus altered via a standard computerised algorithm to measure retinal sensitivity at various points of the visual field. One eye is tested at a time, where the other eye not under test is patched.

4.1.5.3.1 Humphrey Field Analyzer

This is one of the most readily found system used in clinical areas. The standard set up includes:

- **The projection system** = the bowl where stimulus is presented. The distance between the centre of the bowl to the eye is set at 30cm.
- **The optical system** = the location of the stimulus on the bowl correlates to the retinal area to be tested. To minimise the effect of glare, the bowl surface has a matte finish.
- **Central processor** = Controls testing strategy via computerised algorithm, with continuous adjustment of stimulus based on each response by the patient.
- **Patient interface** = Chin rest, forehead rest, chair and trial lens holder are positioned optimally for patient comfort and testing criteria. Trial lens holder (37mm lens size) is used to test central areas. However, for fields

more than 30 degrees the lens holder may obstruct vision and present artefacts on the perimetric results.

Figure 4.5:
The Perimetry setup. The subject maintains position by resting both their chin and forehead against the rest on the machine. The subject has a 'clicker'; a button is pressed when stimulus is detected.

4.1.6 Reliability Indices

The current perimetric testing software can appraise the subject's testing ability through consideration of fixation losses, false positive catch trials and false negatives; cumulatively known as "Reliability Indices".

4.1.6.1 Fixation loss

Fixation stability is an essential part of perimetry that can be monitored in modern perimetry through 'Eye-tracking'. One of the earliest method of 'eye-tracking' is by first localising and establishing the area of the physiological 'blind spot'. The Heijl-Krakau technique projects a stimulus (Goldman size III) onto the established blindspot region at various times during the examination. If the stimulus is detected by the subject, this will be counted as an episode of fixation loss. In general, fixation losses above 20% will render the test results unreliable.

Another common method of eye tracking is the "Gaze tracker", a feature of the modern Humphrey Field Analyser. This technique first measures the distance between first corneal reflex and the centre of the pupil prior to the start of the test, using a preset fixation target. During the test, the change in distance is measured as a deviation from the established baseline. This is recorded on the test result as a line bar chart, that requires clinician to deduce subjective correlations.

High rates of fixation losses can be erroneously induced in the presence of high false positives and misplotting of the 'blind spot'.

4.1.6.2 False Positive catch trials

A subject with high levels of false positives on a visual field test is often labelled as 'trigger-happy'. During the test, the patient responds in the absence of a positive stimulus.

Automated perimetry evaluates a false positive either by presenting a mechanical noise in the absence of a light stimulus (a catch trial, additional time to test), or a positive response when the patient is not expected to react to the stimulus, between reaction time of 180 – 200ms (de Boer *et al.*, 1982).

High false positive can occur if the patient misunderstood the instructions for the examination, or lost concentration due to anxiety and pressure to perform during the test. In the Swedish Interactive Threshold Algorithms (SITA) automated perimetry, false positive higher than 15% can render the examination result unreliable (Bengtsson and Heijl, 2000).

4.1.6.3 False Negative

When a patient does not respond to a stimulus that has been previously detected at a lower luminance, a false negative is recorded. The earlier versions of the automated field analyser (Full threshold and FASTPAC algorithm) the brightness of the stimulus used in the catch trial is 9dB brighter than the earlier detected stimulus. The SITA has developed a more sophisticated method which runs smaller numbers of catch trials (drives down testing time), and statistically calculates the probability of a false negative response.

False negative was initially intended to investigate patient reliability during testing. Lack of attention has been attributed to high rates of false negatives, although some authors suggest higher rates of false negatives are seen in patients with advance field loss(Katz and Sommer, 1988; Bengtsson and Heijl, 2000).

The 'Clover leaf' pattern is characteristic of a result with high levels of false negatives. Recognition of this pattern prevent misdiagnoses of peripheral field constriction, and must be repeated.

4.1.7 Factors that can affect the visual fields

The visual fields examination is a popular form of assessment used to map the field of vision. The advantages are clear – it is safe, non-invasive, economical to run, cost-effective and requires an operator with some basic training in perimetry.

There are several potential limitations to consider, particularly when testing a cohort like ours. Patients with epilepsy are reported to have slower response times, partially contributed by decreased alertness (Hawker and Astbury, 2008; Clayton *et al.*, 2013).

<u>Physical factors that can affect performance during visual fields examination:</u>

4.1.7.1 Age

The older population perform less well on visual fields examination due to combination of factors more commonly associated with the ageing population (Kosmin *et al.*, 1996). Specifically, the examination requires a patient to multitask; to focus on a single spot while inducing heightened awareness of light stimulus, upon when the button should be clicked. This high level of concentration will need to be maintained for a few minutes per eye and can prove to be a challenge. Common testing algorithms run for longer

when it detects issue with performance reliability (fixation loss, increased eye movements, high false negative or false positive). Reduced contrast sensitivity on the flicker perimetry has been associated with age(Bernardi, Costa and Shiroma, 2007). Reduced sensitivity on the blue-on-yellow perimetry was also observed in the older population (Johnson *et al.*, 1988).

The impact of mental fatigue should be considered when evaluating the results (Johnson, Adams and Lewis, 1988). Previous studies have reported evidence for reduced cognitive and technical performance, following prolonged periods of cognitively demanding tasks (Marcora, Staiano and Manning, 2009). Often when visual fields results are inaccurate, the test is repeated to improve performance. In the presence of mental fatigue, that translates into testing fatigue performance can decline, therefore affecting true results.

4.1.7.2 Defocus

Defocusing of the retinal image are commonly caused by the following:

- Incorrect trial lenses
- Poor positioning or trial lenses
- Pupil sizes

Defocusing of the retinal image from incorrect trial lenses or poor positioning during the examination can affect the visibility of the stimulus. Uncorrected refractive error can

affect the threshold estimation in non-suprathreshold testing strategies (Heuer *et al.*, 1987; Henson and Morris, 1993).

Defocusing is also dependent on pupil size, which can be affected by age, medication (miotics or mydriatics) and pre-existing neuro-ophthalmological conditions. The pupil aperture affects retinal illumination and visual field sensitivity where a small constricted pupil dims the intensity of both the stimulus and the background (Lindenmuth *et al.*, 1989). On the other hand, a dilated pupil reduces peripheral threshold sensitivity (Lindenmuth *et al.*, 1990).

4.1.7.3 Media opacities

The presence of any form of opacities obscuring the visual axis can compromise the accuracy of the visual fields (Takada *et al.*, 2003). Most reports that investigated the effect of cataract report generalised reduced threshold for retinal sensitivity. Other forms of media opacities can also produce the same effect:

Anterior segment: Cataract, corneal scarring, hyphaema or hypopyon
Posterior segment: Vitreous condensation (inflammatory), vitreous haemorrhage

The generalised effect observed particularly on threshold perimetry must lead the interpreter to consider issues with media opacities before committing to diagnosing a defect based on the visual field test. Rapid or unexpected changes in the test results also warrants slit lamp examination to exclude other causes that can interfere with the final visual field result.

4.1.7.4 Psychological

Perimetry has been described to be is a form of psychophysical examination that requires a high degree of patient cooperation and concentration. The effect of mental fatigue has been briefly discussed previously. The learning effect phenomenon associated with this examination is well documented. To gain reliable results, it is recommended that patients undergo several tests sessions for practice in order to improve accuracy of test results. Logistically this can be challenging to overcome, especially in a setting like the NHS, where outpatient review sessions are increasingly limited.

4.1.7.5 The Learning Effect of Perimetry

It is now accepted that experience in perimetric examination significantly influences performance and result. An author even stated "learning effect is an artefact of automated perimetry in that masks the real defect" (Chandrinos and Tzamouranis, 2020). This phenomenon has been observed mainly in patients with glaucoma and their control counterparts. Some authors report improvement in threshold sensitivity in the form of mean deviation (MD) and pattern standard deviation (PSD) with practice, with significant difference in the reliability indices (Pierre-Filho *et al.*, 2010).

Heijl et al in 1989 documented the effect of previous testing experience in perimetry. Common deviations found in unexperienced subjects include peripheral field loss with reduced peripheral sensitivities (Heijl, Lindgren and Olsson, 1989). When repeated, the

threshold sensitivity improves from the peripheral field. To minimise the impact of the learning effect, recommendations include allowing repeated testing in the inexperienced patient, conduct a practice test prior to the full/actual perimetry test as well as incorporate the 'Learning index', into the statistical software (Chandrinos and Tzamouranis, 2020)

4.1.7.6 Visual Fields appraisal method in this work

References to Wild's classification is made in the early sections of this thesis to show consideration to a common method used to appraise visual fields in patients with Vigabatrin, primarily to allow comparisons to other published studies. Historically, this classification was first published in 1999 and allow the severity of visual field loss secondary to Vigabatrin be graded in terms of a 3-point ordinal grading scale of Mild, Moderate or Severe. As the classification was derived from kinetic perimetry, it is based on the extent of isopters, of the intensity and size of the 14e stimulus. However, as our patients are assessed using suprathreshold static perimetry the classification had to be modified and converted to degrees of eccentricity from fixation. This classification will not be used for detailed analysis due to unsuitable data format for the intended quantitative analysis.

Perimetry Score

This novel method to appraise visual fields was devised for the specific purpose to enable quantitative work for this study. Before a visual field is assigned a score, it must

also meet the other specified criterias relating to Vigabatrin associated visual loss (Bilateral, concentric and symmetrical). A visual field that does not meet the full criteria will not be included. The main aim of this method is to produce a continuous dataset that has the advantage of allowing quantitative analysis for correlation with other dataset in this study.

Perimetry Score X

x denotes the average from both eyes of the number of 'seen' retinal stimulus, over the total of 120 total stimulus covering 60 degrees retinal region from fixation.

$$\textit{Perimetry score, } \boldsymbol{x} = \frac{\textbf{(Right eye 'seen' stimuli + Left eye 'seen' stimuli)}}{\boldsymbol{2}}$$

As the test delivers stimuli for 120 retinal point, the higher score indicate that the subject has seen more stimuli, therefore less peripheral constriction and vice-versa. This is used in chapter 4.2. The average values from both eyes is used to pair with the corresponding independent variable of that subject (Vigabatrin burden). As visual loss from Vigabatrin is believed to be bilateral and symmetrical, it is felt to be logical approach for deducing a single score per subject.

Perimetry score Z

Z denotes the number of 'seen' retinal stimulus, out of the total 120 stimulus covering 60 degrees of retinal area from fixation from each eye. Unlike x, z reflects only the score from ONE eye. A higher z score indicate that the subject has the respective number of stimuli, therefore less peripheral constriction. This scoring is used in chapter 5.3, where z score is matched to an independent variable (Volume or thickness data from OCT) from each eye. The advantage of this approach is the increase in data points that could be included for analysis.

CHAPTER 4.2: EXPERIMENTAL WORK

THE RELATIONSHIP BETWEEN VIGABATRIN BURDEN AND VISUAL FIELDS, BY CONSIDERING 2MS TIMING DELAY IN WIDE-FIELD MULTIFOCAL ELECTRORETINOGRAM: A QUANTITATIVE APPROACH.

The first report of visual toxicity secondary to vigabatrin use by Eke in 1997 was based on the finding of visual fields constriction. Subsequent reports following this publication also described visual field loss as the main characteristic of vision change and disturbance. Other features such as visual acuity, colour vision, changes in retinal appearances and responses were also described in the literature, but none gained the same standing for consistency as detection of visual field loss from perimetry or visual field testing.

Visual field loss from vigabatrin toxicity is typically characterised as being bilaterally concentric (begin peripherally and progresses centrally), progressive but arrests when Vigabatrin is stopped, and is generally irreversible in nature.(Lawden *et al.*, 1999; Malmgren, Ben-Menachem and Frisén, 2001; Wild *et al.*, 2009; Wild, Smith and Knupp, 2019) Most patients are asymptomatic until the field loss reaches a severe stage where central vision is affected. The advantage of visual fields testing is that the test is widely available and economical to run, and the operator can be easily trained. The disadvantages of visual field testing include the variability of testing protocols, and

dependent on the Visual Fields machine available at each centre. The test also requires the operator to be constantly on alert to the patient during the test to encourage compliance or record any issues that could affect the result. Patients on Vigabatrin are known to have slow response times, possibly attributed by the decreased alertness observed in patients with epilepsy.(Hawker and Astbury, 2008; Clayton *et al.*, 2013) Therefore reliability indices of the test is often poor, and degraded due to high levels of fixation losses, false positives and false negatives. This leads to loss of valuable data that was intended to guide visual monitoring while on Vigabatrin.

The role of multifocal electrophysiological testing in Vigabatrin treated patients have received limited attention mainly because it is considered a highly specialised form of examination that is not widely available, require specialist operator and experienced result interpreter. Our centre previously reported abnormal Wide Field multifocal electroretinogram (WF-mfERG) responses in the form of implicit timing delays between central and peripheral field of more than 2ms, to be reflective of retinal dysfunction from Vigabatrin toxicity.

The effect of the cumulative Vigabatrin burden has been implicated in the past to reflect overall exposure to the treatment. Visual field loss from toxicity was reported to be rapidly progressing early, within 2 years (approximately 2kg total burden)(European Medicines Agency, 1999), before plateauing, after approximately 6 years duration of vigabatrin use (approximately 5kg total burden) (Wild *et al.*, 2013).

The aim of this study is to evaluate the relationship between visual fields and Vigabatrin burden, through consideration of the presence or absence of the timing delay of more than 2ms between the peripheral and central field in their WF-mfERG results.

Method

All patients underwent full ocular examination prior to inclusion into this study. Visual acuity, pupil examination and slit lamp examination which includes intraocular pressure measurements, anterior segment examination and dilated fundoscopy. The visual fields were assessed with the Humphrey 120-point suprathreshold, three-zone static perimetry test using the Humphrey Field Analyzer (Carl Zeiss, Meditec, Dublin CA, USA).

Each pair of visual fields is assigned a perimetry score of x, only if it met the inclusion criteria related to Vigabatrin associated visual field loss. As part of the larger study, all subjects have also undergone multifocal electrophysiological examination, blood tests and optical coherence tomography. The WF-mfERG responses were assessed with respect to the amplitude and latency (implicit time) of individual response element. Multifocal electrophysiology results are interpreted by two clinical scientists with total combined duration of 35 years' experience in the subject.

Subjects who have completed the multifocal electrophysiology testing, with confirmed estimated vigabatrin burden over the duration of their treatment are included for further analysis. Their visual field results (current and historical) in the research centre were retrieved and inspected for study suitability (type of test, reliability indices,

determined vigabatrin burden). The visual fields results were only included for further analysis if they met minimum reliability index (<20% fixation loss), displayed bilateral symmetrical and concentric field loss.

Data analysis

All statistical analysis were performed using the SPSS (IBM® SPSS® Statistics, version 27). In all three sets of analysis, two separate variables are defined. Vigabatrin burden is regarded as the independent variable and expressed in kilograms (kg). Perimetry score is the dependant variable, expressed as an absolute number to signify $\boldsymbol{x}/120$ (120 to reflect the total number of stimulus points on the perimetry test). Prior to analysis, each dataset was checked for outliers by determining the residuals/standard error value.

Each dataset is tested using linear regression, with graphical representation of the data spread, the linear regression equation and best-fit line. R_2 is expressed to imply the variability of the dependent dataset. As part of the linear regression calculation, the ANOVA is employed at each analysis. A *P* value less than 0.05 was considered statistically significant throughout.

Results:

ANALYSIS A: Vigabatrin burden versus perimetry score in current Vigabatrin user

30 pairs visual fields results were identified. The corresponding Vigabatrin burden was determined for all 30; although 8 were excluded as they did not meet the minimum reliability index. The remaining 22 visual fields results were used for further analysis. Two pair of outliers were identified and excluded from further analysis.

Vigabatrin burden (kg)	Perimetry score (x/120)
2.18	82.5
3.5	80.5
4.9	103
5.46	73.5
5.5	104.5
6	41
6.36	103
6.55	75
6.6	84
7.28	96
8.18	62.5
9.5	83.5
12.6	82
12.9	94.5
13.1	47.5
16.38	59.5
17.42	71
18.6	52.5
19.6	62
20.75	53
***2.2**	14
***18**	13

*outlier data

Table 4.2.1a: Dataset containing raw data of Vigabatrin burden and Perimetry score for current vigabatrin users

Descriptive Statistics

	N	Minimum	Maximum	Mean	Std. Deviation
Vigabatrin burden (kg)	20	2.18	20.75	10.1680	5.78385
Perimetry score (x/120)	20	41.00	104.50	75.5500	19.23326
Valid N (listwise)	20				

Table 4.2.1b: Descriptive data for the current vigabatrin group

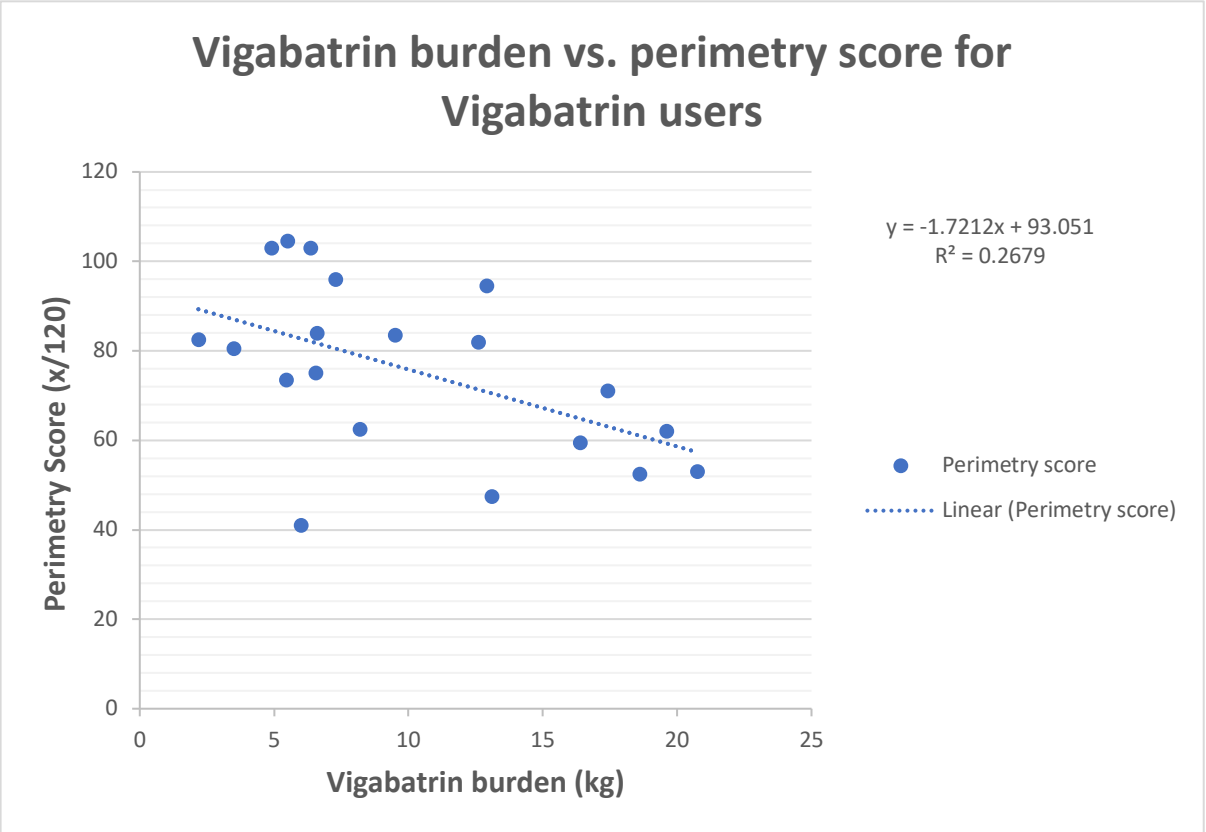

Figure 4.2.1: Scatter and plot graph showing the relationship, spread of data and best-fit line for current Vigabatrin users.

Model Summary

Model	R	R Square	Adjusted R Square	Std. Error of the Estimate
1	.518[a]	.268	.227	16.90738

a. Predictors: (Constant), Vigabatrin burden (kg)

Table 4.2.1c: Model summary showing adjusted R2 and SE of the estimate for this group.

ANOVA[a]

Model		Sum of Squares	df	Mean Square	F	Sig.
1	Regression	1882.978	1	1882.978	6.587	.019[b]
	Residual	5145.472	18	285.860		
	Total	7028.450	19			

a. Dependent Variable: Perimetry score (x/120)

b. Predictors: (Constant), Vigabatrin burden (kg)

Table 4.2.1d: ANOVA test results for the current vigabatrin users

Coefficients[a]

Model		Unstandardized Coefficients		Standardized Coefficients		
		B	Std. Error	Beta	t	Sig.
1	(Constant)	93.051	7.797		11.934	<.001
	Vigabatrin burden (kg)	-1.721	.671	-.518	-2.567	.019

a. Dependent Variable: Perimetry score (x/120)

Table 4.2.1e: Determined co-efficient for the linear regression equation in current vigabatrin users

For this analysis, the linear regression equation is:

$$y = -1.7212x + 93.051$$

$$R^2 = 0.2679$$

This model is statistically significant, where $F(1,18) = 6.587$, $p < 0.05$. In this set of data from current Vigabatrin users, Vigabatrin burden has an inverse relationship with perimetry score, where higher Vigabatrin burden predicts lower perimetry scores.

ANALYSIS B: Vigabatrin burden versus Perimetry score in those with 2ms timing delay (Delayed) in WF – mfERG.

For this analysis, 20 visual field results were identified. Out the 20, Vigabatrin burden was successfully determined and met minimum reliability index for 11 visual fields. 1 outlier was statistically identified through regression analysis and excluded from further calculations.

VIGABATRIN BURDEN (kg)	**Perimetry Score (*x/120*)**	**Comments**
4.9	103	
5.5	104.5	
6.36	103	
6.6	84	
12.6	82	
12.9	94.5	
13.1	47.5	
16.38	59.5	
17.42	71	
18.6	52.5	
30.6	*63.5*	*OUTLIER*

Table 4.2.2a: Dataset containing raw data of Vigabatrin burden and perimetry score in the 'Delayed' group

Descriptive Statistics

	N	Minimum	Maximum	Mean	Std. Deviation
Vigabatrin burden (kg)	10	4.90	18.60	11.4360	5.21695
Perimetry Score (x/120)	10	47.50	104.50	80.1500	21.60768
Valid N (listwise)	10				

Table 4.2.2b: Descriptive data for the 'Delayed' group

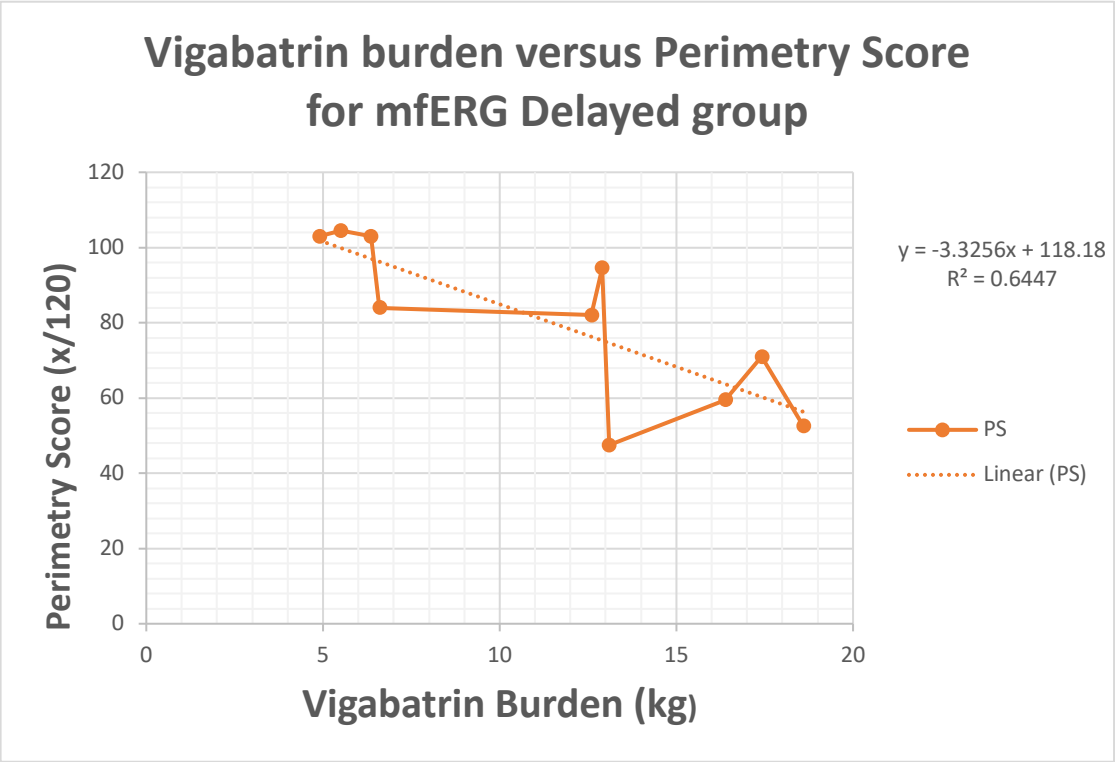

Figure 4.2.2: Scatter and plot graph showing the relationship, spread of data and best-fit line for the 'Delayed' group.

Model Summary

Model	R	R Square	Adjusted R Square	Std. Error of the Estimate
1	.803[a]	.645	.600	13.66128

a. Predictors: (Constant), Vigabatrin Burden (kg)

Table 4.2.2c: Model summary showing adjusted R2 and SE of the estimate for this group.

ANOVA[a]

Model		Sum of Squares	df	Mean Square	F	Sig.
1	Regression	2708.981	1	2708.981	14.515	.005[b]
	Residual	1493.044	8	186.630		
	Total	4202.025	9			

a. Dependent Variable: Perimetric Score (x/120)

b. Predictors: (Constant), Vigabatrin Burden (kg)

Table 4.2.2d: ANOVA test results for the 'Delayed' group

Coefficients[a]

Model		Unstandardized Coefficients		Standardized Coefficients		
		B	Std. Error	Beta	t	Sig.
1	(Constant)	118.181	10.877		10.865	<.001
	Vigabatrin Burden (kg)	-3.326	.873	-.803	-3.810	.005

a. Dependent Variable: Perimetric Score (x/120)

Table 4.2.2e: Determined co-efficient for the linear regression equation for the 'Delayed' group.

In this linear regression model, the equation is:

$$y = -3.3256x + 118.18$$

$$R^2 = 0.6447$$

This model is statistically significant, where $F(1,8) = 14.515$, $p < 0.05$. In this set of data from subjects with timing delay in the WF - mfERG, Vigabatrin burden (kg) has an inverse relationship with perimetry score, where higher Vigabatrin burden predicts lower perimetry score.

ANALYSIS C: Vigabatrin burden versus Perimetry score in those without the 2ms timing delay (Non-delayed) in WF - mfERG

For this analysis, 26 visual fields results were identified. Out of the 26, Vigabatrin burden was successfully determined and met minimum reliability index in 11 visual fields results. 1 outlier was statistically identified through regression analysis and excluded from further calculations.

VIGABATRIN BURDEN (kg)	Perimetry Score (x/120)	Comments
2.2	14	
2.5	11.5	
3.5	80.5	
5.46	73.5	
6	41	
6.55	75	
7.28	96	
8.19	62.5	
9.5	83.5	
9.8	74.5	
18	*13*	*OUTLIER*

Table 4.2.3a: Dataset containing raw data of Vigabatrin burden and perimetry score for the 'Non-delayed' group

Descriptive Statistics

	N	Minimum	Maximum	Mean	Std. Deviation
Vigabatrin burden (kg)	10	2.20	9.80	6.0980	2.71953
Perimetry Score (x/120)	10	11.50	96.00	61.2000	29.26336
Valid N (listwise)	10				

Table 4.2.3b: Descriptive data for the 'Non-delayed' group

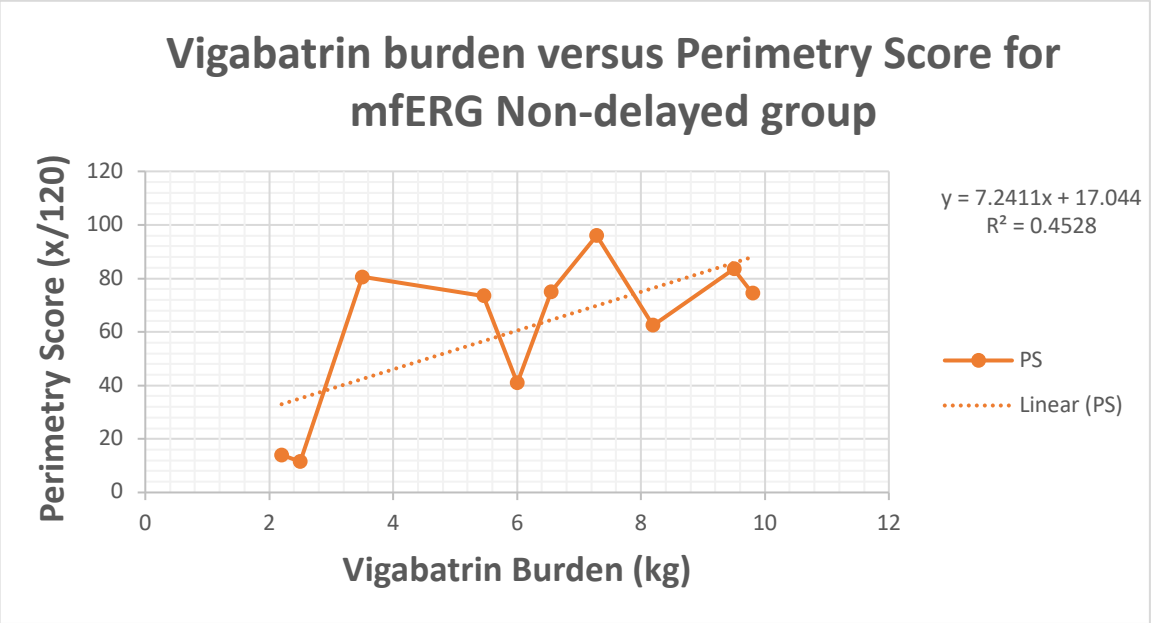

Figure 4.2.3: Scatter and plot graph showing the relationship, spread of data and best-fit line for the 'Non-delayed' group.

Model Summary

Model	R	R Square	Adjusted R Square	Std. Error of the Estimate
1	.673[a]	.453	.384	22.95906

a. Predictors: (Constant), Vigabatrin Burden (kg)

Table 4.2.3c: Model summary showing adjusted R2 and SE of the estimate for the 'Non-delayed' group.

ANOVA[a]

Model		Sum of Squares	df	Mean Square	F	Sig.
1	Regression	3490.151	1	3490.151	6.621	.033[b]
	Residual	4216.949	8	527.119		
	Total	7707.100	9			

a. Dependent Variable: Perimetric Score (x/120)

b. Predictors: (Constant), Vigabatrin Burden (kg)

Table 4.2.3d: ANOVA test results for the 'Non-delayed' group

Coefficients[a]

Model		Unstandardized Coefficients		Standardized Coefficients	t	Sig.
		B	Std. Error	Beta		
1	(Constant)	17.044	18.633		.915	.387
	Vigabatrin Burden (kg)	7.241	2.814	.673	2.573	.033

a. Dependent Variable: Perimetric Score (x/120)

Table 4.2.3e: Determined co-efficient for the linear regression equation in the 'Non-delayed' group.

In this linear regression model, the equation is:

$$y = 7.2411x + 17.044$$

$$R^2 = 0.4528$$

This model is statistically significant, where $F(1,8) = 6.621$, $p < 0.05$. In this set of data from subject with no timing delay in the mfERG central responses, Vigabatrin burden has a linear relationship with perimetry score where higher Vigabatrin burden predicts higher perimetry scores.

Analysis	Group	n (visual fields)	Vigabatrin burden mean (kg)	Perimetry score mean (x/120)	ANOVA significance, p value	Adjusted R_2 value
A	Current user	20	10.1680	75.55	0.019	0.227
B	Delayed	10	11.436	80.150	0.005*	0.600
C	Non-delayed	10	6.098	61.2	0.033	0.384

Table 4.2.4: Summary: Comparing key statistical values from analysis A, B and C.

Discussion:

The relationship between visual toxicity secondary to the cumulative dose of burden of vigabatrin has been previously reported.(European Medicines Agency, 1999; Clayton *et al.*, 2013; Wild *et al.*, 2013; Nowomiejska *et al.*, 2014) While the manufacturers originally estimated 0.14% incidence of visual effects secondary to treatment (Wong, Mawer and Sander, 1997), the current literature reports higher incidence at around 6 – 30%. (Spence and Sankar, 2001) The most common method used to assess for toxicity from Vigabatrin is the visual fields or perimetry; preferably three zone, suprathreshold

static perimetry testing protocol which is normally available in a typical ophthalmic clinical setting.

The aim of our study is to draw novel correlations between visual fields and vigabatrin burden in our cohort. Analysis A demonstrates a relationship which is consistent with previous reports, where higher vigabatrin burden predicts lower perimetry score despite the unusual method of appraising the visual fields. This informs us that there is some validity in this method, provided all the other conditions for visual fields inclusion (bilateral, symmetrical and concentric) and the minimum accepted reliability indices are met. This also provides rationale for us to apply the same analysis to a different set of data; namely those with 2ms timing delay and those without the timing delay as seen in analysis B and C respectively. Interestingly, analysis B appear to display the strongest statistical correlation, where increases in cumulative vigabatrin strongly predicts lower perimetry score in subjects where there is a delay of more than 2ms between the peripheral from central field in their WF-mfERG. This finding supports the earlier recommendation the 2ms timing delay is likely to be reflective of pathological retinal response secondary to Vigabatrin.(McDonagh *et al.*, 2003b; Gonzalez *et al.*, 2009)

While Wild et al has done tremendous work to plot and predict progression of vigabatrin specific visual toxicity through meticulous visual fields analyses (Wild *et al.*, 2019; Wild, Smith and Knupp, 2019), robust data to confirm pattern of progression for visual field loss, patient susceptibility and test specificity is still lacking. In our experience patient retention and cooperation during testing remains a significant challenge. Quality of monitoring while on vigabatrin is often hampered by lack of clinic attendance, and the

quality of test results degraded by poor reliability parameters. We know presence of visual field loss does not necessarily imply toxicity, as up to 25% of patients were documented to have visual field loss at baseline. (Sergott *et al.*, 2016b) Through wide-field multifocal ERG, specific changes in the form of marked reduction in b-wave amplitudes and delay in implicit timings between peripheral and central fields were reported and believed to be pathological of Vigabatrin related toxic effects.(McDonagh *et al.*, 2003b; Gonzalez *et al.*, 2009) Our results could further inform the ongoing efforts to identify distinct biomarkers related specifically to Vigabatrin toxicity, through the recognition of 2ms timing delay.

Our finding in C is unexpected yet noteworthy; one possible explanation is that the observed relationship demonstrates the visual fields test 'learning effect' among subjects (Marra and Flammer, 1991; Yenice and Temel, 2005), which laterally was not overcome in analysis B, presumably due to retinal toxicity. The main weakness of this study is the small number of subjects and visual fields tests available for analysis. The main strength of this study is the integration of relevant WF-mfERG results for exploration of detailed examination of the relationship between Vigabatrin exposure and visual field results. We acknowledge that the method we employed to evaluate the visual fields is unconventional. To maximise data analysis for a unique cohort, particularly when data is scarce calls for more novel approach to navigate through the available data. To compensate for this modification, all visual fields were inspected to ensure they met the additional criteria for inclusion.

The challenge remains in identifying a widely acceptable testing method that can draw a clear distinction around visual toxicity related to Vigabatrin, from other type of visual abnormalities. The literature heavily reports on the finding of peripheral field loss; however central visual function involving the cones at the fovea has also been reported, where co-existent impaired cone response amplitudes were found in the ERG in those with peripheral field defect (Banin *et al.*, 2003).

The full anatomical, structural and functional correlation to this finding remains elusive, although we have offered potential explanations as part of the larger study (see other chapters). Our advantage is the access to the wealth of WF-mfERG data relating to vigabatrin toxicity, that could be further developed for wider correlations that could be applied to other conventional testing methods of the visual pathway apart from the visual fields, such as the optical coherence tomography.

CHAPTER 5:

OPTICAL COHERENCE TOMOGRAPHY

5.1 Introduction

Optical coherence tomography (OCT) is an examination tool that allows detailed examination of the retina and optic disc microstructures. It is an imaging technique that utilises low-coherence light to capture high-resolution images in 2-dimensional form from an optical scatter media (retinal tissue). Testing with the OCT is rapid, non-contact and non-invasive. OCT has been proposed to be an alternative way to test for visual toxicity in Vigabatrin-exposed patients, as it allows objective assessment of the retinal tissues. Several groups have published findings related to Vigabatrin use including optic disc atrophy(Ravindran *et al.*, 2001b), attenuation of the retinal nerve fibre layers (Clayton *et al.*, 2013)(Lawthom, Smith and Wild, 2009)(Peng *et al.*, 2017) and more recently retinal thickening in the fovea and retinal nerve fibre layers .

This can especially be advantageous for monitoring vigabatrin effects, given that patients can have slow response times when undergoing perimetry assessments, partially attributed to decreased alertness observed in patients with epilepsy(Hawker and Astbury, 2008)(Clayton *et al.*, 2013).

5.1.1 History of OCT

The technology and potential capability of the Optical coherence tomography to perform 'Optical biopsy' was first reported in 1991 by Huang et al. Their prototype employed both low coherence light and ultrashort laser pulses to create an optical signal that could penetrate and be reflected back through biological tissues. The reflected signals are measured from the echo time delay via the Michelson interferometer, which involves movement of reference mirror. The collected spatial information then generates two-dimensional map of the tissue. The first commercially available **Time-Domain** OCT scanner was made available in 1996 was produced by Zeiss OCT. The later models of this can produce 400 A-scans per second, with up to 8µm axial resolution.

The **Spectral-Domain OCT** differs from the Time-Domain described where the reference mirror remains stationary, and the light signal from the interferometer is then measured with a spectrometer. Advancement of the spectral domain technology now allows information from the spectrometer to be transformed into axial measurements of the tissue, via Fourier technique (hence it also named the Fourier-Domain OCT). This allows more rapid and higher resolution of two-dimensional images to be produced. This allowed increase in scanning speed up to 50 times that of the time domain OCT. Commercial application of the Fourier domain/Spectral domain OCT was only in 2002.

Swept Source OCT is also a modification to the OCT technology, which utilises a frequency-swept light source and a light detector instead of the spectrometer. This advancement allowed longer wavelengths to be employed to reduce scattering from the

dark retinal pigment epithelium layer (RPE). The scanning speed is >100,000 A-scans per sec, with the ability to acquire wider scans of the macula (up to 12mm) and more accurate visualisation of other tissues around and within the retina such as the vitreous, choroid and blood vessels.

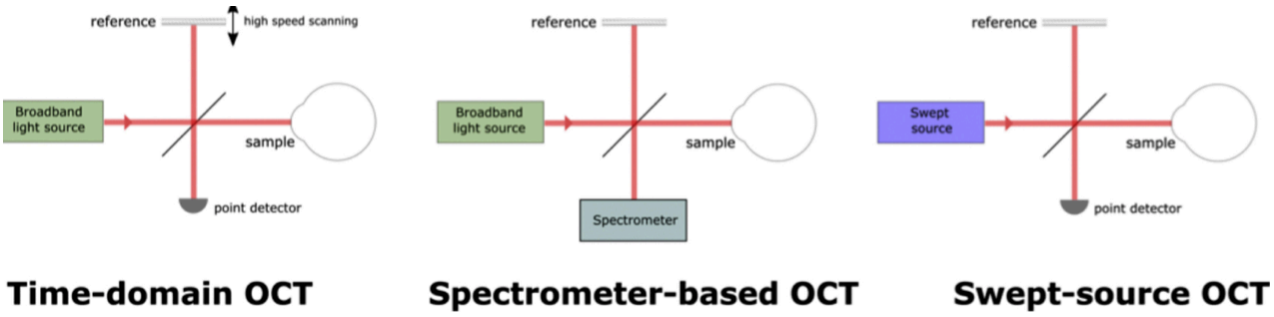

Figure 5.1.1: Block diagram demonstrating differences in the current types of OCT. (Image credit to (Ang *et al.*, 2018) 'Anterior segment optical coherence tomography' Progress in retinal and eye research 66(1): 132-56)

Interdomain measurements

Despite the similar technologies, measurements from one domain cannot be compared to measurement of the same tissue sample from another domain OCT, despite good reproducibility of results from both. Lack of correlation is worse in pathologic eyes (Forte *et al.*, 2009) as the ability to detect subtle changes differ between TD-OCT and SD-OCT (Folgar *et al.*, 2014).

5.1.2 Eye Tracking in OCT

Despite the progression in the OCT technology, the results can be hampered by movement causing imaging and signal artefacts. Both voluntary and involuntary eye movements are common cause of signal degradation even in high-speed systems (Vienola *et al.*, 2012). Movement interferes with data averaging of high volume of B-scans used to improve the signal-to-noise ratio. Some artefacts can be corrected by post-processing algorithms, but large movements produce gaps in volume imaging.

The eye-tracking capability in the SPECTRALIS® is based on image tracking, where eye motions are extracted, and the OCT beam follows the image to keep the input and area of scanning 'stationery'. 1,000 retinal points from the infra-red scanning laser ophthalmoscopy (SLO) imaging is used to keep up with motion during the scanning time.

5.1.3 Why Spectral-Domain OCT?

The Spectral domain OCT machine used for this study is the SPECTRALIS® by Heidelberg Engineering, Heidelberg, Germany. Previous OCT related studies in Vigabatrin patients have used a mix of both Time-Domain and Spectral-Domain systems; earlier studies are likely to have employed the Time-Domain scanner, and later studies tend to use spectral-domain systems. In the US, the OCT has been approved for use in monitoring of Vigabatrin related toxicity. Even though the type of OCT was not specified, it is likely to be spectral-domain. This is in line with the progression of technology, where later

generations of OCT are spectral-domain. Choosing to use a SD-OCT in this study with allow comparisons with future studies, and ongoing monitoring effort.

5.1.4 The OCT scanning protocol

5.1.4.1 Retinal nerve fibre layer (RNFL) protocol

Single layer retinal analysis was performed by the SPECTRALIS.

For result presentation, the SPECTRALIS is supplied with the Heidelberg Eye Explorer that presents the results in the form of

a) fundus image showing area of scan with respect to the speculated area of the fovea (point of fixation)
b) line-scan of the peripapillary retina, highlighting the RNFL (green line at the outer limit, red line on the inner limit/start of the internal limiting membrane [ILM])
c) diagram of the optic nerve head, showing quantitative values for thickness in µm by segments (Superior, temporal, inferior and nasal)
d) graphical illustration of measured RNFL thickness in µm, against a colour-coded background illustrating three categories of thickness (based on normative data):
    - Green (Normal)
    - Yellow (Borderline thinning)
    - Red (Abnormal thinning)
    - Green line (expected Normal)

The SPECTRALIS device is equipped with internal fixation points for patients to focus on during the test. The laser tracking is activated once the fundus image is registered by the software and throughout the scanning duration.

5.1.4.2 Macula Volume protocol

On the macula, 25-line raster scans are acquired to construct a 6mm x 6mm macular cube. The Heidelberg Eye Explorer application presents the result of the macula cube in the form of thickness profile (line-by-line analysis of the cube) and thickness map which gives average thickness and volume of each segment.

For volume analysis, the 1, 3, 6mm ETDRS concentric ring is applied to the macula as the software generates the calculated volumed for the scanned area, based on the 25-line raster cube.

Auto segmentation of each individual layers (RNFL, ganglion cell layer (GCL), Inner plexiform layer (IPL), Inner nuclear layer (INL), Outer Plexiform layer (OPL), Outer nuclear layer (ONL), Retinal pigment epithelium (RPE)) as well as broader categorisation of Inner retinal layers (RNFL, GCL, IPL, INL, OPL) and Outer retinal layers (ONL, ELM, Photoreceptor layer ,RPE and Bruch's membrane) based on the software manufacturers description (*Know your retinal layers*, 2016).

Individual microstructures/microlayers	Inner retinal macrolayers	Outer retinal macrolayers
Retinal nerve fibre layer	✓	
Ganglion cell layer	✓	
Inner plexiform layer	✓	
Inner nuclear layer	✓	
Outer plexiform layer	✓	
Outer nuclear layer		✓
Retinal pigment epithelium		✓

Table 4.2.5 The auto-segmentation of retinal layers used in this study based on the manufacturer's handout.

5.1.5

Inclusion of OCT data

Only images with signal-to-noise ratio greater than 25dB were included (automated acceptance by the software).

Exclusion of OCT data

Poor quality scans are excluded from further analysis. This includes scans with poor signal strengths as determined by the OCT software. Signal strength is gauged by the signal-to noise ratio and signal uniformity during the scan and can affect the accuracy of the scan and lead to auto-segmentation errors. The software's ability to perform

accurate segmentation is also affected by the presence of disease(Sadda *et al.*, 2006; Domalpally *et al.*, 2009; Alshareef *et al.*, 2017).

Common cause for poor scans can also include:

- Failure to track fixation due to:
    - High rate of blinking
    - Large eye movements
    - Light sensitivity
- Circle decentration
- Scan misalignment

5.1.6 OCT of the retina

The reflective ability of biological tissues allows separate population of tissues to be distinguished from its neighbours. They are described as hyperreflective (bright) or hyporeflective (dark) bands.

The 3 key features of OCT imaging are:

a) Cellular layer = hyporeflective
b) Fibrous layer = hyperreflective
c) Boundaries = hyperreflective

(as described by Yoshimura and Hangai, OCT Atlas, ©Springer-Verlag Berlin Heidelberg 2014)

Cellular layers of the retina are weakly reflective and are mainly composed of neuronal cell bodies. The ganglion cell layer, inner nuclear layer and the outer nuclear layer are classed as hypo-reflective on the OCT scans.

The **fibrous layers** of the OCT are hyperreflective as it runs perpendicular to the path of the OCT beam, creating intense backscatter and reflection. The retinal nerve fibre layer (NFL) and the inner plexiform layer (IPL) produce this characteristic on the OCT scan. The nerve fibres of the outer plexiform layer (OPL) though expected to be highly reflective is an exception. This is because the Henle Fibre layer (part of the OPL) changes its orientation, where its forward tilt causes it to be obliquely angled to the OCT beam, making it weakly reflective (Otani, Yamaguchi and Kishi, 2011).

The highly reflective **boundaries / lines** seen on the OCT scans are thin layers of highly aligned cell layers; the external limiting membrane, the photoreceptor inner segment/outer segment junction, cone outer segment tip and the retinal pigment epithelium (apex and base as 2 separate and distinct lines).

Structure Function correlation with the OCT

This chapter examines the retinal structure to visual function relationship in Vigabatrin treated patients in two separate studies.

1. Evaluate relationship between retinal OCT microstructures RNFL thickness to WF-mfERG

2. Evaluate relationship between retinal OCT microstructures and RNFL thickness to visual fields

CHAPTER 5.2: EXPERIMENTAL WORK

THE ROLE OF OPTICAL COHERENCE TOMOGRAPHY IN VIGABATRIN EXPOSED PATIENTS: RETINAL NERVE FIBRE LAYER AND MACULA VOLUME MICROSTRUCTURES ANALYSIS.

Introduction:

The rapid advances in OCT technology can prove to be the answer in our search for the ideal examination and monitoring tool for Vigabatrin related visual toxicity. The advantages of OCT testing are obvious as testing is rapid, non-contact and non-invasive. Its ability to capture high-definition images of the retina with advanced functional tools for objective measurements makes it an exceptionally valuable tool the clinical setting. Its use in monitoring for Vigabatrin related toxicity at present is limited to research purposes. Several groups have published relevant retinal findings from Vigabatrin use that could be objectively evaluated with the OCT. Clinical findings include optic disc atrophy(Ravindran *et al.*, 2001b), attenuation of the retinal nerve fibre layers (Clayton *et al.*, 2013)(Lawthom, Smith and Wild, 2009)(Peng *et al.*, 2017) and more recently retinal thickening in the fovea and retinal nerve fibre layers .

Our centre published multifocal ERG results on epileptic patients and found Vigabatrin related visual change is associated with 2ms delay in the peripheral field versus central

field in multifocal ERG, with 100% sensitivity and 86% specificity (Gonzalez *et al.*, 2009). It is a form of objective testing of the visual system that can overcome the usual challenges encountered in visual fields testing, especially in patients with concentration and attention problems (McDonagh *et al.*, 2001)(McDonagh *et al.*, 2003b). The downside of this test is the lengthy duration required, the need for a highly skilled operator to conduct the examination and an experienced result interpreter. Despite the striking findings, the explanation behind the observed timing delays in this test has never been fully elucidated.

In this study we aim to investigate if OCT examination of the retinal microstructures and retinal nerve fibre layer thickness could potentially reveal a structural cause behind the WF-mfERG findings in our cohort of patients.

Method:

All patients underwent full ocular examination prior to inclusion into this study. Visual acuity, pupil examination and slit lamp examination which includes intraocular pressure measurements, anterior segment examination and dilated fundoscopy.

As part of the larger study, all subjects have also undergone multifocal electrophysiological examination, blood tests and optical coherence tomography. The WF-mfERG responses were assessed with respect to the amplitude and latency (implicit time) of individual response element. Multifocal electrophysiology results are

interpreted by two clinical scientists with total combined duration of 35 years' experience in the subject.

The WF-mfERG protocol utilises back projection stimulus consisting of 61 element array with independent decimated binary m-sequence covering 90 degrees visual field, conducted by a custom-built software. Electrical responses from the central field (0-45 degrees) were compared to the peripheral field (45-90 degrees).

OCT examination was performed using the spectral-domain OCT, Heidelberg SPECTRALIS, Heidelberg Engineering, Heidelberg, Germany.

Visual fields were assessed using the Humphrey 120-point suprathreshold, three zone static perimetry test. The results were graded based on the modified Wild's classification (Wild *et al.*, 1999) as normal, mild, moderate and severe.

All statistical analysis was performed using the SPSS (IBM® SPSS® version 27). In all analyses, data are grouped into either 'Delayed' and 'Non-Delayed'. Data samples are compared using descriptive statistics and independent samples T-test. Values are expressed in mm^3 for volume and micrometer (µm) for thickness. Boxplot graphs are used to illustrate the spread of data.

The study was approved by the West of Scotland Ethics committee.

Results:

28 subjects completed the study and only those with good quality OCT results were included in this part of the analysis. For the OCT analysis, subjects were grouped based on their WF-mfERG results under Delayed (2ms delay in the peripheral field (45-90 degrees, compared to central 0 - 45 degree field) or Non-Delayed group. Those who were excluded had abnormal OCT findings that had spuriously affect the results of the auto segmentation program (epiretinal membrane, central serous retinopathy) or poor-quality OCT images. Retinal nerve fibre layer (RNFL), both macula and macula microstructures volumes were investigated for correlation with the spatial delays (2ms or more) recorded in the WF-mfERG result.

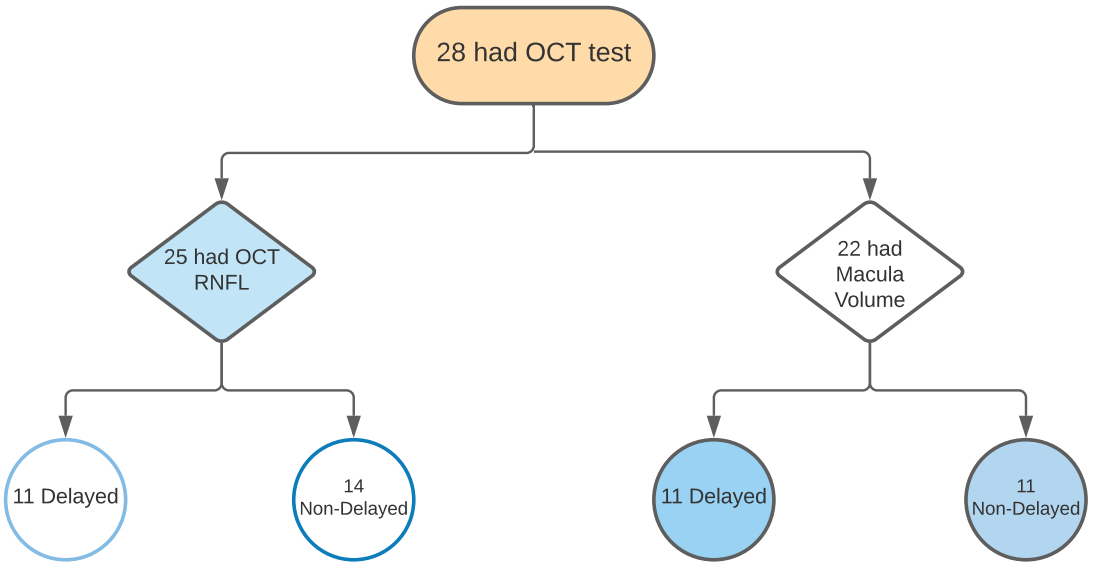

Figure 5.2.1: Distribution of subjects based of availability of OCT and WF-mfERG results.

For the RNFL thickness scans, results from 3 subjects were excluded due to scan decentration. For the macula volume scan, results from 6 subjects were excluded; 1 due

to epiretinal membrane, 1 due to central serous retinopathy, 4 due to incomplete scans from significant blinking artefacts.

All groups were matched in age. Statistical analysis for the Delayed and Non-Delayed group was performed using the independent samples t-test, the analysis comparing OCT results based of visual field grades with the ANOVA single factor.

Retinal nerve fibre layer analysis

25 patients were included in the OCT RNFL analysis, with 11 in the 'Delayed' group versus 14 in the 'Non-delayed' group. 3 out of 28 patients were excluded due to incomplete WF-mfERG results. Analysis was performed by group comparison of the retinal nerve fibre layer thickness in each quadrant. The thickness value of a segment used is the average from the corresponding segments in both eyes.

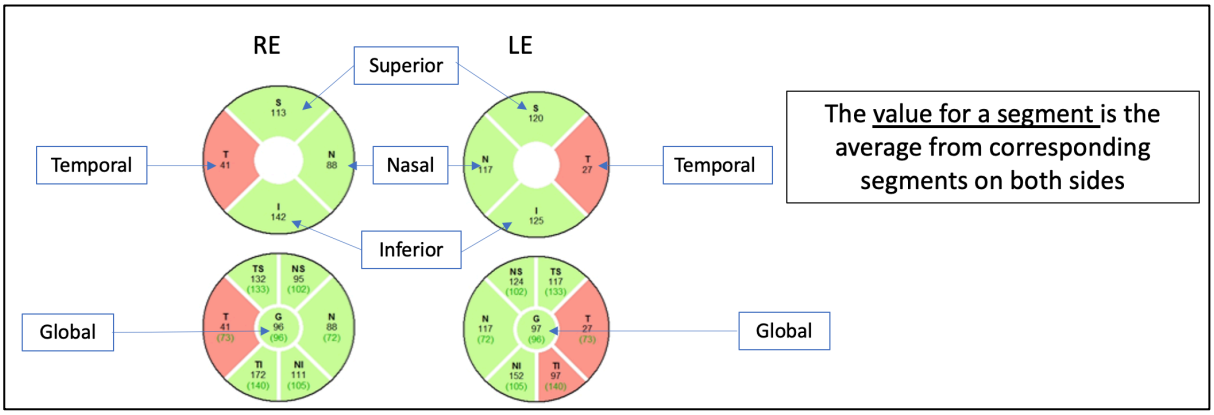

Figure 5.2.3: Retinal nerve fibre layer measurements based on the OCT.

RNFL thickness comparison between the Delayed vs Non-delayed group

Descriptives

	WF-mfERG			Statistic	Std. Error
Global RNFL (micrometer)	Delayed	Mean		72.5000	4.64220
		95% Confidence Interval for Mean	Lower Bound	62.1565	
			Upper Bound	82.8435	
		5% Trimmed Mean		72.2778	
		Median		72.0000	
		Variance		237.050	
		Std. Deviation		15.39643	
		Minimum		52.00	
		Maximum		97.00	
		Range		45.00	
		Interquartile Range		33.00	
		Skewness		.362	.661
		Kurtosis		-1.011	1.279
	Non-Delayed	Mean		69.0000	3.52035
		95% Confidence Interval for Mean	Lower Bound	61.3947	
			Upper Bound	76.6053	
		5% Trimmed Mean		68.8611	
		Median		70.0000	
		Variance		173.500	
		Std. Deviation		13.17194	
		Minimum		50.00	
		Maximum		90.50	
		Range		40.50	
		Interquartile Range		21.88	
		Skewness		.175	.597
		Kurtosis		-1.349	1.154
Superior RNFL (micrometer)	Delayed	Mean		86.2273	6.93914
		95% Confidence Interval for Mean	Lower Bound	70.7659	
			Upper Bound	101.6886	
		5% Trimmed Mean		85.7525	
		Median		81.5000	
		Variance		529.668	
		Std. Deviation		23.01452	
		Minimum		55.00	
		Maximum		126.00	
		Range		71.00	
		Interquartile Range		37.00	
		Skewness		.465	.661
		Kurtosis		-.606	1.279
	Non-Delayed	Mean		84.3929	5.56361
		95% Confidence Interval for Mean	Lower Bound	72.3734	
			Upper Bound	96.4123	
		5% Trimmed Mean		83.9365	
		Median		83.7500	
		Variance		433.353	
		Std. Deviation		20.81713	
		Minimum		57.50	
		Maximum		119.50	
		Range		62.00	
		Interquartile Range		39.00	
		Skewness		.252	.597
		Kurtosis		-1.320	1.154

Temporal RNFL (micrometer)	Delayed	Mean		67.7273	1.94745
		95% Confidence Interval for Mean	Lower Bound	63.3881	
			Upper Bound	72.0665	
		5% Trimmed Mean		67.8081	
		Median		69.0000	
		Variance		41.718	
		Std. Deviation		6.45896	
		Minimum		57.00	
		Maximum		77.00	
		Range		20.00	
		Interquartile Range		11.50	
		Skewness		-.534	.661
		Kurtosis		-.676	1.279
	Non-Delayed	Mean		56.7500	3.15652
		95% Confidence Interval for Mean	Lower Bound	49.9308	
			Upper Bound	63.5692	
		5% Trimmed Mean		56.6389	
		Median		54.7500	
		Variance		139.490	
		Std. Deviation		11.81060	
		Minimum		36.50	
		Maximum		79.00	
		Range		42.50	
		Interquartile Range		17.88	
		Skewness		.309	.597
		Kurtosis		-.416	1.154
Inferior RNFL (micrometer)	Delayed	Mean		88.5455	7.49983
		95% Confidence Interval for Mean	Lower Bound	71.8348	
			Upper Bound	105.2561	
		5% Trimmed Mean		88.2727	
		Median		83.0000	
		Variance		618.723	
		Std. Deviation		24.87414	
		Minimum		55.00	
		Maximum		127.00	
		Range		72.00	
		Interquartile Range		48.00	
		Skewness		.415	.661
		Kurtosis		-1.129	1.279
	Non-Delayed	Mean		84.2857	5.20321
		95% Confidence Interval for Mean	Lower Bound	73.0449	
			Upper Bound	95.5266	
		5% Trimmed Mean		84.0397	
		Median		76.5000	
		Variance		379.027	
		Std. Deviation		19.46863	
		Minimum		56.50	
		Maximum		116.50	
		Range		60.00	
		Interquartile Range		31.38	
		Skewness		.476	.597
		Kurtosis		-1.125	1.154

Nasal RNFL (micrometer)	Delayed	Mean		46.3182	4.21646
		95% Confidence Interval for Mean	Lower Bound	36.9233	
			Upper Bound	55.7130	
		5% Trimmed Mean		46.4646	
		Median		48.5000	
		Variance		195.564	
		Std. Deviation		13.98441	
		Minimum		21.00	
		Maximum		69.00	
		Range		48.00	
		Interquartile Range		25.00	
		Skewness		-.241	.661
		Kurtosis		-.382	1.279
	Non-Delayed	Mean		47.7500	3.59897
		95% Confidence Interval for Mean	Lower Bound	39.9749	
			Upper Bound	55.5251	
		5% Trimmed Mean		47.1944	
		Median		43.7500	
		Variance		181.337	
		Std. Deviation		13.46613	
		Minimum		33.50	
		Maximum		72.00	
		Range		38.50	
		Interquartile Range		20.38	
		Skewness		.889	.597
		Kurtosis		-.481	1.154

Table 5.2.1: Descriptive statistics of both Delayed and Non-delayed groups, based on the RNFL quadrants.

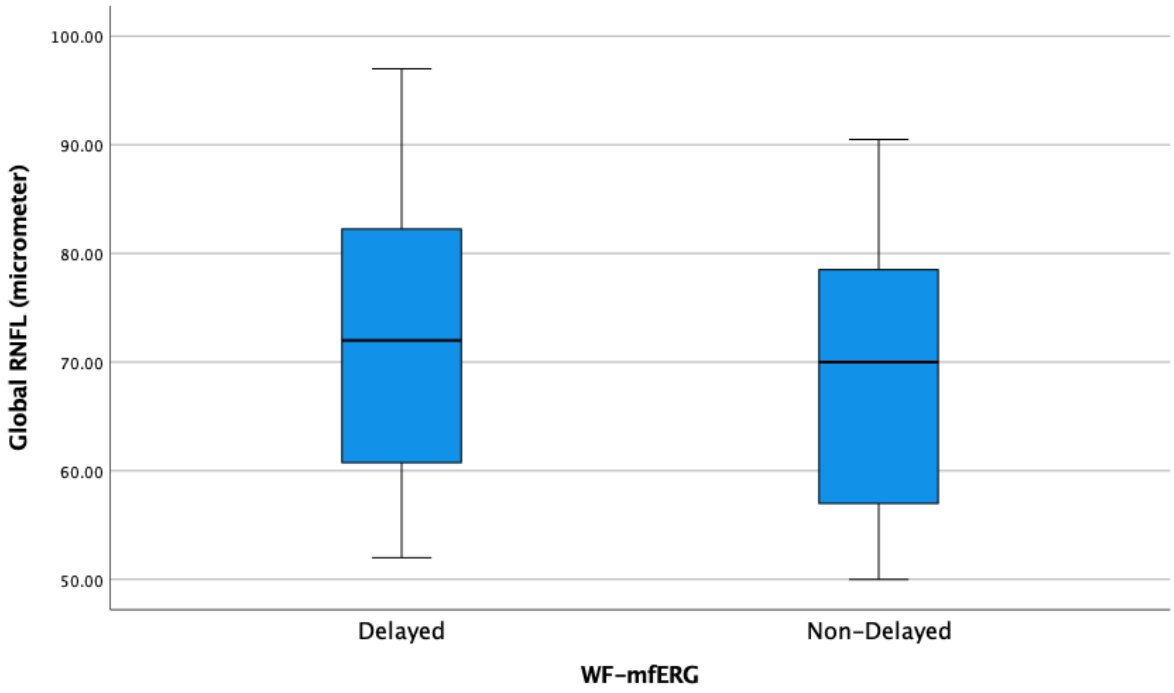

Figure 5.2.4: Boxplot graph demonstrating the Global RNFL thickness in both groups, p = 0.546

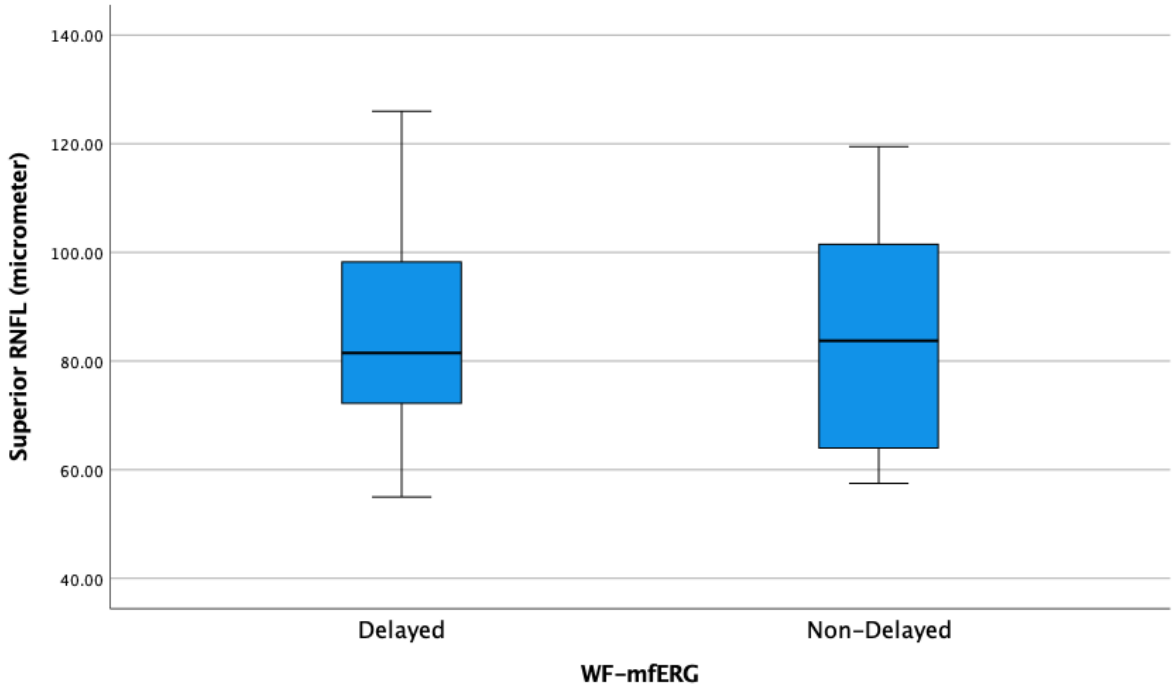

Figure 5.2.5: Boxplot demonstrating the superior RNFL thickness in both groups, p = 0.836.

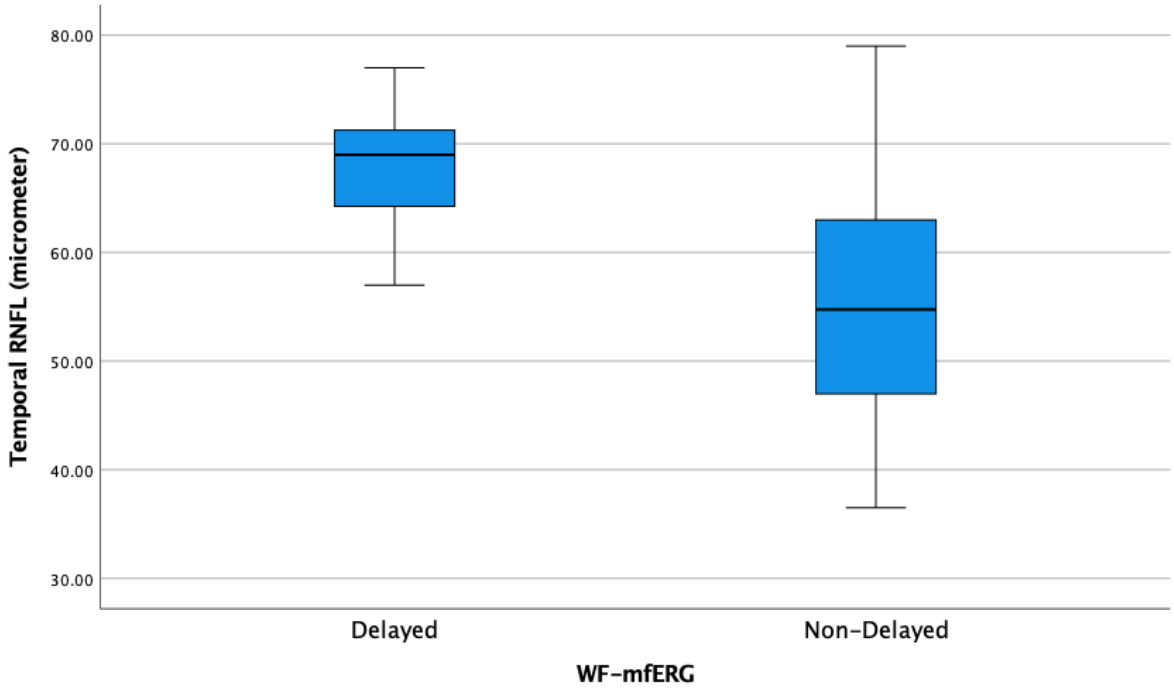

Figure 5.2.6: Boxplot demonstrating the temporal RNFL thickness in both groups, p <0.05.

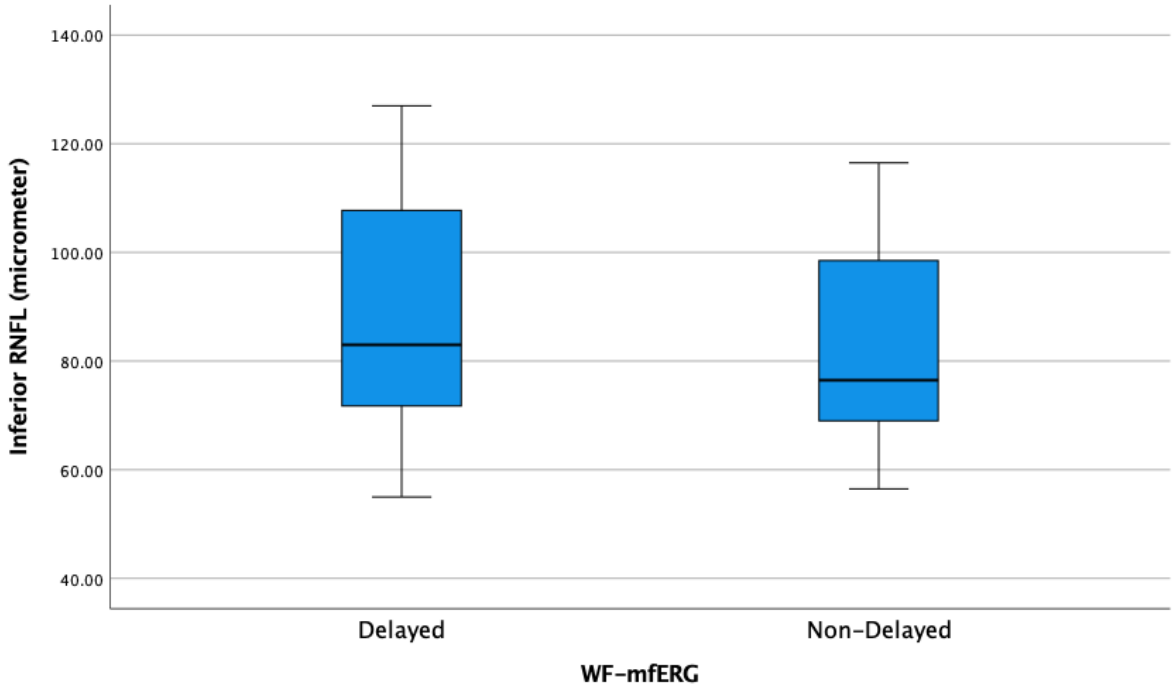

Figure 5.2.7: Boxplot demonstrating inferior RNFL thickness in both groups, p = 0.635

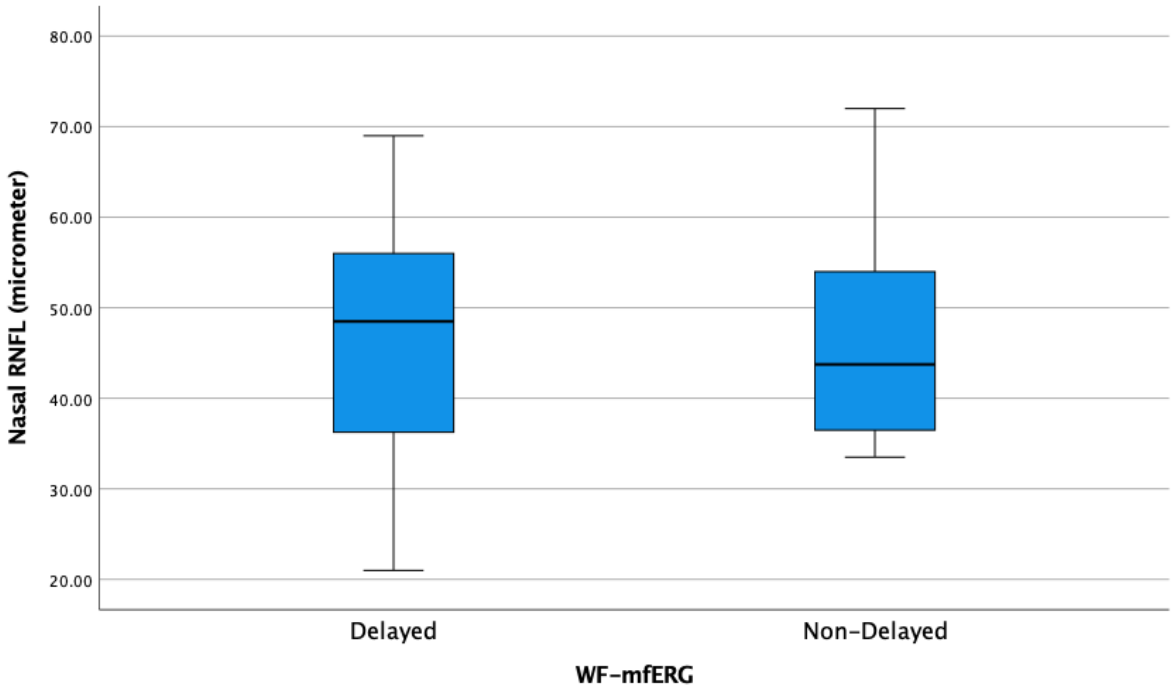

Figure 5.2.8: Boxplot demonstrating nasal RNFL thickness in both groups, p = 0.798.

ANOVA

		Sum of Squares	df	Mean Square	F	Sig.
Global RNFL (micrometer)	Between Groups	75.460	1	75.460	.375	.546
	Within Groups	4626.000	23	201.130		
	Total	4701.460	24			
Superior RNFL (micrometer)	Between Groups	20.729	1	20.729	.044	.836
	Within Groups	10930.271	23	475.229		
	Total	10951.000	24			
Temporal RNFL (micrometer)	Between Groups	742.283	1	742.283	7.654	.011
	Within Groups	2230.557	23	96.981		
	Total	2972.840	24			
Inferior RNFL (micrometer)	Between Groups	111.776	1	111.776	.231	.635
	Within Groups	11114.584	23	483.243		
	Total	11226.360	24			
Nasal RNFL (micrometer)	Between Groups	12.629	1	12.629	.067	.798
	Within Groups	4313.011	23	187.522		
	Total	4325.640	24			

Table 5.2.2: The results of the ANOVA comparison, based on RNFL thickness in both groups.

Quadrants	F-value	ANOVA significance, P value
Superior	0.044	0.836
Temporal	7.654	0.011*
Inferior	0.231	0.635
Nasal	0.067	0.798
Global	0.375	0.546

Table 5.2.3: Key statistical values, comparing p-values of RNFL quadrants between the delayed and non-delayed group.

In the RNFL thickness analysis, the temporal quadrant is found to be thicker in the Delayed group ($p<0.0001$, 95% CI, $t=6.688$). No significant results were found when comparing other quadrants.

Macula volume analysis

22 participants were included with 11 in the 2ms peripheral delay group versus 11 in the non-delay group. All subjects had macula volume scans, and the 1, 3, 6 mm concentric rings applied on the macula volume analysis software. Additional analysis was done through auto-segmentation of the retinal layers. The auto-segmented layers were visually inspected for accuracy prior to final analysis.

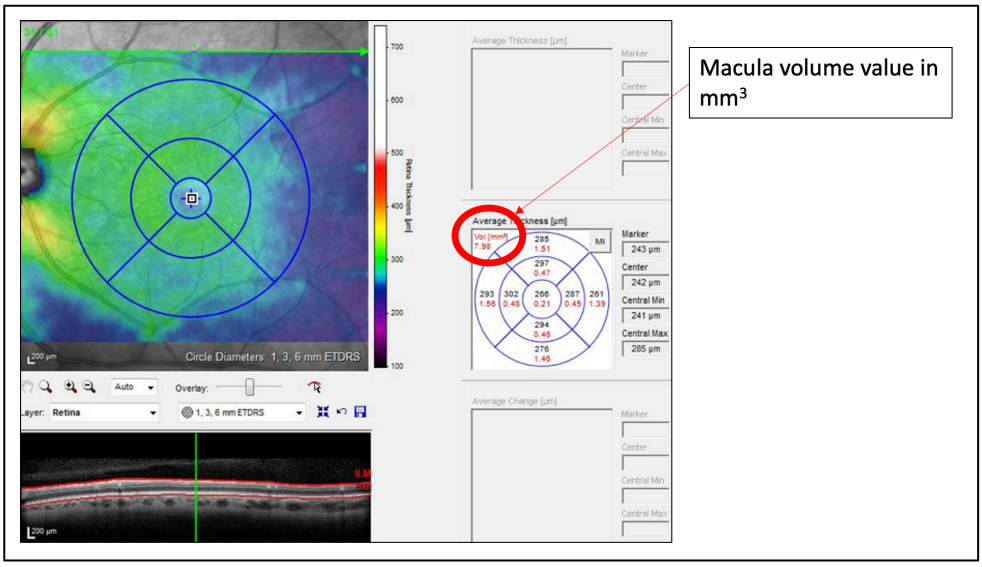

Figure 5.2.9: Macula volume measurements from the OCT, based on the 1, 3, 6mm concentric rings.

Descriptives

	WF-mfERG status			Statistic	Std. Error
Nerve fibre layer volume (mm3)	Delayed	Mean		.87591	.042221
		95% Confidence Interval for Mean	Lower Bound	.78183	
			Upper Bound	.96998	
		5% Trimmed Mean		.87212	
		Median		.86000	
		Variance		.020	
		Std. Deviation		.140032	
		Minimum		.705	
		Maximum		1.115	
		Range		.410	
		Interquartile Range		.245	
		Skewness		.765	.661
		Kurtosis		-.590	1.279
	Non-Delayed	Mean		.74818	.030423
		95% Confidence Interval for Mean	Lower Bound	.68039	
			Upper Bound	.81597	
		5% Trimmed Mean		.74354	
		Median		.74000	
		Variance		.010	
		Std. Deviation		.100903	
		Minimum		.625	
		Maximum		.955	
		Range		.330	
		Interquartile Range		.165	
		Skewness		.764	.661
		Kurtosis		.336	1.279
Ganglion cell layer volume (mm3)	Delayed	Mean		1.00591	.020625
		95% Confidence Interval for Mean	Lower Bound	.95995	
			Upper Bound	1.05186	
		5% Trimmed Mean		1.00823	
		Median		1.03500	
		Variance		.005	
		Std. Deviation		.068404	
		Minimum		.890	
		Maximum		1.080	
		Range		.190	
		Interquartile Range		.140	
		Skewness		-.545	.661
		Kurtosis		-1.332	1.279
	Non-Delayed	Mean		.90000	.020780
		95% Confidence Interval for Mean	Lower Bound	.85370	
			Upper Bound	.94630	
		5% Trimmed Mean		.89583	
		Median		.88500	
		Variance		.005	
		Std. Deviation		.068920	
		Minimum		.825	
		Maximum		1.050	
		Range		.225	
		Interquartile Range		.080	
		Skewness		1.155	.661
		Kurtosis		1.044	1.279
Inner plexiform layer volume (mm3)	Delayed	Mean		.83455	.014293
		95% Confidence Interval for Mean	Lower Bound	.80270	
			Upper Bound	.86639	
		5% Trimmed Mean		.83422	
		Median		.84500	
		Variance		.002	
		Std. Deviation		.047405	
		Minimum		.765	
		Maximum		.910	
		Range		.145	
		Interquartile Range		.090	
		Skewness		-.214	.661
		Kurtosis		-1.150	1.279
	Non-Delayed	Mean		.77091	.012735
		95% Confidence Interval for Mean	Lower Bound	.74253	
			Upper Bound	.79929	
		5% Trimmed Mean		.76879	
		Median		.76000	
		Variance		.002	
		Std. Deviation		.042239	
		Minimum		.710	
		Maximum		.870	
		Range		.160	
		Interquartile Range		.030	
		Skewness		1.174	.661
		Kurtosis		2.492	1.279

Inner nuclear layer volume (mm3)	Delayed	Mean		.99091	.021115
		95% Confidence Interval for Mean	Lower Bound	.94386	
			Upper Bound	1.03796	
		5% Trimmed Mean		.99073	
		Median		.95500	
		Variance		.005	
		Std. Deviation		.070029	
		Minimum		.880	
		Maximum		1.105	
		Range		.225	
		Interquartile Range		.115	
		Skewness		.337	.661
		Kurtosis		-.817	1.279
	Non-Delayed	Mean		.94227	.013856
		95% Confidence Interval for Mean	Lower Bound	.91140	
			Upper Bound	.97315	
		5% Trimmed Mean		.94086	
		Median		.95000	
		Variance		.002	
		Std. Deviation		.045955	
		Minimum		.875	
		Maximum		1.035	
		Range		.160	
		Interquartile Range		.075	
		Skewness		.388	.661
		Kurtosis		.315	1.279
Outer plexiform layer volume (mm3)	Delayed	Mean		.86500	.031866
		95% Confidence Interval for Mean	Lower Bound	.79400	
			Upper Bound	.93600	
		5% Trimmed Mean		.86167	
		Median		.85000	
		Variance		.011	
		Std. Deviation		.105688	
		Minimum		.750	
		Maximum		1.040	
		Range		.290	
		Interquartile Range		.220	
		Skewness		.709	.661
		Kurtosis		-1.059	1.279
	Non-Delayed	Mean		.78636	.015493
		95% Confidence Interval for Mean	Lower Bound	.75184	
			Upper Bound	.82088	
		5% Trimmed Mean		.78346	
		Median		.78000	
		Variance		.003	
		Std. Deviation		.051385	
		Minimum		.725	
		Maximum		.900	
		Range		.175	
		Interquartile Range		.085	
		Skewness		1.009	.661
		Kurtosis		1.071	1.279
Outer nuclear layer volume (mm3)	Delayed	Mean		1.87909	.031231
		95% Confidence Interval for Mean	Lower Bound	1.80950	
			Upper Bound	1.94868	
		5% Trimmed Mean		1.88121	
		Median		1.88000	
		Variance		.011	
		Std. Deviation		.103581	
		Minimum		1.700	
		Maximum		2.020	
		Range		.320	
		Interquartile Range		.175	
		Skewness		-.392	.661
		Kurtosis		-1.084	1.279
	Non-Delayed	Mean		1.61455	.061705
		95% Confidence Interval for Mean	Lower Bound	1.47706	
			Upper Bound	1.75203	
		5% Trimmed Mean		1.61283	
		Median		1.55000	
		Variance		.042	
		Std. Deviation		.204652	
		Minimum		1.290	
		Maximum		1.970	
		Range		.680	
		Interquartile Range		.185	
		Skewness		.663	.661
		Kurtosis		.362	1.279

Retinal pigment epithelium volume (mm3)	Delayed	Mean		.38636	.009320
		95% Confidence Interval for Mean	Lower Bound	.36560	
			Upper Bound	.40713	
		5% Trimmed Mean		.38596	
		Median		.38500	
		Variance		.001	
		Std. Deviation		.030910	
		Minimum		.340	
		Maximum		.440	
		Range		.100	
		Interquartile Range		.035	
		Skewness		.709	.661
		Kurtosis		.284	1.279
	Non-Delayed	Mean		.36818	.008265
		95% Confidence Interval for Mean	Lower Bound	.34977	
			Upper Bound	.38660	
		5% Trimmed Mean		.36854	
		Median		.37000	
		Variance		.001	
		Std. Deviation		.027411	
		Minimum		.325	
		Maximum		.405	
		Range		.080	
		Interquartile Range		.045	
		Skewness		-.222	.661
		Kurtosis		-.964	1.279
Inner Retinal Layers volume (mm3)	Delayed	Mean		6.45545	.091123
		95% Confidence Interval for Mean	Lower Bound	6.25242	
			Upper Bound	6.65849	
		5% Trimmed Mean		6.44884	
		Median		6.43000	
		Variance		.091	
		Std. Deviation		.302221	
		Minimum		6.070	
		Maximum		6.960	
		Range		.890	
		Interquartile Range		.460	
		Skewness		.583	.661
		Kurtosis		-.790	1.279
	Non-Delayed	Mean		5.76409	.065425
		95% Confidence Interval for Mean	Lower Bound	5.61832	
			Upper Bound	5.90987	
		5% Trimmed Mean		5.76816	
		Median		5.74000	
		Variance		.047	
		Std. Deviation		.216989	
		Minimum		5.380	
		Maximum		6.075	
		Range		.695	
		Interquartile Range		.380	
		Skewness		-.051	.661
		Kurtosis		-.735	1.279
Outer Retinal Layers volume (mm3)	Delayed	Mean		2.22636	.021225
		95% Confidence Interval for Mean	Lower Bound	2.17907	
			Upper Bound	2.27366	
		5% Trimmed Mean		2.22374	
		Median		2.21000	
		Variance		.005	
		Std. Deviation		.070395	
		Minimum		2.140	
		Maximum		2.360	
		Range		.220	
		Interquartile Range		.125	
		Skewness		.752	.661
		Kurtosis		-.475	1.279
	Non-Delayed	Mean		2.17909	.014860
		95% Confidence Interval for Mean	Lower Bound	2.14598	
			Upper Bound	2.21220	
		5% Trimmed Mean		2.17871	
		Median		2.18500	
		Variance		.002	
		Std. Deviation		.049286	
		Minimum		2.095	
		Maximum		2.270	
		Range		.175	
		Interquartile Range		.070	
		Skewness		.273	.661
		Kurtosis		.134	1.279

Table 5.2.4: Descriptive statistics for macula OCT microlayers for the delayed and non-delayed group.

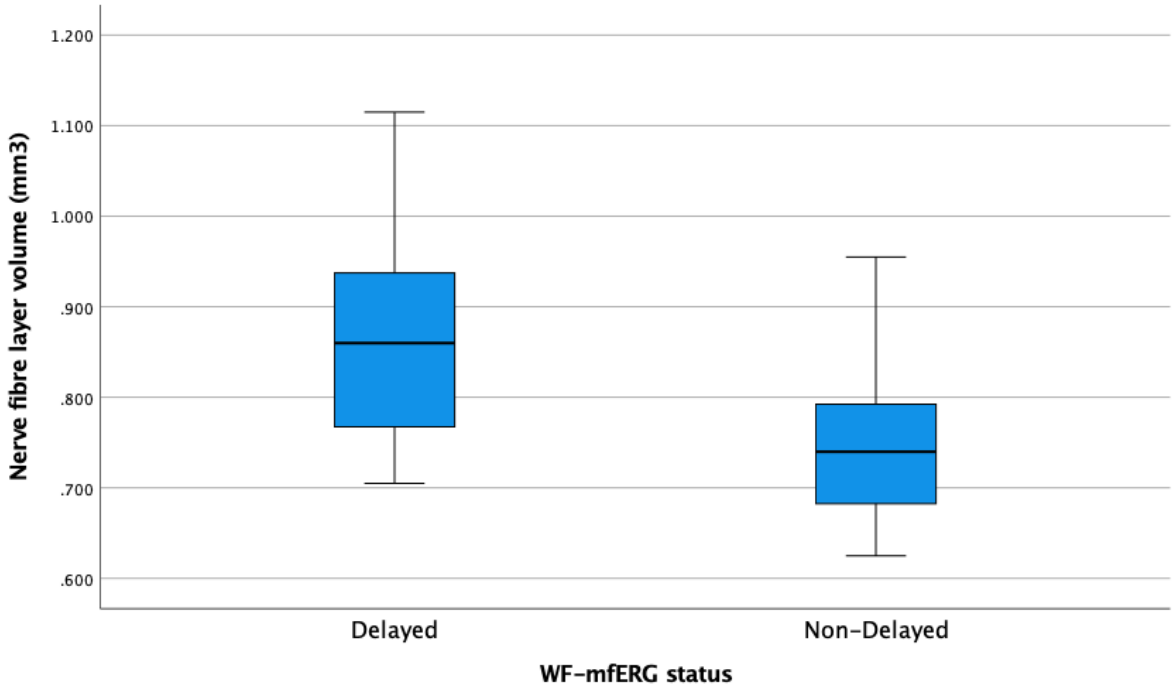

Figure 5.2.10: Boxplot demonstrating nerve fibre layer volume in both groups, $p<0.05$

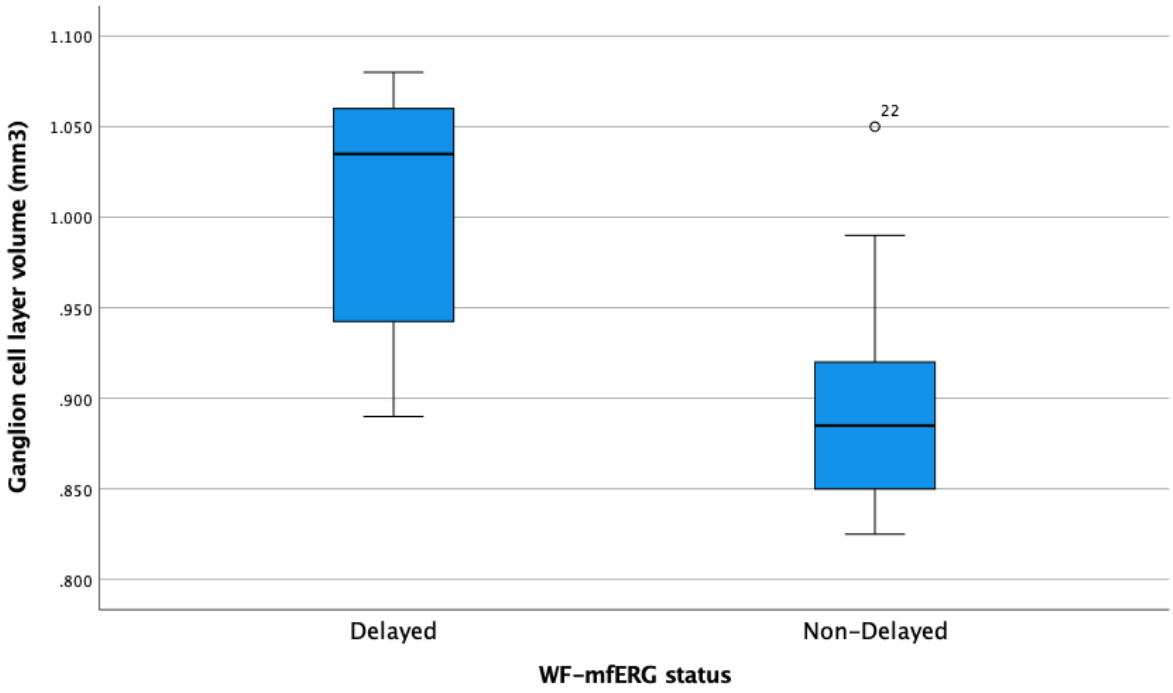

Figure 5.2.11 Boxplot demonstrating ganglion cell layer volume in both groups, p<0.05

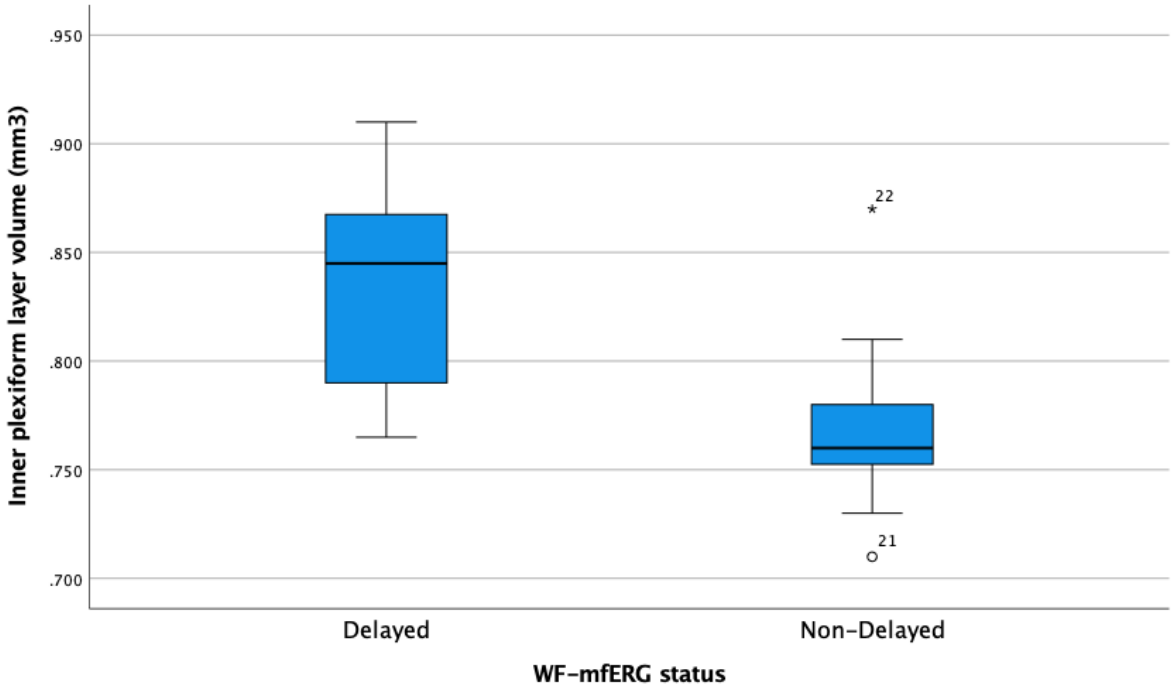

Figure 5.2.12 Boxplot demonstrating inner plexiform layer volume in both groups, p<0.05

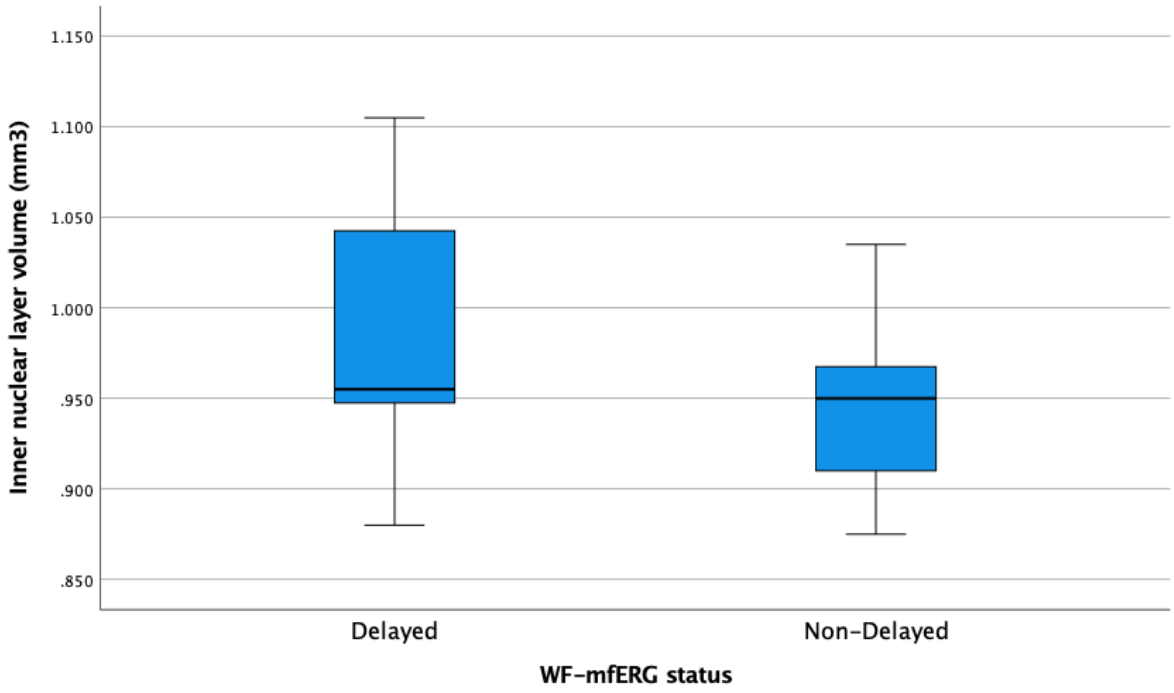

Figure 5.2.13 Boxplot demonstrating inner nuclear layer volume in both groups, p = 0.068

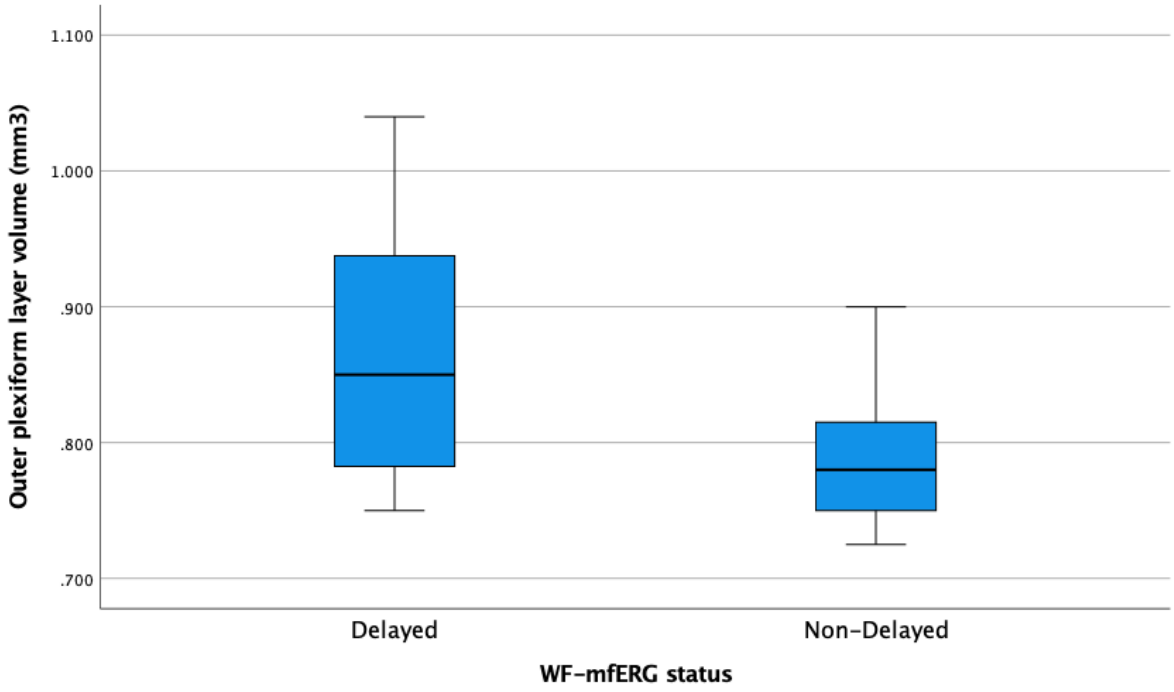

Figure 5.2.14 Boxplot demonstrating outer plexiform layer volume in both groups, p<0.05

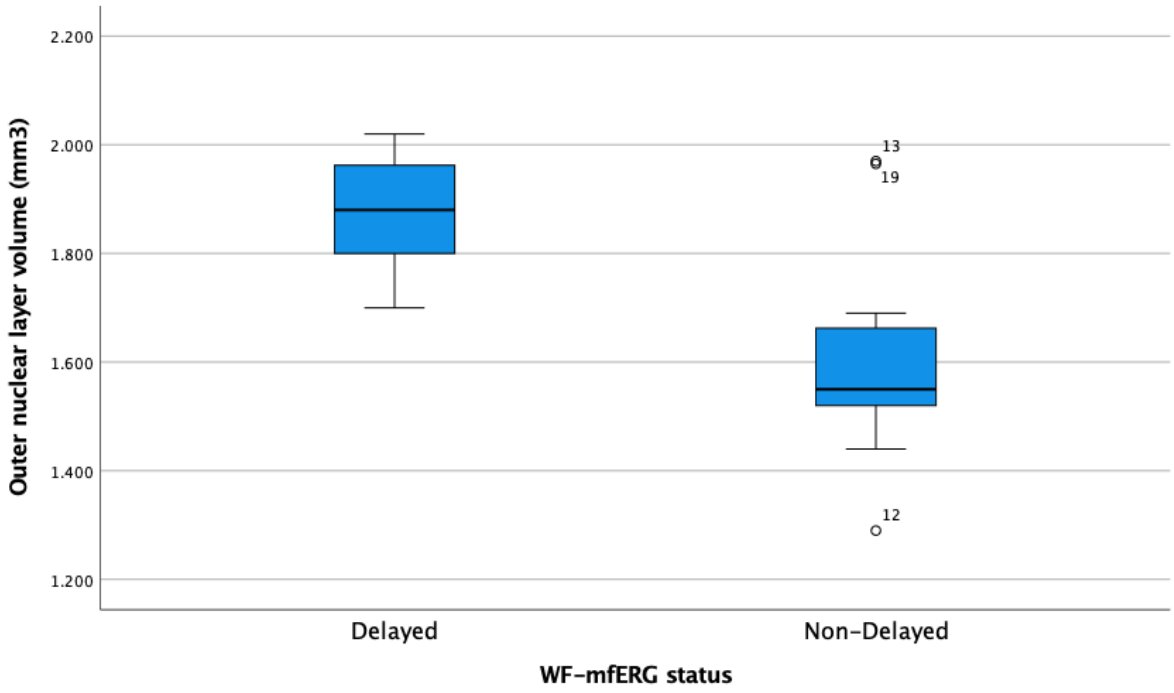

Figure 5.2.15 Boxplot demonstrating outer nuclear layer volume in both groups, p<0.05

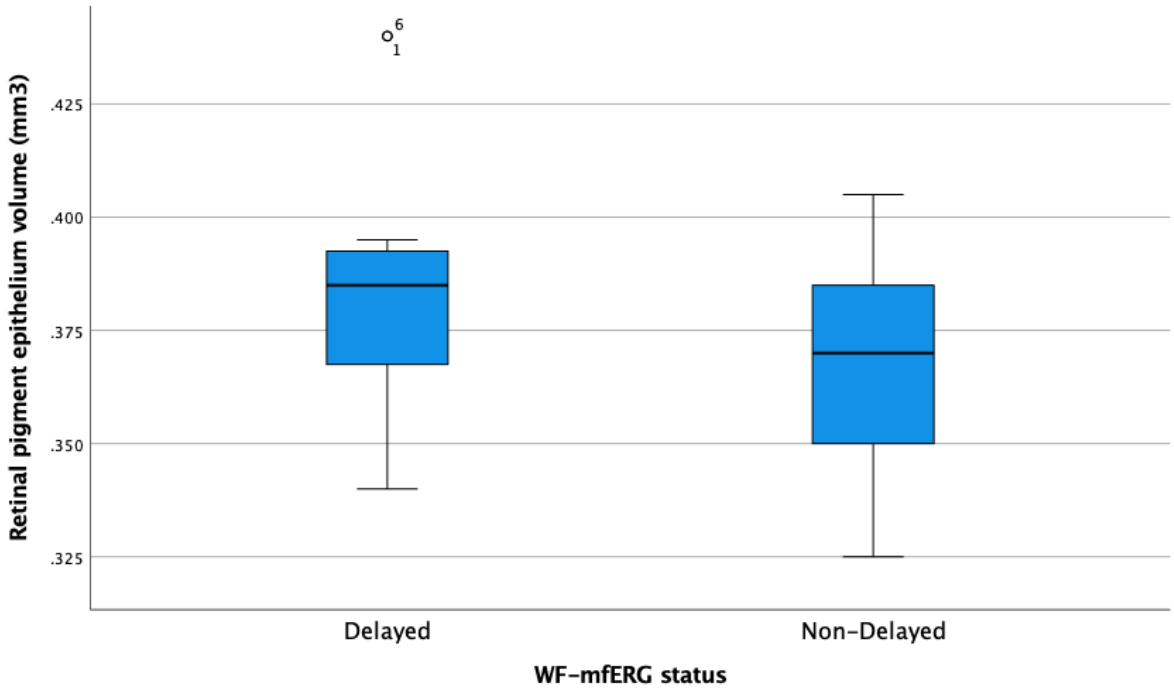

Figure 5.2.16 Boxplot demonstrating retinal pigment epithelium volume in both groups, p = 0.16

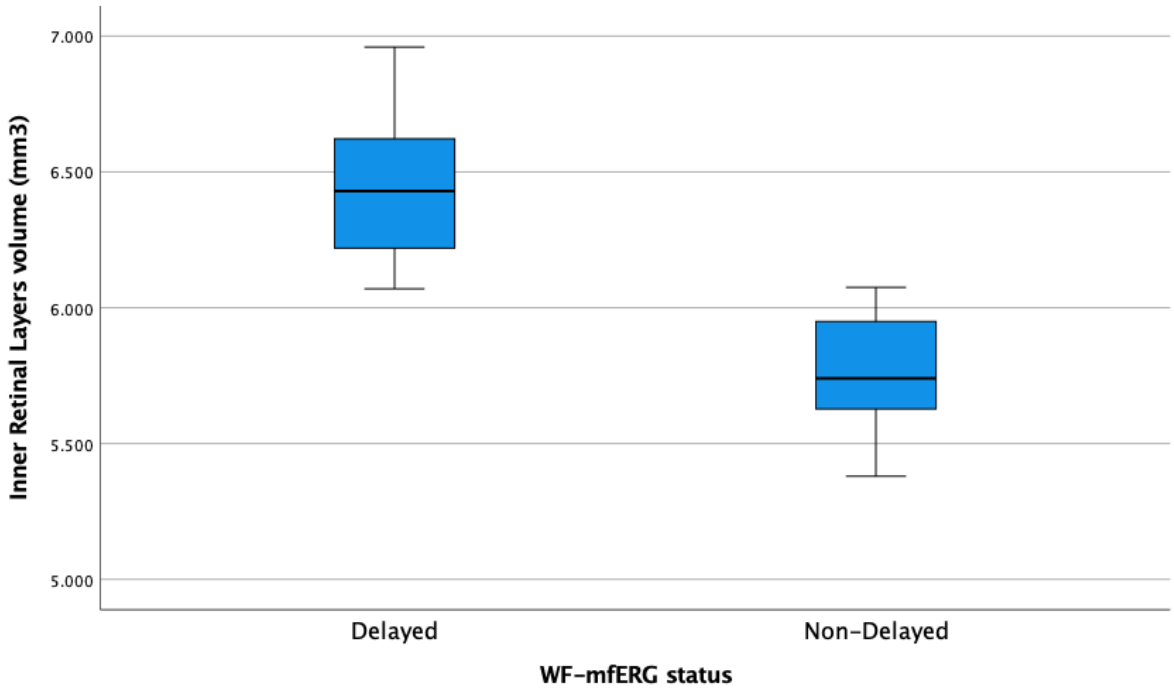

Figure 5.2.17 Boxplot demonstrating inner retinal macrolayer volume in both groups, $p<0.05$

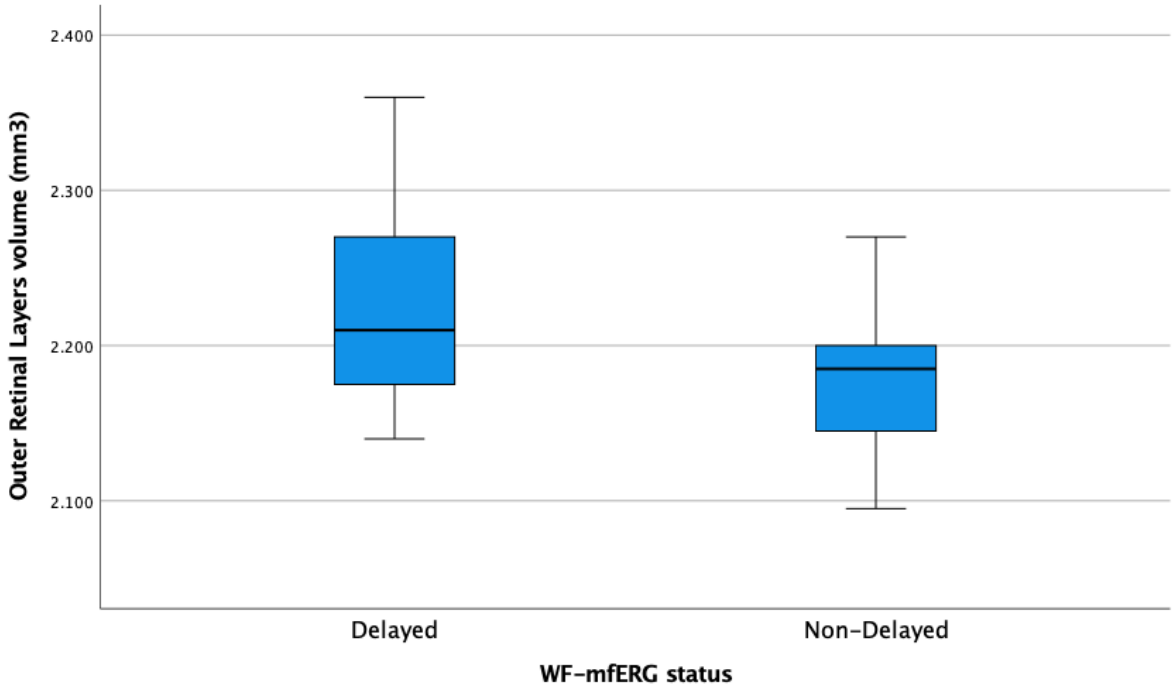

Figure 5.2.18 Boxplot demonstrating outer retinal macrolayers volume in both groups, $p = 0.083$

Macula volume comparison between the Delayed vs Non-delayed group

ANOVA

		Sum of Squares	df	Mean Square	F	Sig.
Nerve fibre layer volume (mm3)	Between Groups	.090	1	.090	6.024	.023
	Within Groups	.298	20	.015		
	Total	.388	21			
Ganglion cell layer volume (mm3)	Between Groups	.062	1	.062	13.085	.002
	Within Groups	.094	20	.005		
	Total	.156	21			
Inner plexiform layer volume (mm3)	Between Groups	.022	1	.022	11.050	.003
	Within Groups	.040	20	.002		
	Total	.063	21			
Inner nuclear layer volume (mm3)	Between Groups	.013	1	.013	3.709	.068
	Within Groups	.070	20	.004		
	Total	.083	21			
Outer plexiform layer volume (mm3)	Between Groups	.034	1	.034	4.925	.038
	Within Groups	.138	20	.007		
	Total	.172	21			
Outer nuclear layer volume (mm3)	Between Groups	.385	1	.385	14.632	.001
	Within Groups	.526	20	.026		
	Total	.911	21			
Retinal pigment epithelium volume (mm3)	Between Groups	.002	1	.002	2.130	.160
	Within Groups	.017	20	.001		
	Total	.019	21			
Inner Retinal Layers volume (mm3)	Between Groups	2.629	1	2.629	37.984	<.001
	Within Groups	1.384	20	.069		
	Total	4.013	21			
Outer Retinal Layers volume (mm3)	Between Groups	.012	1	.012	3.329	.083
	Within Groups	.074	20	.004		
	Total	.086	21			

Table 5.2.5: The ANOVA comparison between both groups, based on retinal microlayers

Microlayers	Delayed	Non-delayed	p-values
Nerve fibre	0.876	0.748	0.023
Ganglion cell	1.006	0.900	0.002
Inner Plexiform	0.835	0.771	0.003
Inner Nuclear	0.991	0.942	0.068
Outer Plexiform	0.865	0.786	0.038
Outer nuclear	1.879	1.615	0.001
RPE	0.386	0.368	0.160
Inner retinal	6.455	5.764	<0.001
Outer retinal	2.226	2.179	0.083

Table 5.2.6: Key statistical value, highlighting mean (mm^3) and the significance where statistically significant results are printed in red.

When analysing the macula volume, the Delayed group had higher macula volume compared to the non-delayed group ($p<0.001$, 95% CI, $t=6.456$), and this was further localised to the 3 segments within the inner retinal layer ($p<0.001$, 95%CI, $t=6.163$); ganglion cell layer ($p<0.01$, 95% CI, $t=3.617$), Inner plexiform layer ($p<0.01$, 95% CI, $t=3.324$) and Outer nuclear layer ($p<0.01$, 95% CI, $t=3.825$).

Discussion:

In the early days of vigabatrin toxicity, the reported eye findings are mainly degenerative in nature such as optic atrophy (Ravindran *et al.*, 2001b) (Buncic *et al.*, 2004), chrorioretinal atrophy (Sorri *et al.*, 2010), RNFL attenuation and thinning (Lawthom, Smith and Wild, 2009)(Clayton *et al.*, 2013)(Peng *et al.*, 2017)(Wild *et al.*, 2006) . Sills et al (2001) had demonstrated the accumulation of vigabatrin in the retina, believing that site of vigabatrin related toxicity is within the retinal tissue itself. Severe disorganisation of the ganglion cell layer has been reported as well as disruption in the outer nuclear layer (Wang *et al.*, 2008)(Duboc *et al.*, 2004).

More recently, Sergott et al, Tügcu et al and Foroozan reported increased tissue thickness in patients exposed to Vigabatrin, although the clinical significance has not been fully accounted for(Sergott *et al.*, 2016b)(Tuğcu *et al.*, 2017)(Foroozan, 2018). Referring to our earlier studies, 2ms delay in the peripheral retinal responses was found to be highly specific in identifying vigabatrin associated retinal toxicity, separating this group from those with visual field loss from other causes (McDonagh *et al.*, 2003b). This was further confirmed in a larger study involving 202 patients by Gonzalez et al(Gonzalez *et al.*, 2009). With the benefit of high-resolution images from the OCT, our results demonstrated that those in the peripheral delay group had thicker temporal quadrants in the RNFL measurements. Foroozan et al reported similar findings in most of his patients exposed to Vigabatrin, compared to their own baseline after 1 year.

How does it compare with retinal histopathological reports in Vigabatrin toxicity?

When analysing the macula volume, the difference in the macula volume between the 2 groups achieved statistical significance, which was followed through by further subanalysis showing the most distinct change in the ganglion cell layer, inner plexiform layer and outer nuclear layer. One of the striking observations in this study is how the general morphology of the retina does not appear to be affected, and the disruption to the ONL, IPL and the RGC is only revealed when compared for analysis.

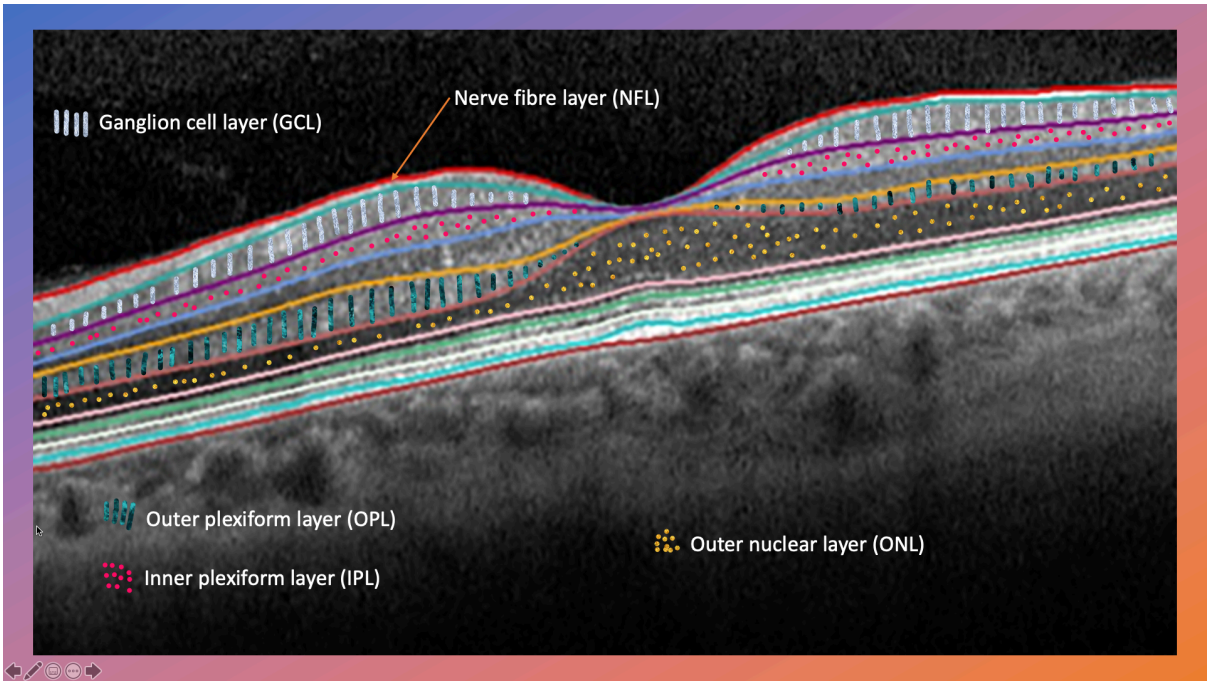

Figure 5.2.19 Auto-segmentation of macula microstructures, with the affected layers annotated

Looking at our results, generally all layers (except the RPE) show that they may have been affected to some degree, although this is much more pronounced in the 5 layers outlined above. The ganglion cell layer and the outer nuclear layer contain nuclei of cells

as a common entity. One can argue that possibly the distal component of the ganglion cell within the IPL is primarily affected explaining our observation of IPL involvement.

The changes detected from this study point towards the possibility of damage which predominantly occur in the ONL, IPL and the RGC. These findings are consistent with histopathological reports of VGB treated mice and rats, where the disorganisation of the ONL layer and changes to the RGC has been reported. Although our cohort has been investigated by the OCT instead of conventional histopathological analysis, our findings are in agreement with reports of widespread cellular changes that occurs without change in the general retinal morphology (Duboc *et al.*, 2004; Wang *et al.*, 2008; Foroozan, 2018).

As mentioned above, our centre's earlier publications by Gonzalez et al and McDonagh et al had exclusively pointed out 2ms delay in the peripheral field responses compared to central responses in the WF-mfERG to be relevant in our study of vigabatrin related toxicity, although no explanation was elucidated at the time. By using this specific finding in the WF-mfERG results as a discriminatory feature to differentiate between Vigabatrin and non-vigabatrin changes has provided us with statistically significant results that reassures us that OCT microstructures volume examination could be used to monitor and detect vigabatrin related toxicity in patients.

How do we explain peripheral, rather than central visual loss?

How do we explain and correlate our findings from the macula region to the observed peripheral visual field loss seen in this group of patients? We theorise that it is likely that peripheral visual loss that has been observed is due to naturally thinner retinal bulk in the periphery, with therefore less tissue reserve compared to the macula, causing subsequent loss of function. Although we cannot find any published evidence for this, our current knowledge of the gradual thinning of retinal tissue as it stretches towards the periphery would be in line with this theory. The advancement of OCT technology has seen that the ultra widefield OCT now being available and could potentially provide as a promising direction for future research especially in this cohort. We believe that our observation in this study from the macula region provide important clues on the structural state of the peripheral retina. As the peripheral retina is deemed thinner, with reduced retinal cell density, there is subsequently modest tissue reserve unable to maintain normal visual function when there is a damaging mechanism at play.

Conclusion:

The toxic effects of Vigabatrin in humans have been studied mainly from the form of the retinal function rather than retinal histopathology and physiology. Where human histopathological studies are rare, the advancement of the OCT allowing closed and detailed examination of the retinal microstructures has allowed us the advantage of non-invasive histological examination of the retina. This is also the first time specific retinal microstructures have been highlighted to be the likely site of damage from vigabatrin in humans. This gives us some confidence in our search for a reliable and

practical tool such as the OCT could be used in the assessment and monitoring of VGB related toxicity.

CHAPTER 5.3: EXPERIMENTAL WORK

THE RELATIONSHIP BETWEEN OCT RETINAL MICROSTRUCTURES AND RNFL TO VISUAL FIELDS IN VIGABATRIN TREATED PATIENTS

Aim:

The aim of this study is to evaluate the relationship between OCT retinal structure and visual fields in Vigabatrin patients. The main difference between this experiment and the previous is that here we attempt to draw some structure-function correlation between the OCT microlayers and the corresponding visual fields.

Method:

All patients underwent full ocular examination prior to inclusion into this study. Visual acuity, pupil examination and slit lamp examination which includes intraocular pressure measurements, anterior segment examination and dilated fundoscopy. The visual fields were assessed with the Humphrey 120-point suprathreshold, three-zone static perimetry test using the Humphrey Field Analyzer (Carl Zeiss, Meditec, Dublin CA, USA).

Perimetry results are included for further study analysis only if subsequent review of case notes met the inclusion criteria. As part of the larger study, all subjects have also

undergone multifocal electrophysiological examination, blood tests and optical coherence tomography. The WF-mfERG responses were assessed with respect to the amplitude and latency (implicit time) of individual response element. Multifocal electrophysiology results are interpreted by two clinical scientists with total combined duration of 35 years' experience in the subject.

Subjects who have completed visual field tests and OCT scans at the same visit are considered for inclusion. The visual fields results were only included for further analysis if they met minimum reliability index (<20% fixation loss), displayed bilateral symmetrical and concentric field loss. Visual field test are inspected separately and assigned a ***z*** score (see below)

Perimetry Score

Each visual fields is assigned a perimetry score of z, only if they met the inclusion criteria related to Vigabatrin associated visual field loss. A higher z score indicate that the subject has the respective number of stimuli, therefore less peripheral constriction. The z score is then tabulated alongside the respective value from the OCT scans.
(Background on perimetry score is explained on page 114)

OCT scan

The scanning protocol is described in detail in chapter 2. For the OCT RNFL, a circular line scan of 3.4mm centred on the optic nerve head is captured. For macula volume scans, 25-line raster scans covering 6mm x 6mm is used. The auto-segmentation

protocol is inbuild as part of the SPECTRALIS software. Poor quality images are excluded from further analysis.

Data analysis

OCT data in the form of microlayer volume (units = micrometer^3 or μm^3) and optic disc nerve fibre layer thickness (unit = micrometer or μm) is paired with a z value, which represent visual fields from the corresponding eye. In the first stage, all the data pairs will be analysed together for correlation. In the second stage, only data from the Delayed group will be analysed for the same correlation as in stage 1.

All statistical analysis were performed using the SPSS (IBM® SPSS® Statistics, version 27). In all analysis, the dependent and independent variables are defined. Perimetry score is the dependent variable, expressed as an absolute number to signify ***z***/120 (120 to reflect the total number of stimulus points on the perimetry test). OCT values are regarded as the independent variable and expressed in micrometer (μm). Prior to analysis, each dataset was checked for outliers by determining the residuals/standard error value.

The statistical analysis performed is simple linear regression for each of the independent variables, for all subjects. Each dataset is tested using simple linear regression, with graphical representation of the data spread, the linear regression equation and best-fit line and p value to determine the significance of the overall model. R_2 and 'adjusted R_2' is expressed to illustrate the variability of the dependent dataset. As part of the linear

regression calculation, the ANOVA is employed at each analysis. A *P* value less than 0.05 was considered statistically significant throughout.

Results:

OCT macula microstructures analysis

NEW ID	Z SCORE	NFL	GCL	IPL	INL	OPL	ONL	RPE	IRL	ORL
A1	42	0.77	0.89	0.76	0.89	0.84	1.53	0.39	5.67	2.22
B1	19	0.74	0.91	0.76	0.94	0.76	1.95	0.4	6.08	2.27
B2	38	0.71	0.86	0.76	0.97	0.77	1.99	0.41	6.07	2.27
C2	87	0.67	0.88	0.74	1	0.78	1.66	0.4	5.66	2.24
D1	108	0.74	0.83	0.75	0.93	0.9	1.44	0.38	5.59	2.21
E1	36	1.17	1.03	0.84	1.06	0.75	1.7	0.39	6.55	2.16
E2	38	1.03	1.06	0.88	0.99	0.77	1.7	0.38	6.43	2.16
F1	60	0.74	0.83	0.71	0.86	0.75	1.45	0.33	5.33	2.19
F2	53	0.74	0.82	0.71	0.89	0.72	1.56	0.32	5.43	2.18
G1	67	0.79	1.03	0.88	0.94	0.79	1.89	0.36	6.32	2.18
G2	54	0.73	1.04	0.86	0.95	0.77	1.87	0.36	6.22	2.2
H1	51	0.91	0.95	0.77	0.96	0.78	1.87	0.38	6.23	2.15
H2	45	0.83	0.92	0.76	0.94	0.79	1.87	0.39	6.12	2.19
L1	83	0.83	1.08	0.87	0.96	0.9	1.79	0.4	6.42	2.25
L2	81	0.9	1.07	0.86	0.94	0.85	1.82	0.39	6.44	2.17
M1	75	1.01	1.04	0.85	1.04	1.06	1.97	0.37	6.96	2.23
M2	52	1	0.99	0.84	1.08	1.02	1.97	0.35	6.96	2.22
O1	99	0.86	1.1	0.91	1	0.83	2	0.45	6.71	2.28
O2	90	0.81	1.05	0.91	1	0.87	1.94	0.43	6.58	2.31
P1	43	0.74	0.91	0.78	1.1	0.81	1.8	0.44	6.14	2.36
P2	50	0.67	0.87	0.77	1.07	0.91	1.71	0.44	6	2.36
Q1	118	0.77	1.04	0.86	0.94	0.98	1.95	0.38	6.54	2.3
Q2	118	0.78	1.04	0.88	0.97	1.02	1.96	0.38	6.66	2.33

Table 5.3.1: OCT macula: Raw data for all included subjects. Green cells indicate data from subjects with no timing delay from their WF-mfERG, yellow cells indicate data from subjects with >2ms delay in their WF-mfERG. Data under the columns of NFL, GCL, IPL, INL, OPL, ONL, RPE, IRL and ORL are in micrometer^3 or µm^3.

23 Visual fields with accompanying macula scans were available for analysis. 16 were from subjects with >2ms timing delay (hereon referred to as the Delayed group), 7 were from subjects who did not have >2ms timing delay.

In the first stage of analysis, all 23 subjects are included irrespective of their WF-mfERG results. In the second analysis, only those in the Delayed group (n=16) are included.

Nerve Fibre layer (NFL)

The linear regression equation is:

y=94.68-35.41*x,
where R_2 = 0.026

This model is not statistically significant, where F (1,21) = 0.562, p = 0.462. The adjusted R_2 value is -0.20 which means none of the data variability can be explained by this model. The null hypothesis is accepted here, where NFL volume does not predict z scores.

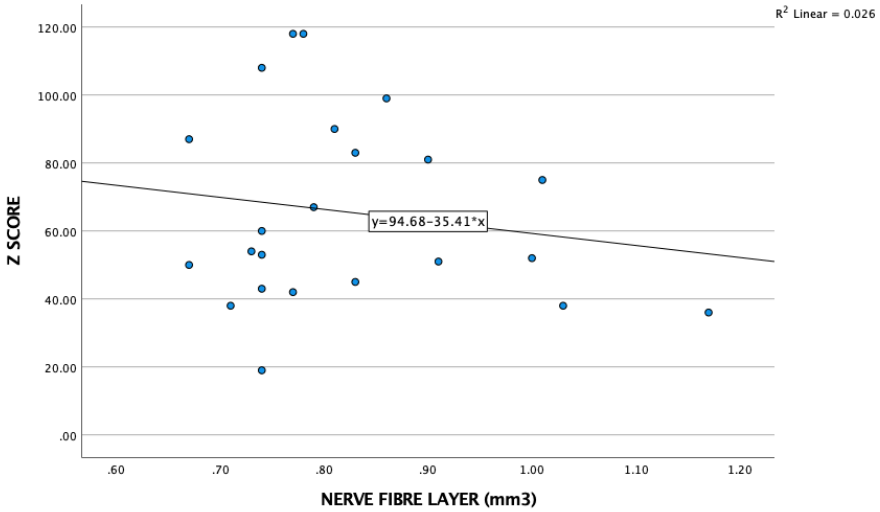

Figure 5.3.1: Scatter plot graph demonstrating relationship between nerve fibre layer and z score, p = 0.462.

Model Summary

Model	R	R Square	Adjusted R Square	Std. Error of the Estimate
1	.161[a]	.026	-.020	28.17595

a. Predictors: (Constant), NERVE FIBRE LAYER

ANOVA[a]

Model		Sum of Squares	df	Mean Square	F	Sig.
1	Regression	446.176	1	446.176	.562	.462[b]
	Residual	16671.563	21	793.884		
	Total	17117.739	22			

a. Dependent Variable: Z SCORE

b. Predictors: (Constant), NERVE FIBRE LAYER

Table 5.3.2: Key statistical values analysing relationship between Nerve fibre layer volume to z score.

Ganglion cell layer (GCL)

The calculated linear regression equation here is:

Y=-33.01+1.02*x,
where R_2 = 0.115

This model is not statistically significant, where F (1,21) = 2.717, p = 0.114. The adjusted R_2 value is 0.72, which means 7% of the data variability can be explained by this model.

The null hypothesis is accepted here, where GCL volume does not predict z score.

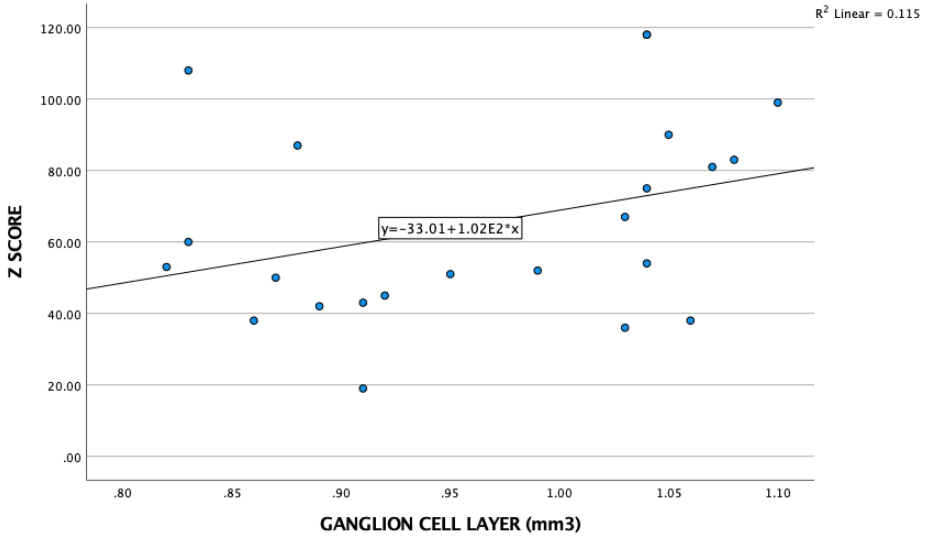

Figure 5.3.2: Scatter plot graph demonstrating relationship between ganglion cell layer and z score, p = 0.114.

Model Summary[b]

Model	R	R Square	Adjusted R Square	Std. Error of the Estimate
1	.338[a]	.115	.072	26.86530

a. Predictors: (Constant), GANGLION CELL LAYER

b. Dependent Variable: Z SCORE

ANOVA[a]

Model		Sum of Squares	df	Mean Square	F	Sig.
1	Regression	1961.113	1	1961.113	2.717	.114[b]
	Residual	15156.626	21	721.744		
	Total	17117.739	22			

a. Dependent Variable: Z SCORE

b. Predictors: (Constant), GANGLION CELL LAYER

Table 5.3.3 Key statistical values analysing relationship between ganglion cell layer volume and z score.

Inner Plexiform Layer (IPL)

The calculated linear regression equation here is:

Y = -77.92 + 176x,

where R_2 = 0.166

This model is not statistically significant, where F (1,21) = 4.187, p = 0.053. The adjusted R_2 value is 0.127, which means 13% of the data variability can be explained by this model. The null hypothesis is accepted here, where IPL volume does not predict z scores.

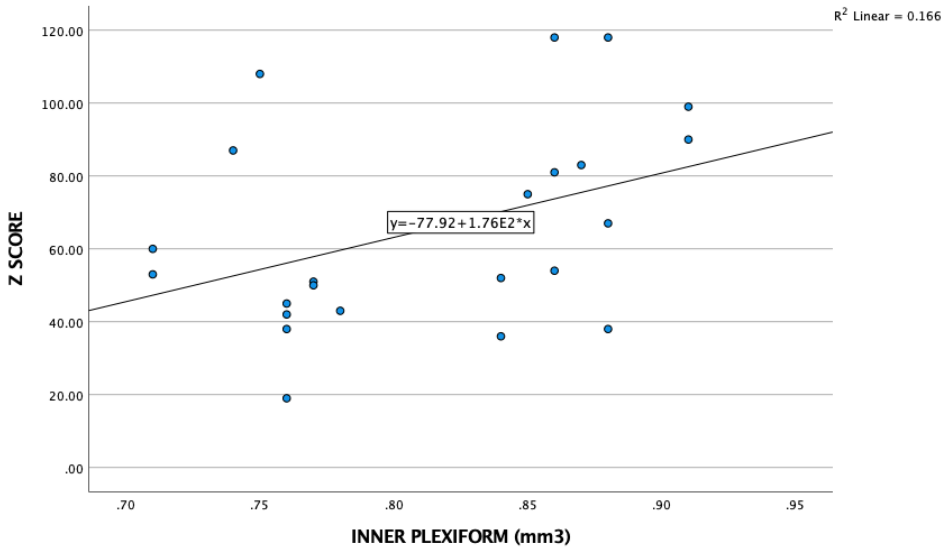

Figure 5.3.3: Scatter plot graph demonstrating relationship between inner plexiform layer and z score, p = 0.053.

Model Summary[b]

Model	R	R Square	Adjusted R Square	Std. Error of the Estimate
1	.408[a]	.166	.127	26.06954

a. Predictors: (Constant), INNER PLEXIFORM

b. Dependent Variable: Z SCORE

ANOVA[a]

Model		Sum of Squares	df	Mean Square	F	Sig.
1	Regression	2845.701	1	2845.701	4.187	.053[b]
	Residual	14272.039	21	679.621		
	Total	17117.739	22			

a. Dependent Variable: Z SCORE

b. Predictors: (Constant), INNER PLEXIFORM

Table 5.3.4 Key statistical values analysing the relationship between inner plexiform layer volume and z score.

Inner Nuclear layer (INL)

The calculated linear regression equation here is:

Y = 113-48.82x,
where R_2 = 0.012.

This model is not statistically significant, where F (1,21) = 0.255, p = 0.619. The adjusted R_2 value here is -0.35, which means none of the data variability can be explained by the model. The null hypothesis is accepted in this dataset where the INL volume does not predict z score.

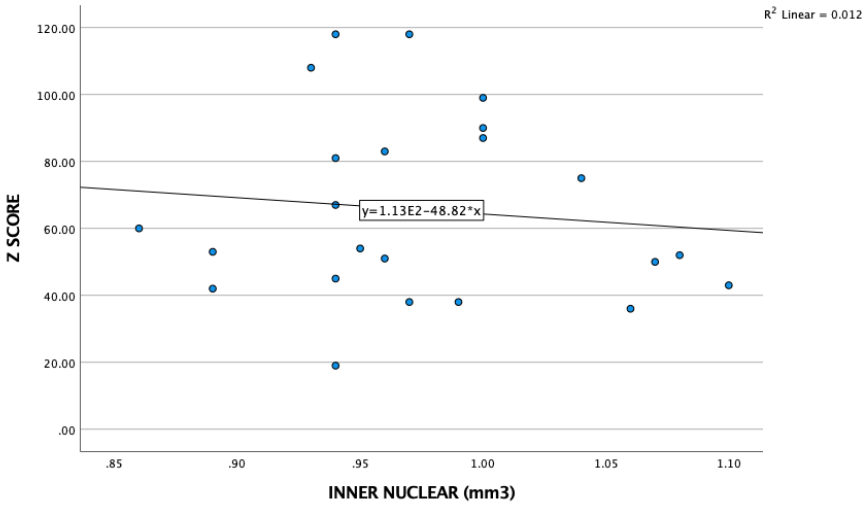

Figure 5.3.4: Scatter plot graph demonstrating relationship between inner nuclear layer volume and z score, p = 0.619.

Model Summary[b]

Model	R	R Square	Adjusted R Square	Std. Error of the Estimate
1	.110[a]	.012	-.035	28.37866

a. Predictors: (Constant), INNER NUCLEAR

b. Dependent Variable: Z SCORE

ANOVA[a]

Model		Sum of Squares	df	Mean Square	F	Sig.
1	Regression	205.423	1	205.423	.255	.619[b]
	Residual	16912.316	21	805.348		
	Total	17117.739	22			

a. Dependent Variable: Z SCORE

b. Predictors: (Constant), INNER NUCLEAR

Table 5.3.5 Key statistical values analysing the relationship between inner nuclear layer volume and z score.

Outer Plexiform layer (OPL)

The calculated linear regression equation here is:

Y = -69.97 +160x,
where R_2 = 0.316

This model is statistically significant, where F (1,21) = 9.723, p < 0.05. The adjusted R_2 value in this calculation is 0.284, where 28% of variability in the data can be explained by this R model. The null hypothesis is rejected in this model, where the OPL volume predicts z score.

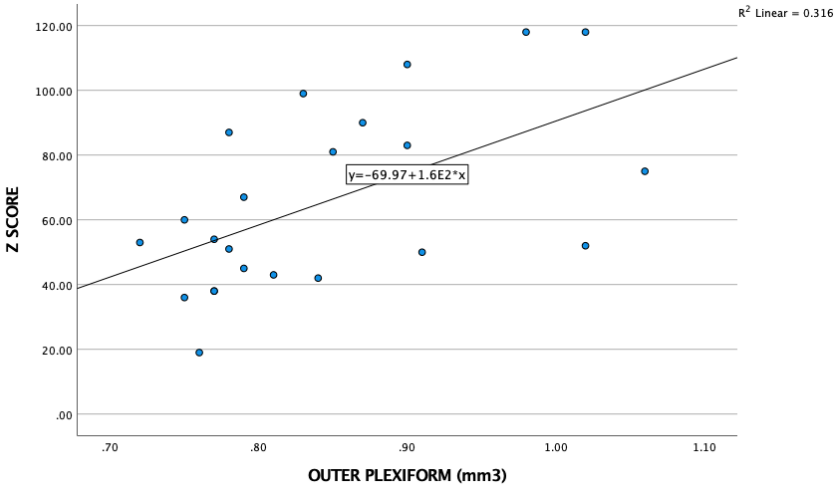

Figure 5.3.5: Scatter plot graph demonstrating relationship between outer plexiform layer and z score, p<0.05.

Model Summary[b]

Model	R	R Square	Adjusted R Square	Std. Error of the Estimate
1	.563[a]	.316	.284	23.60442

a. Predictors: (Constant), OUTER PLEXIFORM

b. Dependent Variable: Z SCORE

ANOVA[a]

Model		Sum of Squares	df	Mean Square	F	Sig.
1	Regression	5417.202	1	5417.202	9.723	.005[b]
	Residual	11700.537	21	557.168		
	Total	17117.739	22			

a. Dependent Variable: Z SCORE

b. Predictors: (Constant), OUTER PLEXIFORM

Table 5.3.6 Key statistical values analysing the relationship between outer plexiform layer volume and z score.

Outer nuclear layer (ONL)

The calculated linear regression equation here is:

Y = 37.39 + 15.63x,
where R_2 = 0.01

This model is not statistically significant, where F (1,21) = 0.205, p = 0.655. The adjusted R_2 value is -0.037, which means none of the data variability is predicted by this model. The null hypothesis is accepted in this dataset where ONL volume does not predict z scores.

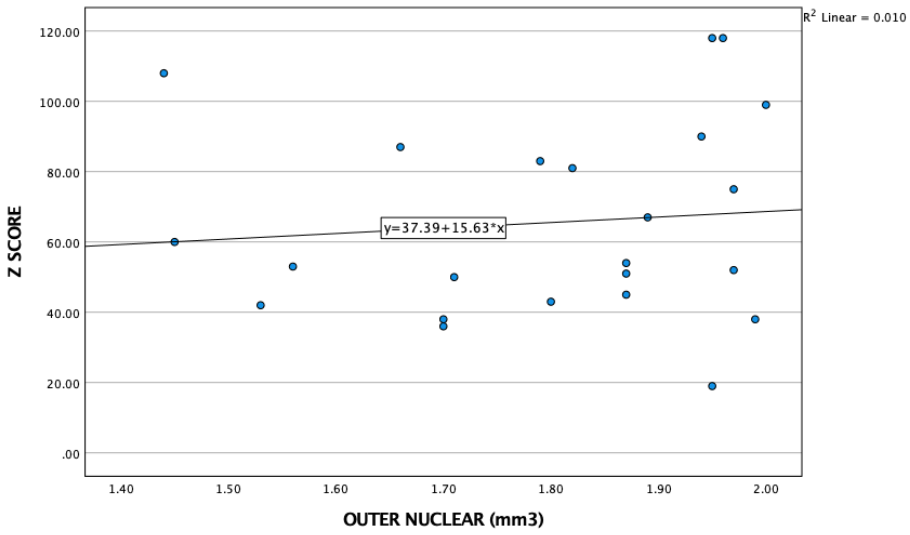

Figure 5.3.6: Scatter plot graph demonstrating relationship between outer nuclear layer and z score, p = 0.655.

Model Summary[b]

Model	R	R Square	Adjusted R Square	Std. Error of the Estimate
1	.098[a]	.010	-.037	28.41201

a. Predictors: (Constant), OUTER NUCLEAR

b. Dependent Variable: Z SCORE

ANOVA[a]

Model		Sum of Squares	df	Mean Square	F	Sig.
1	Regression	165.648	1	165.648	.205	.655[b]
	Residual	16952.092	21	807.242		
	Total	17117.739	22			

a. Dependent Variable: Z SCORE

b. Predictors: (Constant), OUTER NUCLEAR

Table 5.3.7 Key statistical values analysing the relationship between outer nuclear layer volume and z score.

Retinal Pigment Epithelium (RPE)

The calculated linear regression equation here is:

Y = 44.71 + 53.67x,
where R_2 = 0.004.

This model is not statistically significant, where F (1,21) = 0.084, p = 0.775. The adjusted R_2 value is -0.043 which means none of the data variability is explained by this model.

The null hypothesis is accepted here where RPE volume does not predict z score.

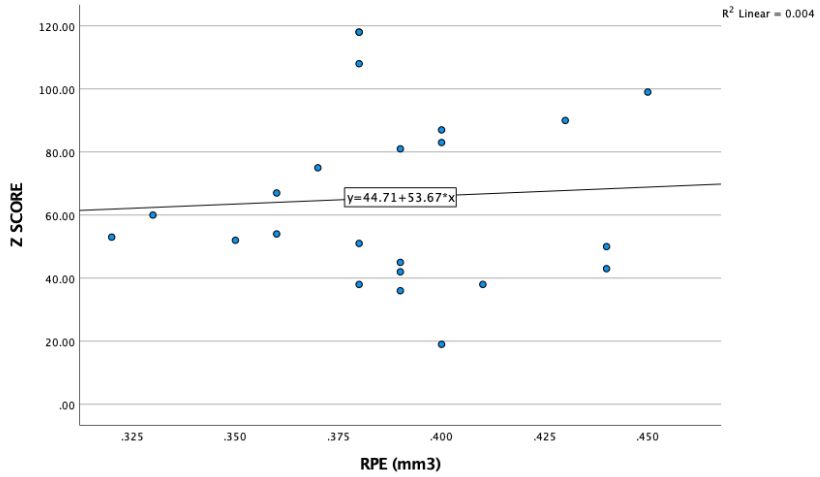

Figure 5.3.7: Scatter plot graph demonstrating relationship between RPE layer volume and z score, p = 0.775.

Model Summary[b]

Model	R	R Square	Adjusted R Square	Std. Error of the Estimate
1	.063[a]	.004	-.043	28.49377

a. Predictors: (Constant), RPE

b. Dependent Variable: Z SCORE

ANOVA[a]

Model		Sum of Squares	df	Mean Square	F	Sig.
1	Regression	67.948	1	67.948	.084	.775[b]
	Residual	17049.791	21	811.895		
	Total	17117.739	22			

a. Dependent Variable: Z SCORE

b. Predictors: (Constant), RPE

Table 5.3.8 Key statistical values analysing the relationship between retinal pigment epithelium layer volume and z score.

Inner retinal layers (IRL)

The calculated linear regression equation here is:

Y = -17.04 + 13.27x,

where R_2 = 0.047.

This model is not statistically significant, where F (1,21) = 1.031, p = 0.322. The adjusted R_2 value is 0.001, where about none of the data variability can be explained by this model. The null hypothesis is accepted here where IRL volume does not predict z score.

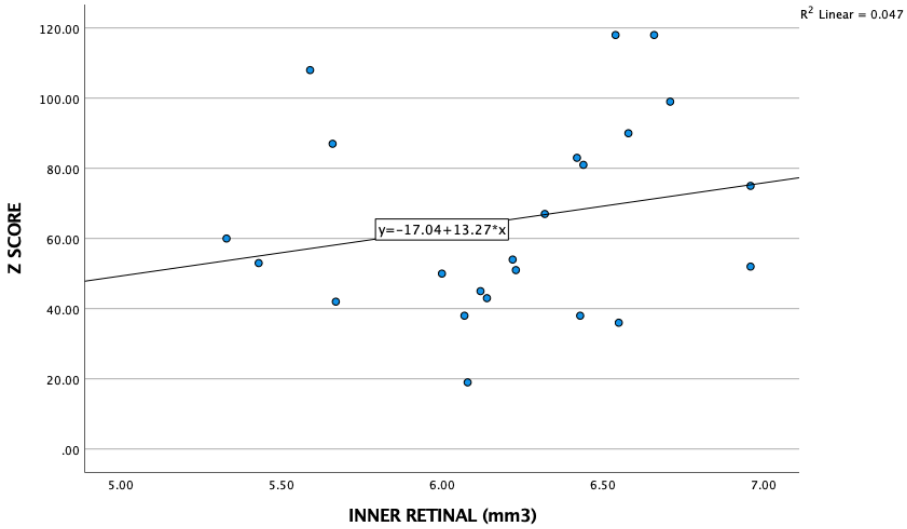

Figure 5.3.8: Scatter plot graph demonstrating relationship between inner retinal macrolayer volume and z score, p = 0.462.

Model Summary[b]

Model	R	R Square	Adjusted R Square	Std. Error of the Estimate
1	.216[a]	.047	.001	27.87462

a. Predictors: (Constant), INNER RETINAL

b. Dependent Variable: Z SCORE

ANOVA[a]

Model		Sum of Squares	df	Mean Square	F	Sig.
1	Regression	800.853	1	800.853	1.031	.322[b]
	Residual	16316.886	21	776.995		
	Total	17117.739	22			

a. Dependent Variable: Z SCORE

b. Predictors: (Constant), INNER RETINAL

Table 5.3.9 Key statistical values analysing the relationship between inner retinal macrolayer volume and z score.

Outer retinal layers

The calculated linear regression equation here is:

Y = -205 + 1.21x,
R_2 = 0.077

This model is statistically significant, where F (1,21) = 1.755, p = 0.199. The adjusted R_2 value is 0.033, where about 3% of the data variability is explained by the model. The null hypothesis is accepted here, where ORL volume does not predict z score.

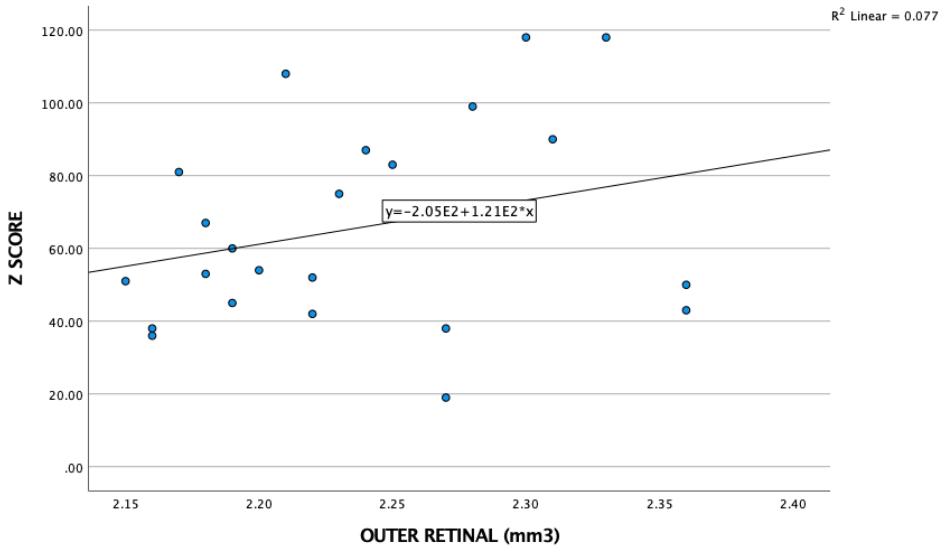

Figure 5.3.9: Scatter plot graph demonstrating relationship between outer retinal macrolayer and z score, p = 0.199.

Model Summary

Model	R	R Square	Adjusted R Square	Std. Error of the Estimate
1	.278[a]	.077	.033	27.42748

a. Predictors: (Constant), OUTER RETINAL

ANOVA[a]

Model		Sum of Squares	df	Mean Square	F	Sig.
1	Regression	1320.139	1	1320.139	1.755	.199[b]
	Residual	15797.600	21	752.267		
	Total	17117.739	22			

a. Dependent Variable: Z SCORE

b. Predictors: (Constant), OUTER RETINAL

Table 5.3.10 Key statistical values analysing the relationship between outer retinal layer volume and z score.

Sub Analysis Linear regression for subjects with >2ms delay in WF-mfERG

The second stage of analysis is sub-group analysis of those with >2ms timing delay on their WF-mfERG. Similar statistical steps as above are taken.

Delayed group: Nerve Fibre layer (NFL)

The calculated linear regression equation here is:

$$Y = 127 - 67.34x,$$

$$\text{where } R_2 = 0.108.$$

This model is not statistically significant, where F (1,14) = 1.691, p = 0.214. The adjusted R_2 value is 0.044, where about 4% of the data variability could be explained by the model. The null hypothesis is accepted here, where NFL volume does not predict z score.

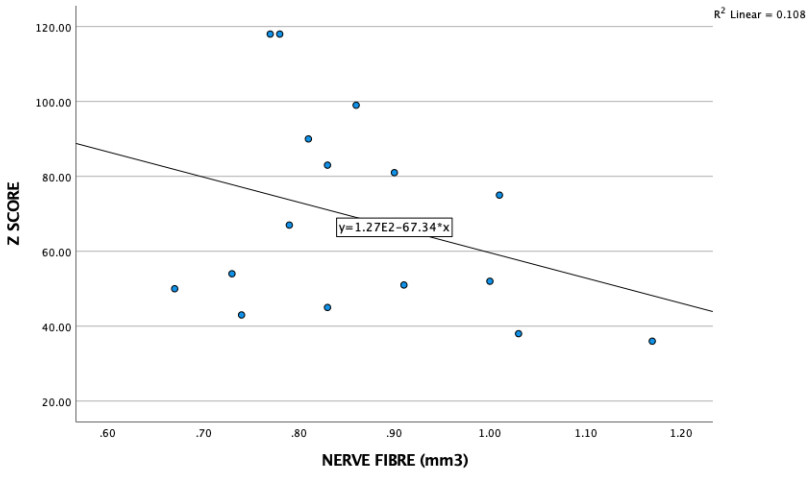

Figure 5.3.10: Scatter plot graph demonstrating relationship between nerve fibre layer and z score in the delayed group, p = 0.214.

Model Summary[b]

Model	R	R Square	Adjusted R Square	Std. Error of the Estimate
1	.328[a]	.108	.044	26.50467

a. Predictors: (Constant), NERVE FIBRE

b. Dependent Variable: Z SCORE

ANOVA[a]

Model		Sum of Squares	df	Mean Square	F	Sig.
1	Regression	1188.035	1	1188.035	1.691	.214[b]
	Residual	9834.965	14	702.497		
	Total	11023.000	15			

a. Dependent Variable: Z SCORE

b. Predictors: (Constant), NERVE FIBRE

Table 5.3.11 Key statistical values analysing the relationship between nerve fibre layer volume and z score in the delayed group.

Delayed group: Ganglion cell layer (GCL)

The calculated linear regression equation here is:

y = - 152 + 218x,

where R_2 = 0.287.

This model is statistically significant where F (1,14) = 5.638, p < 0.05. The adjusted R_2 value is 0.236, where approximately 24% of the data variability could be explained by this model. The null hypothesis is rejected here, where GCL volume predicts z scores.

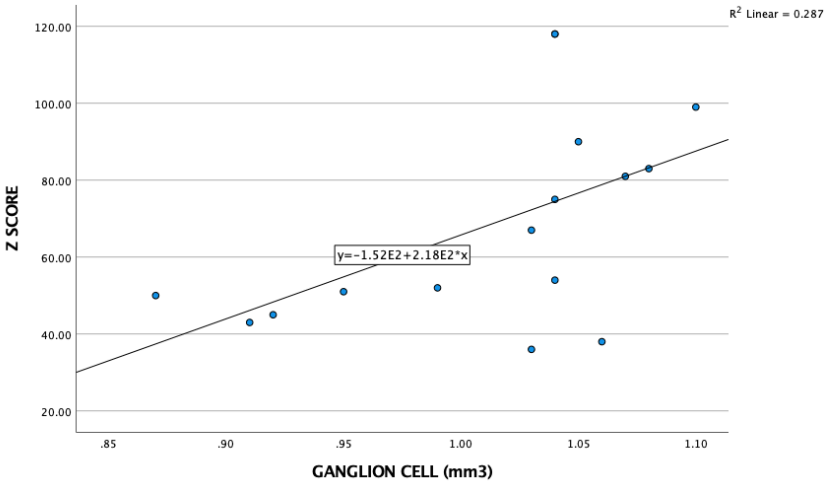

Figure 5.3.11: Scatter plot graph demonstrating relationship between ganglion cell layer volume and z score in the delayed group, p <0.05.

Model Summary[b]

Model	R	R Square	Adjusted R Square	Std. Error of the Estimate
1	.536[a]	.287	.236	23.69203

a. Predictors: (Constant), GANGLION CELL

b. Dependent Variable: Z SCORE

ANOVA[a]

Model		Sum of Squares	df	Mean Square	F	Sig.
1	Regression	3164.630	1	3164.630	5.638	.032[b]
	Residual	7858.370	14	561.312		
	Total	11023.000	15			

a. Dependent Variable: Z SCORE

b. Predictors: (Constant), GANGLION CELL

Table 5.3.12 Key statistical values analysing the relationship between ganglion cell layer volume and z score in the delayed group.

Delayed group: Inner plexiform layer (IPL)

The calculated linear regression equation here is:

Y = -204 + 323x,

where R_2 = 0.343.

The model is statistically significant here, where F (1,14) = 7.311, p < 0.05. The adjusted R_2 value is 0.296, where 30% of the data variability can be explained by the model. The null hypothesis is rejected here, where the IPL volume predicts z scores.

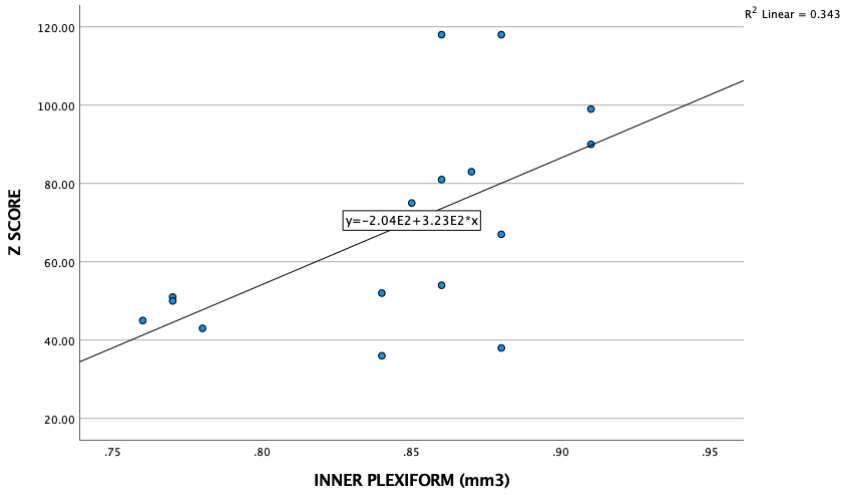

Figure 5.3.12: Scatter plot graph demonstrating relationship between inner plexiform layer volume and z score in the delayed group, p <0.05.

Model Summary[b]

Model	R	R Square	Adjusted R Square	Std. Error of the Estimate	Change Statistics				
					R Square Change	F Change	df1	df2	Sig. F Change
1	.586[a]	.343	.296	22.74314	.343	7.311	1	14	.017

a. Predictors: (Constant), INNER PLEXIFORM
b. Dependent Variable: Z SCORE

ANOVA[a]

Model		Sum of Squares	df	Mean Square	F	Sig.
1	Regression	3781.492	1	3781.492	7.311	.017[b]
	Residual	7241.508	14	517.251		
	Total	11023.000	15			

a. Dependent Variable: Z SCORE
b. Predictors: (Constant), INNER PLEXIFORM

Table 5.3.13 Key statistical values analysing the relationship between inner plexiform layer volume and z score in the delayed group.

Delayed group: Inner nuclear layer

The calculated liner regression equation here is:

Y = 266 – 198x,

where R_2 is 0.169.

This model is not statistically significant, where F (1,14) = 2.848, p = 0.114. The adjusted R_2 value of 0.11 indicates that about 11% of the data variability can be explained by this model. The null hypothesis is accepted here, where INL volume does not predict z score.

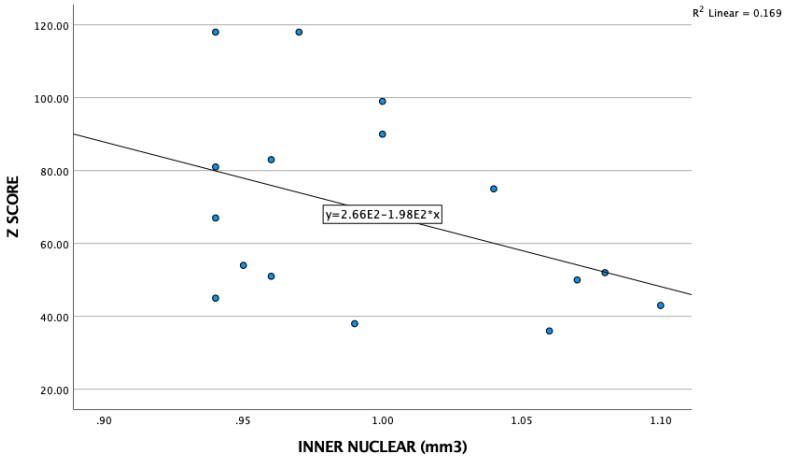

Figure 5.3.13: Scatter plot graph demonstrating relationship between inner nuclear layer volume and z score in the delayed group, p = 0.114.

Model Summary[b]

Model	R	R Square	Adjusted R Square	Std. Error of the Estimate	Change Statistics				
					R Square Change	F Change	df1	df2	Sig. F Change
1	.411[a]	.169	.110	25.57882	.169	2.848	1	14	.114

a. Predictors: (Constant), INNER NUCLEAR

b. Dependent Variable: Z SCORE

ANOVA[a]

Model		Sum of Squares	df	Mean Square	F	Sig.
1	Regression	1863.135	1	1863.135	2.848	.114[b]
	Residual	9159.865	14	654.276		
	Total	11023.000	15			

a. Dependent Variable: Z SCORE

b. Predictors: (Constant), INNER NUCLEAR

Table 5.3.14 Key statistical values analysing the relationship between inner nuclear layer volume and z score in the delayed group.

Delayed group: Outer plexiform layer

The calculated linear regression equation here is:

Y = -60.89 + 149x,

where $R_2 = 0.316$

This model is statistically significant where F (1,14) = 6.477, p <0.05. The adjusted R_2 value is 0.267, where about 27% of the data variability can be explained by the model. The null hypothesis is rejected here where OPL volume predicts z score.

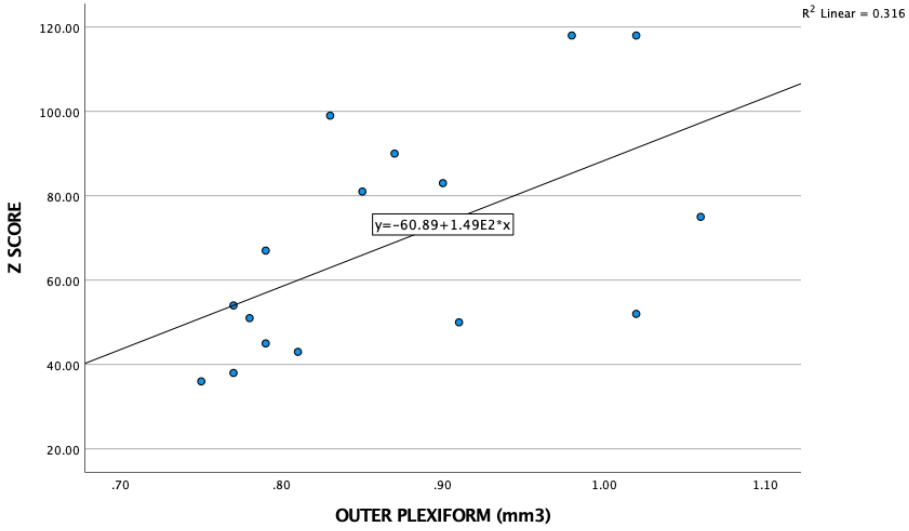

Figure 5.3.14: Scatter plot graph demonstrating relationship between outer plexiform layer volume and z score in the delayed group, p <0.05.

Model Summary[b]

Model	R	R Square	Adjusted R Square	Std. Error of the Estimate	Change Statistics				
					R Square Change	F Change	df1	df2	Sig. F Change
1	.562[a]	.316	.267	23.20151	.316	6.477	1	14	.023

a. Predictors: (Constant), OUTER PLEXIFORM

b. Dependent Variable: Z SCORE

ANOVA[a]

Model		Sum of Squares	df	Mean Square	F	Sig.
1	Regression	3486.656	1	3486.656	6.477	.023[b]
	Residual	7536.344	14	538.310		
	Total	11023.000	15			

a. Dependent Variable: Z SCORE

b. Predictors: (Constant), OUTER PLEXIFORM

Table 5.3.15 Key statistical values analysing the relationship between outer plexiform layer volume and z score in the delayed group.

Delayed group: Outer nuclear layer

The calculated linear regression equation here is:

Y = -254 +173x,

where R_2 = 0.418

This model is statistically significant, where F (1,14) = 10.040, p < 0.05. The adjusted R_2 value is 0.376, where approximately 38% of data variability can be accounted for by this model. The null hypothesis is rejected here, where ONL volume predicts z score.

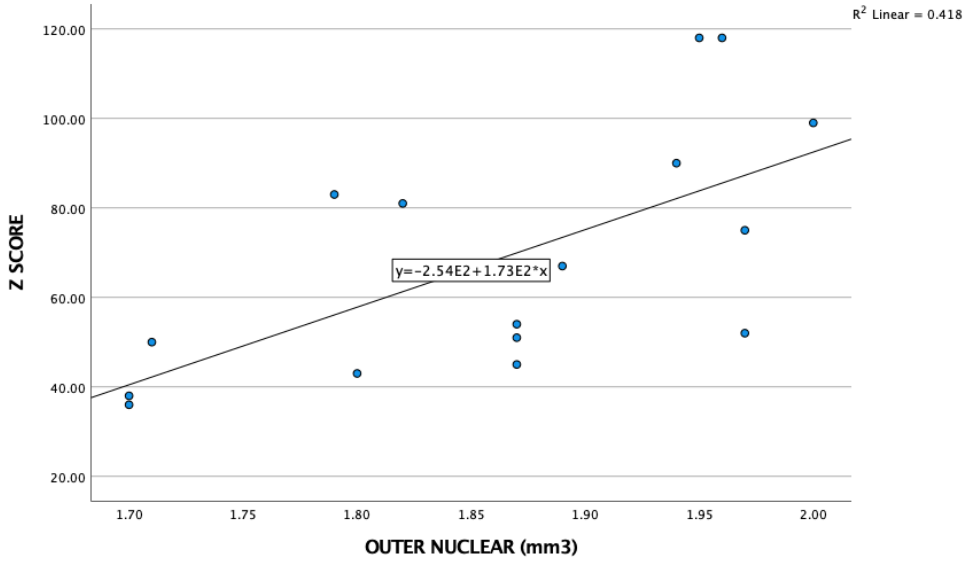

Figure 5.3.15: Scatter plot graph demonstrating relationship between outer nuclear layer volume and z score in the delayed group, p <0.05.

Model Summary[b]

Model	R	R Square	Adjusted R Square	Std. Error of the Estimate	Change Statistics				
					R Square Change	F Change	df1	df2	Sig. F Change
1	.646[a]	.418	.376	21.41303	.418	10.040	1	14	.007

a. Predictors: (Constant), OUTER NUCLEAR
b. Dependent Variable: Z SCORE

ANOVA[a]

Model		Sum of Squares	df	Mean Square	F	Sig.
1	Regression	4603.748	1	4603.748	10.040	.007[b]
	Residual	6419.252	14	458.518		
	Total	11023.000	15			

a. Dependent Variable: Z SCORE
b. Predictors: (Constant), OUTER NUCLEAR

Table 5.3.16 Key statistical values analysing the relationship between outer nuclear layer volume and z score in the delayed group.

Delayed group: Retinal Pigment epithelium (RPE)

The calculated linear regression equation here is:

Y = 37.99 + 78.26x,

where R_2 = 0.008

This model is not statistically significant, where F (1,14) = 0.112, p = 0.742. The adjusted R_2 value is – 0.063 where none of the data variability could be explained by this model.

The null hypothesis is accepted here where RPE volume does not predict z score.

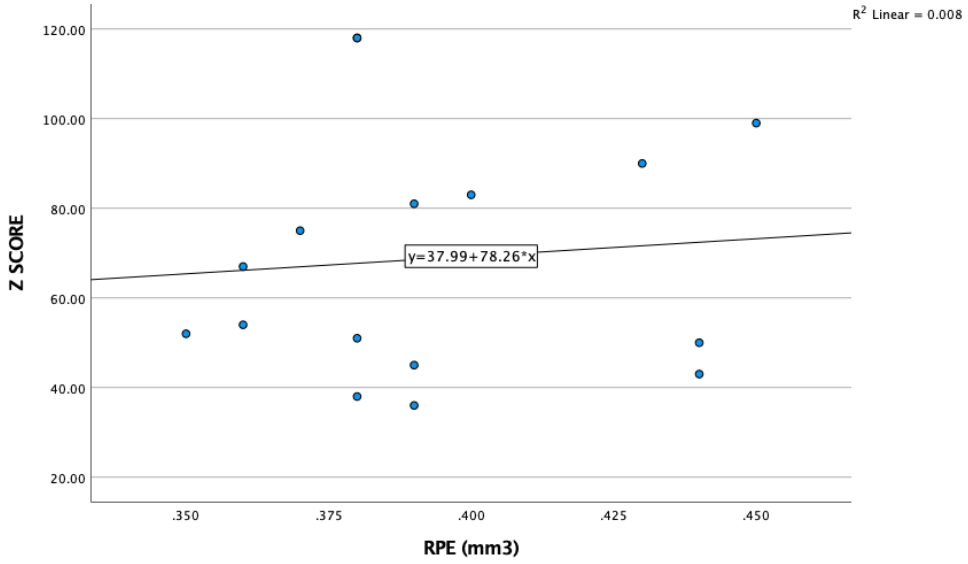

Figure 5.3.16: Scatter plot graph demonstrating relationship between RPE layer volume and z score in the delayed group, p = 0.742.

Model Summary[b]

Model	R	R Square	Adjusted R Square	Std. Error of the Estimate	Change Statistics				
					R Square Change	F Change	df1	df2	Sig. F Change
1	.089[a]	.008	-.063	27.94786	.008	.112	1	14	.742

a. Predictors: (Constant), RPE
b. Dependent Variable: Z SCORE

ANOVA[a]

Model		Sum of Squares	df	Mean Square	F	Sig.
1	Regression	87.844	1	87.844	.112	.742[b]
	Residual	10935.156	14	781.083		
	Total	11023.000	15			

a. Dependent Variable: Z SCORE
b. Predictors: (Constant), RPE

Table 5.3.17 Key statistical values analysing the relationship between RPE layer volume and z score in the delayed group.

Delayed group: Inner retinal layers

The calculated linear equation calculation here is:

Y = - 194 + 40.73x,
where R_2 = 0.18

This model is not statistically significant where F (1,14) = 3.066, p = 0.102. The adjusted R_2 value is 0.121, where approximately 12% of the data variability could be explained by this model. The null hypothesis is accepted here where IRL volume does not predict z score.

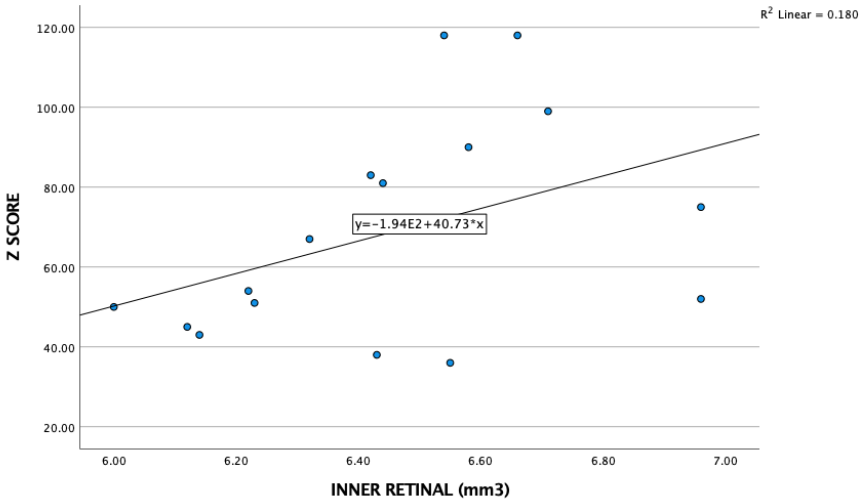

Figure 5.3.17: Scatter plot graph demonstrating relationship between inner retinal macrolayer volume and z score in the delayed group, p = 0.102.

Model Summary[b]

Model	R	R Square	Adjusted R Square	Std. Error of the Estimate	Change Statistics				
					R Square Change	F Change	df1	df2	Sig. F Change
1	.424[a]	.180	.121	25.41445	.180	3.066	1	14	.102

a. Predictors: (Constant), INNER RETINAL
b. Dependent Variable: Z SCORE

ANOVA[a]

Model		Sum of Squares	df	Mean Square	F	Sig.
1	Regression	1980.483	1	1980.483	3.066	.102[b]
	Residual	9042.517	14	645.894		
	Total	11023.000	15			

a. Dependent Variable: Z SCORE
b. Predictors: (Constant), INNER RETINAL

Table 5.3.18 Key statistical values analysing the relationship between inner retinal macrolayer volume and z score in the delayed group.

Delayed group: Outer retinal layers (ORL)

The calculated linear regression equation here is:

Y = -287 + 159x,

where R_2 = 0.185

This model is not statistically significant, where F (1,14) = 3.18, p = 0.096. The adjusted R_2 value is 0.127, where about 13% of the data variability could be explained by this model. The null hypothesis is accepted here where ORL volume does not predict z score.

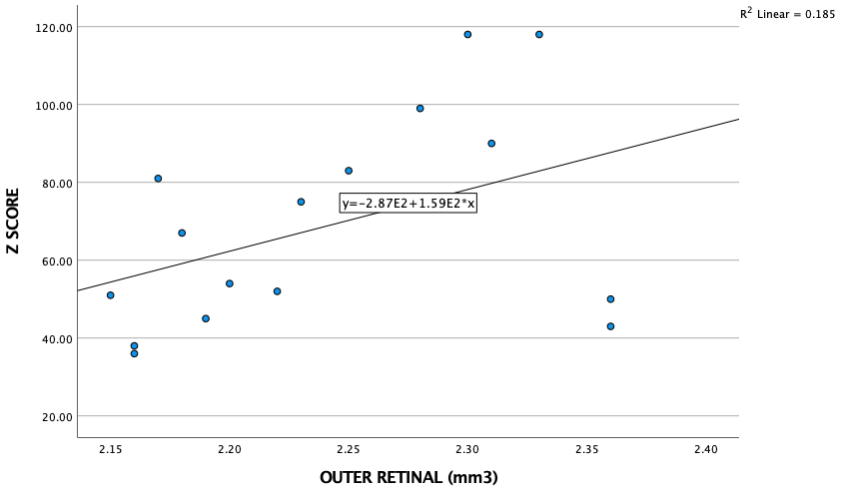

Figure 5.3.18: Scatter plot graph demonstrating relationship between outer retinal macrolayer volume and z score in the delayed group, p = 0.096.

Model Summary[b]

Model	R	R Square	Adjusted R Square	Std. Error of the Estimate	Change Statistics				
					R Square Change	F Change	df1	df2	Sig. F Change
1	.430[a]	.185	.127	25.33045	.185	3.180	1	14	.096

a. Predictors: (Constant), OUTER RETINAL
b. Dependent Variable: Z SCORE

ANOVA[a]

Model		Sum of Squares	df	Mean Square	F	Sig.
1	Regression	2040.156	1	2040.156	3.180	.096[b]
	Residual	8982.844	14	641.632		
	Total	11023.000	15			

a. Dependent Variable: Z SCORE
b. Predictors: (Constant), OUTER RETINAL

Table 5.3.19 Key statistical values analysing the relationship between outer retinal macrolayer volume and z score in the delayed group.

OCT disc Retinal nerve fibre layer circumferential line scan

For OCT RNFL thickness, 25 visual fields with the corresponding VF z score is available for analsysis, regardless of WF-mfERG results and form stage 1 of the analysis in this section. In stage 2, only 16 visual fields with corresponding OCT data from those who display >2ms delay in their WF-mfERG is available for the same analysis.

ID	z score	Global	Superior	Temporal	Inferior	Nasal
A1	42	86	97	58	116	72
B1	19	58	72	52	70	38
B2	38	56	66	49	68	41
C2	87	95	125	61	119	76
D1	108	74	100	49	82	63
E1	36	73	75	79	87	51
E2	38	73	86	70	79	52
F1	60	50	58	54	57	32
F2	53	50	57	53	56	35
G1	67	90	123	75	105	55
G2	54	96	131	65	129	60
H1	51	55	55	61	73	32
H2	45	56	61	60	71	34
J1	71	59	67	64	65	39
J2	78	52	61	39	73	36
L1	83	72	90	73	76	51
L2	81	72	86	63	81	57
M1	75	67	75	78	74	42
M2	52	63	65	76	69	44
O1	99	89	104	77	120	52
O2	90	90	110	63	119	66
P1	43	58	86	55	61	31
P2	50	55	77	59	49	35
Q1	118	90	106	70	125	60
Q2	118	89	108	74	121	52

Table 5.3.20: OCT disc RNFL: *Raw data for all included subjects. Green cells indicate data from subjects with no timing delay from their WF-mfERG, yellow cells indicate data from subjects with >2ms delay in their WF-mfERG. Data under the columns of Global, Superior, Temporal, Inferior and Nasal are in micrometer or µm.*

Global RNFL

The calculated linear regression equation here is:

Y = 4.24 + 0.88x, where R_2 = 0.264.

This model is statistically significant, where F (1,23) = 8.255, p<0.05. The adjust R_2 value is 0.232, which means about 23% of the data variability can be accounted for by this model. The null hypothesis is rejected here, where average global RNFL thickness can predict z score.

Model Summary

Model	R	R Square	Adjusted R Square	Std. Error of the Estimate
1	.514[a]	.264	.232	23.52054

a. Predictors: (Constant), Global RNFL

ANOVA[a]

Model		Sum of Squares	df	Mean Square	F	Sig.
1	Regression	4566.599	1	4566.599	8.255	.009[b]
	Residual	12723.961	23	553.216		
	Total	17290.560	24			

a. Dependent Variable: Z score

b. Predictors: (Constant), Global RNFL

Coefficients[a]

Model		Unstandardized Coefficients		Standardized Coefficients		
		B	Std. Error	Beta	t	Sig.
1	(Constant)	4.238	22.087		.192	.850
	Global RNFL	.877	.305	.514	2.873	.009

a. Dependent Variable: Z score

Table 5.3.21: Key statistical values analysing the relationship between global RNFL thickness and z score.

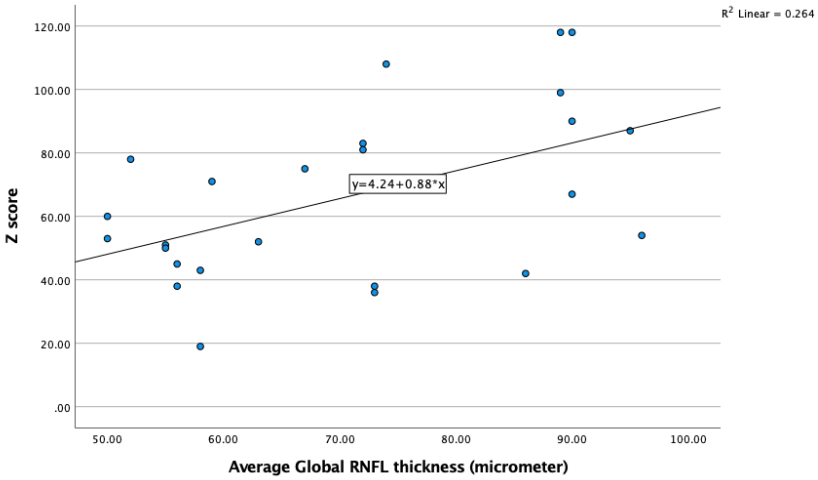

Figure 5.3.19: Scatter plot graph demonstrating relationship between average global RNFL thickness and z score, $p < 0.05$.

Superior RNFL

The calculated linear regression equation here is:

Y = 17.99 + 0.56x, where R_2 is 0.231

This model is also statistically significant, where F(1,23) = 6.912, p<0.05. The adjust R_2 value is 0.198, which means approximately 20% of the data variability can be accounted for by this model. The null hypothesis is rejected here, where average superior RNFL thickness is predictive of the z score.

Model Summary

Model	R	R Square	Adjusted R Square	Std. Error of the Estimate
1	.481[a]	.231	.198	24.04272

a. Predictors: (Constant), Superior RNFL

ANOVA[a]

Model		Sum of Squares	df	Mean Square	F	Sig.
1	Regression	3995.353	1	3995.353	6.912	.015[b]
	Residual	13295.207	23	578.052		
	Total	17290.560	24			

a. Dependent Variable: Z score

b. Predictors: (Constant), Superior RNFL

Coefficients[a]

Model		Unstandardized Coefficients		Standardized Coefficients		
		B	Std. Error	Beta	t	Sig.
1	(Constant)	17.988	18.973		.948	.353
	Superior RNFL	.563	.214	.481	2.629	.015

a. Dependent Variable: Z score

Table 5.3.22: Key statistical values analysing the relationship between superior RNFL thickness and z score.

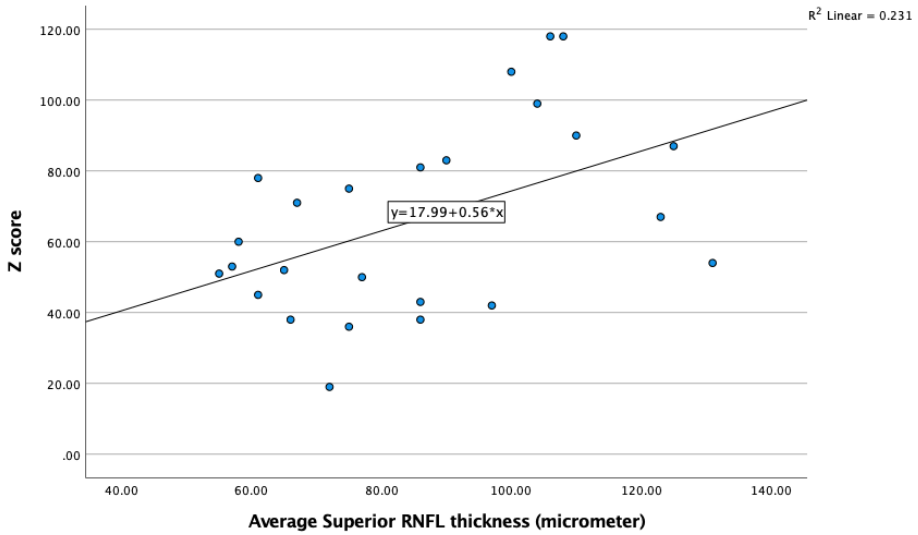

Figure 5.3.20: Scatter plot graph demonstrating relationship between average superior RNFL thickness and z score, $p < 0.05$.

Temporal RNFL

The calculated linear regression equation here is:

Y = 31.89 + 0.54x, where R_2 = 0.046

This model is not statistically significant, where F (1,23) = 1.119, p = 0.301. The adjusted R_2 value is 0.005, which means less than 1% of the data variability can be be explained by this model. The null hypothesis is accepted here where average temporal RNFL thickness is not predictive of the z score.

Model Summary

Model	R	R Square	Adjusted R Square	Std. Error of the Estimate
1	.215[a]	.046	.005	26.77452

a. Predictors: (Constant), Temporal RNFL

ANOVA[a]

Model		Sum of Squares	df	Mean Square	F	Sig.
1	Regression	802.435	1	802.435	1.119	.301[b]
	Residual	16488.125	23	716.875		
	Total	17290.560	24			

a. Dependent Variable: Z score

b. Predictors: (Constant), Temporal RNFL

Coefficients[a]

Model		Unstandardized Coefficients		Standardized Coefficients		
		B	Std. Error	Beta	t	Sig.
1	(Constant)	31.889	32.907		.969	.343
	Temporal RNFL	.545	.515	.215	1.058	.301

a. Dependent Variable: Z score

Table 5.3.23: Key statistical values analysing the relationship between temporal RNFL thickness and z score.

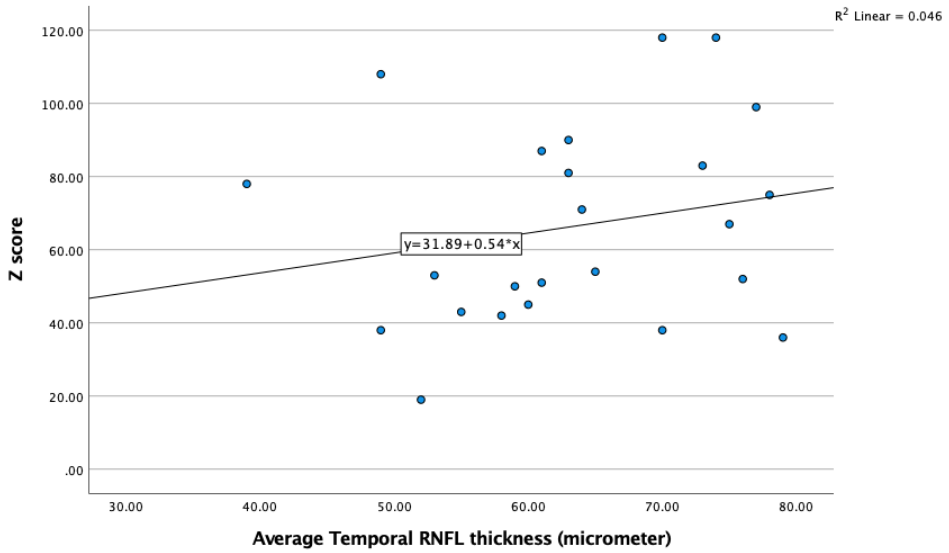

Figure 5.3.21: Scatter plot graph demonstrating relationship between average temporal RNFL thickness and z score, p = 0.301.

Inferior RNFL

The calculated linear regression equation here is:

Y = 18.85 + 0.55x, where R_2 = 0.267

This model is statistically significant, where F (1,23) = 8.378, p <0.05. The adjusted R_2 value is 0.235, whereby 23.5% of the data variability can be explained by this model. The null hypothesis is rejected here, as average Inferior RNFL thickness is predictive of the z score.

Model Summary

Model	R	R Square	Adjusted R Square	Std. Error of the Estimate
1	.517[a]	.267	.235	23.47421

a. Predictors: (Constant), Inferior RNFL

ANOVA[a]

Model		Sum of Squares	df	Mean Square	F	Sig.
1	Regression	4616.674	1	4616.674	8.378	.008[b]
	Residual	12673.886	23	551.039		
	Total	17290.560	24			

a. Dependent Variable: Z score

b. Predictors: (Constant), Inferior RNFL

Coefficients[a]

Model		Unstandardized Coefficients		Standardized Coefficients		
		B	Std. Error	Beta	t	Sig.
1	(Constant)	18.848	17.033		1.107	.280
	Inferior RNFL	.552	.191	.517	2.895	.008

a. Dependent Variable: Z score

Table 5.3.24: Key statistical values analysing the relationship between inferior RNFL thickness and z score.

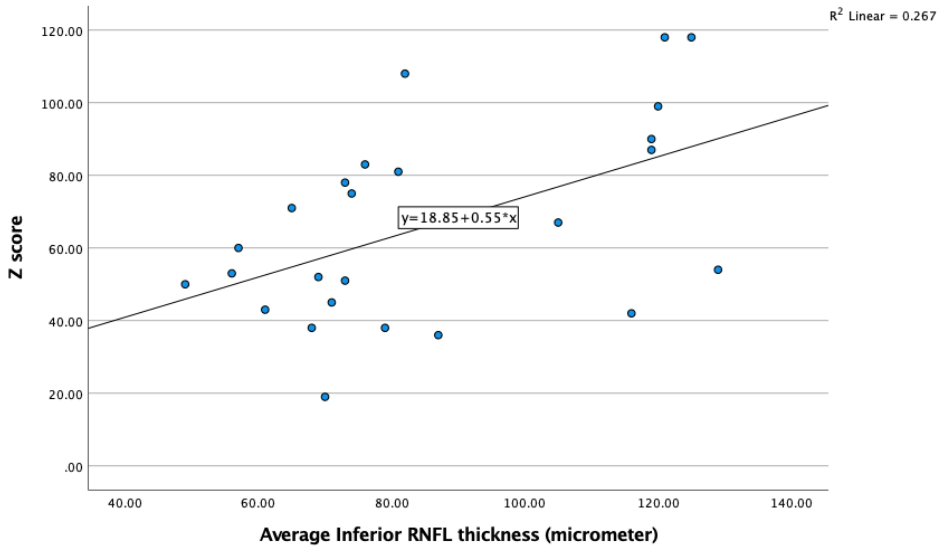

Figure 5.3.22: Scatter plot graph demonstrating relationship between average inferior RNFL thickness and z score, $p < 0.05$.

Nasal RNFL

The calculated linear regression equation here is:

Y = 22.55 + 0.91x, where R_2 = 0.197.

This model is statistically significant, where F (1,23) = 5.641, p < 0.05. The adjust R_2 value is 0.162, where 16% of the data variability can be explained by the model. The null hypothesis is rejected here, as average nasal RNFL thickness is predictive of the z score.

Model Summary

Model	R	R Square	Adjusted R Square	Std. Error of the Estimate
1	.444[a]	.197	.162	24.57021

a. Predictors: (Constant), Nasal RNFL

ANOVA[a]

Model		Sum of Squares	df	Mean Square	F	Sig.
1	Regression	3405.565	1	3405.565	5.641	.026[b]
	Residual	13884.995	23	603.695		
	Total	17290.560	24			

a. Dependent Variable: Z score

b. Predictors: (Constant), Nasal RNFL

Coefficients[a]

Model		Unstandardized Coefficients		Standardized Coefficients		
		B	Std. Error	Beta	t	Sig.
1	(Constant)	22.554	19.038		1.185	.248
	Nasal RNFL	.906	.381	.444	2.375	.026

a. Dependent Variable: Z score

Table 5.3.25: Key statistical values analysing the relationship between nasal RNFL thickness and z score.

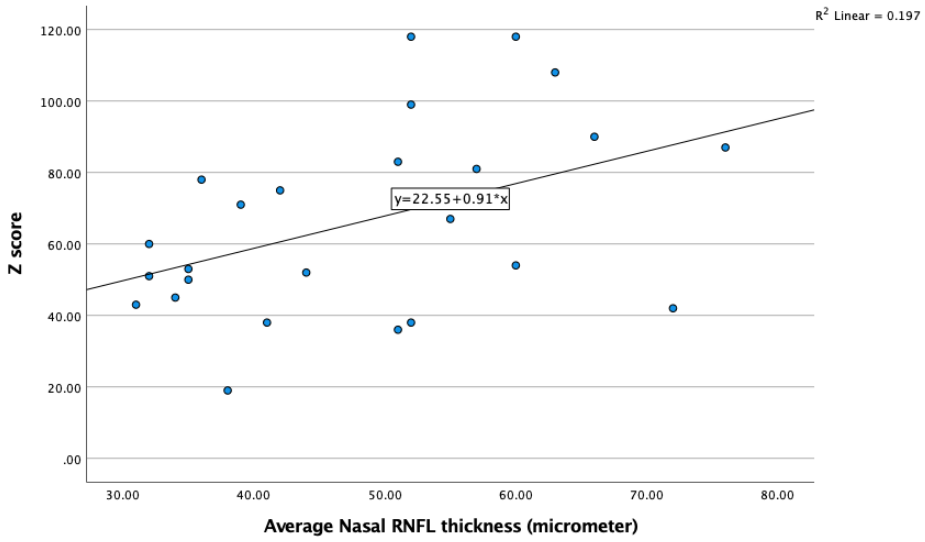

Figure 5.3.23: Scatter plot graph demonstrating relationship between average nasal RNFL thickness and z score, $p < 0.05$.

Delayed Group: Global RNFL

The calculated linear regression model here is:

Y = - 16.44 + 1.15x, where R_2 = 0.38

This model is statistically significant, where F (1, 14) = 8.585, p<0.05. The adjusted R_2 value is 0.336, where 33.6% of the data variability can be explained by this model. The null hypothesis is rejected here, as average global RNFL thickness is predictive of the z score.

Model Summary

Model	R	R Square	Adjusted R Square	Std. Error of the Estimate
1	.617[a]	.380	.336	22.09217

a. Predictors: (Constant), Average Global RNFL (micrometer)

ANOVA[a]

Model		Sum of Squares	df	Mean Square	F	Sig.
1	Regression	4190.105	1	4190.105	8.585	.011[b]
	Residual	6832.895	14	488.064		
	Total	11023.000	15			

a. Dependent Variable: Z score

b. Predictors: (Constant), Average Global RNFL (micrometer)

Coefficients[a]

Model		Unstandardized Coefficients		Standardized Coefficients		
		B	Std. Error	Beta	t	Sig.
1	(Constant)	-16.440	29.595		-.556	.587
	Average Global RNFL (micrometer)	1.147	.392	.617	2.930	.011

a. Dependent Variable: Z score

Table 5.3.26: Key statistical values analysing the relationship between global RNFL thickness and z score in the delayed group

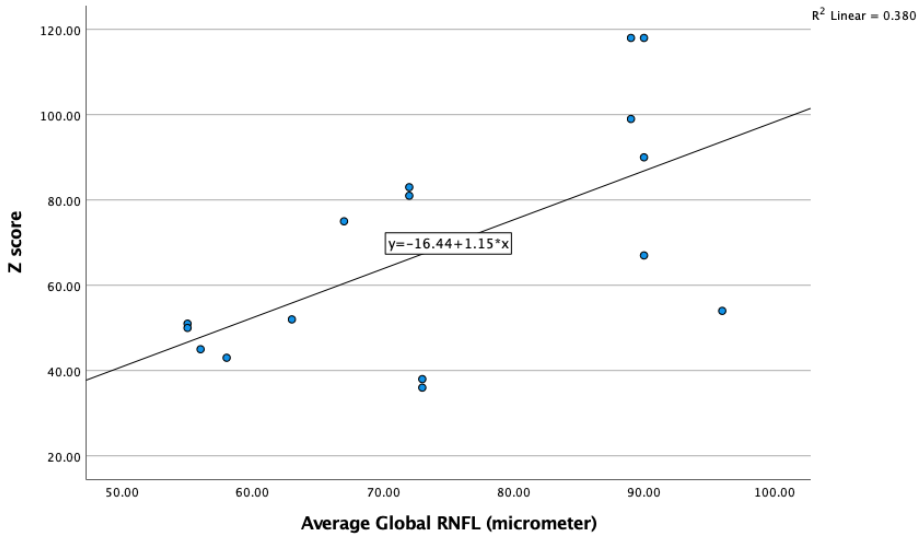

Figure 5.3.24: Scatter plot graph demonstrating relationship between average global RNFL thickness and z score in the delayed group, p <0.05.

Delayed group: Superior RNFL

The calculated linear regression equation here is:

Y = 14.51 + 0.6x, where R_2 = 0.241.

This model is not statistically significant, where F (1,14) = 4.452, p = 0.053. The adjusted R_2 value is 0.187, which means 19% of the data variability can be explained by this model. The null hypothesis is accepted here where average superior RNFL thickness is not predictive of the z score.

Model Summary

Model	R	R Square	Adjusted R Square	Std. Error of the Estimate
1	.491[a]	.241	.187	24.44127

a. Predictors: (Constant), Average Superior RNFL (micrometer)

ANOVA[a]

Model		Sum of Squares	df	Mean Square	F	Sig.
1	Regression	2659.737	1	2659.737	4.452	.053[b]
	Residual	8363.263	14	597.376		
	Total	11023.000	15			

a. Dependent Variable: Z score

b. Predictors: (Constant), Average Superior RNFL (micrometer)

Coefficients[a]

Model		Unstandardized Coefficients		Standardized Coefficients		
		B	Std. Error	Beta	t	Sig.
1	(Constant)	14.514	26.420		.549	.591
	Average Superior RNFL (micrometer)	.603	.286	.491	2.110	.053

a. Dependent Variable: Z score

Table 5.3.27: Key statistical values analysing the relationship between superior RNFL thickness and z score in the delayed group

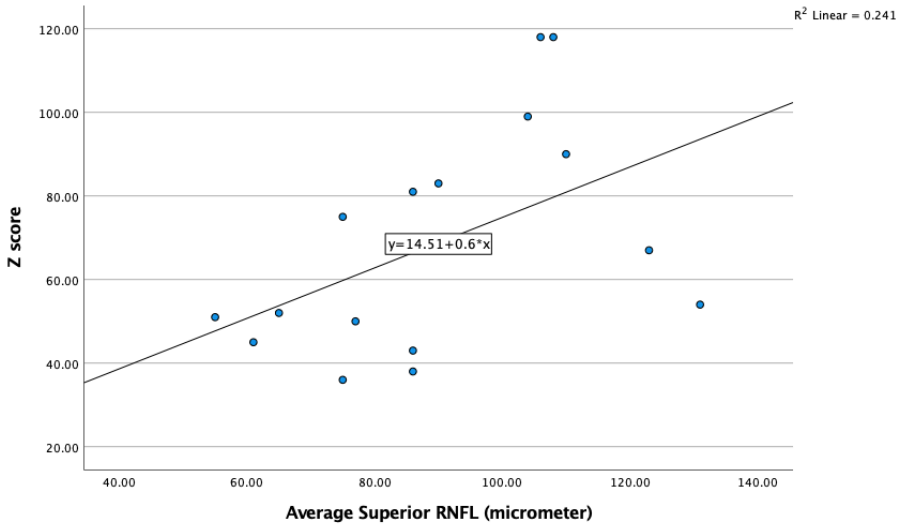

Figure 5.3.25: Scatter plot graph demonstrating relationship between average superior RNFL thickness and z score in the delayed group, p = 0.053.

Delayed group: Temporal RNFL

The calculated linear regression equation is:

Y = -1.92 + 1.03x, where R_2 = 0.087.

This model is not statistically significant, where F (1, 14) = 1.327, p = 0.269. The adjusted R_2 value is 0.021, which means only 2% of the data variability can be explained by this model. The null hypothesis is accepted here where average RNFL thickness is not predictive of the z score.

Model Summary

Model	R	R Square	Adjusted R Square	Std. Error of the Estimate
1	.294[a]	.087	.021	26.81811

a. Predictors: (Constant), Average Temporal RNFL (micrometer)

ANOVA[a]

Model		Sum of Squares	df	Mean Square	F	Sig.
1	Regression	954.045	1	954.045	1.327	.269[b]
	Residual	10068.955	14	719.211		
	Total	11023.000	15			

a. Dependent Variable: Z score

b. Predictors: (Constant), Average Temporal RNFL (micrometer)

Coefficients[a]

Model		Unstandardized Coefficients		Standardized Coefficients		
		B	Std. Error	Beta	t	Sig.
1	(Constant)	-1.915	61.720		-.031	.976
	Average Temporal RNFL (micrometer)	1.030	.894	.294	1.152	.269

a. Dependent Variable: Z score

Table 5.3.28: Key statistical values analysing the relationship between temporal RNFL thickness and z score in the delayed group

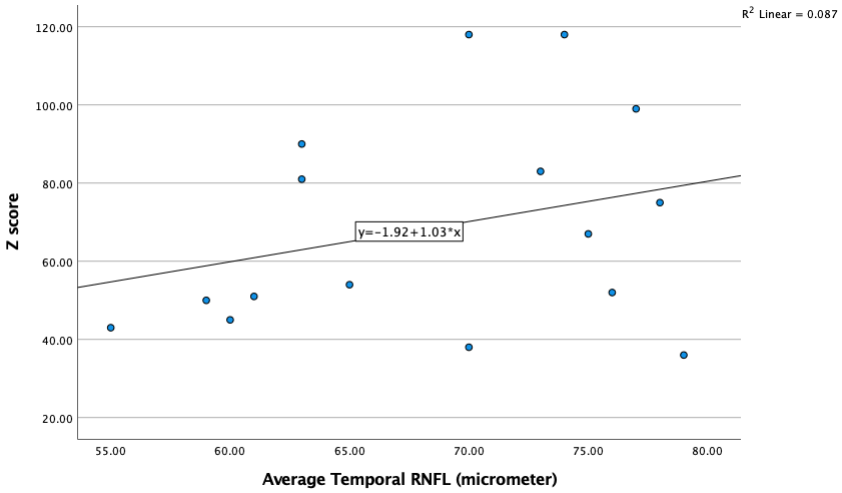

Figure 5.3.26: Scatter plot graph demonstrating relationship between average temporal RNFL thickness and z score in the delayed group, p = 0.269

Delayed group: Inferior RNFL

The calculated linear regression equation here is:

Y = 7.1 + 0.69x, where R_2 = 0.424.

This model is statistically significant, where F (1, 14) = 10.309, $p < 0.05$. The adjusted R_2 value is 0.383 which means 38.3% of the data variability can be explained by this model. The null hypothesis is rejected here where the average inferior RNFL thickness is predictive of the z score.

Model Summary

Model	R	R Square	Adjusted R Square	Std. Error of the Estimate
1	.651[a]	.424	.383	21.29425

a. Predictors: (Constant), Average Inferior RNFL (micrometer)

ANOVA[a]

Model		Sum of Squares	df	Mean Square	F	Sig.
1	Regression	4674.770	1	4674.770	10.309	.006[b]
	Residual	6348.230	14	453.445		
	Total	11023.000	15			

a. Dependent Variable: Z score

b. Predictors: (Constant), Average Inferior RNFL (micrometer)

Coefficients[a]

Model		Unstandardized Coefficients		Standardized Coefficients		
		B	Std. Error	Beta	t	Sig.
1	(Constant)	7.100	19.925		.356	.727
	Average Inferior RNFL (micrometer)	.685	.213	.651	3.211	.006

a. Dependent Variable: Z score

Table 5.3.29: Key statistical values analysing the relationship between inferior RNFL thickness and z score in the delayed group

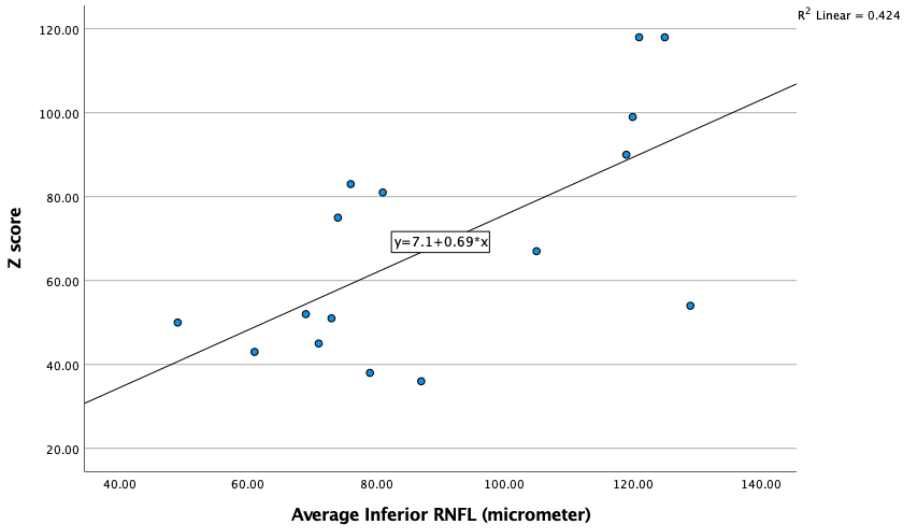

Figure 5.3.27: Scatter plot graph demonstrating relationship between average inferior RNFL thickness and z score in the delayed group, p <0.05.

Delayed Group: Nasal RNFL

The calculated linear regression equation here is:

Y = 4.13 + 1.34x, where R_2 = 0.286.

This model is statistically significant, where F (1, 14) = 5.613, $p < 0.05$. The adjusted R_2 value is 0.235, which means 23.5% of the data variability can be accounted for by this model. The null hypothesis is rejected here where average nasal RNFL thickness is predictive of the z score.

Model Summary

Model	R	R Square	Adjusted R Square	Std. Error of the Estimate
1	.535[a]	.286	.235	23.70702

a. Predictors: (Constant), Average Nasal RNFL (micrometer)

ANOVA[a]

Model		Sum of Squares	df	Mean Square	F	Sig.
1	Regression	3154.678	1	3154.678	5.613	.033[b]
	Residual	7868.322	14	562.023		
	Total	11023.000	15			

a. Dependent Variable: Z score

b. Predictors: (Constant), Average Nasal RNFL (micrometer)

Coefficients[a]

Model		Unstandardized Coefficients		Standardized Coefficients		
		B	Std. Error	Beta	t	Sig.
1	(Constant)	4.127	27.913		.148	.885
	Average Nasal RNFL (micrometer)	1.336	.564	.535	2.369	.033

a. Dependent Variable: Z score

Table 5.3.30: Key statistical values analysing the relationship between nasal RNFL thickness and z score in the delayed group

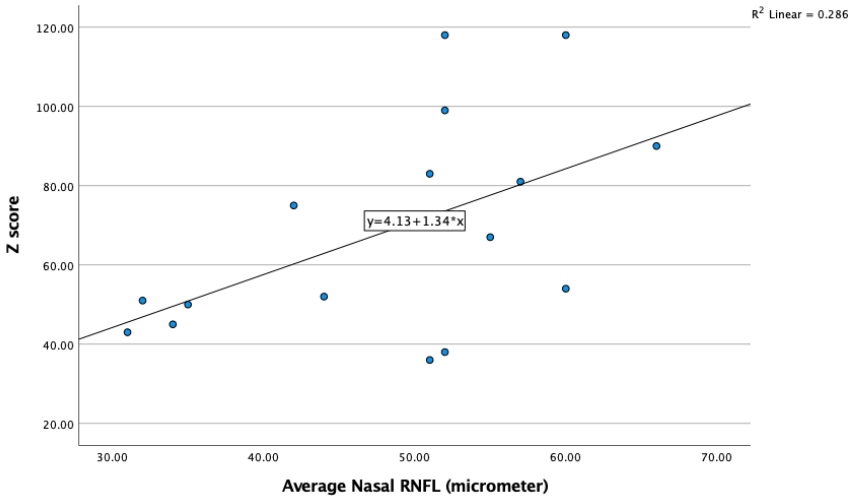

Figure 5.3.28: Scatter plot graph demonstrating relationship between average nasal RNFL thickness and z score in the delayed group, p <0.05.

Summary of findings:

Independent variable (layers)	ANOVA significance, p value	
	All	Delayed group only
Nerve fibre	0.462	0.214
Ganglion cell	0.114	0.032*
Inner plexiform	0.053	0.017*
Inner nuclear	0.619	0.114
Outer plexiform	0.005*	0.023*
Outer nuclear	0.655	0.007*
Retinal pigment epithelium	0.775	0.742
Inner retinal (macrolayers)	0.322	0.102
Outer retinal (macrolayers)	0.199	0.096

Table 5.3.31: Summary of key statistical findings for linear regression calculations where z score is the dependent variable and the retinal microstructures are the independent variable. Values that reached statistical significance is printed in red.

Independent variable (RNFL Quadrants)	ANOVA significance, p value	
	All	Delayed group only
Global	0.009*	0.011*
Superior	0.015*	0.053
Temporal	0.301	0.269
Inferior	0.008*	0.006*
Nasal	0.026*	0.033*

Table 5.3.32: Summary of key statistical values from all linear regression calculations where z score is the dependent variable and the quadrants are the independent variable. Values that reached statistical significance are printed in red.

Discussion:

The integration of OCT technology into the assessment of visual function is continually advanced by newer generations of OCT devices. The advances have now allowed more rapid and accurate capture of data, micrometer resolution of images and development of OCT based structure-function corresponding software for detailed analysis. The validity of OCT retinal structure and visual function correlation is well accepted. The gathered scientific evidence OCT based structure function correlation is primarily in glaucoma (Wu *et al.*, 2015; Tatham and Medeiros, 2017; Renard, Fénolland and Giraud, 2019). Other conditions have also been investigated such as diabetic retinopathy (Zeng *et al.*, 2019), and neuro-ophthalmological conditions (Kardon, 2011) and other neurological diagnoses such as Leber's Hereditary Optic neuropathy (LHON) (Wang *et al.*, 2020).

The efforts in investigating the role of OCT as a biomarker were initially exploratory; although it's utility and clinical relevance in glaucoma is now widely accepted. Commercially available OCT devices now have OCT structure with corresponding visual fields function analysis tool built-in as part of the software. Nerve fibre layer changes with sequential ganglion cell complex thinning is correlated to reduced retinal sensitivity. In LHON, ganglion cell dysfunction was found to be correlated to GCL and IPL thinning in both acute and chronic patients. Changes related to multifocal ERG found localised macular dysfunction also in both acute and chronic sufferers (Wang *et al.*, 2020). In diabetes, ERG changes in the form of delayed implicit times and decreased amplitude with reduced peripapillary RNFL on the OCT was seen even before any visible retinal lesions were seen (Zeng *et al.*, 2019).

Thinning and atrophic changes

One of the earliest publication that reported structure function correlation in Vigabatrin treated individuals was a case report of an 18 year old with bilateral concentric field loss, with photographic evidence of retinal nerve fibre layer loss with correlation to OCT disc RNFL thinning in all quadrants bar the temporal region (Choi and Kim, 2004). Further studies to support the implication of RNFL tissue changes was published (Wild *et al.*, 2006; Lawthom, Smith and Wild, 2009; Moseng *et al.*, 2011; Clayton *et al.*, 2013). Vigabatrin associated visual loss can exist in the absence of any gross fundal abnormalities (Newman, Tocher and Acheson, 2002). Reported fundal abnormalities include optic disc pallor (Daneshvar *et al.*, 1999; Malmgren, Ben-Menachem and Frisén, 2001; Buncic *et al.*, 2004), epiretinal membrane (Gregory L. Krauss, Johnson and Miller,

1998), attenuated retinal vessels (Gregory L. Krauss, Johnson and Miller, 1998; Wild *et al.*, 1999), abnormal macula pigmentation (Krauss and Miller, 1999) and abnormal pigmentation in the peripheral retina (Lawden *et al.*, 1999). The effect of medication in what we suspect is 'toxic' effect is theoretically expected to give atrophic and degenerative types changes, which was seen in the early OCT publications.

The reverse: Thickening?

More recently, increase in tissue thickness is reported which is peculiar when compared to previous publications. It is likely that advancement on the OCT devices and development of better monitoring schedules have allowed us to visualise changes on OCT scans that related to time from exposure to Vigabatrin. In a US-based trial, disc RNFL thickening was observed in almost all patients, with no other associated peculiar clinical manifestations. The authors theorised that these changes are precursor to more permanent changes when visual loss ensues (Sergott *et al.*, 2016b). Tuğcu et al found generalised RNFL thinning with associated higher foveal thickness in the patient group, compared to normal controls (Tuğcu *et al.*, 2017). We found similar finding of increased tissue volume in those who had >2ms peripheral timing delay (see chapter 5, unpublished)

Microlayers

In our study we attempt to investigate if a linear relationship could be drawn between our novel perimetry score z and retinal microstructures. This relationship is further

harnessed in a more focused analysis looking at those specifically with peripheral timing delay in their WF-mfERG. When we tried to correlate visual fields in all our subjects to their respective macula microlayer volume, our analysis shows statistical significance in the linear regression model when correlated to the outer plexiform layer volume. As far as we know, the OPL is not a common microlayer that has been implicated as a sole target site for damage in visual diseases. It is also known as the outer synaptic layer, where fibres from the rods and cones synapse with cells from the inner nuclear layer. OPL abnormalities have been reported in Behcet's disease, with focal bumpy areas (Kido *et al.*, 2018).

Interestingly, focused sub-analysis on those who displayed peripheral delay in their WF-mfERG revealed statistically significant linear regression model in 4 layers; ganglion cell layer, inner plexiform layer, outer plexiform layer and outer nuclear layer. Ganglion cell layer was the first implicated retinal microlayer (Choi and Kim, 2004) in vigabatrin related visual loss. Postmortem retinal analysis of another patient with vigabatrin associated visual loss found extensive loss of ganglion cells, with some sparing within the macula region. The authors also reported partial loss of nuclei from the Inner nuclear layer, outer nuclear layer with atrophy of the inner and outer plexiform layers (Ravindran *et al.*, 2001b), all of which are the same layers found to be predictive of visual field score in our study. Histological reports in rats exposed to Vigabatrin showed disorganisation of the photoreceptor layers peripherally (Butler, Ford and Newberne, 1987; Duboc *et al.*, 2004). The implication of OPL in the first analysis is noteworthy since it continued to reach statistical relevance even in the sub group analyses. It is possible

that the OPL changes occur as it contains distal end of damaged cells from adjacent layers.

Disc RNFL quadrants

Our findings in both the main analyses and the subanalyses for RNFL thickness display similarities in their relationship with the z score. While other studies were generally comparative reports, characteristic nasal peripapillary thinning with preservation of the temporal quadrant was reported (Lawthom, Smith and Wild, 2009; Moseng *et al.*, 2011; Clayton *et al.*, 2013) in the treated group and compared to non-exposed controls. Non-involvement of other quadrants were also specifically reported (Lawthom, Smith and Wild, 2009). One case series reported attenuated RNFL was found in 75% of the patients, with preservation of the temporal quadrant found in all (Kjellström, Andréasson and Ponjavic, 2014). The equivocal conclusion from our RNFL quadrants analysis suggest that the observed thinning may not be the pathological component in vigabatrin related retinal toxicity, and may represent an inherent characteristic of patients with epilepsy. Patients with epilepsy have been reported to have thinner RNFL when compared to normal controls, even in the absence of Vigabatrin exposure. (Balestrini *et al.*, 2016)

Overall, we are reassured that the microlayers highlighted in our second analysis appears to be in line with histological reports. Firstly, it gives some validity to our z score, which was originally an attempt to assign a simple numerical score to a visual field result to enable quantitative analysis. We recognise that our method for evaluating visual fields is unconventional so in order to compensate for the modifications,

additional criteria including concentric pattern must also be present. Previous publications had the advantage of various adjustable parameters such isopters and stimuli size and intensity for more detailed spatial correlation with the OCT. The 120-point suprathreshold screening test was employed in this study for a historical reason – most subjects have been tested on this perimetry protocol, and it was judged to beneficial to continue the same testing protocol to facilitate any analytical need in future research. To maximise data analysis for a unique cohort, particularly when data is scarce calls for more novel approach to navigate through the available data. Therefore the analysis here pertains per eye, rather than per subject (one value assigned to both eye). The advantage in our dataset is that the visual fields and the OCT are normally taken on the same study visit, so visual fields results would be in 'real-time' as the OCT.

Secondly, our finding continues to add weight to the role of WF-mfERG in this condition, as significant pattern of results emerge when subjects are segregated based on the finding of >2ms timing delay of the peripheral 45° - 90°, compared to the central 0° - 45°. (McDonagh *et al.*, 2003a; Gonzalez *et al.*, 2009)

Despite good quality data from our centre with WF-mfERG, other centres have not been able to replicate the same result – and likely because they used a different software to ours.

The advantage of this study is the availability of WF-mfERG data that could be incorporated for correlation to produce new information that could help progress our understanding of Vigabatrin related visual toxicity. The limitations of this study includes

the lack of a control group, especially in the evaluation of the OCT and also low number data/subjects per group.

Finally, it is likely that we are closer to pinning down the site of retinal damage from Vigabatrin. In our study the GCL, IPL, OPL and ONL appear to be predictive of the z score and is in line with histological publications that observed the same. Ideally it would desirable to translate this knowledge into an examination tool that is epilepsy patient-friendly; rapid, requires minimal cooperation and sensitive to early detection of Vigabatrin related retinal toxicity.

CHAPTER 6:

TAURINE AND ORNITHINE

Taurine

The potential role for Taurine in the retina was first raised following the observation of retinal dysfunction in cats when fed on a taurine-free diet (Hayes, Carey and Schmidt, 1975). Its level is presumed to be reduced within the retina in the presence of Vigabatrin, which inhibits its uptake (Jammoul *et al.*, 2009). Taurine is an amino acid discovered in 1827 and was first isolated from the bile of an Ox in 1838. It is found in small quantities in some greens, seeds and tubers (Lähdesmäki, 1986). It is also found in high quantities in mammalian tissues; mammals such as the cat, monkey and man depend on oral consumption of taurine-rich food source to sustain its requirement (Lombardini, 1991). On the other hand, the rat species are able to synthesise taurine endogenously for its own need. Interestingly, taurine is highly abundant in the retina of the rat, making up to 50% of the total amino acid (Lombardini, 1991). Immunocytological staining in certain species were able to confirm presence of taurine in the photoreceptor inner segments and synaptic terminals(Lake and Verdone-Smith, 1989).

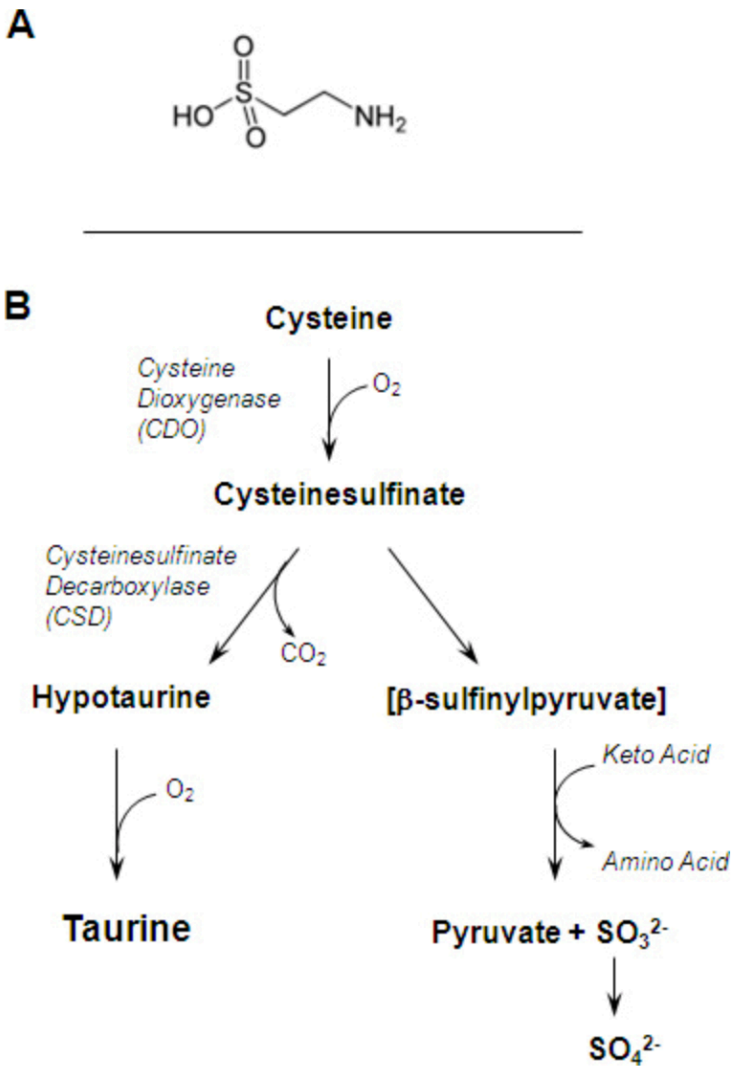

Figure 6.1.1. Diagram A shows the molecular structure of Taurine. Diagram B shows the keys steps involved in the metabolic pathway from Cysteine to Taurine. (Image credit to Ripps and Shen "Review: Taurine: A 'very essential' amino acid" Mol Vis. 2012; 18: 2673–2686.)

Taurine is also known as 2-aminoethanesulfonic acid, a β-amino sulfonic acid. It is a naturally occurring amino acid resulting from the metabolism of cysteine and methionine.

The Molecular formula $NH_2CH_2CH_2SO_3H$ or $C_2H_7NO_3S$, with a molecular weight of 125.15g/mol. In general the exact mechanism in which Taurine plays a role in biological processes is yet to be understood, it is seen to play a major function in osmoregulation, modulation of neurotransmitter action, regulation of adipose tissue, and membrane stabilisation (Froger *et al.*, 2014). There is sufficient evidence to demonstrate release of Taurine from the retina under a range of conditions, dependent on the species and stimulus (Salazar *et al.*, 1986)(Neal, Collins and Massey, 1979). While there is stronger evidence to demonstrate poorer retinal activity with reduced taurine levels, there is limited evidence to show the reverse.

The observed electroretinographic (ERG) changes associated with Taurine depletion include decreases in a-wave and b-wave amplitudes, suggesting changes to both the outer and inner retina(Quesada, Picones and Pasantes-Morales, 1988)(Jacobson *et al.*, 1987; Shimada *et al.*, 1992). However the damage appears to be predominantly in the photoreceptor layer where disarray in the organisation of the structures was recorded. (Hayes, Carey and Schmidt, 1975; Anderson *et al.*, 1979; Gaucher *et al.*, 2012)(Barnett and Burger, 1980; Imaki *et al.*, 1993)(Leon, Levick and Sarossy, 1995). This includes swollen inner segments and nuclei, disarray in disk stacks and its membrane,

accumulation of membrane-bound vesicles at the base of the photoreceptor cells, and overall reduction in the size of the photoreceptor layer(Gaucher *et al.*, 2012).

Ornithine

High serum concentration of ornithine was identified as the cause of gyrate atrophy of the retina and the choroid. Hyperornithinaemia is implicated by unusually high levels of Ornithine caused by deficient level of activity and of the enzyme ornithine 5-aminotransferase (OAT). Ornithine a product of the urea cycle, where excess ornithine is further broken down by 2 catabolic enzymes, ornithine 5-transferase and ornithine decarboxylase.

Deficiency of the OAT is a form of rare autosomal recessive disorder, predominantly found in Finland (Takki and Simell, 1974). Clinically, patients demonstrate loss of peripheral vision in the first decade of life, alongside reduction of night vision and myopia. Visual impairment is normally progressive, resulting complete visual loss before reaching the age of 50. (Takki and Simell, 1974; Heinänen *et al.*, 1998). While learning disability does not form part of this condition, early degenerative and atrophic changes with abnormal EEG activities are reported with some patients (Valtonen *et al.*, 1999).

Reduction in the activity of Ornithine-δ-aminotransferase (OAT) is believed to be the cause for elevated / accumulated levels of ornithine. An additional consequence of this is reduced levels of glutamate as the excitatory neurotransmitter; leading to reduced

overall GABA neurotransmitter levels. Some hypothesise that in the presence of Vigabatrin, reduced OAT activity produces hyperornithinaemia and over time manifestations of Gyrate atrophy within the fundus of the eye(Sorri *et al.*, 2010).

CHAPTER 6.2: EXPERIMENTAL WORK

PLASMA CONCENTRATION OF TAURINE AND ORNITHINE IN PATIENTS EXPOSED TO VIGABATRIN

Introduction

The antiseizure medication Vigabatrin is well known to cause visual implications, primarily in the form of visual field defect. One of the potential hypothesis behind this phenomenon is the metabolomic perspective, where Vigabatrin interferes and causes disturbance in amino acid tissue levels, particularly Taurine and Ornithine.

Our centre previously published findings that associated implicit timing delay of more than 2ms in wide field multifocal electroretinography (WF-mfERG) to be reflective of Vigabatrin toxicity, with 100% sensitivity, and 86% specificity (McDonagh *et al.*, 2001, 2003b; Gonzalez *et al.*, 2009). The reason behind the observed timing delays have not been fully elucidated. WF-mfERG has the advantage of providing objective measure of visual function and is especially beneficial in patients with concentration difficulties. The drawback is not insignificant as it requires a highly specialised operator, experienced result interpreter and lengthy testing duration.

The aim of this study is to evaluate the significance of serum concentrations of both amino acids in patients exposed to Vigabatrin, by taking into consideration the presence or absence of >2ms timing delay in their WF-mfERG results.

Method

All patients underwent full ocular examination prior to inclusion into this study. Visual acuity, pupil examination and slit lamp examination which includes intraocular pressure measurements, anterior segment examination and dilated fundoscopy.

As part of the larger study, all subjects have also undergone multifocal electrophysiological examination, blood tests and optical coherence tomography. The WF-mfERG responses were assessed with respect to the amplitude and latency (implicit time) of individual response element. Multifocal electrophysiology results are interpreted by two clinical scientists with total combined duration of 35 years' experience in the subject.

The WF-mfERG protocol utilises back projection stimulus consisting of 61 element array with independent decimated binary m-sequence covering 90 degrees visual field, conducted by a custom-built software. Electrical responses from the central field (0-45 degrees) were compared to the peripheral field (45-90 degrees).

Blood samples were collected from patients in haemolysis tubes containing sodium heparin. The samples were labeled and stored appropriately before transfer to the biochemistry laboratory in the NHS Greater Glasgow and Clyde for analysis. Analysis for Taurine and Ornithine was performed using the High Performance Liquid chromatography (HPLC) with suitable amino acid detectors. The results were provided in absolute values.

Serum concentrations of Taurine and Ornithine are evaluated by the following comparisons:

- Current versus previous Vigabatrin user
- Delayed versus non-delayed

All statistical analysis were performed using SPSS (IBM®SPSS® Statistics, Version 27).
In all four sets of analyses, data samples are compared using descriptive statistics and analysed with the independent samples T-test. The subjects are categorised as either current or previous Vigabatrin user in analyses 1A and 1B, and Delayed or Non-Delayed in analyses 2A and 2B. Serum concentration of amino acids are expressed in µmol/l. Boxplot graphs are used to illustrate spread of data.

The study was approved by the West of Scotland Ethics Committee.

Results

28 patients attended the study visit. Out of the 28, 11 were still on Vigabatrin while 17 were previous users of vigabatrin.

Of the 25 patients who completed the WF-mfERG testing, 11 showed >2ms timing delay in the peripheral field compared to the central field. (Diagram 2)

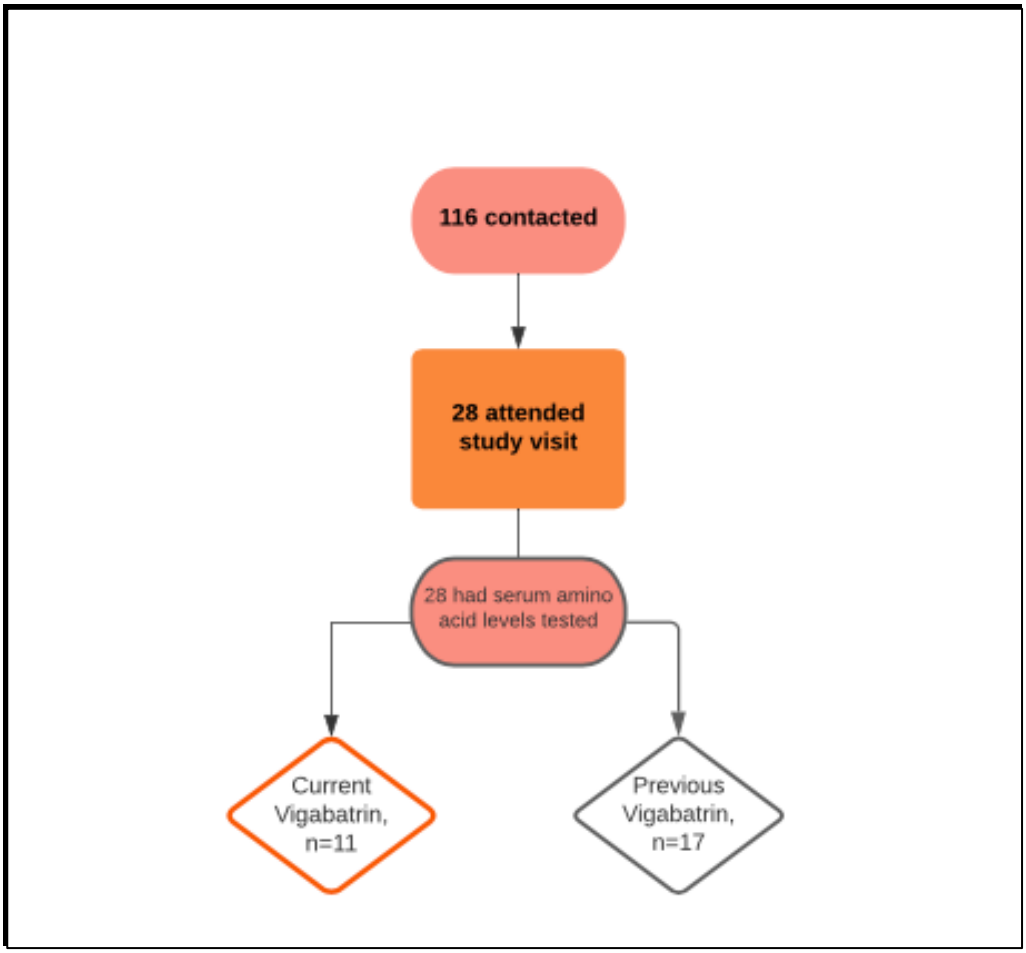

Figure 6.2.1: Flowchart showing distribution of subjects used in analysis 1A and 1B.

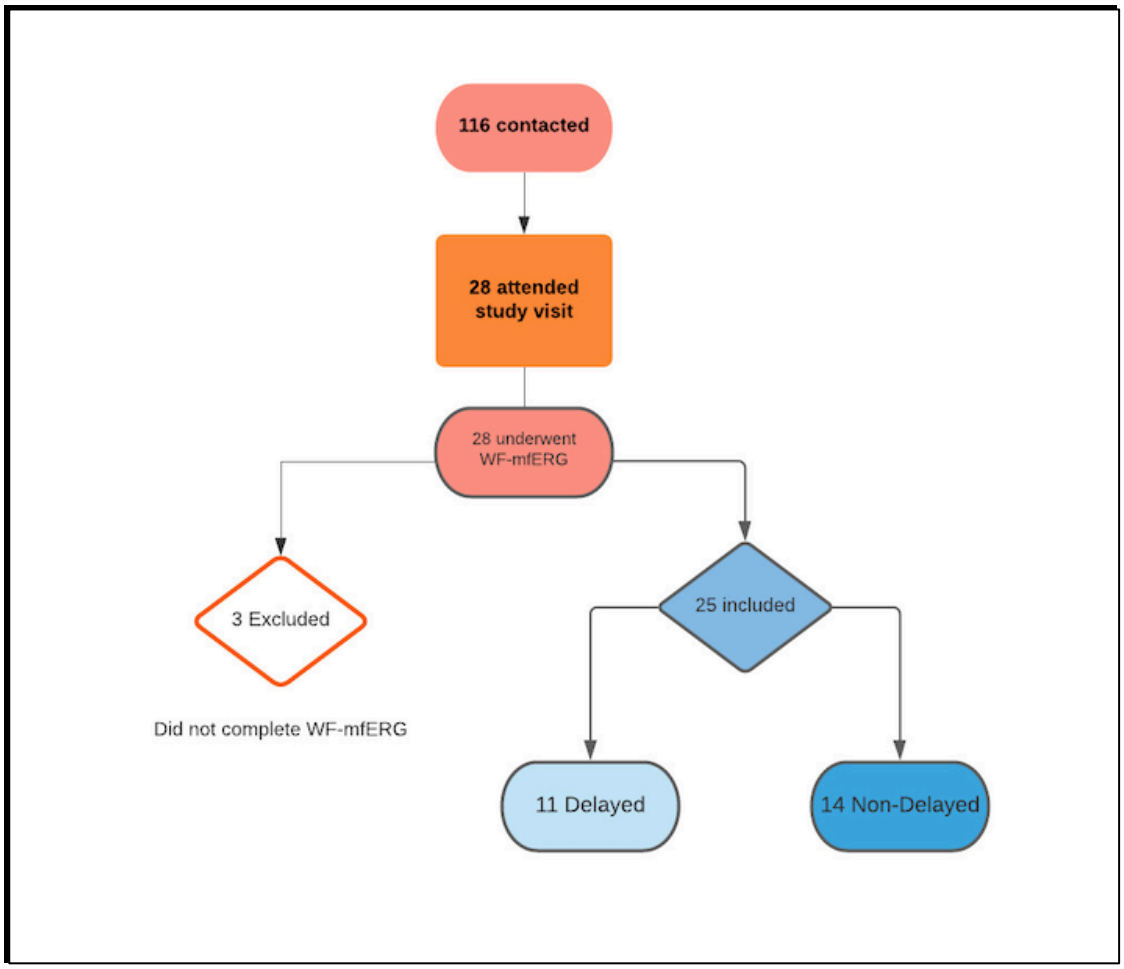

Figure 6.2.2: Flowchart showing distribution of subjects used in analysis 2A and 2B.

The results are tabulated based on the following categories of analyses:

1A: Taurine concentration in Current versus Previous Vigabatrin user

1B: Ornithine concentration in Current versus Previous Vigabatrin user

2A: Taurine concentration based on WF-mfERG results; Delayed versus non-delayed

2B: Ornithine concentration based on WF-mfERG results: Delayed versus non-delayed

Analyses 1:

Current versus Previous Vigabatrin use

28 patients were included in this analysis, where 11 are current users and 17 are recorded as previous users of Vigabatrin. The cumulative Vigabatrin burden was 10.9kg – 30.6kg for the current user group. All current users are on one to three other antiseizure medications, alongside Vigabatrin. In the ex-user group, the cumulative Vigabatrin burden is 1.64kg – 22.9kg.

Analysis 1A: Comparing serum concentrations of Taurine between current and previous users of Vigabatrin.

In this analysis 28 data points were included, 11 for 'current' group and 17 for 'previous' group. In the Current group, the values ranged from 59 µmol/L – 129µmol/L, and the median value of 92.5 µmol/L. In the Previous group, the values ranged 43.9 µmol/L – 101 µmol/L, with the median value of 78.5 µmol/L. When comparing the mean with the two-tailed independent samples t-test, no statistical significance was found at $p = 0.117$. Graph 1 demonstrates the spread of data in both groups.

Case Processing Summary

		Cases					
		Valid		Missing		Total	
	Vigabatrin status	N	Percent	N	Percent	N	Percent
Taurine Concentration (micromol/L)	Current	11	100.0%	0	0.0%	11	100.0%
	Previous	17	100.0%	0	0.0%	17	100.0%

Descriptives

	Vigabatrin status			Statistic	Std. Error
Taurine Concentration (micromol/L)	Current	Mean		88.9182	7.15812
		95% Confidence Interval for Mean	Lower Bound	72.9689	
			Upper Bound	104.8675	
		5% Trimmed Mean		88.3535	
		Median		92.5000	
		Variance		563.626	
		Std. Deviation		23.74080	
		Minimum		59.00	
		Maximum		129.00	
		Range		70.00	
		Interquartile Range		42.70	
		Skewness		.273	.661
		Kurtosis		-1.347	1.279
	Previous	Mean		75.1353	4.31515
		95% Confidence Interval for Mean	Lower Bound	65.9876	
			Upper Bound	84.2830	
		5% Trimmed Mean		75.4337	
		Median		78.5000	
		Variance		316.549	
		Std. Deviation		17.79181	
		Minimum		43.90	
		Maximum		101.00	
		Range		57.10	
		Interquartile Range		29.60	
		Skewness		-.388	.550
		Kurtosis		-1.014	1.063

Table 6.2.1 a, b: Summary of statistical descriptive values in the Taurine concentration analysis for current and previous users of Vigabatrin.

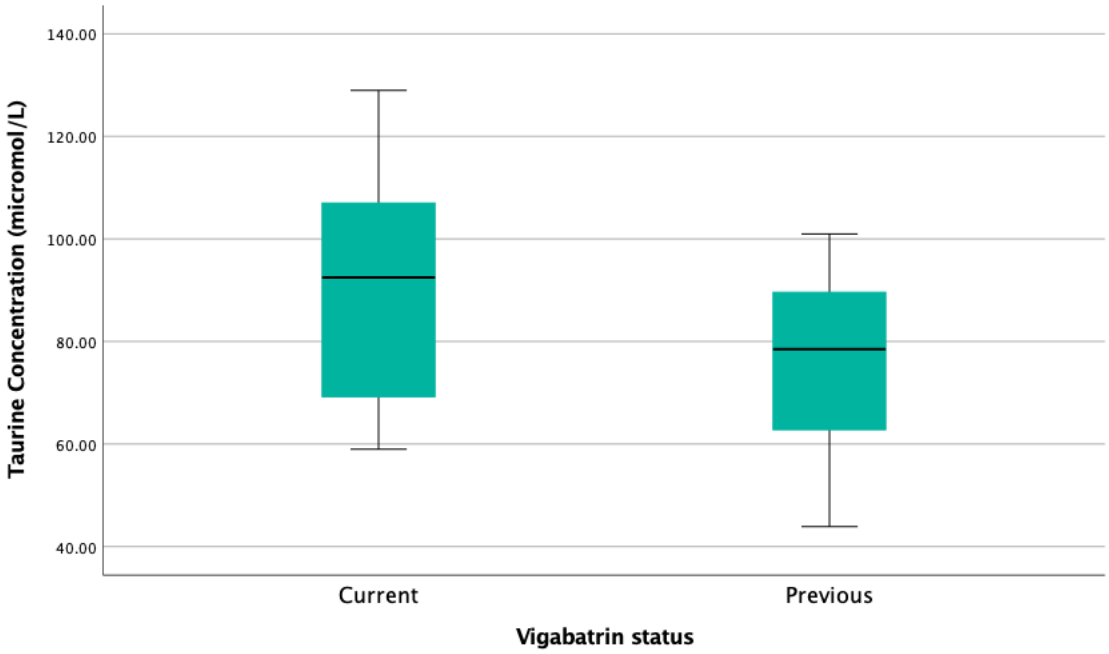

Figure 6.2.3: Boxplot graph comparing serum concentrations of Taurine in current and previous users of Vigabatrin. No significant difference between the spread of data in both groups is found, p = 0.117.

Analysis 1B: Comparing serum ornithine levels in current Vigabatrin users versus ex-Vigabatrin users.

The mean for the 'current' group is 119.28, with a median value of 121. The values ranged from 73.9 µmol/L – 165 µmol/L. The mean value in the 'previous' group is 124.07 µmol/L, with median of 125 µmol/L. The values ranged from 70.1 µmol/L – 203 µmol/L. When comparing the mean with the two-tailed independent samples t-test, no statistical significance was found at p = 0.668. Graph 2 demonstrates the spread of data in both groups.

Case Processing Summary

		Cases					
		Valid		Missing		Total	
	Vigabatrin status	N	Percent	N	Percent	N	Percent
Ornithine concentration (micromol/L)	Current	11	100.0%	0	0.0%	11	100.0%
	Previous	17	100.0%	0	0.0%	17	100.0%

Descriptives

	Vigabatrin status			Statistic	Std. Error
Ornithine concentration (micromol/L)	Current	Mean		119.2818	8.17721
		95% Confidence Interval for Mean	Lower Bound	101.0619	
			Upper Bound	137.5018	
		5% Trimmed Mean		119.2631	
		Median		121.0000	
		Variance		735.534	
		Std. Deviation		27.12072	
		Minimum		73.90	
		Maximum		165.00	
		Range		91.10	
		Interquartile Range		38.60	
		Skewness		-.073	.661
		Kurtosis		-.343	1.279
	Previous	Mean		124.0706	7.37073
		95% Confidence Interval for Mean	Lower Bound	108.4453	
			Upper Bound	139.6958	
		5% Trimmed Mean		122.6840	
		Median		125.0000	
		Variance		923.571	
		Std. Deviation		30.39031	
		Minimum		70.10	
		Maximum		203.00	
		Range		132.90	
		Interquartile Range		29.00	
		Skewness		.559	.550
		Kurtosis		2.109	1.063

Table 6.2.2a,b: Summary of statistical descriptive values in the serum Ornithine concentration analysis for current and previous users of Vigabatrin.

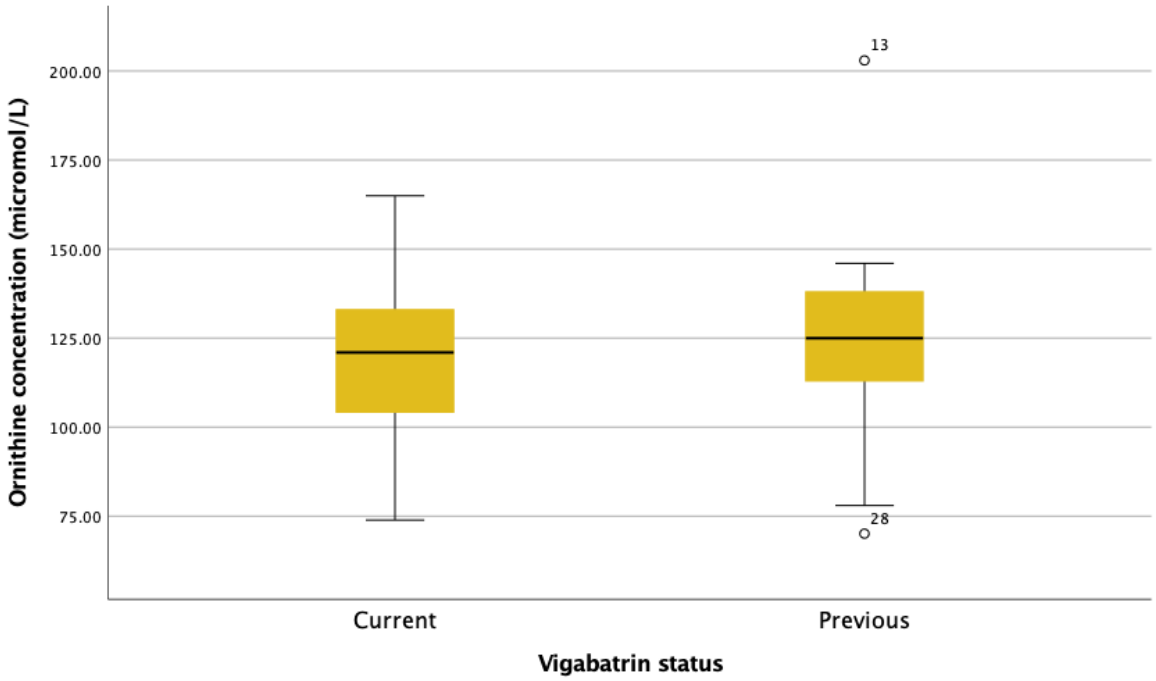

Figure 6.2.4: Boxplot graph comparing serum concentrations of ornithine in current and previous users of Vigabatrin. No significant difference in this comparison is found, p = 0.668.

Global analysis for 1A and 1B:

For serum taurine, the mean concentration for the current group is higher at 88.92, compared to 75.13 for the previous users. Even though there appear to be some difference in the mean and spread of data between both groups in 1A and 1B, where taurine appear to be higher in the 'current' group, ornithine higher in the 'previous' group, both comparisons did not reach statistical significance.

Group Statistics

	Vigabatrin status	N	Mean	Std. Deviation	Std. Error Mean
Taurine Concentration (micromol/L)	Current	11	88.9182	23.74080	7.15812
	Previous	17	75.1353	17.79181	4.31515
Ornithine concentration (micromol/L)	Current	11	119.2818	27.12072	8.17721
	Previous	17	124.0706	30.39031	7.37073

Independent Samples Test

		Levene's Test for Equality of Variances		t-test for Equality of Means						
									95% Confidence Interval of the Difference	
		F	Sig.	t	df	Sig. (2-tailed)	Mean Difference	Std. Error Difference	Lower	Upper
Taurine Concentration (micromol/L)	Equal variances assumed	2.323	.140	1.756	26	.091	13.78289	7.85027	-2.35357	29.91934
	Equal variances not assumed			1.649	17.171	.117	13.78289	8.35818	-3.83793	31.40371
Ornithine concentration (micromol/L)	Equal variances assumed	.015	.903	-.424	26	.675	-4.78877	11.28981	-27.99530	18.41776
	Equal variances not assumed			-.435	23.256	.668	-4.78877	11.00883	-27.54842	17.97088

Independent Samples Effect Sizes

		Standardizer[a]	Point Estimate	95% Confidence Interval	
				Lower	Upper
Taurine Concentration (micromol/L)	Cohen's d	20.28739	.679	-.107	1.454
	Hedges' correction	20.89704	.660	-.104	1.411
	Glass's delta	17.79181	.775	-.040	1.568
Ornithine concentration (micromol/L)	Cohen's d	29.17617	-.164	-.922	.597
	Hedges' correction	30.05292	-.159	-.895	.580
	Glass's delta	30.39031	-.158	-.915	.605

a. The denominator used in estimating the effect sizes.
Cohen's d uses the pooled standard deviation.
Hedges' correction uses the pooled standard deviation, plus a correction factor.
Glass's delta uses the sample standard deviation of the control group.

Table 6.2.3a, b, c: Summary of descriptive statistics for Analyses 1. Table 1b Shows the results for independent samples t-test results for both Taurine and Ornithine serum concentrations in current and previous user groups.

ANALYSES 2

Delayed versus Non-Delayed group.

Of the 28 who completed the study, 25 were included in this analysis. 3 were excluded as they did not complete the mfERG phase of testing.

Of the 25, 11 were 'delayed' and 14 were 'non-delayed'.

In the delayed group 6 are current vigabatrin users, versus 3 current users in the non-delayed group.

Analysis 2A: Comparing serum taurine levels in Delayed versus Non-delayed group, based on WF-mfERG results.

The mean value for Taurine in the Delayed group is 85.84 µmol/L, and the median is 89.6 µmol/L. The values ranged from 62.8 µmol/L to 111 µmol/L. In the Non-Delayed group, the mean is 76.43 µmol/L with the median 74.35 µmol/L. The values ranged from 47.1 µmol/L – 114 µmol/L. When comparing the mean with the two-tailed independent samples t-test, no statistical significance was found at $p = 0.199$. Graph 3 demonstrates the spread of data in both groups.

Case Processing Summary

		Cases					
		Valid		Missing		Total	
	mfERG	N	Percent	N	Percent	N	Percent
Taurine concentration (micromol/L)	Delayed	11	100.0%	0	0.0%	11	100.0%
	Non-Delayed	14	100.0%	0	0.0%	14	100.0%

Descriptives

	mfERG			Statistic	Std. Error
Taurine concentration (micromol/L)	Delayed	Mean		85.8364	4.74476
		95% Confidence Interval for Mean	Lower Bound	75.2644	
			Upper Bound	96.4084	
		5% Trimmed Mean		85.7182	
		Median		89.6000	
		Variance		247.641	
		Std. Deviation		15.73660	
		Minimum		62.80	
		Maximum		111.00	
		Range		48.20	
		Interquartile Range		25.80	
		Skewness		-.138	.661
		Kurtosis		-.904	1.279
	Non-Delayed	Mean		76.4286	5.29744
		95% Confidence Interval for Mean	Lower Bound	64.9841	
			Upper Bound	87.8730	
		5% Trimmed Mean		75.9706	
		Median		74.3500	
		Variance		392.881	
		Std. Deviation		19.82122	
		Minimum		47.10	
		Maximum		114.00	
		Range		66.90	
		Interquartile Range		34.65	
		Skewness		.311	.597
		Kurtosis		-.709	1.154

Table 6.2.4a, b: **Summary of statistical descriptive values in the serum Taurine concentration analysis for the Delayed and Non-Delayed groups.**

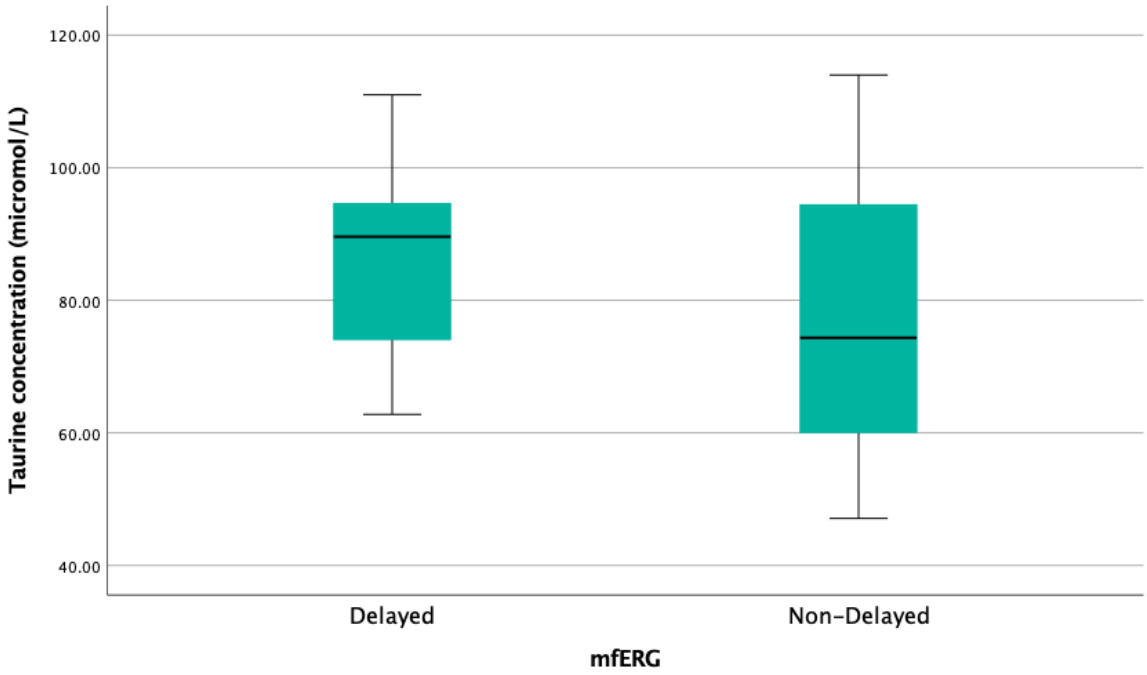

Figure 6.2.5: Boxplot graph comparing serum concentrations of Taurine between the Delayed and Non-delayed group. No significance difference in this comparison is found, p = 0.199.

Analysis 2B: Comparing serum ornithine levels in delayed versus non-delayed group, based on WF-mfERG results.

The mean value for Ornithine in the Delayed group is 128.41 µmol/L, and the median is 133 µmol/L. The values ranged from 89.1 µmol/L to 165 µmol/L. In the Non-Delayed group, the mean is 127.07 µmol/L with the median 121 µmol/L. The values ranged from 78 µmol/L – 203 µmol/L. When comparing the mean with the two-tailed independent samples t-test, no statistical significance was found at p = 0.896. Graph 4 demonstrates the spread of data in both groups.

Case Processing Summary

		Cases					
		Valid		Missing		Total	
	mfERG	N	Percent	N	Percent	N	Percent
Ornithine concentration (micromol/L)	Delayed	11	100.0%	0	0.0%	11	100.0%
	Non-Delayed	14	100.0%	0	0.0%	14	100.0%

Descriptives

	mfERG			Statistic	Std. Error
Ornithine concentration (micromol/L)	Delayed	Mean		128.4091	6.84114
		95% Confidence Interval for Mean	Lower Bound	113.1661	
			Upper Bound	143.6521	
		5% Trimmed Mean		128.5601	
		Median		133.0000	
		Variance		514.813	
		Std. Deviation		22.68949	
		Minimum		89.10	
		Maximum		165.00	
		Range		75.90	
		Interquartile Range		32.00	
		Skewness		-.395	.661
		Kurtosis		-.252	1.279
	Non-Delayed	Mean		127.0714	7.41580
		95% Confidence Interval for Mean	Lower Bound	111.0506	
			Upper Bound	143.0923	
		5% Trimmed Mean		125.5794	
		Median		121.0000	
		Variance		769.918	
		Std. Deviation		27.74739	
		Minimum		78.00	
		Maximum		203.00	
		Range		125.00	
		Interquartile Range		22.75	
		Skewness		1.352	.597
		Kurtosis		4.329	1.154

Table 6.2.5a, b: **Summary of statistical descriptive values in the serum Ornithine concentration analysis for the Delayed and Non-Delayed groups.**

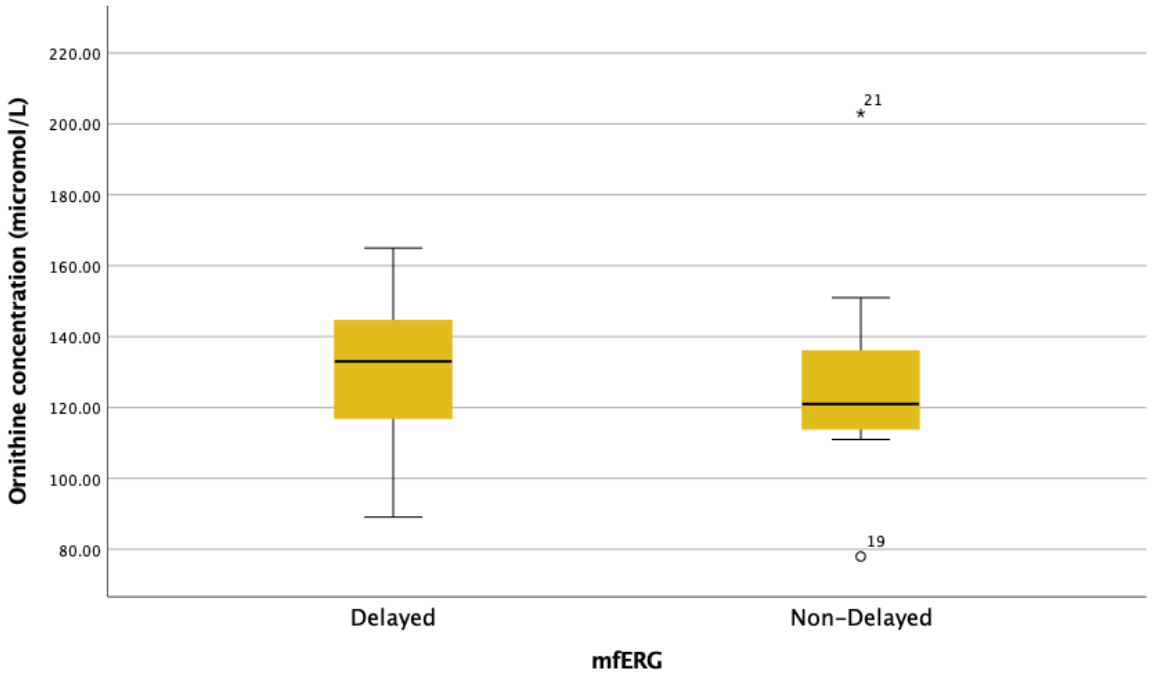

Figure 6.2.6: Boxplot graph comparing serum concentrations of Ornithine between the Delayed and Non-Delayed group. No significant difference in this comparison is found at p = 0.896.

In the global analysis for 2A and 2B, the Taurine concentrations appear higher in the Delayed group but did not achieve statistical significance. There was little difference in the ornithine concentrations between both groups.

Group Statistics

	mfERG	N	Mean	Std. Deviation	Std. Error Mean
Taurine concentration (micromol/L)	Delayed	11	85.8364	15.73660	4.74476
	Non-Delayed	14	76.4286	19.82122	5.29744
Ornithine concentration (micromol/L)	Delayed	11	128.4091	22.68949	6.84114
	Non-Delayed	14	127.0714	27.74739	7.41580

Independent Samples Test

		Levene's Test for Equality of Variances		t-test for Equality of Means						
									95% Confidence Interval of the Difference	
		F	Sig.	t	df	Sig. (2-tailed)	Mean Difference	Std. Error Difference	Lower	Upper
Taurine concentration (micromol/L)	Equal variances assumed	.831	.372	1.286	23	.211	9.40779	7.31629	-5.72710	24.54268
	Equal variances not assumed			1.323	22.990	.199	9.40779	7.11166	-5.30415	24.11973
Ornithine concentration (micromol/L)	Equal variances assumed	.013	.909	.129	23	.898	1.33766	10.34316	-20.05879	22.73412
	Equal variances not assumed			.133	22.942	.896	1.33766	10.08937	-19.53671	22.21204

Independent Samples Effect Sizes

		Standardizer[a]	Point Estimate	95% Confidence Interval	
				Lower	Upper
Taurine concentration (micromol/L)	Cohen's d	18.15855	.518	-.291	1.316
	Hedges' correction	18.77877	.501	-.281	1.273
	Glass's delta	19.82122	.475	-.344	1.276
Ornithine concentration (micromol/L)	Cohen's d	25.67104	.052	-.738	.841
	Hedges' correction	26.54786	.050	-.714	.814
	Glass's delta	27.74739	.048	-.743	.837

a. The denominator used in estimating the effect sizes.
Cohen's d uses the pooled standard deviation.
Hedges' correction uses the pooled standard deviation, plus a correction factor.
Glass's delta uses the sample standard deviation of the control group.

Table 6.2.6a, b, c: Summary of descriptive statistics for Analyses 2. Table 6.2.6b shows the calculations for independent samples t-test results for both Taurine and Ornithine serum concentrations in the Delayed and non-delayed groups

Groups	n (subjects)	Analyses	Comparison group	Mean (µmol/L)	Independent samples t-test, p value	t value
Current versus previous user	Current =11	1A	Taurine	Current= 88.92 Previous = 75.14	0.117	1.649
	Previous = 17	1B	Ornithine	Current = 119.28 Previous = 124.07	0.668	-0.435
Delayed versus non-delayed	Delayed = 11	2A	Taurine	Delayed = 85.84 Non-Delayed = 76.42	0.199	1.323
	Non-Delayed = 14	2B	Ornithine	Delayed = 128.41 Non-delayed = 127.07	0.896	0.133

Table 6.2.7: Comparing key statistical values from each group and analyses.

Discussion:

It appears that the most common outcome when ascertaining risks factors that might be related to VaRT, not all patients display the same vulnerability. The distinctive feature/clue that separates those who are vulnerable to the toxic effects is still undetermined. Our strategy is to investigate if the delay in timing responses observed in

the multifocal ERG changes, as well as if current exposure to Vigabatrin can be a distinctive feature that could be narrowed further by examining serum concentrations of taurine and ornithine.

Serum Taurine

The role of taurine in mediating the function of the retina lead to the hypothesis that taurine may be affected in Vigabatrin users. Pre-clinical animal studies found depletion of Taurine levels alongside vigabatrin use is associated with retinopathy. To date no clinical studies have convincingly reported a relationship between plasma Taurine concentrations and vigabatrin use. It interesting to note that to date there is only a single publication studying taurine levels in vigabatrin users in humans (Spelbrink *et al.*, 2016). They found no correlation between the use of Vigabatrin and taurine in their small paediatric cohort, but also acknowledge that they made no distinction between those with visual or retinal pathologies.

Authors	**Nature**	**Subject number**	**Main finding**
Spellbrink et al 2016	Retrospective Clinical	16 paediatrics	Normal plasma taurine levels in Vigabatrin exposed subjects

Table 6.2.8: Summary of clinical/human studies between Vigabatrin and Taurine.

More convincing findings have been drawn primarily from pre-clinical studies involving rats, rodents and cats; as a result taurine levels monitoring and supplementation are recommended in children taking Vigabatrin by the Tuberous Sclerosis Alliance. Halonen

et al reported no difference in the CSF taurine levels after long term Vigabatrin use in both rodents and humans (Halonen, Pitkänen and Riekkinen, 1990).
Interestingly, a more recent study found dysregulation of taurine and ornithine, which appear to be confined to the retina in vigabatrin treated murine models (Walters *et al.*, 2021). This would explain both sides of the hypothesis, where disruption in taurine have reduced its neuroprotective effect on the retina, and yet such changes are not detectable in our serum.In our study, serum taurine in both analyses did not reach statistical significance. In all groups the mean level was within normal limits. The main limitation of this analyses would be the small number of subjects analysed each group.

Serum Ornithine

The recent findings by Walters et al would also echo an early suggestion raised by Roubertie et al that ornithine levels may be implicated in the vigabatrin associated retinal toxicity (Roubertie, Bellet and Echenne, 1998). This was on the basis that Vigabatrin is known to have inhibitory action on several transaminases, thereby inducing secondary metabolic interference. Ornithine is the product of the urea cycle; originates from dietary arginine from by arginase and catabolised by ornithine-d-aminotrasferase (OAT) to glutamate-γ semialdehyde and glutamate. In the presence of Vigabatrin, OAT activity is reduced, thereby causing hyperornithinaemia. Over time hyperornithinaemia is known to cause gyrate atrophy within the fundus. Sorri et al found reduced OAT activities in vigabatrin exposed patients with documented visual field defect. Reduced levels of the OAT enzyme lead to a build-up of ornithine levels within tissues and a reduction of the neuroexcitatory glutamate, and overall reduced GABA levels. The

subsequent effect of hyperornithinaemia is believed to be toxic to the choroid and the retina, although the exact mechanism is still unknown. Even though previous work has supported the hypothesis that ornithine levels are implicated in patients who used Vigabatrin, there has been insufficient human studies to demonstrate that this. In our study, serum measurement levels of ornithine in both analyses did not reach statistical significance. In all groups the mean level was within normal limits. Krauss et al reported the same in his 2 patients (G. L. Krauss, Johnson and Miller, 1998). The limitations of these analyses would be the small number of subjects within each group, as well as the lack of data for OAT activity. Serum Ornithine levels are also highly influenced by dietary intake, which were not recorded in this study due to the complex nature of patients.

The following table summarises available published reports on the interaction between Vigabatrin and ornithine.

Authors	**Nature**	**Subject number**	**Main finding**
Sorri et al 2010	Clinical Prospective	47	Ornithine aminotransferase (OAT) activity is reduced in Vigabatrin exposed patients with visual field defects
Hisama FM et al 2001	Genetic and molecular analysis	17	No clinically significant genetic mutation detected.
Krauss et al 1998	Clinical Prospective (unpublished)	2	Normal serum ornithine in Vigabatrin exposed patients

Table 6.2.9: Summary of clinical/human studies between Vigabatrin and Ornithine

The lack of relationship demonstrated in this study could be due to the selective vulnerability in the development of visual toxicity that cannot be tested sufficiently within small numbers of subjects. This is also the issue encountered by other published work, although direct comparison with our work is not feasible due to different categories compared for analyses.

The lack of relationship between Vigabatrin, and the amino acids Taurine and Ornithine through serum testing certainly does not eliminate the notion of their involvement, especially as localised dysregulation of Taurine and Ornithine was observed in the retina of experimental models (Walters *et al.*, 2021).

On the positive side it demonstrates that serum Taurine and Ornithine concentrations are generally maintained within normal range in patients where vigabatrin related visual effects is a risk. However, our finding does not exclude the possible relationship that may exist between the amino acids and the function of the retina; but suggest that other categories of comparison should be considered to fully explore the role of the amino acids, especially Taurine in this patient group.

CHAPTER 7:

DISCUSSION OF THE THESIS

General discussion

This was a prospective study examining the visual function of 28 patients who have been exposed to Vigabatrin. Our project aimed to examine several aspects of visual function for correlation with Vigabatrin associated retinal toxicity (VaRT), based on multifocal ERG readings. The key findings of the experimental work are discussed under the following themes:

1. OCT RNFL is not a suitable marker for detection and monitoring of Vigabatrin associated retinal toxicity
2. OCT volume microstructures is highly correlated to >2 ms timing delay of the peripheral field compared to central field in multifocal ERG.
3. Vigabatrin associated retinal toxicity affects multiple layers of the retina
4. Serum concentrations of Taurine and Ornithine is unaffected by Vigabatrin

OCT RNFL IS NOT A SUITABLE MARKER FOR DETECTING AND MONITORING OF VIGABATRIN ASSOCIATED RETINAL TOXICITY

Previous work examining structure-function correlation made from OCT scans are predominantly drawn from patients with glaucoma, which is a gradually progressive optic neuropathy often associated with raised intraocular pressure. The structural damage that occur in glaucomatous eyes is predominantly thought to be due to retinal ganglion cell loss, believed to be the final result of multiple biochemical alteration of trophic factors and neuroprotectants resulting in axonal cell death (Osborne *et al.*, 1999). The pattern for visual field defect in glaucoma is highly predictable, following specific patterns from arcuate defect, nasal step that progresses to encroach onto the central vision. The structure function correlation for glaucoma based on OCT RNFL is surprisingly less than predictable, given the amount of interest and resources directed into it. The characteristics of ganglion cell complex progression appear more defined than RNFL thinning (Renard, Fénolland and Giraud, 2019). Moderate correlation between peripapillary RNFL thickness and visual field severity indices, with the greater association in the inferior quadrant (Kang *et al.*, 2015).

It is important to bear in mind the distinct differences in the aetiology of both conditions, and to not apply the same structure-function filters to VaRT. For instance the ganglion cell layer complex appear to implicated in macula analysis of glaucomatous eyes, while in our study it appears several different cell layers are implicated (discussed

in the next theme). The disc RNFL findings in VaRT at present appears to be a mixed bag, ranging from nasal RNFL thinning, while the other quadrants appear preserved, to temporal RNFL thickening in the first year from Vigabatrin use (Lawthom, Smith and Wild, 2009; Moseng *et al.*, 2011; Clayton *et al.*, 2013; Sergott *et al.*, 2016b). The appropriateness of using RNFL as a biomarker is further challenged by the finding of thinner RNFL in patients with epilepsy with no prior exposure to Vigabatrin.

Cumulatively, these observations are not entirely paradoxical, considering the key disc RNFL findings applicable to this cohort. One theory is that thickening of RNFL occurs in all but least in the nasal quadrant. When this is superimposed on a patient with thinned pre-existing RNFL, it could give the impression of tissue preservation when in fact the 'original thinning' is masked by a secondary pathology that could be attributed by Vigabatrin.

When considering data from our cohort, the thickening of the temporal RNFL quadrant is significant in those with >2ms peripheral timing delay, and could reflect a more compelling reaction from Vigabatrin and can imply 'tissue toxicity'.

The interpretation of the strong relationship between RNFL quadrants thickness and perimetry score in our study is a challenge. The relationship appears in both 'all' and 'delayed only' group for the global, inferior and nasal quadrants. This is likely to simply illustrate the general severity of cell loss from the cumulative effect of the inherent structural changes from epilepsy as well as from Vigabatrin, causing general decline in retinal function. Stratification of the results based on Visual fields severity grading is not

feasible due to the small data sample, although would be interesting as a direction for future research.

In summary, there is simply insufficient evidence to fully conclude on a definitive role of OCT disc RNFL in VaRT. At present the cumulative observation from various publications adds to the current knowledge base particularly on the distinctive pattern of thickening or thinning of RNFL in epileptic population, and how this pattern differs from other forms of optic neuropathies.

OCT volume microstructures are highly correlated to the >2ms peripheral timing delay seen in multifocal ERG.

The strong relationship between >2ms peripheral timing delay with retinal microstructure and visual fields is encouraging and reassures us that our WF-mfERG observation is likely to reflect VaRT. The strong relationship between the variables also degrades significantly when the WF-mfERG is removed from the equation. In both experimental works (chapters 5.2 and 5.3), several retinal layers are involved. When correlated with visual fields, the ganglion cell, inner plexiform, outer plexiform and outer nuclear layers appear to have strong predictive linear relationship with perimetry score in the delayed group. This was also echoed in the study looking at differences in microlayer volumes, where higher volumes were observed in the delayed group for nerve fibre, ganglion cell, inner plexiform, outer plexiform, outer nuclear and the overall inner retinal layers. The summary is provided below.

Microlayers	*Delayed (mean in mm^3)*	*Non-delayed (mean in mm^3)*	*p-values*	*ANOVA sig (p-values in Delayed vs VF)*	*ANOVA sig (p-values in All vs VF)*
Nerve fibre	0.876	0.748	0.023	0.214	0.462
Ganglion cell	1.006	0.900	0.002	0.032	0.114
Inner Plexiform	0.835	0.771	0.003	0.017	0.053
Inner Nuclear	0.991	0.942	0.068	0.114	0.619
Outer Plexiform	0.865	0.786	0.038	0.023	0.005
Outer nuclear	1.879	1.615	0.001	0.007	0.655
RPE	0.386	0.368	0.160	0.742	0.775
Inner retinal	6.455	5.764	<0.001	0.102	0.322
Outer retinal	2.226	2.179	0.083	0.096	0.199

Table 7.1 Table illustrating key statistical values for microlayers from analyses in chapters 5.2 and 5.3.

One would wonder how structural changes of the macula, which is primarily responsible for our central vision, is relevant in a disease that predominantly affects the peripheral vision. After all, central field of vision is typically reported as unchanged or unaffected in Vigabatrin exposed patients. We feel this striking observation parallel some earlier thinking that VaRT is in fact a diffuse disease rather than restricted to the peripheral retina. The lack of concordance between ERG and Visual fields observed by an author led them to suspect a diffuse retinal disease (Hilton *et al.*, 2002; Jensen *et al.*, 2002). Unpublished data from our center also found some correlation between the N1/P1 ratio in the mfERG central rings in the delayed group. Naturally such subtle changes may be

missed by a full field ERG, as the signals are produced from assessment of the global retinal function. The peripheral field loss recorded in VaRT is most likely to be due to higher vulnerability of the peripheral retina from lower cell density, compared to the macula which has a higher density of müller cells as protection (Daneshvar *et al.*, 1999).

During the time of this study there is no commercially available OCT device that can directly examine the peripheral retinal structure for direct correlation with our WF-mfERG findings. Now, Ultra widefield OCT is available and will no doubt be helpful for future research in this topic.

Vigabatrin associated retinal toxicity affects multiple layers of the retina

Our study also supports the thinking that toxic effects from vigabatrin is multi layered and not confined to a specific cell type. Structurally, our study confirms the involvement of several microlayers (see Table 7) of the retina. It is encouraging to also find considerable concordance between our data and published histopathological reports in both experimental models and humans. Ganglion cell layer was first implicated through structural photographs (not OCT) where 'thinning' was observed (Choi and Kim, 2004). Post mortem pathological analysis of the retina in a deceased patient with VaRT showed widespread loss of ganglion cell, with some sparing of the macula. Disruption in the cellular structure and organisation was also reported in the inner nuclear, outer nuclear, inner and outer plexiform layers (Ravindran *et al.*, 2001a).

The conspicuous enigma here would be the higher tissue volume observed in our data, which would naturally suggest tissue 'thickening'. This would contrast the GCL thinning observation made by Choi et al, although their observation was via photography, and not OCT. The observation made by Ravindran et al did not comment on general tissue volume but rather 'loss' which almost always imply thinning, but we cannot be sure. Speculation of the effect on tissue volume from the reported cellular structure and disorganisation also could not be drawn. Higher foveal thickness in vigabatrin treated patients compared to controls were also observed in another study, although not in the perifovea or parafoveal region (Tuğcu *et al.*, 2017).

To date, the thickening or increased volume seen in our cohort and other reports (Sergott *et al.*, 2016a; Tuğcu *et al.*, 2017) is baffling. Prospective studies to specifically monitor the retinal changes that occur on a microstructure level will be able to shed more light into the aetiology of this condition.

Development of customised analytical algorithm involving retinal autosegmentation in an OCT software could assist further study and help us progress in the right direction in the detection and monitoring of VaRT.

Serum concentrations of Taurine and Ornithine is unaffected by Vigabatrin use

In our pursuit to seek a practical and ideal biomarker for VaRT, we strategized to test serum concentrations of taurine and ornithine. Our analyses however did not reveal a significant pattern that could be extended into the clinical setting. Similar findings were found by other researchers. The lack of relationship in serum testing does not preclude the involvement of Taurine and Ornithine altogether, as localised retinal dysregulation of Taurine and Ornithine was uncovered in an experimental work. This would explain both sides of the hypothesis, where disruption in Taurine have reduced its neuroprotective effect on the retina, and Ornithine indeed is affected and yet such changes are not detectable in our serum, making it an unsuitable serum biomarker for VaRT.

Summary

Overall, it has been a delightful experience to uncover some significant structural correlations with the >2ms peripheral timing delay in our WF-mfERG, shedding more light and adding weight to this mfERG abnormality. This is important as it currently is a standalone yardstick, as other centres have not been able to replicate the same results.

VaRT is undoubtedly a retinal disease, as supported not only by our studies but many others through rigorous examination of animal models and meticulous data extraction and innovative data reconstruction to better understand the aetiology of VaRT. We hope data from this study can help narrow down a more specific and practical biomarker to detect and monitor the progression of VaRT.

BIBLIOGRAPHY

Allen, M. P. (1997) 'The problem of multicollinearity', in *Understanding Regression Analysis*. Boston, MA: Springer US, pp. 176–180. doi: 10.1007/978-0-585-25657-3_37.

Alshareef, R. A. *et al.* (2017) 'Segmentation errors in macular ganglion cell analysis as determined by optical coherence tomography in eyes with macular pathology.', *International journal of retina and vitreous*, 3, p. 25. doi: 10.1186/s40942-017-0078-7.

Anderson, P. A. *et al.* (1979) 'Biochemical lesions associated with taurine deficiency in the cat.', *Journal of animal science*, 49(5), pp. 1227–34. doi: 10.2527/jas1979.4951227x.

Ang, M. *et al.* (2018) 'Anterior segment optical coherence tomography', *Progress in Retinal and Eye Research*, 66, pp. 132–156. doi: 10.1016/j.preteyeres.2018.04.002.

Arndt, C. F. *et al.* (1999) 'Outer retinal dysfunction in patients treated with vigabatrin.', *Neurology*, 52(6), pp. 1201–5. doi: 10.1212/wnl.52.6.1201.

Arya, B. *et al.* (2015) 'Pointwise linear regression analysis of serial Humphrey visual fields and a correlation with electroretinography in birdshot chorioretinopathy.', *The British journal of ophthalmology*, 99(7), pp. 973–8. doi: 10.1136/bjophthalmol-2014-306003.

Balestrini, S. *et al.* (2016) 'Retinal nerve fibre layer thinning is associated with drug resistance in epilepsy.', *Journal of neurology, neurosurgery, and psychiatry*, 87(4), pp. 396–401. doi: 10.1136/jnnp-2015-310521.

Banin, E. *et al.* (2003) 'Retinal function abnormalities in patients treated with vigabatrin.', *Archives of ophthalmology (Chicago, Ill. : 1960)*, 121(6), pp. 811–6. doi: 10.1001/archopht.121.6.811.

Barnett, K. C. and Burger, I. H. (1980) 'Taurine deficiency retinopathy in the cat.', *The Journal of small animal practice*, 21(10), pp. 521–34. doi: 10.1111/j.1748-5827.1980.tb01354.x.

Barrett, D. *et al.* (2014) 'Vigabatrin Retinal Toxicity First Detected with Electroretinographic Changes: A Case Report.', *Journal of clinical & experimental ophthalmology*, 5(5). doi: 10.4172/2155-9570.1000363.

Ben-Menachem, E. *et al.* (1989) 'The effect of different vigabatrin treatment regimens on CSF biochemistry and seizure control in epileptic patients.', *British journal of clinical pharmacology*, 27 Suppl 1, pp. 79S-85S. doi: 10.1111/j.1365-2125.1989.tb03466.x.

Ben-Menachem, E. *et al.* (1991) 'Effect of long-term vigabatrin therapy on selected neurotransmitter concentrations in cerebrospinal fluid.', *Journal of child neurology*, Suppl 2, pp. S11-6. Available at: http://www.ncbi.nlm.nih.gov/pubmed/1719063.

Bengtsson, B. and Heijl, A. (2000) 'False-Negative Responses in Glaucoma Perimetry: Indicators of Patient Performance or Test Reliability?', *Investigative Ophthalmology & Visual Science*, 41(8), pp. 2201–2204.

Bernardi, L., Costa, V. P. and Shiroma, L. O. (2007) 'Flicker perimetry in healthy subjects: influence of age and gender, learning effect and short-term fluctuation', *Arquivos Brasileiros de Oftalmologia*, 70(1), pp. 91–99. doi: 10.1590/S0004-27492007000100017.

Bernasconi, R. *et al.* (1988) 'Gamma-vinyl GABA: comparison of neurochemical and anticonvulsant effects in mice.', *Journal of neural transmission*, 72(3), pp. 213–33. doi: 10.1007/BF01243421.

Besch, D. *et al.* (2002) 'Visual field constriction and electrophysiological changes associated with vigabatrin.', *Documenta ophthalmologica. Advances in ophthalmology*, 104(2), pp. 151–70. doi: 10.1023/a:1014644307518.

de Boer, R. W. *et al.* (1982) 'Concepts for automatic perimetry, as applied to the Scoperimeter, an experimental automatic perimeter', *International Ophthalmology*, 5(3), pp. 181–191. doi: 10.1007/BF00149152.

Bormann, J. and Feigenspan, A. (1995) 'GABAC receptors.', *Trends in neurosciences*, 18(12), pp. 515–9. doi: 10.1016/0166-2236(95)98370-e.

Bresnahan, R. *et al.* (2020) 'Vigabatrin add-on therapy for drug-resistant focal epilepsy.', *The Cochrane database of systematic reviews*, 7, p. CD007302. doi: 10.1002/14651858.CD007302.pub3.

Brodie, M. J. and Mumford, J. P. (1999) 'Double-blind substitution of vigabatrin and valproate in carbamazepine- resistant partial epilepsy', *Epilepsy Research*. doi: 10.1016/S0920-1211(98)00110-7.

Browne, T. R. *et al.* (1987) 'Vigabatrin for refractory complex partial seizures: multicenter single-blind study with long-term follow-up.', *Neurology*, 37(2), pp. 184–9. doi: 10.1212/wnl.37.2.184.

Buncic, J. R. *et al.* (2004) 'Characteristic retinal atrophy with secondary "inverse" optic atrophy identifies vigabatrin toxicity in children', *Ophthalmology*. doi: 10.1016/j.ophtha.2004.03.036.

Butler, W. H. (1989) 'The Neuropathology of Vigabatrin', *Epilepsia*. doi: 10.1111/j.1528-1157.1989.tb05827.x.

Butler, W. H., Ford, G. P. and Newberne, J. W. (1987) 'A Study of the Effects of Vigabatrin on the Central Nervous System and Retina of Sprague Dawley and Lister-Hooded Rats', *Toxicologic Pathology*. doi: 10.1177/019262338701500203.

Chan, H. L. and Mohidin, N. (2003) 'Variation of multifocal electroretinogram with axial length.', *Ophthalmic & physiological optics : the journal of the British College of*

Ophthalmic Opticians (Optometrists), 23(2), pp. 133–40. doi: 10.1046/j.1475-1313.2003.00097.x.

Chan, K. *et al.* (2020) 'Vigabatrin-Induced Retinal Functional Alterations and Second-Order Neuron Plasticity in C57BL/6J Mice.', *Investigative ophthalmology & visual science*, 61(2), p. 17. doi: 10.1167/iovs.61.2.17.

Chandrinos, A. and Tzamouranis, D.-D. (2020) 'A Review of Learning Effect in Perimetry', *Ophthalmology Research: An International Journal*, pp. 23–30. doi: 10.9734/or/2020/v12i230144.

Chaudhuri, A. and Behan, P. O. (2004) 'Fatigue in neurological disorders.', *Lancet (London, England)*, 363(9413), pp. 978–88. doi: 10.1016/S0140-6736(04)15794-2.

Chew, S. S. L. *et al.* (2016) 'Anxiety in visual field testing.', *The British journal of ophthalmology*, 100(8), pp. 1128–33. doi: 10.1136/bjophthalmol-2015-307110.

Chin, M. P. *et al.* (2015) 'Human electroretinal responses to grating patterns and defocus changes by global flash multifocal electroretinogram.', *PloS one*, 10(4), p. e0123480. doi: 10.1371/journal.pone.0123480.

Choi, H. J. and Kim, D. M. (2004) 'Visual field constriction associated with vigabatrin: retinal nerve fiber layer photographic correlation', *Journal of Neurology, Neurosurgery & Psychiatry*, 75(10), pp. 1395 LP – 1395. doi: 10.1136/jnnp.2004.036301.

Clayton, L. M. *et al.* (2013) 'Evolution of visual field loss over ten years in individuals taking vigabatrin', *Epilepsy Research*. Elsevier B.V., 105(3), pp. 262–271. doi: 10.1016/j.eplepsyres.2013.02.014.

Comaish, I. F. *et al.* (2002) 'The effects of vigabatrin on electrophysiology and visual fields in epileptics: a controlled study with a discussion of possible mechanisms.', *Documenta ophthalmologica. Advances in ophthalmology*, 104(2), pp. 195–212. doi:

10.1023/a:1014603229383.

Conway, M. L. *et al.* (2014) 'Does the Swedish Interactive Threshold Algorithm (SITA) accurately map visual field loss attributed to vigabatrin?', *BMC Ophthalmology*, 14(1), pp. 1–10. doi: 10.1186/1471-2415-14-166.

Coupland, S. G. *et al.* (2001) 'Vigabatrin effect on inner retinal function.', *Ophthalmology*, 108(8), pp. 1493–6; discussion 1497-8. doi: 10.1016/s0161-6420(01)00638-8.

Daneshvar, H. *et al.* (1999) 'Symptomatic and asymptomatic visual loss in patients taking vigabatrin.', *Ophthalmology*, 106(9), pp. 1792–8. doi: 10.1016/S0161-6420(99)90345-7.

Dewar, J. and M Ckendrick, J. G. (1873) 'On the Physiological Action of Light: No. II.', *Journal of anatomy and physiology*, 7(Pt 2), pp. 278–82. Available at: http://www.ncbi.nlm.nih.gov/pubmed/17230980.

Domalpally, A. *et al.* (2009) 'Quality issues in interpretation of optical coherence tomograms in macular diseases.', *Retina (Philadelphia, Pa.)*, 29(6), pp. 775–81. doi: 10.1097/IAE.0b013e3181a0848b.

Duboc, A. *et al.* (2004) 'Vigabatrin, the gaba-transaminase inhibitor, damages cone photoreceptors in rats', *American Journal of Ophthalmology*. doi: 10.1016/j.ajo.2004.07.014.

Eke, T., Talbot, J. F. and Lawden, M. C. (1997) 'Severe persistent visual field constriction associated with vigabatrin', *British Medical Journal*. doi: 10.1136/bmj.314.7095.1693a.

Ettinger, A. B. *et al.* (1998) 'Fatigue and Depression in Epilepsy', *Journal of Epilepsy*, 11(2), pp. 105–109. doi: 10.1016/S0896-6974(97)00139-4.

European Medicines Agency (1999) *Opinion of the Committee for proprietry medicinal products pursuant to Article 12 of Council Directive 75/319/EEC as amended for*

Vigabatrin. Annex 1. Scientific conclusions and grounds for amendment of the summaries of product characteristics presented by. Available at: https://www.ema.europa.eu/en/documents/referral/opinion-committee-proprietary-medicinal-products-pursuant-article-12-council-directive-75/319/eec-amended-vigabatrin-annexes-i-ii-iii-iv_en.pdf.

Faedda, M. *et al.* (1993) 'Terapia con Vigabatrin nelle epilessie parziali resistenti', *G Neuropsicofarmacol*, (15), pp. 105–8.

Fisher, R. *et al.* (1996) 'Newer antiepileptic drugs as monotherapy: data on vigabatrin.', *Neurology*, 47(1 Suppl 1), pp. S2-5. doi: 10.1212/wnl.47.1_suppl_1.2s.

Folgar, F. A. *et al.* (2014) 'Comparison of optical coherence tomography assessments in the comparison of age-related macular degeneration treatments trials.', *Ophthalmology*, 121(10), pp. 1956–65. doi: 10.1016/j.ophtha.2014.04.020.

Foroozan, R. (2018) 'Vigabatrin: Lessons Learned from the United States Experience', *Journal of Neuro-Ophthalmology*, 38(4), pp. 442–450. doi: 10.1097/WNO.0000000000000609.

Forte, R. *et al.* (2009) 'Comparison of time domain Stratus OCT and spectral domain SLO/OCT for assessment of macular thickness and volume.', *Eye (London, England)*, 23(11), pp. 2071–8. doi: 10.1038/eye.2008.363.

Frierson, H. T. and Hoban, J. D. (1992) 'The effects of acute test anxiety on NBME Part I performance.', *Journal of the National Medical Association*, 84(8), pp. 686–9. Available at: http://www.ncbi.nlm.nih.gov/pubmed/1507259.

Froger, N. *et al.* (2014) 'Taurine: The comeback of a neutraceutical in the prevention of retinal degenerations', *Progress in Retinal and Eye Research*. doi: 10.1016/j.preteyeres.2014.03.001.

Gaucher, D. *et al.* (2012) 'Taurine deficiency damages retinal neurones: Cone photoreceptors and retinal ganglion cells', *Amino Acids*, 43(5), pp. 1979–1993. doi: 10.1007/s00726-012-1273-3.

Gibson, J. P. *et al.* (1990) 'Chronic toxicity studies with vigabatrin, a GABA-transaminase inhibitor.', *Toxicologic pathology*, 18(2), pp. 225–38. doi: 10.1177/019262339001800201.

Glen, F. C., Baker, H. and Crabb, D. P. (2014) 'A qualitative investigation into patients' views on visual field testing for glaucoma monitoring', *BMJ Open*, 4(1), p. e003996. doi: 10.1136/bmjopen-2013-003996.

Gonzalez, P. *et al.* (2004) 'The effects of pupil size on the multifocal electroretinogram.', *Documenta ophthalmologica. Advances in ophthalmology*, 109(1), pp. 67–72. doi: 10.1007/s10633-004-1545-7.

Gonzalez, P. *et al.* (2009) 'Binasal visual field defects are not specific to vigabatrin', *Epilepsy and Behavior*. doi: 10.1016/j.yebeh.2009.09.003.

Gram, L. *et al.* (1988) 'Effects of valproate, vigabatrin and aminooxyacetic acid on release of endogenous and exogenous GABA from cultured neurons.', *Epilepsy research*, 2(2), pp. 87–95. doi: 10.1016/0920-1211(88)90024-1.

Grant, S. M. and Heel, R. C. (1991) 'Vigabatrin', *Drugs*, 41(6), pp. 889–926. doi: 10.2165/00003495-199141060-00007.

Grove, J., Alken, R. G. and Schechter, P. J. (1984) 'Assay of gamma-vinyl-gamma-aminobutyric acid (4-amino-hex-5-enoic acid) in plasma and urine by automatic amino acid analysis. Application to human pharmacokinetics.', *Journal of chromatography*, 306, pp. 383–7. doi: 10.1016/s0378-4347(00)80903-2.

Grzybowski, A. (2009) 'Harry Moss Traquair (1875-1954), Scottish ophthalmologist and

perimetrist', *Acta Ophthalmologica*, 87(4), pp. 455–459. doi: 10.1111/j.1755-3768.2008.01286.x.

Guberman, A. (1996) 'Vigabatrin.', *The Canadian journal of neurological sciences. Le journal canadien des sciences neurologiques*, 23(4 Suppl 2), pp. S13-7. doi: 10.1017/s0317167100020928.

Haegele, K. D. *et al.* (1988) 'Pharmacokinetics of vigabatrin: implications of creatinine clearance.', *Clinical pharmacology and therapeutics*, 44(5), pp. 558–65. doi: 10.1038/clpt.1988.194.

Haegele, K. D. and Schechter, P. J. (1986) 'Kinetics of the enantiomers of vigabatrin after an oral dose of the racemate or the active S-enantiomer.', *Clinical pharmacology and therapeutics*, 40(5), pp. 581–6. doi: 10.1038/clpt.1986.227.

Halonen, T., Pitkänen, A. and Riekkinen, P. J. (1990) 'Administration of vigabatrin (gamma-vinyl-gamma-aminobutyric acid) affects the levels of both inhibitory and excitatory amino acids in rat cerebrospinal fluid.', *Journal of neurochemistry*, 55(6), pp. 1870–4. doi: 10.1111/j.1471-4159.1990.tb05770.x.

Hammond, E. J. and Wilder, B. J. (1985) 'Gamma-vinyl GABA: a new antiepileptic drug.', *Clinical neuropharmacology*, 8(1), pp. 1–12. doi: 10.1097/00002826-198503000-00001.

Harding, G. F. . *et al.* (2000) 'Separating the retinal electrophysiologic effects of vigabatrin. treatment versus field loss', *American Journal of Ophthalmology*. doi: 10.1016/s0002-9394(00)00763-7.

Harding, G. F. A., Mackenzie, R. and Klistorner, A. (1998) 'Severe persistent visual field constriction associated with vigabatrin', *BMJ*. doi: 10.1136/bmj.316.7126.232.

Hardus, P. *et al.* (2001) 'The value of electrophysiology results in patients with epilepsy and vigabatrin associated visual field loss.', *Acta ophthalmologica Scandinavica*, 79(2),

pp. 169–74. doi: 10.1034/j.1600-0420.2001.079002169.x.

Hawker, M. J. and Astbury, N. J. (2008) 'The ocular side effects of vigabatrin (Sabril): Information and guidance for screening', *Eye*. doi: 10.1038/eye.2008.139.

Hayes, K. C., Carey, R. E. and Schmidt, S. Y. (1975) 'Retinal degeneration associated with taurine deficiency in the cat', *Science*. doi: 10.1126/science.1138364.

Heijl, A., Lindgren, G. and Olsson, J. (1989) 'The effect of perimetric experience in normal subjects.', *Archives of ophthalmology (Chicago, Ill. : 1960)*, 107(1), pp. 81–6. doi: 10.1001/archopht.1989.01070010083032.

Heinänen, K. *et al.* (1998) 'Gyrate atrophy of the choroid and retina: lymphocyte ornithine-delta-aminotransferase activity in different mutations and carriers.', *Pediatric research*, 44(3), pp. 381–5. doi: 10.1203/00006450-199809000-00019.

Henson, D. B. and Morris, E. J. (1993) 'Effect of uncorrected refractive errors upon central visual field testing.', *Ophthalmic & physiological optics : the journal of the British College of Ophthalmic Opticians (Optometrists)*, 13(4), pp. 339–43. doi: 10.1111/j.1475-1313.1993.tb00488.x.

Heuer, D. K. *et al.* (1987) 'The Influence of Refraction Accuracy on Automated Perimetric Threshold Measurements', *Ophthalmology*, 94(12), pp. 1550–1553. doi: 10.1016/S0161-6420(87)33248-8.

Hilton, E. J. R. *et al.* (2002) 'Patients treated with vigabatrin exhibit central visual function loss.', *Epilepsia*, 43(11), pp. 1351–9. doi: 10.1046/j.1528-1157.2002.00502.x.

Hoffmann, M. B. *et al.* (2021) 'ISCEV standard for clinical multifocal electroretinography (mfERG) (2021 update)', *Documenta Ophthalmologica*, 142(1), pp. 5–16. doi: 10.1007/s10633-020-09812-w.

Hood, D. C. (2000) 'Assessing retinal function with the multifocal technique.', *Progress in*

retinal and eye research, 19(5), pp. 607–46. doi: 10.1016/s1350-9462(00)00013-6.

Hwang, Y. H. *et al.* (2016) 'Retinal Nerve Fiber Layer Thickness Measurement Repeatability for Cirrus HD-OCT Retinal Tracking System During Eye Movement.', *Journal of glaucoma*, 25(3), pp. e214-9. doi: 10.1097/IJG.0000000000000250.

Imaki, H. *et al.* (1993) 'Retinal morphology and visual pigment levels in 6-and 12-month-old rhesus monkeys fed a taurine-free human infant formula', *Journal of Neuroscience Research*, 36(3), pp. 290–304. doi: 10.1002/jnr.490360307.

Jackson, G. R. *et al.* (2002) 'Aging-related changes in the multifocal electroretinogram.', *Journal of the Optical Society of America. A, Optics, image science, and vision*, 19(1), pp. 185–9. doi: 10.1364/josaa.19.000185.

Jacobson, S. G. *et al.* (1987) 'Rhodopsin topography and rod-mediated function in cats with the retinal degeneration of taurine deficiency.', *Experimental eye research*, 45(4), pp. 481–90. doi: 10.1016/s0014-4835(87)80059-3.

Jammoul, F. *et al.* (2009) 'Taurine deficiency Is a cause of vigabatrin-induced retinal phototoxicity', *Annals of Neurology*. doi: 10.1002/ana.21526.

Jensen, H. *et al.* (2002) 'Vigabatrin and retinal changes.', *Documenta ophthalmologica. Advances in ophthalmology*, 104(2), pp. 171–80. doi: 10.1023/a:1014679804792.

Johnson, C. A. *et al.* (1988) 'Age-related changes in the central visual field for short-wavelength-sensitive pathways', *Journal of the Optical Society of America A*, 5(12), p. 2131. doi: 10.1364/JOSAA.5.002131.

Johnson, C. A. (2013) 'Psychophysical factors that have been applied to clinical perimetry', *Vision Research*, 90, pp. 25–31. doi: 10.1016/j.visres.2013.07.005.

Johnson, C. A., Adams, C. W. and Lewis, R. A. (1988) 'Fatigue effects in automated perimetry', *Applied Optics*, 27(6), p. 1030. doi: 10.1364/AO.27.001030.

Jung, M. J. *et al.* (1977) ?'-VINYL GABA (4-amino-hex-5-enoic acid), A NEW SELECTIVE IRREVERSIBLE INHIBITOR OF GABA-T: EFFECTS ON BRAIN GABA METABOLISM IN MICE', *Journal of Neurochemistry*, 29(5), pp. 797–802. doi: 10.1111/j.1471-4159.1977.tb10721.x.

Jung, M J *et al.* (1977) 'The effect of 4-amino hex-5-ynoic acid (gamma-acetylenic GABA, gammma-ethynyl GABA) a catalytic inhibitor of GABA transaminase, on brain GABA metabolism in vivo.', *Journal of neurochemistry*, 28(4), pp. 717–23. doi: 10.1111/j.1471-4159.1977.tb10618.x.

Jung, M. J. and Metcalf, B. W. (1975) 'Catalytic inhibition of gamma-aminobutyric acid - alpha-ketoglutarate transaminase of bacterial origin by 4-aminohex-5-ynoic acid, a substrate analog.', *Biochemical and biophysical research communications*, 67(1), pp. 301–6. doi: 10.1016/0006-291x(75)90316-2.

Kälviäinen, R. *et al.* (1995) 'Vigabatrin vs carbamazepine monotherapy in patients with newly diagnosed epilepsy. A randomized, controlled study.', *Archives of neurology*, 52(10), pp. 989–96. doi: 10.1001/archneur.1995.00540340081016.

Kang, E. M. *et al.* (2015) 'Relationship between Peripapillary Retinal Nerve Fiber Layer Thickness Measured by Optical Coherence Tomography and Visual Field Severity Indices.', *Korean journal of ophthalmology : KJO*, 29(4), pp. 263–9. doi: 10.3341/kjo.2015.29.4.263.

Kardon, R. H. (2011) 'Role of the macular optical coherence tomography scan in neuro-ophthalmology.', *Journal of neuro-ophthalmology : the official journal of the North American Neuro-Ophthalmology Society*, 31(4), pp. 353–61. doi: 10.1097/WNO.0b013e318238b9cb.

Katz, J. and Sommer, A. (1988) 'Reliability Indexes of Automated Perimetric Tests',

Archives of Ophthalmology, 106(9), pp. 1252–1254. doi: 10.1001/archopht.1988.01060140412043.

Kawabata, H. and Adachi-Usami, E. (1997) 'Multifocal electroretinogram in myopia.', *Investigative ophthalmology & visual science*, 38(13), pp. 2844–51. Available at: http://www.ncbi.nlm.nih.gov/pubmed/9418738.

Keating, D. *et al.* (2001) 'A comparison of CRT and digital stimulus delivery methods in the multifocal ERG.', *Documenta ophthalmologica. Advances in ophthalmology*, 102(2), pp. 95–114. doi: 10.1023/a:1017527006572.

Keating, D., Parks, S. and Evans, A. (2000) 'Technical aspects of multifocal ERG recording', *Documenta Ophthalmologica*, 100(2), pp. 77–98. doi: 10.1023/A:1002723501303.

Kido, A. *et al.* (2018) 'Outer Plexiform Layer Elevations as a Marker for Prior Ocular Attacks in Patients With Behcet's Disease', *Investigative Ophthalmology & Visual Science*, 59(7), pp. 2828–2832. doi: 10.1167/iovs.18-24348.

Kjellström, U., Andréasson, S. and Ponjavic, V. (2014) 'Attenuation of the retinal nerve fibre layer and reduced retinal function assessed by optical coherence tomography and full-field electroretinography in patients exposed to vigabatrin medication', *Acta Ophthalmologica*, 92(2), pp. 149–157. doi: 10.1111/aos.12030.

Know your retinal layers (2016) *Heidelberg Engineering*. Available at: https://business-lounge.heidelbergengineering.com/us/en/news/news/know-your-retinal-layers-33401465 (Accessed: 17 August 2021).

Kosmin, A. *et al.* (1996) 'Ageing changes in automated perimetry. A comparison of flicker and luminance sensitivity in normal subjects', in *Perimetry Upate 1996/1997. Proceedings of the XIIth International Perimetric Society Meeting Würzburg, Germany*,

pp. 229–233.

Koulen, P. *et al.* (1998) 'Presynaptic and postsynaptic localization of GABA(B) receptors in neurons of the rat retina.', *The European journal of neuroscience*, 10(4), pp. 1446–56. doi: 10.1046/j.1460-9568.1998.00156.x.

Krauss, G. *et al.* (2016) 'Sabril® registry 5-year results: Characteristics of adult patients treated with vigabatrin', *Epilepsy and Behavior*. doi: 10.1016/j.yebeh.2015.12.004.

Krauss, Gregory L., Johnson, M. A. and Miller, N. R. (1998) 'Vigabatrin-associated retinal cone system dysfunction: Electroretinogram and ophthalmologic findings', *Neurology*, 50(3), pp. 614–618. doi: 10.1212/WNL.50.3.614.

Krauss, G. L., Johnson, M. A. and Miller, N. R. (1998) 'Vigabatrin-associated retinal cone system dysfunction', *Neurology*. doi: 10.1212/wnl.51.6.1779-b.

Krauss, G. L. and Miller, N. R. (1999) 'Vigabatrin: An Effective antiepilepsy drug - Balancing the risk of visual dysfunction', *Annals of Pharmacotherapy*. doi: 10.1345/aph.19308.

Lagogianni, C., Gatzonis, S. and Patrikelis, P. (2021) 'Fatigue and cognitive functions in epilepsy: A review of the literature', *Epilepsy & Behavior*, 114, p. 107541. doi: 10.1016/j.yebeh.2020.107541.

Lähdesmäki, P. (1986) 'Determination of taurine and other acidic amino acids in plants', *Phytochemistry*, 25(10), pp. 2409–2411. doi: 10.1016/S0031-9422(00)81707-0.

Lake, N. and Verdone-Smith, C. (1989) 'Immunocytochemical localization of taurine in the mammalian retina.', *Current eye research*, 8(2), pp. 163–73. doi: 10.3109/02713688908995188.

Larsson, O. M. *et al.* (1986) 'Differential effect of gamma-vinyl GABA and valproate on GABA-transaminase from cultured neurones and astrocytes.', *Neuropharmacology*,

25(6), pp. 617–25. doi: 10.1016/0028-3908(86)90214-5.

Lawden, M. C. *et al.* (1999) 'Visual field defects associated with vigabatrin therapy', *Journal of Neurology Neurosurgery and Psychiatry*. doi: 10.1136/jnnp.67.6.716.

Lawthom, C., Smith, P. E. M. and Wild, J. M. (2009) 'Nasal Retinal Nerve Fiber Layer Attenuation: A Biomarker for Vigabatrin Toxicity', *Ophthalmology*. doi: 10.1016/j.ophtha.2008.09.047.

Leach, J. P. *et al.* (1996) 'Effects of tiagabine and vigabatrin on GABA uptake into primary cultures of rat cortical astrocytes', *Seizure*. doi: 10.1016/S1059-1311(96)80041-0.

Leon, A., Levick, W. R. and Sarossy, M. G. (1995) 'Lesion topography and new histological features in feline taurine deficiency retinopathy', *Experimental Eye Research*, 61(6), pp. 731–741. doi: 10.1016/S0014-4835(05)80024-7.

Lindenmuth, K. A. *et al.* (1989) 'Effects of PuPiliary Constriction on Automated Perimetry in Normal Eyes', *Ophthalmology*, 96(9), pp. 1298–1301. doi: 10.1016/S0161-6420(89)32723-0.

Lindenmuth, K. A. *et al.* (1990) 'Effects of pupillary dilation on automated perimetry in normal patients.', *Ophthalmology*, 97(3), pp. 367–70. doi: 10.1016/s0161-6420(90)32580-0.

Lippert, B. *et al.* (1977) '4-amino-hex-5-enoic acid, a selective catalytic inhibitor of 4-aminobutyric-acid aminotransferase in mammalian brain.', *European journal of biochemistry*, 74(3), pp. 441–5. doi: 10.1111/j.1432-1033.1977.tb11410.x.

Loiseau, P. *et al.* (1986) 'Double-blind, placebo-controlled study of vigabatrin (gamma-vinyl GABA) in drug-resistant epilepsy.', *Epilepsia*, 27(2), pp. 115–20. doi: 10.1111/j.1528-1157.1986.tb03512.x.

Lombardini, J. B. (1991) 'Taurine: retinal function', *Brain Research Reviews*, 16(2), pp.

151–169. doi: 10.1016/0165-0173(91)90003-Q.

Löscher, W. (1980) 'A comparative study of the pharmacology of inhibitors of GABA-metabolism', *Naunyn-Schmiedeberg's Archives of Pharmacology*, 315(2), pp. 119–128. doi: 10.1007/BF00499254.

Lukasiewicz, P. D. and Shields, C. R. (1998) 'A diversity of GABA receptors in the retina.', *Seminars in cell & developmental biology*, 9(3), pp. 293–9. doi: 10.1006/scdb.1998.0238.

Malmgren, K., Ben-Menachem, E. and Frisén, L. (2001) 'Vigabatrin visual toxicity: evolution and dose dependence.', *Epilepsia*, 42(5), pp. 609–15. doi: 10.1046/j.1528-1157.2001.28600.x.

Marcora, S. M., Staiano, W. and Manning, V. (2009) 'Mental fatigue impairs physical performance in humans', *Journal of Applied Physiology*, 106(3), pp. 857–864. doi: 10.1152/japplphysiol.91324.2008.

Marra, G. and Flammer, J. (1991) 'The learning and fatigue effect in automated perimetry.', *Graefe's archive for clinical and experimental ophthalmology = Albrecht von Graefes Archiv fur klinische und experimentelle Ophthalmologie*, 229(6), pp. 501–4. doi: 10.1007/BF00203309.

McCulloch, D. L. *et al.* (2015) 'ISCEV Standard for full-field clinical electroretinography (2015 update)', *Documenta Ophthalmologica*, 130(1), pp. 1–12. doi: 10.1007/s10633-014-9473-7.

McDonagh, J. *et al.* (2001) 'The wide field multifocal ERG reveals a retinal defect caused by vigabatrin toxicity? [12]', *British Journal of Ophthalmology*. doi: 10.1136/bjo.85.1.110k.

McDonagh, J. *et al.* (2003a) 'Peripheral retinal dysfunction in patients taking vigabatrin', *Neurology*. doi: 10.1212/01.WNL.0000098938.80082.25.

McDonagh, J. *et al.* (2003b) 'Peripheral retinal dysfunction in patients taking vigabatrin', *Neurology*, 61(12), pp. 1690–1694. doi: 10.1212/01.WNL.0000098938.80082.25.

Michelucci, R. and Tassinari, C. A. (1989) 'Response to vigabatrin in relation to seizure type.', *British journal of clinical pharmacology*, 27 Suppl 1, pp. 119S-124S. doi: 10.1111/j.1365-2125.1989.tb03472.x.

Midelfart, A., Midelfart, E. and Brodtkorb, E. (2000) 'Visual field defects in patients taking vigabatrin', *Acta Ophthalmologica Scandinavica*. doi: 10.1034/j.1600-0420.2000.078005580.x.

Mohidin, N., Yap, M. K. and Jacobs, R. J. (1997) 'The repeatability and variability of the multifocal electroretinogram for four different electrodes.', *Ophthalmic & physiological optics : the journal of the British College of Ophthalmic Opticians (Optometrists)*, 17(6), pp. 530–5. Available at: http://www.ncbi.nlm.nih.gov/pubmed/9666928.

Mohidin, N., Yap, M. K. and Jacobs, R. J. (1999) 'Influence of age on the multifocal electroretinography.', *Ophthalmic & physiological optics : the journal of the British College of Ophthalmic Opticians (Optometrists)*, 19(6), pp. 481–8. doi: 10.1046/j.1475-1313.1999.00468.x.

Moseng, L. *et al.* (2011) 'Retinal nerve fibre layer attenuation: clinical indicator for vigabatrin toxicity.', *Acta ophthalmologica*, 89(5), pp. 452–8. doi: 10.1111/j.1755-3768.2010.02077.x.

Mumford, J. P. and Dam, M. (1989) 'Meta-analysis of European placebo controlled studies of vigabatrin in drug resistant epilepsy.', *British journal of clinical pharmacology*, 27 Suppl 1, pp. 101S-107S. doi: 10.1111/j.1365-2125.1989.tb03469.x.

Nabeshima, T. *et al.* (no date) 'Effects of aging on the first and second-order kernels of multifocal electroretinogram.', *Japanese journal of ophthalmology*, 46(3), pp. 261–9. doi:

10.1016/s0021-5155(02)00475-6.

Neal, M. J., Collins, G. G. and Massey, S. C. (1979) 'Inhibition of aspartate release from the retina of the anaesthetised rabbit by stimulation with light flashes.', *Neuroscience letters*, 14(2–3), pp. 241–5. doi: 10.1016/0304-3940(79)96155-x.

Nehring, R. B. *et al.* (2000) 'The metabotropic GABAB receptor directly interacts with the activating transcription factor 4.', *The Journal of biological chemistry*, 275(45), pp. 35185–91. doi: 10.1074/jbc.M002727200.

Newman, W. D., Tocher, K. and Acheson, J. F. (2002) 'Vigabatrin associated visual field loss: a clinical audit to study prevalence, drug history and effects of drug withdrawal.', *Eye (London, England)*, 16(5), pp. 567–71. doi: 10.1038/sj.eye.6700168.

Nowomiejska, K. *et al.* (2014) 'Relationship between the area of isopters and Vigabatrin dosage during two years of observation', *BMC Ophthalmology*. doi: 10.1186/1471-2415-14-56.

OSBORNE, N. N. *et al.* (1999) 'Ganglion cell death in glaucoma: what do we really know?', *British Journal of Ophthalmology*, 83(8), pp. 980 LP – 986. doi: 10.1136/bjo.83.8.980.

Otani, T., Yamaguchi, Y. and Kishi, S. (2011) 'Improved visualization of Henle fiber layer by changing the measurement beam angle on optical coherence tomography.', *Retina (Philadelphia, Pa.)*, 31(3), pp. 497–501. doi: 10.1097/IAE.0b013e3181ed8dae.

Palmowski, A. M. *et al.* (1999) 'Effects of refractive blur on the multifocal electroretinogram', *Documenta Ophthalmologica*, 99(1), p. 41. doi: 10.1023/A:1002432113628.

Pawlikowska, T. *et al.* (1994) 'Population based study of fatigue and psychological distress.', *BMJ (Clinical research ed.)*, 308(6931), pp. 763–6. doi:

10.1136/bmj.308.6931.763.

Pedersen, S. A. *et al.* (1985) 'Long-term study of gamma-vinyl GABA in the treatment of epilepsy.', *Acta neurologica Scandinavica*, 72(3), pp. 295–8. doi: 10.1111/j.1600-0404.1985.tb00873.x.

Peng, Y. *et al.* (2017) 'Reduction of retinal nerve fiber layer thickness in vigabatrin-exposed patients: A meta-analysis', *Clinical Neurology and Neurosurgery*. doi: 10.1016/j.clineuro.2017.04.004.

Petroff, O. A. *et al.* (1998) 'Vigabatrin increases human brain homocarnosine and improves seizure control.', *Annals of neurology*, 44(6), pp. 948–52. doi: 10.1002/ana.410440614.

Pierre-Filho, P. de T. *et al.* (2010) 'Learning effect in visual field testing of healthy subjects using Humphrey Matrix frequency doubling technology perimetry', *Eye*, 24(5), pp. 851–856. doi: 10.1038/eye.2009.210.

Pitkänen, A. *et al.* (1988) 'Levels of total gamma-aminobutyric acid (GABA), free GABA and homocarnosine in cerebrospinal fluid of epileptic patients before and during gamma-vinyl-GABA (vigabatrin) treatment.', *Journal of the neurological sciences*, 88(1–3), pp. 83–93. doi: 10.1016/0022-510x(88)90207-9.

Plant, G. T. and Sergott, R. C. (2011) 'Understanding and interpreting vision safety issues with vigabatrin therapy', *Acta Neurologica Scandinavica*, 124, pp. 57–71. doi: 10.1111/j.1600-0404.2011.01601.x.

Ponjavic, V. and Andréasson, S. (2001) 'Multifocal ERG and full-field ERG in patients on long-term vigabatrin medication.', *Documenta ophthalmologica. Advances in ophthalmology*, 102(1), pp. 63–72. doi: 10.1023/a:1017589301855.

Popova, E. (2015) 'GABAergic neurotransmission and retinal ganglion cell function.',

Journal of comparative physiology. A, Neuroethology, sensory, neural, and behavioral physiology, 201(3), pp. 261–83. doi: 10.1007/s00359-015-0981-z.

Quesada, O., Picones, A. and Pasantes-Morales, H. (1988) 'Effect of light deprivation on the ERG responses of taurine-deficient rats', *Experimental Eye Research*, 46(1), pp. 13–20. doi: 10.1016/S0014-4835(88)80088-5.

R., S. *et al.* (2013) 'Three-year results from the sabril registry continue to yield low rate of visual field defects', *Epilepsy Currents*.

Rajjoub, R. D. *et al.* (2015) 'Reproducibility of retinal nerve fiber layer thickness measures using eye tracking in children with nonglaucomatous optic neuropathy.', *American journal of ophthalmology*, 159(1), pp. 71–7.e1. doi: 10.1016/j.ajo.2014.09.029.

Ravindran, J. *et al.* (2001a) 'Visual field loss associated with vigabatrin: pathological correlations', *American Journal of Ophthalmology*. doi: 10.1016/s0002-9394(01)01227-2.

Ravindran, J. *et al.* (2001b) 'Visual field loss associated with vigabatrin: Pathological correlations', *Journal of Neurology Neurosurgery and Psychiatry*. doi: 10.1136/jnnp.70.6.787.

Renard, J.-P., Fénolland, J.-R. and Giraud, J.-M. (2019) 'Glaucoma progression analysis by Spectral-Domain Optical Coherence Tomography (SD-OCT).', *Journal francais d'ophtalmologie*, 42(5), pp. 499–516. doi: 10.1016/j.jfo.2019.03.001.

Rey, E., Pons, G. and Olive, G. (1992) 'Vigabatrin. Clinical pharmacokinetics.', *Clinical pharmacokinetics*, 23(4), pp. 267–78. doi: 10.2165/00003088-199223040-00003.

Riekkinen, P. J. *et al.* (1989) 'Specificity of vigabatrin for the GABAergic system in human epilepsy.', *Epilepsia*, 30 Suppl 3, pp. S18-22. doi: 10.1111/j.1528-1157.1989.tb05828.x.

Rotolo, T. C. and Dacheux, R. F. (2003) 'Evidence for glycine, GABAA, and GABAB receptors on rabbit OFF-alpha ganglion cells.', *Visual neuroscience*, 20(3), pp. 285–96.

doi: 10.1017/s0952523803203072.

Roubertie, A., Bellet, H. and Echenne, B. (1998) 'Vigabatrin-associated retinal cone system dysfunction.', *Neurology*, 51(6), pp. 1779–81. doi: 10.1212/wnl.51.6.1779-a.

Rowe, F. (2006) *Visual fields via the visual pathway*. Blackwell Publishing Limited.

Ruether, K. *et al.* (1998) 'Electrophysiologic evaluation of a patient with peripheral visual field contraction associated with vigabatrin.', *Archives of ophthalmology (Chicago, Ill. : 1960)*, 116(6), pp. 817–9. Available at: http://www.ncbi.nlm.nih.gov/pubmed/9639460.

Sabers, A. and Gram, L. (1992) 'Pharmacology of vigabatrin.', *Pharmacology & toxicology*, 70(4), pp. 237–43. doi: 10.1111/j.1600-0773.1992.tb00465.x.

'Sabril Drug Information. HIghlights of perscribing information.' (2020). Lundbeck.

Sadda, S. R. *et al.* (2006) 'Errors in retinal thickness measurements obtained by optical coherence tomography.', *Ophthalmology*, 113(2), pp. 285–93. doi: 10.1016/j.ophtha.2005.10.005.

Salazar, P. *et al.* (1986) 'Pharmacological identification of retinal cells releasing taurine by light stimulation.', *Journal of neuroscience research*, 15(3), pp. 383–91. doi: 10.1002/jnr.490150309.

Sarhan, S. and Seiler, N. (1979) 'Metabolic inhibitors and subcellular distribution of GABA.', *Journal of neuroscience research*, 4(5–6), pp. 399–421. doi: 10.1002/jnr.490040508.

Schechter, P. J. *et al.* (1977) 'Audiogenic seizure protection by elevated brain GABA concentration in mice: effects of gamma-acetylenic gaba and gamma-vinyl GABA, two irreversible GABA-T inhibitors.', *European journal of pharmacology*, 45(4), pp. 319–28. doi: 10.1016/0014-2999(77)90270-9.

Schechter, P. J. and Tranier, Y. (1977) 'Effect of GABA-transminase inhibition on rectal

temperature in mice.', *Pharmacology, biochemistry, and behavior*, 6(6), pp. 667–9. doi: 10.1016/0091-3057(77)90092-2.

Sergott, R. C. *et al.* (2016a) 'Retinal structure and function in vigabatrin-treated adult patients with refractory complex partial seizures', *Epilepsia*. doi: 10.1111/epi.13495.

Sergott, R. C. *et al.* (2016b) 'Retinal structure and function in vigabatrin-treated adult patients with refractory complex partial seizures', *Epilepsia*, 57(10), pp. 1634–1642. doi: 10.1111/epi.13495.

Sherafat, H. *et al.* (2003) 'Effect of a patient training video on visual field test reliability', *British Journal of Ophthalmology*, 87(2), pp. 153 LP – 156. doi: 10.1136/bjo.87.2.153.

Shimada, C. *et al.* (1992) 'Beneficial effect of intravenous taurine infusion on electroretinographic disorder in taurine deficient rats.', *Japanese journal of pharmacology*, 59(1), pp. 43–50. doi: 10.1254/jjp.59.43.

Sorri, I. *et al.* (2010) 'Is reduced ornithine-δ-aminotransferase activity the cause of vigabatrin-associated visual field defects?', *Epilepsy Research*. doi: 10.1016/j.eplepsyres.2010.08.006.

Spelbrink, E. M. *et al.* (2016) 'Plasma taurine levels are not affected by vigabatrin in pediatric patients', *Epilepsia*, 57(8), pp. e168–e172. doi: 10.1111/epi.13447.

Spence, S. J. and Sankar, R. (2001) 'Visual field defects and other ophthalmological disturbances associated with vigabatrin.', *Drug safety*, 24(5), pp. 385–404. doi: 10.2165/00002018-200124050-00005.

Sutter, E. E. and Tran, D. (1992) 'The field topography of ERG components in man--I. The photopic luminance response.', *Vision research*, 32(3), pp. 433–46. doi: 10.1016/0042-6989(92)90235-b.

Swaminathan, S. S. *et al.* (2018) 'The Effect of Patient Characteristics and Sleep Quality

on Visual Field Performance Reliability.', *Journal of ophthalmology*, 2018, p. 2731260. doi: 10.1155/2018/2731260.

Takada, S. *et al.* (2003) 'Influence of Media Opacities on Perimetric Threshold Values using W/W, B/Y, HRP, FDT and Flicker Perimetry ', *Investigative Ophthalmology & Visual Science*, 44(13), p. 1919.

Takki, K. and Simell, O. (1974) 'Genetic aspects in gyrate atrophy of the choroid and retina with hyperornithinaemia.', *The British journal of ophthalmology*, 58(11), pp. 907–16. doi: 10.1136/bjo.58.11.907.

Tartara, A. *et al.* (1986) 'Vigabatrin in the treatment of epilepsy: a double-blind, placebo-controlled study.', *Epilepsia*, 27(6), pp. 717–23. doi: 10.1111/j.1528-1157.1986.tb03600.x.

Tassinari, C. A. *et al.* (1987) 'Double-blind study of vigabatrin in the treatment of drug-resistant epilepsy.', *Archives of neurology*, 44(9), pp. 907–10. doi: 10.1001/archneur.1987.00520210009010.

Tatham, A. J. and Medeiros, F. A. (2017) 'Detecting Structural Progression in Glaucoma with Optical Coherence Tomography.', *Ophthalmology*, 124(12S), pp. S57–S65. doi: 10.1016/j.ophtha.2017.07.015.

Tellez-Zenteno, J. F., Matijevic, S. and Wiebe, S. (2005) 'Somatic Comorbidity of Epilepsy in the General Population in Canada', *Epilepsia*, 46(12), pp. 1955–1962. doi: 10.1111/j.1528-1167.2005.00344.x.

Thompson, H. . and Wall, M. (2010) *History of visual fields before perimetry*, *Imaging and Perimetry Society (IPS)*. Available at: http://webeye.ophth.uiowa.edu/ips/perimetryhistory/1-pre-perimetry.htm.

van der Torren, K., Graniewski-Wijnands, H. S. and Polak, B. C. P. (2002) 'Visual field and

electrophysiological abnormalities due to vigabatrin.', *Documenta ophthalmologica. Advances in ophthalmology*, 104(2), pp. 181–8. doi: 10.1023/a:1014615517996.

Treiman, D. M. (2001) 'GABAergic mechanisms in epilepsy.', *Epilepsia*, 42 Suppl 3, pp. 8–12. doi: 10.1046/j.1528-1157.2001.042suppl.3008.x.

Tuğcu, B. *et al.* (2017) 'Evaluation of inner retinal layers with optic coherence tomography in vigabatrin-exposed patients', *Neurological Sciences*. doi: 10.1007/s10072-017-2971-0.

Valtonen, M. *et al.* (1999) 'Central nervous system involvement in gyrate atrophy of the choroid and retina with hyperornithinaemia.', *Journal of inherited metabolic disease*, 22(8), pp. 855–66. doi: 10.1023/a:1005602405349.

Vienola, K. V *et al.* (2012) 'Real-time eye motion compensation for OCT imaging with tracking SLO.', *Biomedical optics express*, 3(11), pp. 2950–63. doi: 10.1364/BOE.3.002950.

Walters, D. C. *et al.* (2019) 'Metabolomic analyses of vigabatrin (VGB)-treated mice: GABA-transaminase inhibition significantly alters amino acid profiles in murine neural and non-neural tissues', *Neurochemistry International*. Elsevier, 125(February), pp. 151–162. doi: 10.1016/j.neuint.2019.02.015.

Walters, D. C. *et al.* (2021) 'Preferential accumulation of the active S-(+) isomer in murine retina highlights novel mechanisms of vigabatrin-associated retinal toxicity.', *Epilepsy research*, 170, p. 106536. doi: 10.1016/j.eplepsyres.2020.106536.

Wang, M. *et al.* (2020) 'Electrophysiological and Structural Changes in Chinese Patients with LHON.', *Journal of ophthalmology*, 2020, p. 4734276. doi: 10.1155/2020/4734276.

Wang, Q. P. *et al.* (2008) 'Treatment of epilepsy: The GABA-transaminase inhibitor, vigabatrin, induces neuronal plasticity in the mouse retina', *European Journal of*

Neuroscience. doi: 10.1111/j.1460-9568.2008.06175.x.

Wild, J. M. *et al.* (1999) 'Characteristics of a unique visual field defect attributed to vigabatrin', *Epilepsia*. doi: 10.1111/j.1528-1157.1999.tb01599.x.

Wild, J. M. *et al.* (2006) 'Detecting vigabatrin toxicity by imaging of the retinal nerve fiber layer', *Investigative Ophthalmology and Visual Science*. doi: 10.1167/iovs.05-0854.

Wild, J. M. *et al.* (2009) 'Visual field loss in patients with refractory partial epilepsy treated with vigabatrin: Final results from an open-label, observational, multicentre study', *CNS Drugs*. doi: 10.2165/11317650-000000000-00000.

Wild, J. M. *et al.* (2013) 'Modelling the risk of visual field loss arising from long-term exposure to the antiepileptic drug vigabatrin: A cross-sectional approach', *CNS Drugs*. doi: 10.1007/s40263-013-0100-z.

Wild, J. M. *et al.* (2019) 'The Topographical Relationship between Visual Field Loss and Peripapillary Retinal Nerve Fibre Layer Thinning Arising from Long-Term Exposure to Vigabatrin.', *CNS drugs*, 33(2), pp. 161–173. doi: 10.1007/s40263-018-0583-8.

Wild, J. M., Smith, P. E. M. and Knupp, C. (2019) 'Objective Derivation of the Morphology and Staging of Visual Field Loss Associated with Long-Term Vigabatrin Therapy', *CNS Drugs*. doi: 10.1007/s40263-019-00634-2.

Wilson, E. A. and Brodie, M. J. (1997) 'Severe persistent visual field constriction associated with vigabatrin. Chronic refractory epilepsy may have role in causing these unusual lesions.', *BMJ (Clinical research ed.)*, 314(7095), p. 1693. Available at: http://www.ncbi.nlm.nih.gov/pubmed/9193311.

Wong, I. C., Mawer, G. E. and Sander, J. W. (1997) 'Severe persistent visual field constriction associated with vigabatrin. Reaction might be dose dependent.', *BMJ (Clinical research ed.)*, 314(7095), pp. 1693–4. Available at:

http://www.ncbi.nlm.nih.gov/pubmed/9193312.

Wu, H. *et al.* (2015) 'Correlation of localized glaucomatous visual field defects and spectral domain optical coherence tomography retinal nerve fiber layer thinning using a modified structure-function map for OCT.', *Eye (London, England)*, 29(4), pp. 525–33. doi: 10.1038/eye.2014.317.

Yenice, O. and Temel, A. (2005) 'Evaluation of two Humphrey perimetry programs: full threshold and SITA standard testing strategy for learning effect.', *European journal of ophthalmology*, 15(2), pp. 209–12. doi: 10.1177/112067210501500205.

Zeng, Y. *et al.* (2019) 'Early retinal neurovascular impairment in patients with diabetes without clinically detectable retinopathy.', *The British journal of ophthalmology*, 103(12), pp. 1747–1752. doi: 10.1136/bjophthalmol-2018-313582.

Zhang, C., Bettler, B. and Duvoisin, R. M. (1998) 'Differential localization of GABA(B) receptors in the mouse retina.', *Neuroreport*, 9(15), pp. 3493–7. doi: 10.1097/00001756-199810260-00029.

Zhang, J. and Slaughter, M. M. (1995) 'Preferential suppression of the ON pathway by GABAC receptors in the amphibian retina.', *Journal of neurophysiology*, 74(4), pp. 1583–92. doi: 10.1152/jn.1995.74.4.1583.

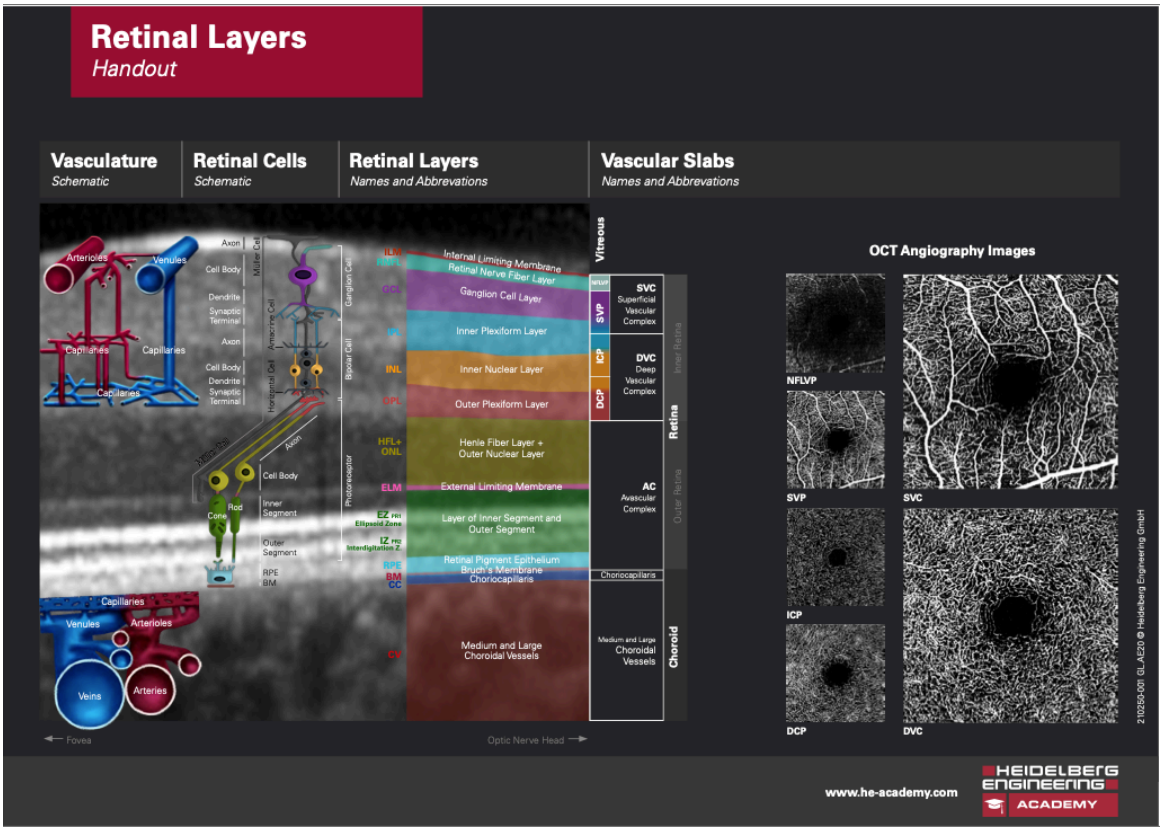
Retinal Layers
Handout
Vasculature
Schematic
Retinal Cells
Schematic
Retinal Layers
Names and Abbrevations
Vascular Slabs
Names and Abbrevations
Arterioles
Venules
Capillaries
Capillaries
Capillaries
Axon
Cell Body
Dendrite
Synaptic Terminal
Axon
Cell Body
Dendrite
Synaptic Terminal
Müller Cell
Amacrine Cell
Horizontal Cell
Ganglion Cell
Bipolar Cell
Photoreceptor
Müller Cell
Axon
Cell Body
Rod
Cone
Inner Segment
Outer Segment
RPE
BM
ILM
RNFL
GCL
IPL
INL
OPL
HFL+
ONL
ELM
EZ
Ellipsoid Zone
IZ
Interdigitation Z.
RPE
BM
CC
CV
Internal Limiting Membrane
Retinal Nerve Fiber Layer
Ganglion Cell Layer
Inner Plexiform Layer
Inner Nuclear Layer
Outer Plexiform Layer
Henle Fiber Layer +
Outer Nuclear Layer
External Limiting Membrane
Layer of Inner Segment and
Outer Segment
Retinal Pigment Epithelium
Bruch's Membrane
Choriocapillaris
Medium and Large
Choroidal Vessels
Capillaries
Venules
Arterioles
Veins
Arteries
Vitreous
SVC
Superficial
Vascular
Complex
SVP
ICP
DVC
Deep
Vascular
Complex
DCP
Inner Retina
Retina
Outer Retina
AC
Avascular
Complex
Choriocapillaris
Choroid
Medium and Large
Choroidal
Vessels
OCT Angiography Images
NFLVP
SVP
SVC
ICP
DCP
DVC
Fovea
Optic Nerve Head
210250-001 GL AE20 © Heidelberg Engineering GmbH
www.he-academy.com
HEIDELBERG
ENGINEERING
ACADEMY